Imperial College London

THE REACTIVITY OF HYDROGEN AND CARBON DIOXIDE MEDIATED BY MAIN GROUP COMPOUNDS

A dissertation submitted to

Imperial College London

for the degree of

Doctor of Philosophy

By

Thomas James Herrington

MChem (Oxon), Imperial College London

May 2014

CID: 00467189

Supervised By

Dr Andrew Ashley & Dr George Britovsek

Chemistry Department

ABSTRACT

The Reactivity of Hydrogen and Carbon Dioxide Mediated by Main Group Compounds

The focus of this thesis has been the design and synthesis of new frustrated Lewis pair (FLP) systems which from structural modifications retain their ability to activate H_2/CO_2, while displaying differing reactivity modes.

Chapter Two describes the first practical synthesis of *tris*[3,5-*bis*(trifluoromethyl)phenyl]borane ($BArF_{18}$). Gutmann-Beckett Lewis acidity measurements reveal that this borane is a more powerful Lewis acid than $B(C_6F_5)_3$, but it nevertheless is found to bind H_2O much more reversibly than $B(C_6F_5)_3$. The $BArF_{18}$/2,2,6,6-tetramethylpiperidine (TMP) FLP provides a rare example of H_2 activation in Et_2O solvent, in which the borohydride salt has been structurally characterised by X-ray crystallography. A novel bridging borohydride $[\mu\text{-}H(BArF_{18})_2]^-$ was revealed, which contrasts to the characteristic terminal borohydrides formed by other borane based mediated FLP systems.

Chapter Three details the design of fluorinated trisalkylboranes including $B[CH(C_6F_5)_2]_3$ which has been synthesised for the first time. This borane has been structurally characterised using X-ray crystallography and displays hydrogen bonding interactions between the *ortho* fluorines on each aryl ring and the adjacent CH proton. Interestingly, and despite this borane showing no Lewis acidity using Gutmann-Beckett and Childs techniques, the $B[CH(C_6F_5)_2]_3$/TMP FLP provides a rare example of H_2 activation in THF solvent.

Chapter Four details the synthesis of two classical trialkylsilylium-phosphane adducts $[R_3Si\text{–}P\textit{t}Bu_3]^+[B(C_6F_5)_4]^-$ [R = Et; R = *i*Pr] derived from the sterically unencumbered silylium ions R_3Si^+ (R = Et, *i*Pr). Both adducts are not found to dissociate at elevated temperature and are appreciably stable towards decomposition. Moreover, adduct formation does not impede archetypal FLP reactivity; admittance of H_2 led to heterolysis at elevated temperatures (90-100 ºC), while CO_2 activation occurs under ambient conditions. The latent stability of the CO_2 adducts has allowed for their crystallographic characterisation. Subsequently, the activation parameters for CO_2 uptake were investigated and support computational calculations.

DECLARATION

The work described in this thesis was carried out within the Chemistry department of Imperial College London from October 2010 to May 2014, under the supervision of Dr Andrew Ashley and Dr George Britovsek. All the work is my own unless stated to the contrary, and has not been previously submitted for any degree at this or any other university.

Thomas James Herrington

May 2014

COPYRIGHT

ACKNOWLEDGEMENTS

I would like to extend my warmest thanks to Dr Andrew Ashley for presenting the tremendous opportunity to study as your first PhD student. I imagine you would agree with me when I say our group hasn't exactly conformed to convention, and to be honest, we couldn't even if we tried. I wish you a 'smorgasbord' of success for the future. Furthermore, I would like to thank my co-supervisor George Britovsek, who has been incredibly approachable over these years.

Much gratitude must be given to all of those individuals who have helped assemble this thesis: Pete Haycock for his unrivalled dedication to all things NMR, Dr A. White for his crystallographic skills and Dr Lisa Haigh for dealing with my mass spectrometry requests. I would to thank Patricia Ho and Bryan Ward of the Hunt research group for their perseverance with the DFT calculations and Dr Alexander Thom for his Monte Carlo analysis. Furthermore, I would like to thank Katie Resner, Elliot J. Lawrence and Dr Gregory Wildgoose of UEA for providing the Cyclic Voltammetry plots and Joe Mcdermott (MSci student (2012-2013)) for his preliminary work on the silylium species. Moreover, I would like to thank Dr Nick Rees of the University of Oxford for providing the low temperature line shape analysis of $B[CH(C_6F_5)_2]_3$.

Massive thanks must be given to Laurence Doyle, who has been an excellent colleague, friend and counterbalance over the years. Although it sickens me to admit your taste in music is markedly better, and I wish you the best of luck with the dinitrogen chemistry. In addition, I would like to say thanks to Daniel Scott, your patience was nothing short of exemplary when it came to proof reading this thesis. You are now the hope of the group when comes to boron based Lewis acids.

To all the other PhDs I have worked with over the last couple of years – Andrew Crawford, Sarah Gates, Peter Hill, and Florian Langmann and Masters students – Duncan Fraser, Caroline Wood, and Louis Oscroft, an immense degree of gratitude for dealing with my mercurial personality. Good luck in whatever the next step may be. Special thanks must be given to those who have worked in the George Britovsek and James Wilton-Ely research groups. More especially Dr A. Tomov, for all your guidance, Matthew Morton with whom I have shared innumerable conversations regarding footy, rugby and post-rock, and Maria Gragert for being so enjoyably German.

To those unconnected with the world of Chemistry I would like to extend my appreciation; Richard Bull, George Willis, Stuart Adams and a now Dr Nick Phillips have all been terrific friends.

Without a doubt no one deserves any more credit than Marguerite Laferrere, who has shown extreme tolerance of my undoubtedly English conduct and provided outstanding support towards the latter stages of this challenging thesis. I am forever grateful and I look forward to our years ahead.

In addition, I would like to thank both the Herrington and Colpitts families for all your support and generosity. In particular, my mother and father who have made this all possible! In short, I hope I have made you both proud.

ABBREVIATIONS

(+I)	Inductively electron donating
(-I)	Inductively electron withdrawing
$\{^1H\}$	Proton decoupled
Ar	Aryl
$BArF_{18}$	$B[3,5\text{-}(CF_3)C_6H_3]_3$
$BArF_{24}$	$B[3,5\text{-}(CF_3)C_6H_3]_4^-$
BCS	Barlett-Condon-Schneider
C	Chemical step
Crotonaldehyde	(2E)-but-2-enal
CSD	Cambridge Structure Database
d	doublet
DABCO	Diazobicylco[2.2.2]octane
DBDMH	1,3-dibromo-5,5-dimethylhydantoin
DFT	Density Functional Theory
DMF	Dimethylformamide
EI	Electron Impact
Et	Ethyl
ET	Electron transfer
Et_2O	Diethyl Ether
FLP	frustrated Lewis pair
HOMO	Highest Occupied Molecular Orbital
HSAB	Hard Soft Acid Base
*i*Pr	*iso*-Propyl
IR	Infrared
LIC-KOR	*n*BuLi/*t*BuOK
LUMO	Lowest Unoccupied Molecular Orbital
Me	Methyl
MHz	Megahertz
Mes	2,4,6-trimethylphenyl
MO	Molecular Orbital
MS	Mass Spectrometry
*n*Bu	*n*-Butyl
NHC	N-heterocyclic carbene
NMP	N-methyl-2-pyrrolidone
nOe	Nuclear Overhauser Effect
NMR	Nuclear Magnetic Resonance
nonaflate	nonafluorobutanesulfonate
Ph	Phenyl
ppm	Parts Per Million
q	quartet
Rbf	Round Bottom Flask
RT	Room Temperature

t	triplet
*t*Bu	*tert*-Butyl
THF	Tetrahydrofuran
TM	Transition Metal
TMP	2,2,6,6-tetramethylpiperidine
TS	Transition state
TSAF	*Tris*(dimethylamino)sulfonium difluorotrimethylsilicate
$\sigma^{p/m}$	Hammett parameter

CONTENTS

CHAPTER ONE

Background & Introduction

1.1 Transition metal *vs.* main group chemistry

Until the last two decades, transition metal complexes were the archetypal catalysts for organic transformations. Their established use in reaction types such as oxidative addition, migratory insertion and reductive elimination promoted their widespread application within petrochemical, pharmaceutical and material industries.[1] For example Wilkinson's rhodium catalyst, $[RhCl(PPh_3)_3]$, continues to be used as a catalyst for the hydrogenation of unsaturated substrates (Figure 1.1).[2] The attraction of this catalyst stems from its high activity and stability coupled with an increasing range of recovery techniques.[3]

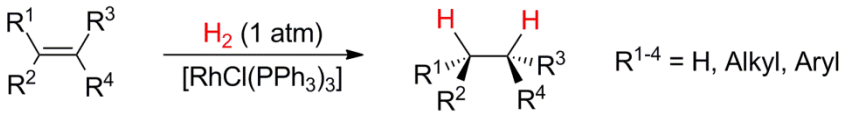

Figure 1.1. Hydrogenation of olefins using $RhCl(PPh_3)_3$.

The ubiquity of transition metal (TM) mediated catalysis stems from the electronic properties of the respective metals, which present energetically accessible occupied and unoccupied frontier orbitals. The cooperativity between these orbitals is exemplified in the Dewar-Chatt-Duncanson model.[4] Here, small molecules such as H_2 and alkenes undergo synergic bonding where σ-donation from the ligand to the metal is concomitant with π-donation from the metal onto the ligand (Figure 1.2). Both interactions result in significant weakening of the H–H or C=C π bond which often leads to their oxidative addition.

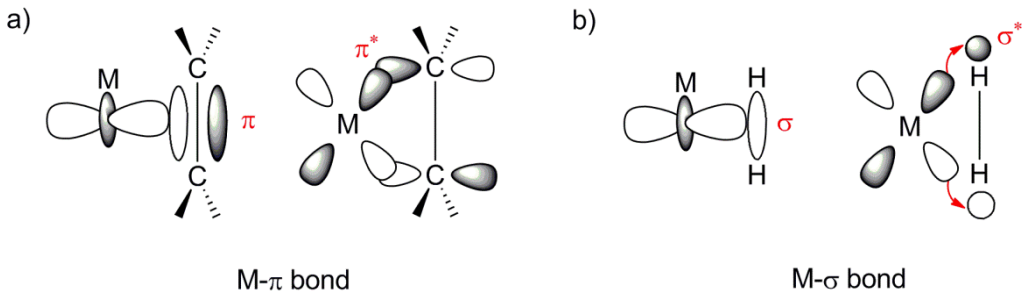

Figure 1.2. Dewar-Chatt-Duncanson Model for olefin and H_2 coordination.

Traditional views towards main-group systems have centred around their valence s and p orbitals which are either fully occupied or empty, coupled with a large energy gap between the highest occupied and lowest unoccupied molecular orbitals (HOMO and LUMO respectively). Consequently, main group systems were anticipated to present poor redox versatility, and unlikely candidates for activating small molecules such as H_2, CO or C_2H_4. The paucity of empirical evidence to suggest otherwise ensured these generalisations remained uncontested for the majority of the 20th century.[5]

1.2 The reactivity of heaver main-group compounds

Recent advances in the chemistry of the heavy main group elements have challenged these opinions.[5] The unsaturated compounds of these elements exhibit large covalent radii and low hybridisation potential (relative to the lighter group elements) which afford weaker σ and π bonds concomitant with significant non-bonding electron density. Table 1.1 presents X-ray crystallographic data for heavy group 14 alkyne analogues in which the M≡M-R bond angles deviate away from the linear geometry observed for C≡C-C structures.[6]

Table 1.1. Structural data for heavier group 14 element alkyne analogues.

Compound	M≡M (Å)	M≡M–C bending angle (°)
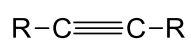	1.1678(1)	178.1
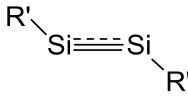	2.0622(9)	137.4
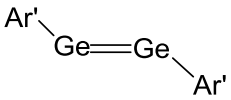	2.285(6)	128.7
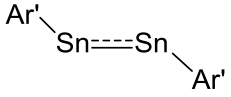	2.6675(4)	125.1
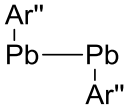	3.181(1)	94.3

R = CO_2H, R' = Si*i*Pr[$CH(SiMe_3)_2$]$_2$, Ar' = C_6H_3-2,6-(C_6H_3-2,6-*i*Pr_2)$_2$, Ar' = C_6H_3-2,6-(C_6H_2-2,4,6-*i*Pr_3)$_2$.

These geometrical distortions are most marked in the case of Pb where minimal hybridisation of the valence orbitals affords two non-bonding (n) 6s orbitals; the two 6p-orbitals bonds are

used to bond to the aryl substituent and Pb partner. Consequently, the M≡M-C bond angle is close to perpedicular (94.3º) in tandem with extreme lengthening of the Pb–Pb bond.[7]

The deviation from a linear geometry is better understood using molecular orbital (MO) theory, which shows a second-order Jahn-Teller distortion effect from mixing of bonding (σ and π) and anti-bonding orbitals (σ* and π*) (Figure 1.3). Importantly, the mixing efficiency is inverse to the energy separation of these orbitals i.e. this interaction is greatest for late row elements where the separation of bonding and antibondings orbitals is sufficiently close to permit mixing. Notably, the unsymmetrical hybrid MO generated from the π and σ* interaction is effectively nonbonding (n_-) and thus E-E bonds in the heavy alkyne analogues are considerably different from C≡C (bond order = 3). The digermynes and distannynes illustrate approximate double bond character (bond order ≈ 2), while Pb-Pb can be effectively considered a single bond (bond order ≈ 1).

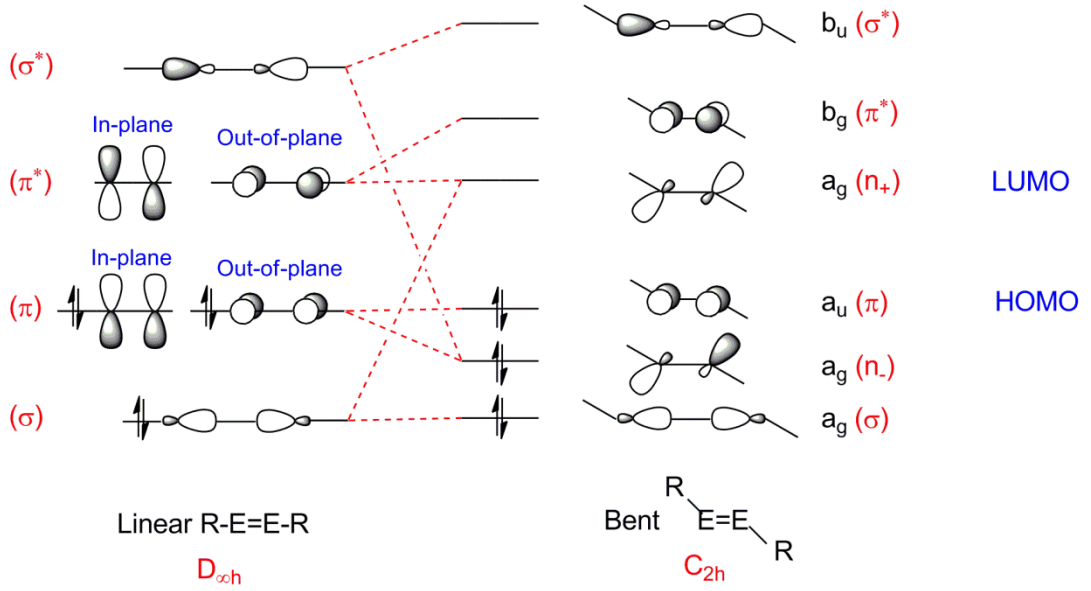

Figure 1.3. The molecular orbital description of bonding in group 14 alkyne analogues which display Jahn-Teller mixing.

In light of these discoveries, Power *et al.* have shown the Ge alkyne analogue Ar'GeGeAr' (Ar' = C_6H_3-2,6-(C_6H_3-2,6-*i*Pr_2)$_2$) react with H_2 to furnish a number of hydrogenated products Ar'GeHGeHAr', Ar'GeH_2GeH_2Ar', and Ar'GeH_3 (Figure 1.4), which represented the first example of H_2 activation by a main group species under mild conditions, in the absence of a metal catalyst. These products were identified by X-ray crystallography[8] and are strongly reminiscent of TM systems. For the initial step, DFT calculations revealed a synergic interaction between the frontier orbitals and H_2. Here, donation from the σ-orbital of

H_2 into the symmetric nonbonding (n_+) LUMO of the Ar'GeGeAr' is concomitant with donation from the π orbital of Ar'GeGeAr' into the σ* of H_2. Consequently, the H–H bond is weakened substantially, enabling oxidative addition. In contrast to the mechanism of TM-mediated H_2 cleavage, back-donation to the σ* does not occur symmetrically, and the H_2 molecule is polarised during its conversion to create a hydride-like hydrogen which attacks the positively polarised germanium centre.

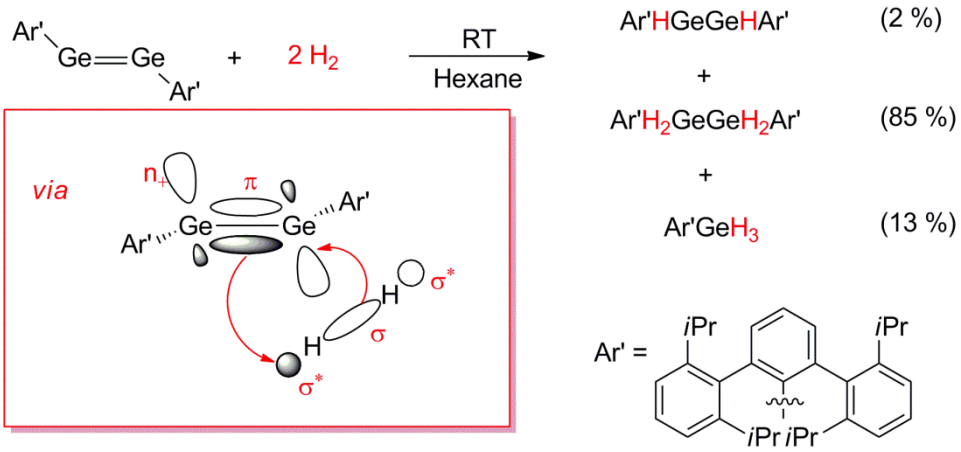

Figure 1.4. The reaction of H_2 with Ar'GeGeAr' to afford a range of hydrogenated products (Ar' = C_6H_3-2,6-(C_6H_3-2,6-iPr$_2$)$_2$). The initial interaction is postulated to proceed *via* the interaction of H_2 with the π-HOMO and the nonbonding (n_+) LUMO of the Ar'GeGeAr'.

Further advances have shown Ar'SnSnAr' (Ar' = C_6H_3-2,6-(C_6H_3-2,6-iPr$_2$)$_2$) to react reversibly with ethylene to yield a double cycloadduct, once again *via* a synergetic interaction between frontier orbitals (Figure 1.5).[9]

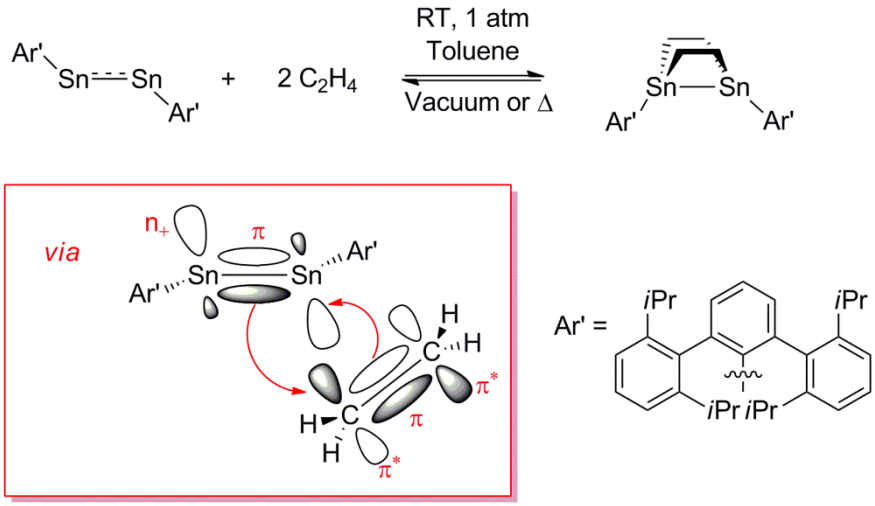

Figure 1.5. The reaction of C_2H_4 with Ar'SnSnAr' to yield a double cycloadduct containing a 1,4-distannabicyclo[2.2.0] butane structure.

Besides the heavier main group systems, Bertrand *et al.* have shown a series of singlet (alkyl)(amino)carbenes, such as **:**C(*t*Bu)N*i*Pr$_2$ to react with H_2 and to deliver the addition product H_2C(*t*Bu)N*i*Pr$_2$.[10] These carbenes possess a vacant p orbital and a filled non-bonding orbital which render them similar to TM centres. DFT studies revealed that the oxidative addition of H_2 proceeds synergistically *via* back donation from the non-bonding orbital into the σ* orbital. Once again this process is non-symmetric, and two equivalent C–H bonds are obtained in the final product. Interestingly, these findings contrast with those for the heavy Sn carbene analogues which, upon addition of H_2, eliminate Ar'H due to steric pressure (Figure 1.6).[11]

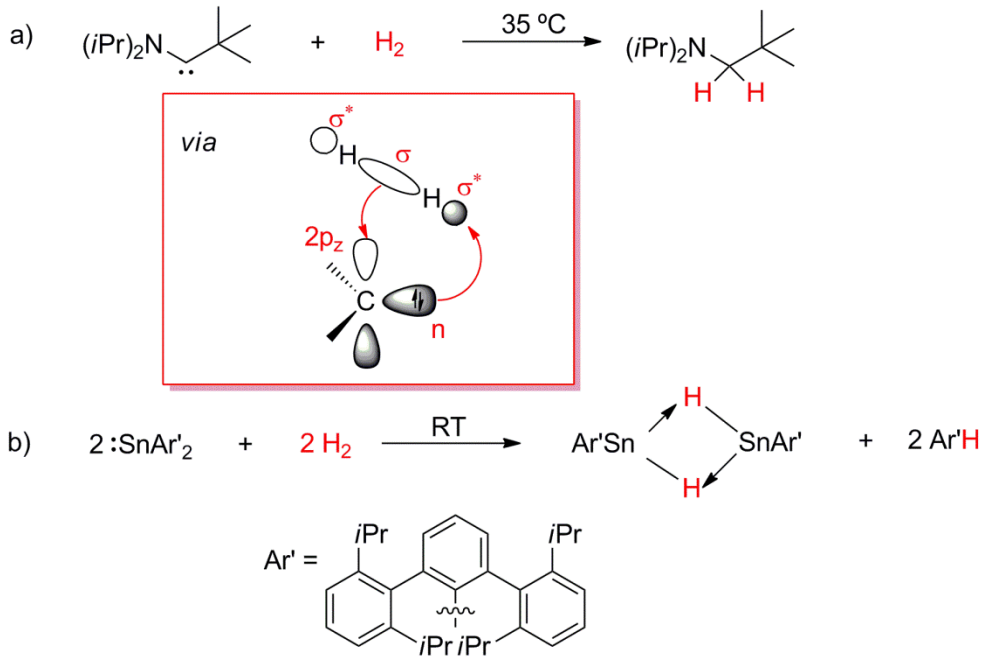

Figure 1.6. a) Activation of H_2 by an (alkyl)(amino) singlet carbene. Mechanistic calculations suggest the initial interaction to proceed analogously to that of a TM system.

1.3 Introduction to FLPs

As of yet, the systems discussed have all demonstrated cooperative electron transfer processes (ET), to direct homolytic bond cleavage. Transition metals are capable of performing both homolytic and heterolytic activations in which the latter commonly occur *via* the participation of a pendant ligand. For example, a cooperative ET strategy may occur between metal and ligand for the activation of H_2, in which σ-donation of H_2 to the metal is in tandem with donation from the lone pair of the ligand into the σ* orbital of H_2 (Figure 1.7) (assistance by a pendant Lewis acidic group has received considerably less attention and few examples are documented).[12]

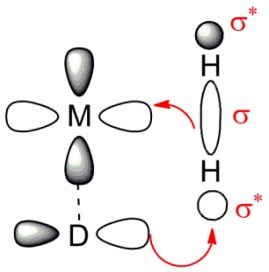

Figure 1.7. Heterolytic mode of H_2 activation.

An alternate and arguably more significant advancement in the domain of main group reactivity arrived following the discovery of main group compounds containing open coordination sites which are sterically inhibited from classic adduct formation. Curiously such systems had been observed as far back as the 1940s, where Brown and co-workers noticed the sterically bulky Lewis base 2,6-dimethylpyridine (lutidine) to be inert to adduct formation with the Lewis acid BMe_3 (Figure 1.8),[13] although only in 2006 was the relevance to reactivity understood.

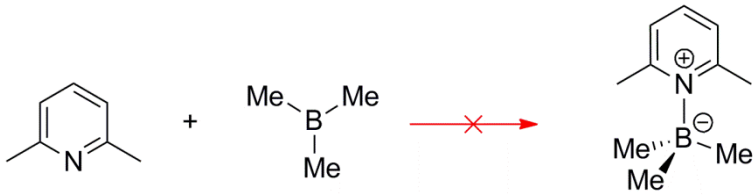

Figure 1.8. The first observation of a 'frustrated Lewis pair'.

By incorporating sterically demanding phosphonium and hydridoborate units within the same molecule, the Stephan research group were able to liberate H_2 at elevated temperatures (> 150 ºC), and remarkably, reform the starting phosphonium borohydride from the reaction with H_2 (1 atm), at room temperature (Figure 1.9).[14]

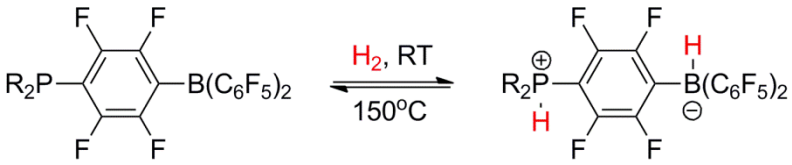

Figure 1.9. Reversible H_2 activation by the seminal phosphonium borate zwitterion $Mes_2PH(C_6F_4)BH(C_6F_5)_2$.

The generality of this type of novel reactivity was demonstrated through rapid expansion into more simple combinations of phosphines and organoboranes [$R_3P/B(C_6F_5)_3$; R = *t*Bu, Mes (Mes = 1,3,5-trimethylbenzene)] which showed analogous reactivity with H_2.[15] This

combination of unquenched acidic and basic functionality inspired the term 'frustrated Lewis pairs' (FLPs) which, by dint of steric hindrance, are restricted from establishing classic-donor acceptor bonds. The unquenched reactivity of these 'frustrated' pairs has facilitated the activation of their small molecules, such as carbon dioxide (CO_2), ethylene (C_2H_4), nitrous oxide (N_2O) and ethers (Figure 1.10).[16]

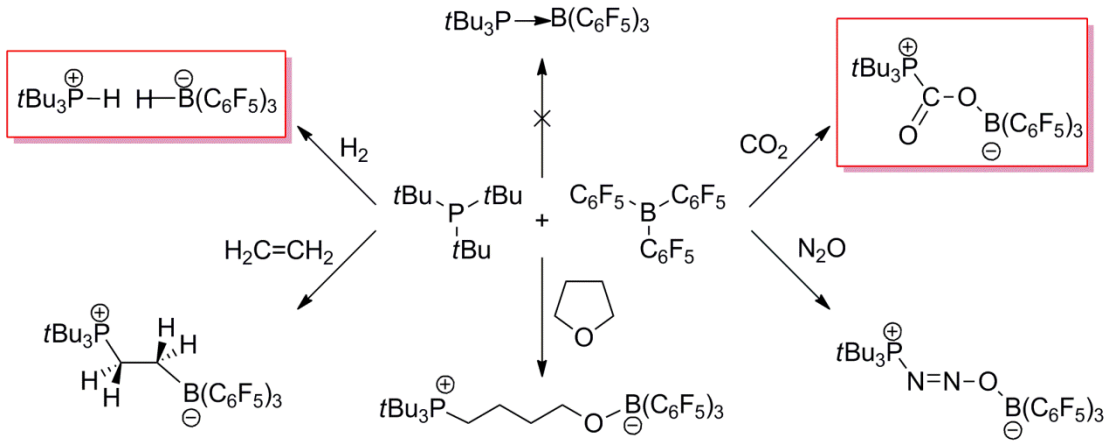

Figure 1.10. Small molecule activation by a tBu$_3$P/B(C$_6$F$_5$)$_3$ FLP system.

Since their discovery, an ever-expanding range of FLP systems, both intra- and inter-molecular, have been investigated for their suitability in small molecule activation (Figure 1.11). While the range of Lewis bases has proliferated rapidly, variation of the Lewis acid has been far less extensively studied.

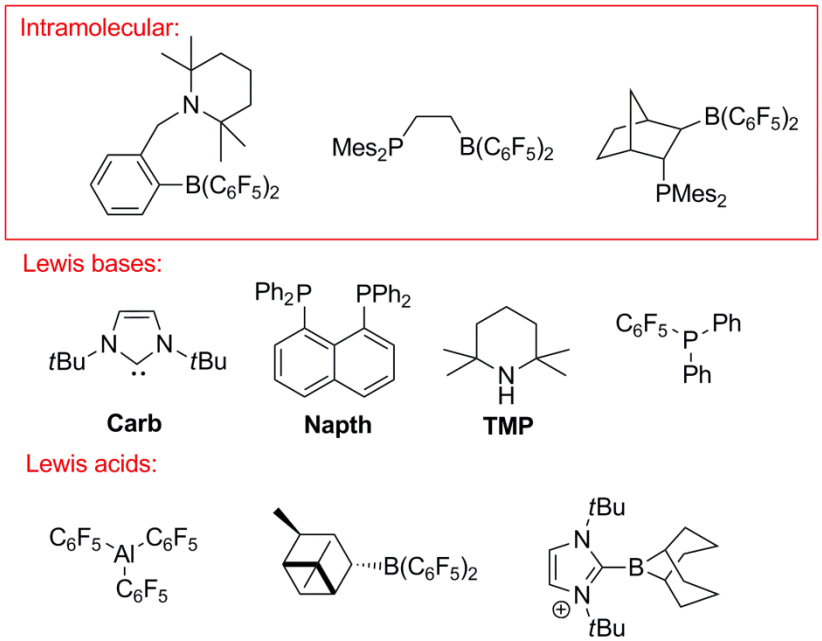

Figure 1.11. Examples of intramoleculer FLP catalysts and constituent Lewis acid/base components of intermolecular FLPs. Where applicable, abbreviations given for Lewis bases.

1.4 H_2 activation by frustrated Lewis pairs

H_2 is perhaps the most significant molecule to be activated by FLP systems. Molecular H_2 has vast applications as both a potential clean energy source and as an efficient reactant in organic and inorganic synthesis. Hydrogenation reactions are some of the most important chemical processes in the production of commodity chemicals, such as NH_3, which help to support a diverse range of global industries.[17] However, H_2 is rather inert which stems from its physical properties: a strong H–H homopolar bond (Bond enthalpy ΔH: 432 kJ mol^{-1}), low polarisability and weak acidity.[18] Chemical activation is therefore dominated by transition metal catalysts (commonly Rh, Ir, Pd, Pt and Ru) and, although these systems present enormous utility, high economic costs are typically associated with their use. In contrast, FLPs present analogous and inexpensive pathways to effect non-metal-mediated H_2 cleavage into 'H^+' and 'H^-' equivalents.

Two conceptually different reactivity models have been proposed to explain the ability of FLPs to activate H_2 (Figure 1.12). For each strategy, activation is assumed to take place *via* reactive intermediates which are preorganised acid/base combinations. The first, the electron transfer (ET) model, postulates H_2 activation to be associated with synergistic electron donation processes which are analogous to those of the heavy main group compounds and transition metals.[19] In effect, there is an available unfilled orbital (LUMO) on the Lewis acid acceptor (A) and a filled donor orbital (HOMO) on the Lewis base (D) which can interact with the H_2 σ and σ* orbitals *via* a low energy pathway.

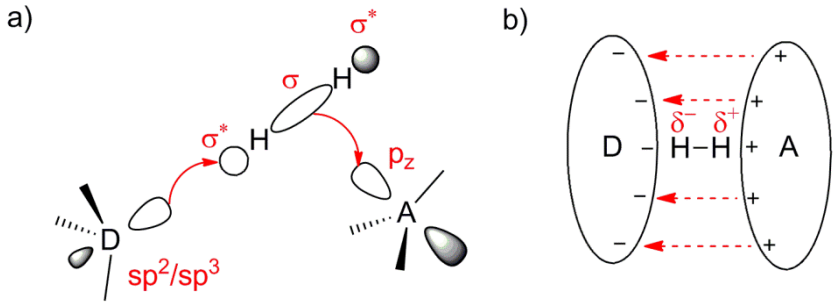

Figure 1.12. a) Electon-transfer and b) electric-field based models for H_2 cleavage by FLPs.

Using DFT analysis, Papai and others have shown this pathway to proceed *via* a bent TS, where H_2 is orientated side-on relative to the acceptor unit. This permits σ-donation from the H_2 molecule to the empty p orbital of the acceptor whilst facilitating overlap between the donor sp^2/sp^3 orbital of the lone-pair and the H_2 σ* orbital (Figure 1.12a).

In contrast, a second model known as the electric field (EF) model, favours polarisation of the hydrogen molecule from exposure to a strong EF present in the cavity between the Lewis acid and base.[20] High level computations favour a barrier-less process in which H_2 is forced into a linear D···H–H···A geometry (Figure 1.12b). Accordingly, separation of the Lewis acid and base intermediates must surpass a critical threshold (4.5 Å in the case of the classic tBu$_3$P/B(C$_6$F$_5$)$_3$ FLP; Figure 1.13) to enable H_2 insertion. Thus, the TS reflects the preorganisation or 'entrance' of H_2.

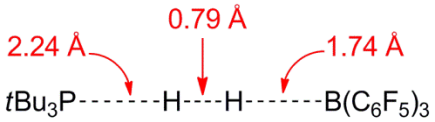

Figure 1.13. Linear TS state proposed by Grimme *et al.* H_2 cleavage by a tBu$_3$P/B(C$_6$F$_5$)$_3$ FLP which only appears at P···B distances > 4.5 Å.

Recently, arguments in support of the EF pathway have waned following further DFT calculations. For example, Papai *et al.* have used improved computational methods, which have shown strong EFs to be absent in the 'cavities' of some FLP systems. In contrast, donor/acceptor interactions of the FLP with H_2 were present for all of the systems investigated.[21] Consequently the ET model is believed to provide a more consistent interpretation of the features along the reaction coordinate.

1.5 The thermodynamic aspects of H_2 cleavage by FLP systems

Preliminary work by Stephan *et al.* on the R$_3$P/B(C$_6$F$_5$) FLP systems highlighted certain examples where H_2 activation occurred either in poor yield or not at all.[15] For example, exposure of H_2 to the tBu$_3$P/B(C$_6$F$_5$)$_3$ FLP in toluene led to the instantaneous precipitation of cleavage products in almost quantitative yield, while activation with tBu$_3$P/BPh$_3$ proceeded in lower yield (33 %). In contrast, tBu$_3$P/BMes$_3$ with H_2 leads to no reaction (Figure 1.14).

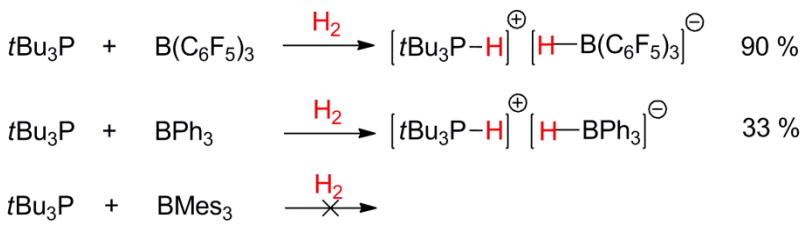

Figure 1.14. Combinations of various Lewis acids and bases and their reactivity with H_2.

Plainly, these results pointed to the need for favourable electronic and steric conditions; the authors concluded that the cumulative Lewis acidity and basicity must be sufficient to effect H_2 cleavage in concert with steric constraints which preclude quenching *via* classical adduct formation. The latter point has since been refined following the discovery of systems which possess dative bonds yet still undergo H_2 cleavage. For these systems, the classical adduct is in equilibrium with the FLP pair.[22] For example, the Lutidine→$B(C_6F_5)$ adduct dissociates sufficiently to allow it to engage in H_2 cleavage (Figure 1.15).

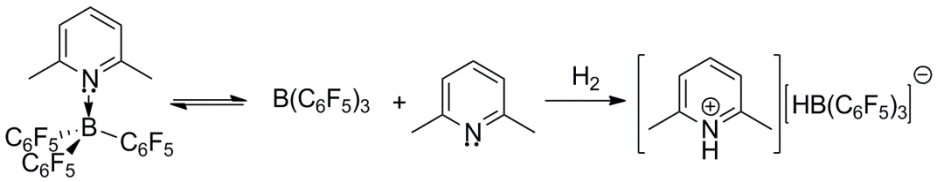

Figure 1.15. Lutidine/$B(C_6F_5)_3$ FLP pair at the boundary of FLP reactivity.

Intrigued by these observations, the Papai research group have studied the energetics for FLP mediated H_2 heterolysis using DFT analysis.[23] For FLPs containing a boron based Lewis acid component, positive ΔG values (298 K), typically greater than +10 kcal mol^{-1} were calculated for those pairs which have been observed to be unreactive towards H_2, while negative values were associated with reactive systems (tBu$_3$P/BPh$_3$ was the sole exception to their calculations ΔG = +18.2 kcal) (Figure 1.16). Values associated with reversible or irreversible H_2 binding were hard to differentiate, although in general reversible systems are said to be slightly exergonic in the direction of H_2 uptake (0 to –10 kcal mol^{-1}). Studies by Paradies and co-workers for reversible H_2 cleavage by a series of *ortho*-fluorinated phosphines/$B(C_6F_5)_3$ FLP systems have since afforded comparable ΔG values (3.4 to –3.7 kcal mol^{-1}; Figure 1.17).[24]

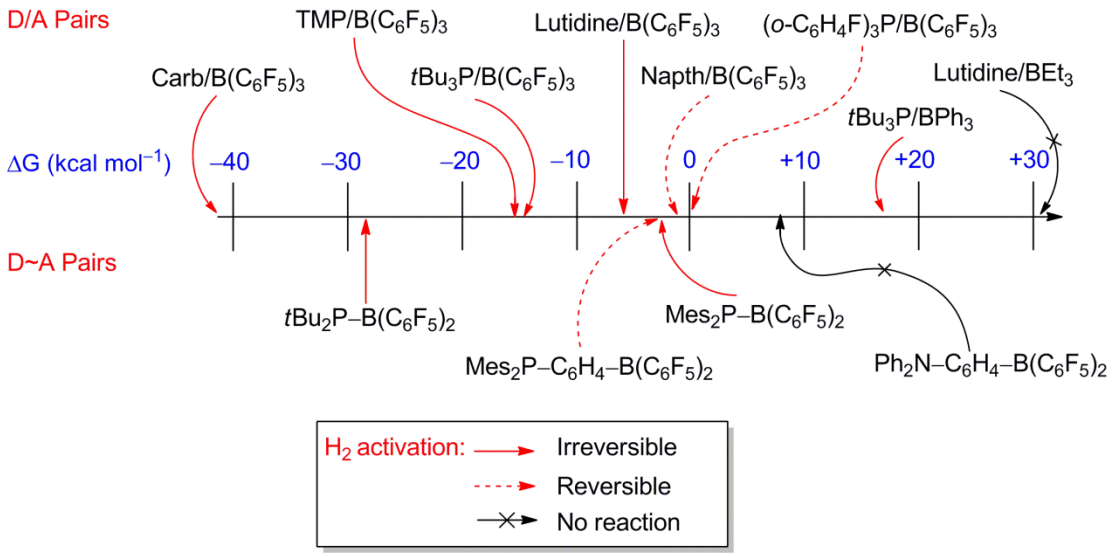

Figure 1.16. Calculated Gibbs free energies for H_2 activation by both intermolecular and intramolecular FLP systems. Napth = 1,8-bis(diphenylphosphino)naphthalene.[23-24]

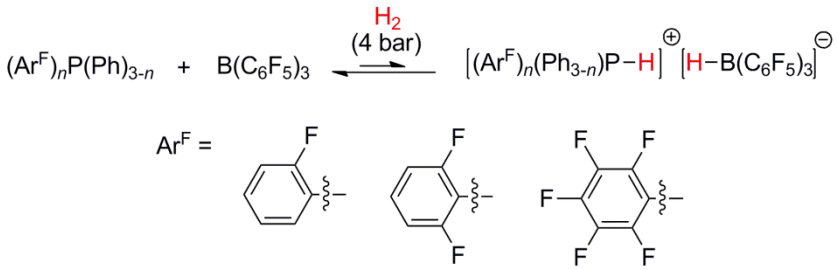

Figure 1.17. Reversible H_2 cleavage by a series of *ortho*-fluorinated triphenylphosphine derivatives (n = 1-3).

Encouraged by these results, Papai and co-worker conceptually partitioned the reaction energy cycle into a number of separate processes that have since proved instrumental for understanding the delicate factors which affect the favourability of H_2 cleavage. The substeps and thermodynamic cycle are shown in Figure 1.18 for intermolecular and intramolecular FLPs.

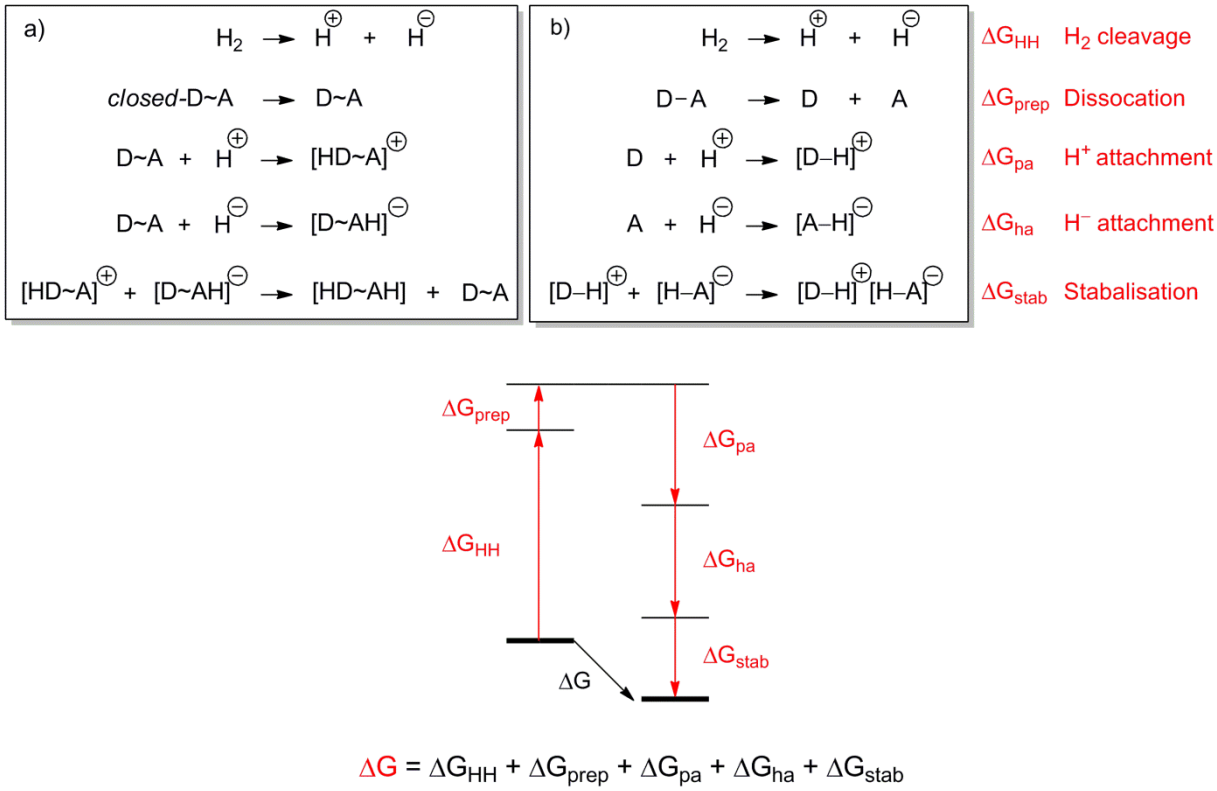

Figure 1.18. Partitioning of the free energy cycle for H_2 cleavage into separate processes for a) intramolecular FLP systems and b) intermolecular systems.

According to this scheme, the first step of the thermodynamic cycle is the heterolytic splitting of H_2 into H^+ and H^-, which for all systems corresponds to a free energy change of ΔG_{HH} = +128.8 kcal mol^{-1}. The second step details the free energy ΔG_{prep} required to separate the Lewis acid and base. This value is practically negligible for FLP systems, in which no dative bonding is observed, and therefore ΔG_{HH} is typically the sole contributor for the uphill step. A positive term is applied for separation of the Lewis acid and base fragments for lutidine→B(C_6F_5) or Me_3P→B(C_6F_5) and is dependent on the steric bulk and acid/base strength of the constituent Lewis pairs. The free energy for stabilisation ΔG_{stab} (the stabilisation energy gained from forming an ion pair) was also calculated to vary only modestly across a range of FLPs (–14 to –24 kcal mol^{-1}) which is attributed to structural similarity between $[DH]^+[HA]^-$ ion pairs. The similarities in the steps described so far are unlikely to account for the variance in FLP reactivity which therefore leaves the energies of proton attachment (ΔG_{pa}) and hydride attachment (ΔG_{ha}) to explain such observations.

The calculated values for ΔG_{pa} and ΔG_{ha} in the studied systems display marked differences (range *ca.* 70 kcal mol^{-1}) which broadly reflect the strength of the donor and acceptor site. Intuitively, one can rationalise the strength of the donor or acceptor site through the electron withdrawing or donating properties of the substituents attached. For

example, replacement of the *para*-F on $B(C_6F_5)_3$ with *para*-H leads to a slight reduction in the electron withdrawing power of the aryl ring and therefore impacts the Lewis acidity and ΔG_{ha} value.[25] A more quantitative examination into donor strength is provided using pK_a values, in which the calculated ΔG_{pa} range of 70 kcal mol^{-1} roughly translates to 50 pK_a units.[23] A quantitative comparison of the hydride strengths in the Lewis acid components is less readily available, and thus thermodynamic quantities related to the reverse processes such as the hydride donor ability or hydride affinity may be employed.[26] Notably, Dubois *et al.* examined experimentally and theoretically the hydride transfer reactions from $Li[HBEt_3]$ to a series of BR_3 Lewis acids (R= O*t*Bu, OC_6F_5, OPh, $OSiMe_3$ and F).[27] Unfortunately these studies were not exhaustive, and where information is missing other measures of Lewis acidity may be substituted (see section 2.5).[28]

1.6 Hydrogenation catalysis

Efficient hydrogenation catalysts require a delicate balance of Lewis acidity and basicity. For systems where the cumulative strength is too high (i.e. ΔG strongly negative) the hydrogenated FLP may behave as a thermodynamic sink in which the system becomes inert to H^-/H^+ transfer. For example the strongly basic N-heterocyclic carbene 1,3-di-*tert*-butyl-1,3-imidazol-2-ylidene (I*t*Bu) forms a FLP with $B(C_6F_5)_3$ at low temperatures which can activate H_2 to give the salt $[I\textit{t}BuH][HB(C_6F_5)_3]$ (Figure 1.19). Addition of an imine substrate *t*BuN=CHPh led to no reduction, in contrast to the zwitterionic salt $Mes_2PH(C_6F_4)BH(C_6F_5)_2$ (*vide infra*).[29] Conversely, should the hydrogenation step become too unfavourable (i.e. positive ΔG) then appreciable H_2 activation will not occur.

The importance of this is well documented by the work of Paradies for the reduction of a series of 1,1-disubstituted olefins. Here, proton transfer for the hydrogenation of trimethyl(2-methylallyl)silane was the rate determining step which increased roughly in the order of pK_a (a proxy for ΔG_{pa}) for the series of triarylphosphine Lewis bases (**a-f**; Figure 1.20); the most electron rich and basic phosphine **c** delivers the greatest concentration of Brønsted-acid in solution which is thereby able to effect the fastest reduction.

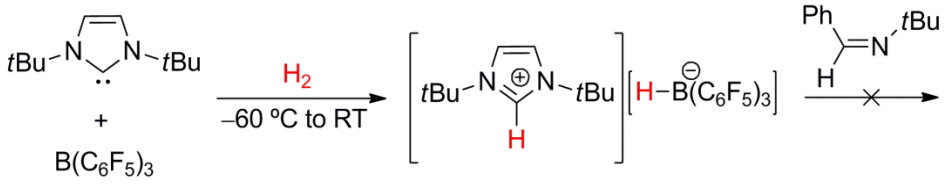

Figure 1.19. H_2 activation by I*t*Bu/$B(C_6F_5)_3$ to form unreactive $[I\textit{t}BuH][HB(C_6F_5)_3]$.

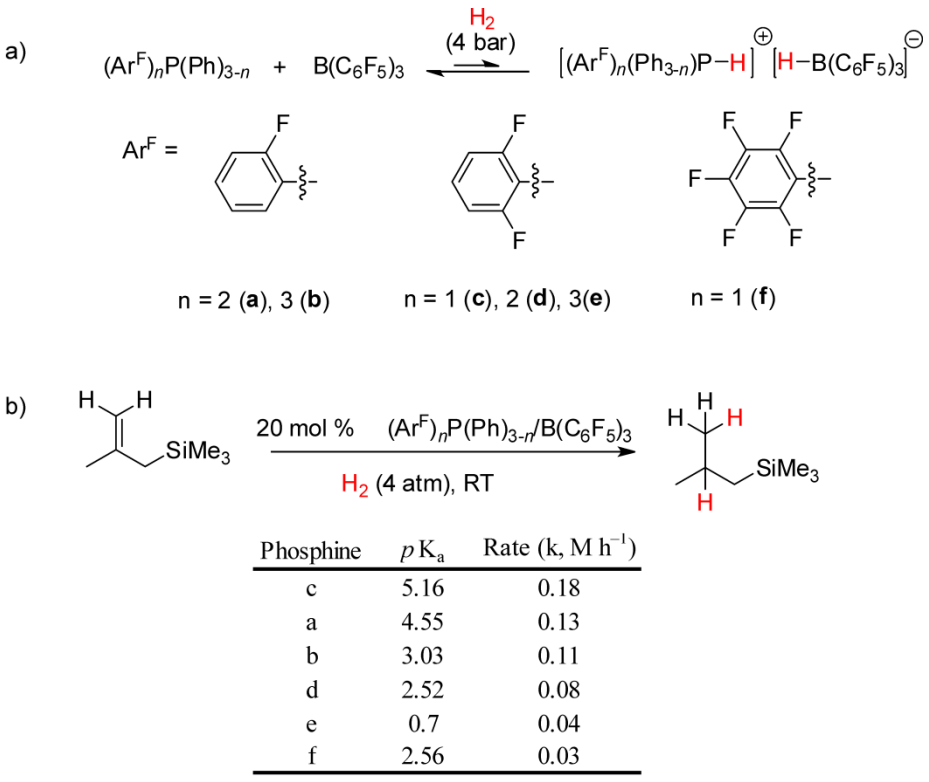

Phosphine	pK_a	Rate (k, M h^{-1})
c	5.16	0.18
a	4.55	0.13
b	3.03	0.11
d	2.52	0.08
e	0.7	0.04
f	2.56	0.03

Figure 1.20. a) Reversible H_2 cleavage by a series of electron deficient triarylphoshphines (a-f). b) The hydrogenation of trimethyl(2-methylallyl)silane accompanied by a table of pK_a values (calculated in 1,2-dichloroethane) and rate constants for this zero order reaction.

Since the discovery of FLP-mediated H_2 cleavage a substantial range of substrates, both polar and non-polar, have been reduced. The first examples of FLP mediated hydrogenation arrived following the discovery of the seminal phosphonium borate $R_2PH(C_6F_4)BH(C_6F_5)_2$ ($R = C_6H_2Me_3$) which was shown to catalytically reduce a series of sterically bulky imines to the corresponding amine (Figure 1.21a). Subsequently, this methodology has been applied to the intermolecular tBu$_3$P/$B(C_6F_5)_3$ FLP systems in which it was shown that the imine could itself behave as the Lewis basic component (Figure 1.21b and Figure 1.22).[30] Undesirable quenching of $B(C_6F_5)_3$ occurs upon use of strong donors and thus this Lewis acid was effective only for imine substrates which surpassed a certain steric threshold. Nevertheless, attempts have been made to extend this methodology to the reduction of related substrates such as nitriles, enamines, and silylenol ethers (Figure 1.21c-e).[30] Strong adduct formation of sterically unhindered nitriles (Figure 1.21c) to the Lewis acidic boranes has been partially circumvented through the addition of sacrificial Lewis acids. These adducts could be catalytically reduced at elevated temperature (120 ºC) using the phosphonium borate $R_2PH(C_6F_4)BH(C_6F_5)_2$ (R = Ph, Me), but to the detriment of atom efficiency.

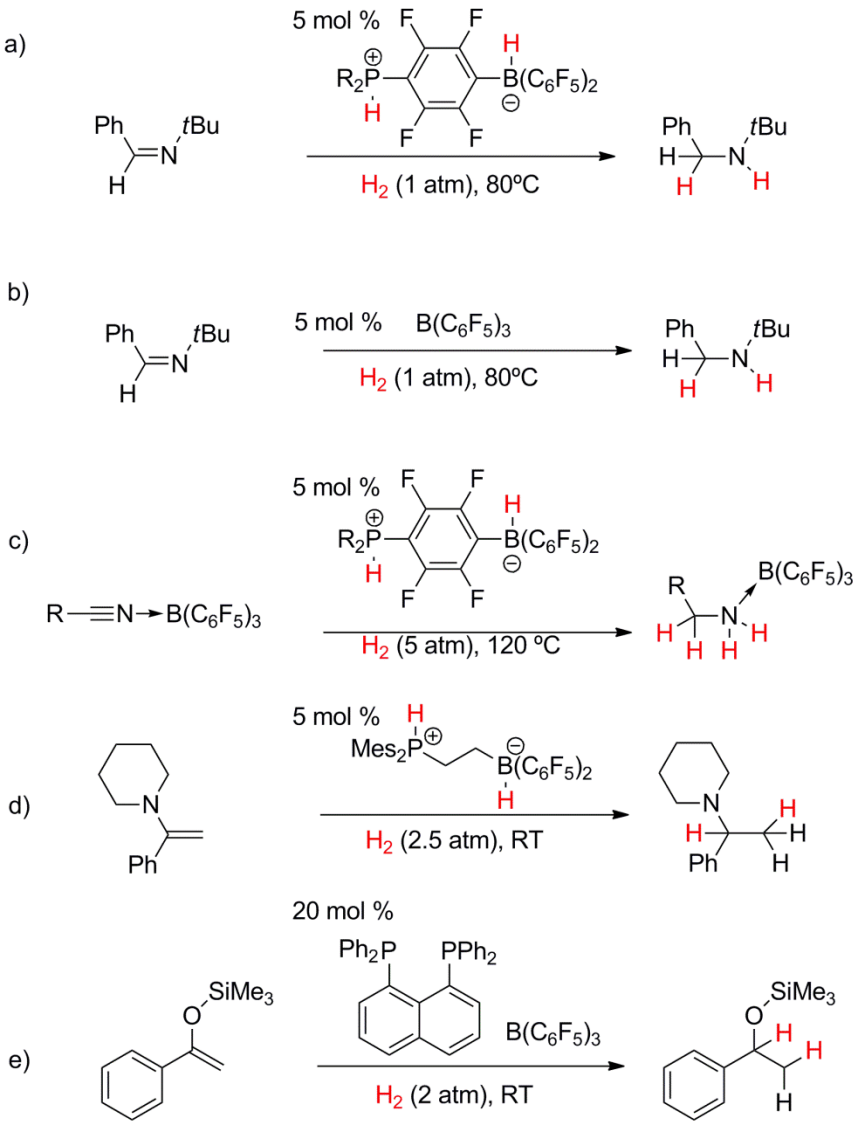

Figure 1.21. Examples of FLP hydrogenation of polar substrates. All reactions conducted in PhMe.[30]

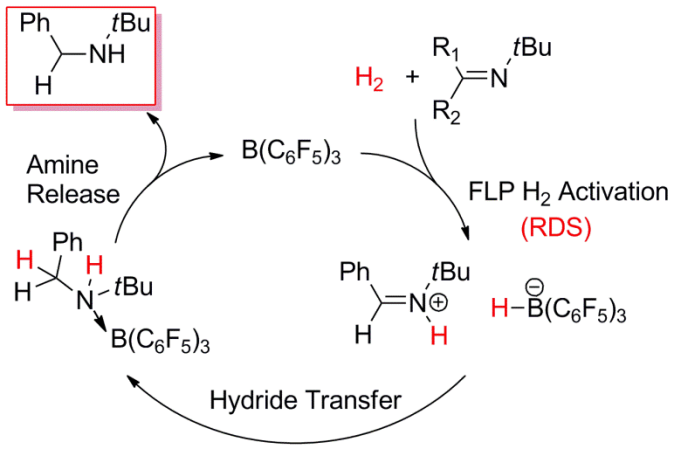

Figure 1.22. Self-reducing FLP pair.[30]

Other developments have focused on improving the tolerance of these Lewis acids to less hindered substrates *via* a 'size exclusion principle'. Soos *et al.* demonstrated the catalytic reduction of less bulky imine substrates using a sterically demanding $MesB(C_6F_5)_2$ borane in combination with TMP (2,2,6,6-tetramethylpiperine) or DABCO (1,4-diazabicyclo[2.2.2]octane).[31] A reverse approach may be to artificially enhance the steric bulk around the unhindered imines *via* incorporation into a mechanically interlocked rotaxane (Figure 1.23).[32] This enhancement permits H_2 cleavage for systems which otherwise are quenched *via* strong adduct formation. This research is still in its infancy and no follow up hydrogenation chemistry has been reported.

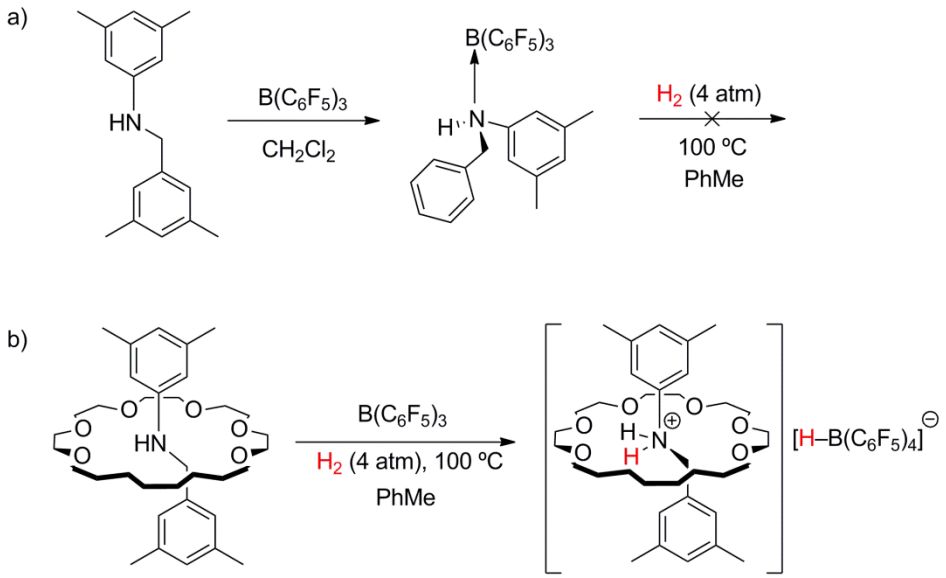

Figure 1.23. a) Strong binding of N-benzylaniline with $B(C_6F_5)_3$ b) H_2 cleavage by the rotaxane and $B(C_6F_5)_3$.

In an unexpected development, the Stephan group reported the ability of small oxygen donors, such as Et_2O, to effect H_2 activation in concert with $B(C_6F_5)_3$ (Figure 1.24).[33] Here, the $B(C_6F_5)_3{\cdot}OEt_2$ adduct was observed using low temperature ^1H NMR spectroscopy to be in equilibrium with the $Et_2O/B(C_6F_5)$ FLP. In the presence of H_2 this system was able to activate H_2 and catalytically hydrogenate olefins 1,1-diphenylethylene and anthracene. The FLP-H_2 species could not be formally characterised due to rapid exchange equilibria, but HD admission to $B(C_6F_5)_3{\cdot}OEt_2$ solutions afforded 2:1:1 statistical mixtures of $HD/H_2/D_2$. The formation of these species in the ^1H NMR spectrum implicated rapid but reversible HD activation/recombination.

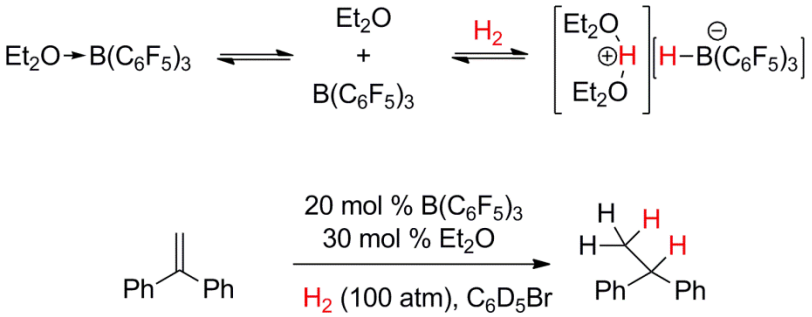

Figure 1.24. Catalytic hydrogenation of 1,1-diphenylethylene by $Et_2O/B(C_6F_5)_3$ under H_2.

Despite these advancements, the catalytic hydrogenation of carbonyl functionalities has yet to be reported. In 2007, the stoichiometric reduction of benzaldehyde was observed by the H_2-activated phosphonium borate $Mes_2PH(CH_2)_2BH(C_6F_5)_2$. The oxophilicity of boron results in the irreversible formation of strong B–O bonds which so far has prevented catalytic turnover (Figure 1.25).[34]

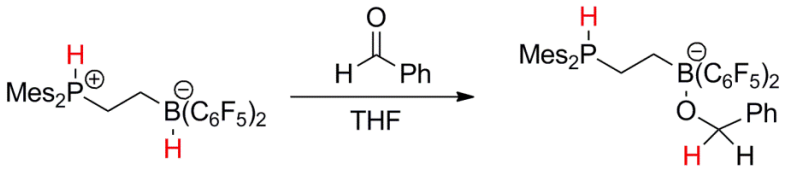

Figure 1.25. Stoichiometric reduction of benzaldehyde by $R_2PH(CH_2)_2BH(C_6F_5)_2$ ($R = C_6H_2Me_3$).

1.7 Hydrosilylation

The trimethylsilylium ion $[SiMe_3]^+$ has been referred to by Villinger as a sterically demanding 'large proton'[35] which is always solvated in the condensed phase forming $[Me_3Si{\cdot}S]^+$ (S = Solvent).[36] For example, H^+ and $[Me_3Si]^+$ will add analogously to anhydrous HF to form $[H\text{-}F\text{-}(H/SiMe_3)]^+$ or to fluorosulfuric acid (HSO_3F) to yield $[(H/SiMe_3)HSO_3F]^+$.

Hydrosilylation, a reaction in which Si–H is added across a C=C, C–O or carbonyl functionality, is mechanistically very similar to that of hydrogenation (Figure 1.26).[37] However, the ease in which a Si–H bond is activated in concert with the strength of the resulting Si–O bond, permits far milder reaction conditions [low temperatures (< 40 ºC) and pressure (4 bar)]. Historically, the catalytic hydrogenation and hydrosilylation of carbonyl compounds has been performed by precious metals such as Rh and Pt, although in recent years a number of cheaper base metal analogues have been developed. Based on the experimental data of a tungsten hydride complex $Cp(CO)_2(IMes)WH$ (IMes = 1,3-*bis*(2,4,6-trimethyphenyl)-imidazol-2-ylidene), the mechanistic similarities between hydrogenation/hydrosilylation are displayed in Figure 1.26. For the former, activation of the

carbonyl complex *via* metal complexation is followed by proton transfer from the metal dihydride to the oxygen lone pair. Ensuing hydride transfer produces a new C–H bond in which subsequent ketone displacement reforms the cationic dihydride complex. For hydrosilylation, displacement of the bound ketone by Et_3SiH yields $[(Cp(CO)_2(IMes)W(SiEt_3)H]^+$ which transfers '$SiEt_3^+$' (in similar fashion to that of H^+) to the ketone to afford a robust Si–O linkage. Hydride transfer from $Et_3Si–H$ furnishes the alkoxysilane whilst also recycling $[(Cp(CO)_2(IMes)W(SiEt_3)H]^+$. In a sense R_3SiH can be viewed as surrogate for molecular H_2 where Si–O bond formation acts as a thermodynamic sink.

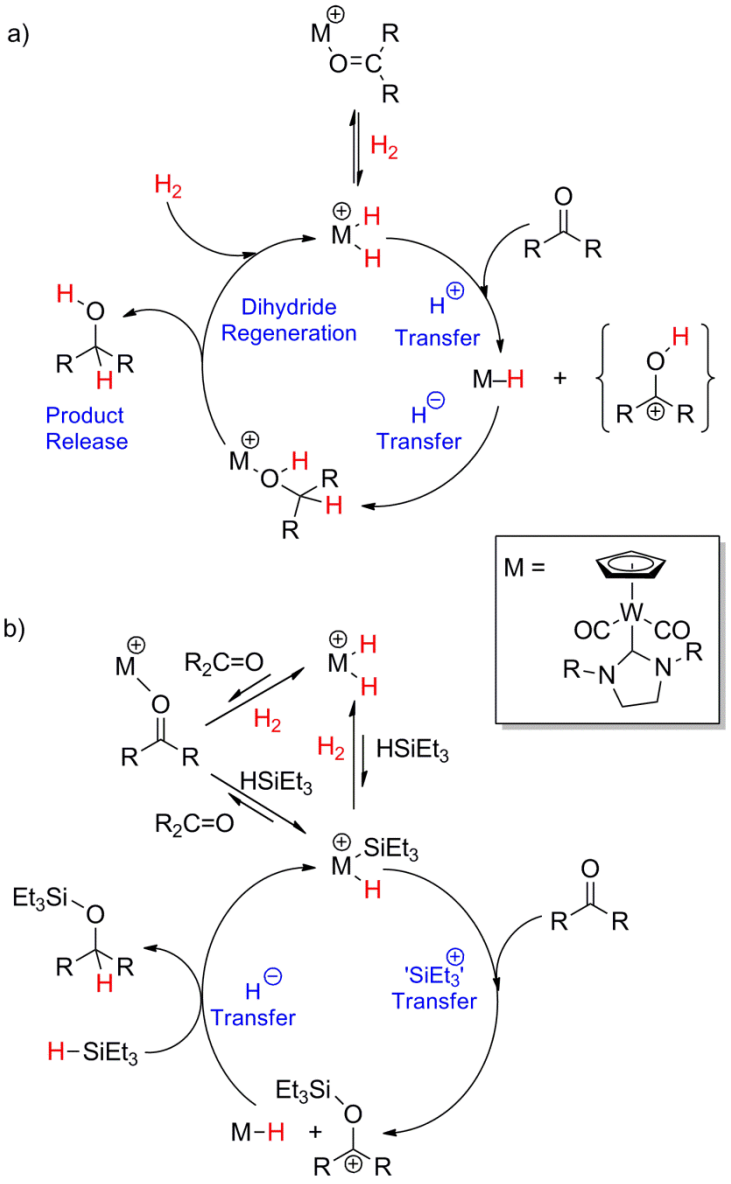

Figure 1.26. Catalytic hydrogenation (a) and hydrosilylation (b) of a ketone by a tungsten hydride complex $(Cp(CO)_2(IMes)WH$ (IMes = 1,3-*bis*(2,4,6-trimethyphenyl)-imidazol-2-ylidene)).

Over the last 20 years, the research groups of Piers and others have examined the use of $B(C_6F_5)_3$ for the catalytic non-metal mediated hydrosilylation of both C=O and C–O bonds (Figure 1.27).[38] Here, typical borane/carbonyl adducts are believed to be circumvented with extensive mechanistic studies supporting an unusual mode of R_3Si–H activation to give the η^1-(Si–H) species $R_3Si^{\delta+}\cdots H\cdots{}^{\delta-}B(C_6F_5)_3$ (Figure 1.28).[38e,39] This species was found to subsequently react with oxygenated substrates to afford silylethers, in which the 'R_3Si' substantially activates the C=O bond towards attack by hydride.

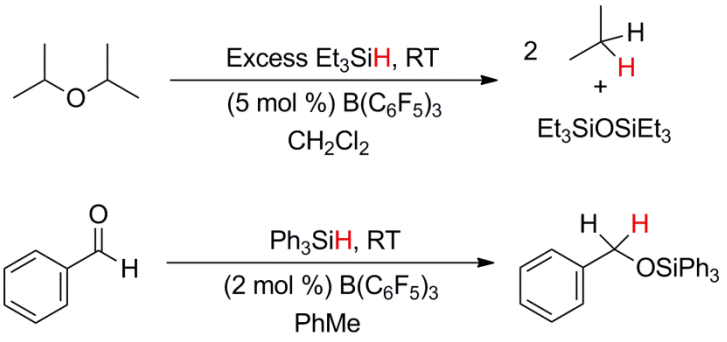

Figure 1.27. Catalytic reductive cleavage of a diisopropylether and benzaldehyde by $B(C_6F_5)_3$ with R_3SiH.

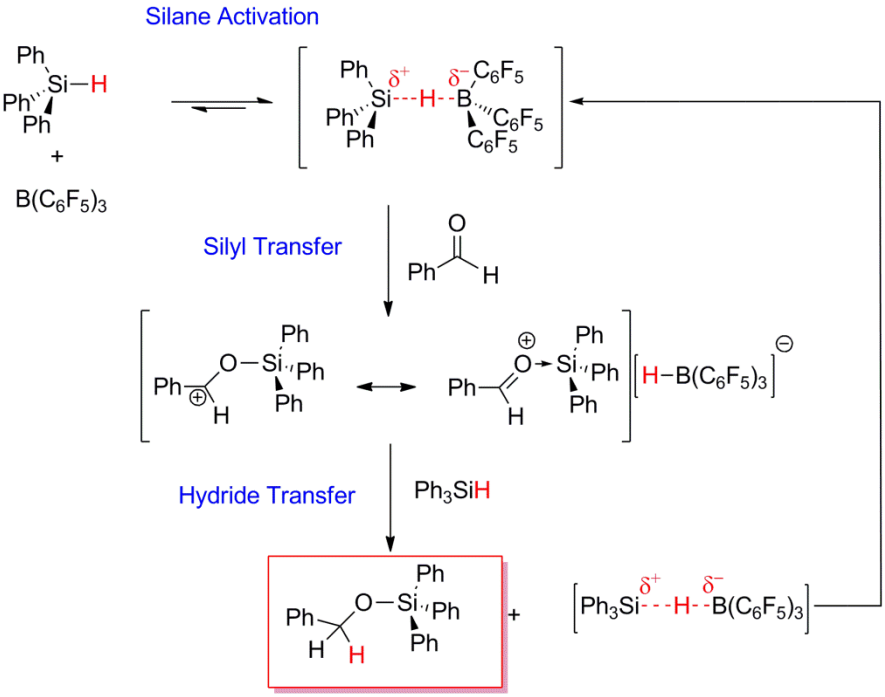

Figure 1.28. Mechanistic proposal for the reduction of benzaldehyde by $[Ph_3Si\cdots H\cdots B(C_6F_5)_3]$.

At the time of publication, Piers and coworkers were unable to categorically prove the existence of η^1-(Si–H). Attempts to garner direct spectroscopic evidence were limited; samples of $B(C_6F_5)_3$ dissolved in C_6D_6 with Ph_3SiH or Et_3SiH showed little evidence of interaction by ^1H NMR spectroscopy. More promisingly, slow cooling of $B(C_6F_5)_3$ dissolved

in neat Et_3SiH shifted the *para* ^{19}F resonance towards a region typically associated with tetracoordinate boron. It was not until the work of Rendler and Oestreich that conclusive evidence of η^1-(Si–H) was reported.[39] Using a chiral silicon reagent, the stereochemical course of the silylation of a ketone was shown to undergo inversion about the Si centre, which pointed to an S_N2 pathway over the alternate S_N1 hydride abstraction route (Figure 1.29).

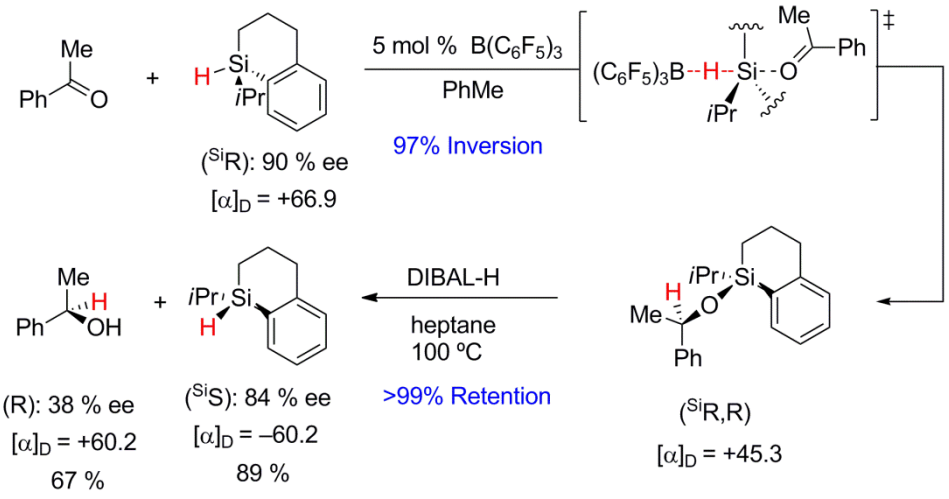

Figure 1.29. Inversion about Si centre from silylation of a ketone.

Since this discovery, Oestreich *et al.* have discussed the similarities of $R_3SiH/B(C_6F_5)_3$ systems to those of a cationic iridium(III) pincer complex, previously generated by Brookhart *et al.* (Figure 1.30). This complex undergoes the same mode of Si–H bond activation to afford an η^1-(Si–H) which was identified using X-ray crystallography and multinuclear solution-phase NMR spectroscopy (^1H, ^{13}C, ^{31}P and ^{29}Si).[40] Furthermore, these complexes undergo mechanistically equivalent silylation pathways upon the addition of an ether, which supports the potential of main group systems as viable alternatives to transition metal catalysts.

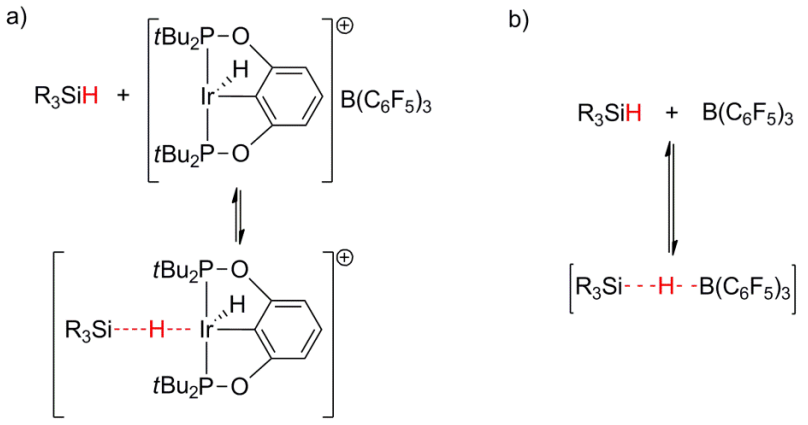

Figure 1.30. Identical modes of Si–H bond activation by a) an iridium(III)pincer complex and b) $B(C_6F_5)_3$.

1.8 CO_2 Activation

In order to combat anthropogenic climate change from emission of greenhouse gases (CO_2, CH_4, N_2O) processes are required which capture or consume these rapidly increasing feedstocks. In this context the sequestration and conversion of CO_2 into fuels such as methanol (CH_3OH) has appeared worthwhile.[41] Furthermore, this C_1 feedstock can be used in large scale Cativa/Monsanto processes to deliver acetic acid.[42] However, the high thermodynamic stability of the non-polar CO_2 molecule has historically necessitated chemical activation *via* use of transition-metal complexes. The hydrogenation of CO_2 into hydrocarbon fuels (C_{1+}) can be envisaged *via* coupling of the reverse water-gas shift reactions (RWGS) and Fischer-Tropsch process (Figure 1.31). The former has been performed homogenously using $M(CO)_6$ (M = Cr, Mo, W) and $Fe(CO)_5$ catalysts, while the latter is currently performed using heterogeneous catalysts (Fe, Ru, Co, Rh, Ni) which exhibit poor selectivity at the high temperatures (150 ºC – 300 ºC) and pressures (25-100 atm) employed.

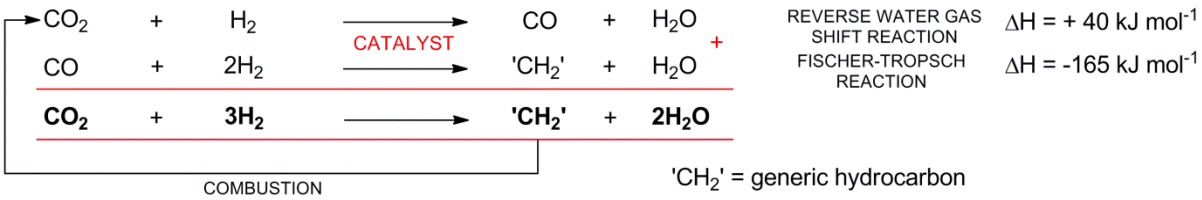

Figure 1.31. RWGS coupled with the Fischer-Tropsch process to afford a distribution of hydrocarbon products.

As demonstrated for H_2 activation, the energetically accessible orbitals of the Lewis acid and base promote FLPs as excellent candidates not only for CO_2 activation but for subsequent ionic hydrogenations. Indeed, FLP-mediated CO_2 fixation has been discovered for a whole series of FLP systems. The first reports by Stephan *et al.* and Erker detailed the use of the intermolecular tBu$_3$P/B(C$_6$F$_5$)$_3$ FLP which rapidly precipitated the zwitterionic tBu$_3$P–C(O)O–B(C$_6$F$_5$)$_3$ upon CO_2 admission (Figure 1.32a);[43] a C=O stretch of 1695 cm^{-1} in the IR spectrum, demonstrated considerable activation of the CO_2 moiety. Interestingly, heating this tBu$_3$P–C(O)O–B(C$_6$F$_5$)$_3$ adduct to 70 ºC promoted CO_2 release and regeneration of the original FLP mixture. These results were furthered by similar admission to the tethered phosphonium borate Mes$_2$P(CH$_2$)$_2$BH(C$_6$F$_5$)$_2$. X-ray crystallography revealed a half chair confirmation of a *cyclo*-Mes$_2$P(CH$_2$)$_2$B(C$_6$F$_5$)$_2$(CO$_2$) species (Figure 1.32b). In contrast to the tBu$_3$P/B(C$_6$F$_5$)$_3$ FLP system, decarboxylation was observed at temperatures above –20 ºC in solution.

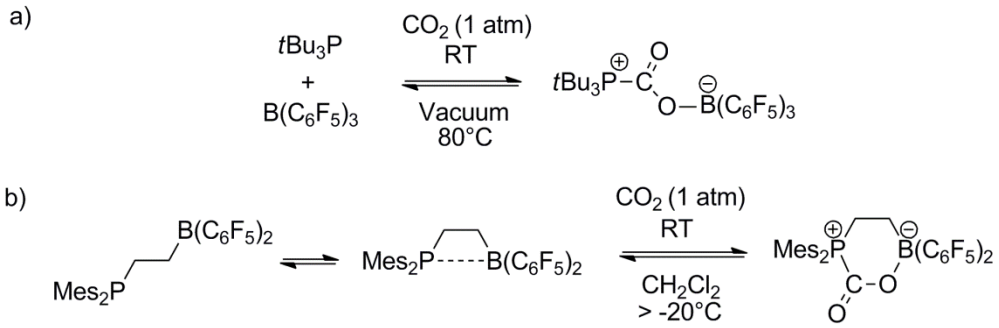

Figure 1.32. Early examples of reversible CO_2 activation by a) tBu$_3$P/B(C$_6$F$_5$)$_3$ and b) Mes$_2$P(C$_6$F$_4$)H(C$_6$F$_5$)$_2$.

The reversibility of these systems has inhibited extraction of the thermodynamic parameters for CO_2 insertion *via* solution phase NMR techniques. Thus, Grimme *et al.* have probed these different thermal stabilities using DFT calculations, which showed the Gibbs free energy of formation for tBu$_3$P–C(O)O–B(C$_6$F$_5$)$_3$ to be 32 kcal mol^{-1} more exothermic than that for Mes$_2$P(CH$_2$)$_2$B(C$_6$F$_5$)$_2$(CO$_2$).[43] Mechanistic calculations supported an early transition state in which P–C and B–O formation occur in a concerted manner (Figure 1.33).

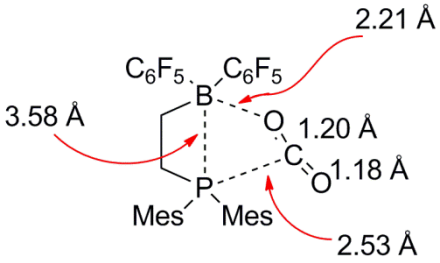

Figure 1.33. Postulated early transition state for the formation of Mes$_2$P(C$_6$F$_4$)B(C$_6$F$_5$)$_2$(CO$_2$).[43]

Follow-up studies on additional phosphine/borane FLPs showed that the cumulative strength of the Lewis acid and base controls the favourability of reaction and, much like H_2 activation; CO_2 adducts of systems with low acidity and basicity were thermally unstable even at temperatures as low as –20 ºC. Their lability was exemplified by their rapid displacement under H_2 atmosphere to afford FLP-H_2 (Figure 1.34).[44] Thus for many systems, derivatisation of the CO_2 molecule is precluded by the thermal instability of the corresponding adducts. Only using boranes of substantial Lewis acidity have follow up transformations been permitted.

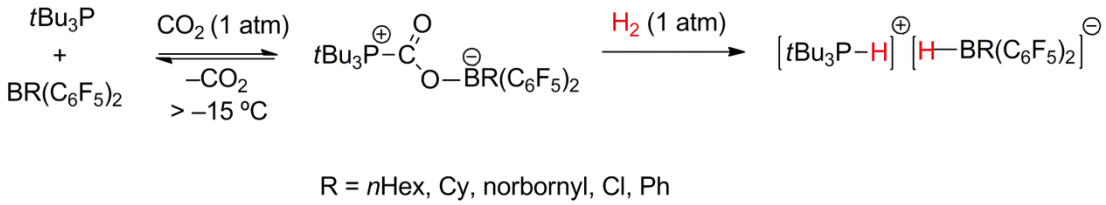

Figure 1.34. Synthesis of various unstable phosphine-borane adducts.

Notably, CO_2 activation has been explored for a series of phosphorus-aluminium FLP systems. In C_6H_5Br, AlX_3 (X = Cl, Br, I) and Mes_3P establish an equilibrium between an FLP mixture and the classical donor acceptor adduct ($Mes_3P{\rightarrow}AlX_3$).[45] Interestingly a solvent assisted mechanism is believed to facilitate this rapid interconversion, with C_6H_5Br forming a weak bromoarenium adduct with AlX_3 to partially compensate for the loss of P–Al bonding.

Admission of CO_2 to these mixtures was shown to lead to double activation through the formation of two Al–O bonds, as evinced in the crystal structure of the $Mes_3PC(OAlX_3)_2$ species (X = Cl, Br, I). The C–O lengths (range 1.233(8)-1.251(8) Å) are considerably shorter than the terminal C=O bond lengths discovered for tBu_3P–C(O)O–$B(C_6F_5)_3$ and $Mes_2PH(C_6F_4)BH(C_6F_5)_2(CO_2)$, which support extensive charge delocalisation through the $C(OAlX_3)_2$ framework (Figure 1.35). Indeed, this strongly activated CO_2 species was shown to display no signs of decarboxylation upon heating to 80 ºC *in vacuo*, although prolonged CO_2 exposure (X = Br, I) resulted in the stoichiometric reduction of CO_2 to CO and the compounds $Mes_3PC(OAlX_2)_2OAlX_3$ (X = Br, I) and $[Mes_3PX][AlX_4]$.[46] The thermodynamic driving force for this process is assumed to be the formation of Al–O bonds in tandem with the oxidation of P(III) to P(IV). The irreversibility of this system permitted a kinetic investigation into the formation of CO, with solution NMR techniques employed to establish the activation parameters ($\Delta H^{\ddagger}$ = 85(5) kJ mol^{-1} and $\Delta S^{\ddagger}$ = –45(15) J mol^{-1} K^{-1}).

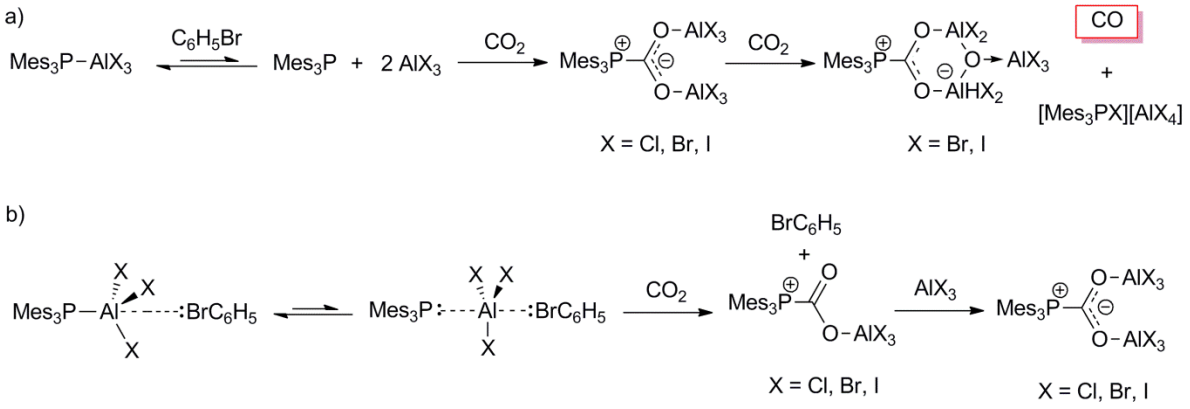

Figure 1.35. a) Reduction of CO_2 to CO b) C_6H_5Br-assisted mechanism as evinced by DFT calculations.

Nitrogen/borane FLP systems, although less widely studies, have arguably contributed the most high profile examples of CO_2 activation and reduction. The FLP pair TMP/$B(C_6F_5)_3$ has been shown to activate H_2,[47] and was subsequently employed by Ashley *et al.* to facilitate the first homogenous hydrogenation of CO_2 to CH_3OH mediated by non-metals (Figure 1.36).[48] Here multinuclear solution NMR spectroscopy (^1H, ^{19}F, ^{11}B and ^{13}C NMR) alongside mechanistic investigations permitted the identification of key intermediates along the reaction pathway. The initial step, formal insertion of CO_2 into a B–H bond, was mediated by the ammonium borohydride salt [TMPH][$HB(C_6F_5)_3$], which at 100 ºC quantitatively afforded a unique formatoborate complex [TMPH][$HC(O)OB(C_6F_5)_3$]. Further heating (140-160 ºC) led to the formation of a doubly activated formate intermediate $[TMPH]_2[H_2C(OB(C_6F_5)_2]$, which was reduced to $CH_3OB(C_6F_5)_3$. Vacuum distillation of the solvent (100 ºC) afforded CH_3OH (17-25% yield) as the sole C_1 product, alongside C_6F_5H and TMP.

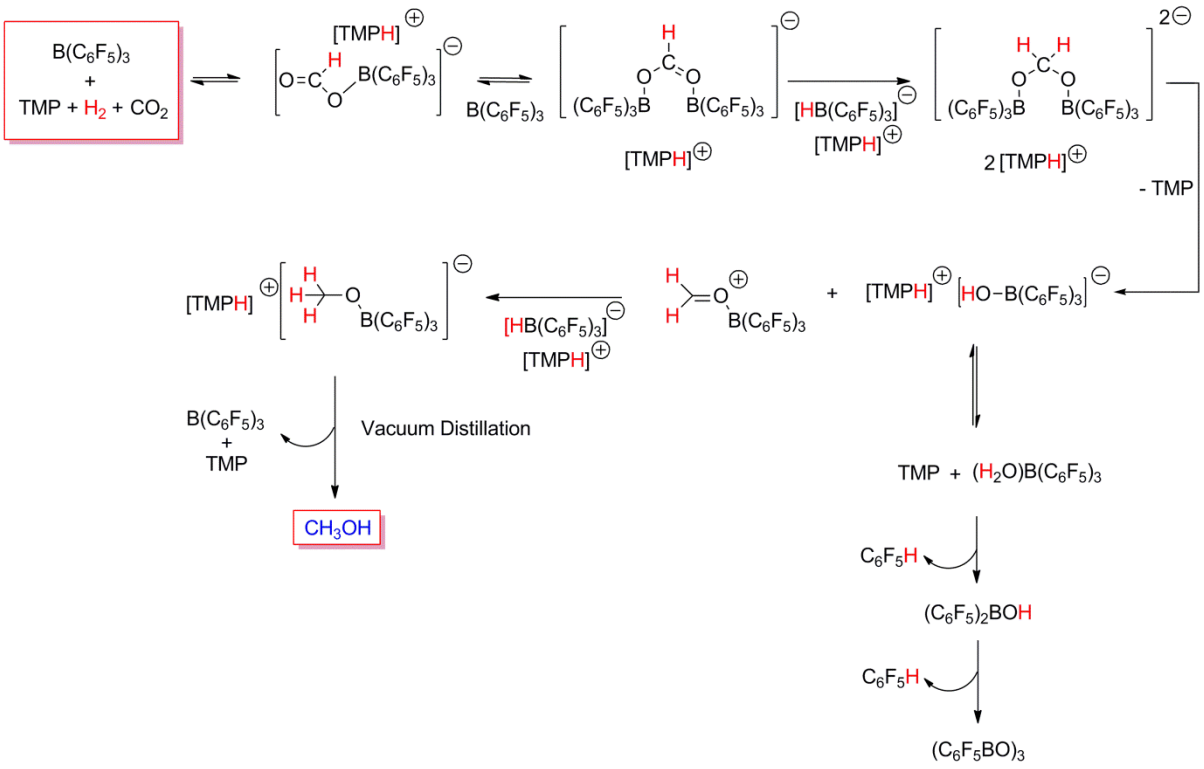

Figure 1.36. 2,2,6,6-tetramethylpiperidine/$B(C_6F_5)_3$ mediated hydrogenation of CO_2.

Since $[TMPH]^+$ provides the only source of labile protons, recombination of the ions to form TMP and ROH·$B(C_6F_5)_3$ (R = Me, H) is reasoned to occur. For a catalytic system, dissociation of these hydroxy adducts would have regenerated the FLP, however under these conditions (150 ºC), H^+ attack on the *ipso*-C is faster which leads to decomposition of the Lewis acid to eventually form an inert boroxine $(C_6F_5BO)_3$, and $CH_3OB(C_6F_5)_2$.

Following this discovery, a number of analogous CO_2 activation systems have been described through using different FLP combinations. For example Mayer and co-workers have examined the lutidinium hydridoborate [LutH][$HB(C_6F_5)_3$] and demonstrated its ability to insert CO_2 to form the formato borate [LutH][$HC(O)OB(C_6F_5)_3$] (Figure 1.37a).[49] Alternatively Stephen *et al.* have effected the room temperature stoichiometric conversion of CO_2 to CH_3OH using the $Mes_3PC(OAlX_3)_2$ (X = Cl, Br) species previously discussed for the conversion of CO_2 to CO.[46] Reaction of this complex with the ammonia borane, NH_3BH_3 (a substitute for H_2) afforded the phosphonium salt [Mes_3PH][$(MeO)_nAlX_{4-n}$], borazine $(BH)_3(NH)_3$ and related products (Figure 1.37b). Addition of H_2O to this aluminium salt resulted in the isolation of CH_3OH (37-51% yield). [45]

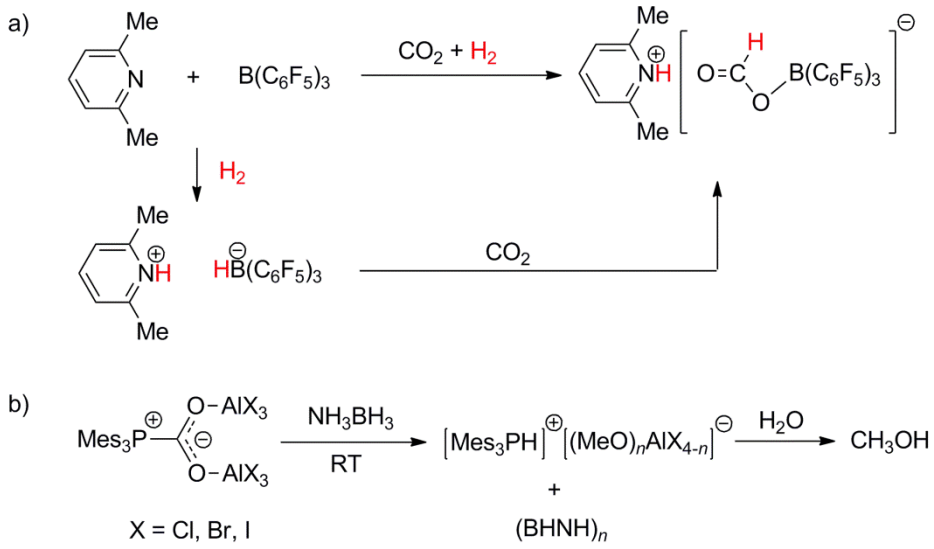

Figure 1.37. a) Reduction of CO_2 by Lut/$B(C_6F_5)_3$ to the formate complex [LutH][$HC(O)OB(C_6F_5)_3$]. b) Stoichiometric reduction of CO_2 to CH_3OH using $Mes_3PC(OAlX_3)_2$ (X = Cl, Br).

1.9 FLP-mediated deoxygenative hydrosilylation of CO_2

Piers and co-workers, encouraged by their hydrosilylation of carbonyl functions and C–O bonds using $B(C_6F_5)_3/R_3SiH$ (R = alkyl, phenyl), have since detailed a tandem FLP catalysed process for the deoxygenative reduction of CO_2 to methane, CH_4 (Figure 1.38).[50] In a similar vein to the work of Ashley *et al.* the ammonium boroyhydride pair [TMPH][$HB(C_6F_5)_3$] was employed in this catalytic cycle.

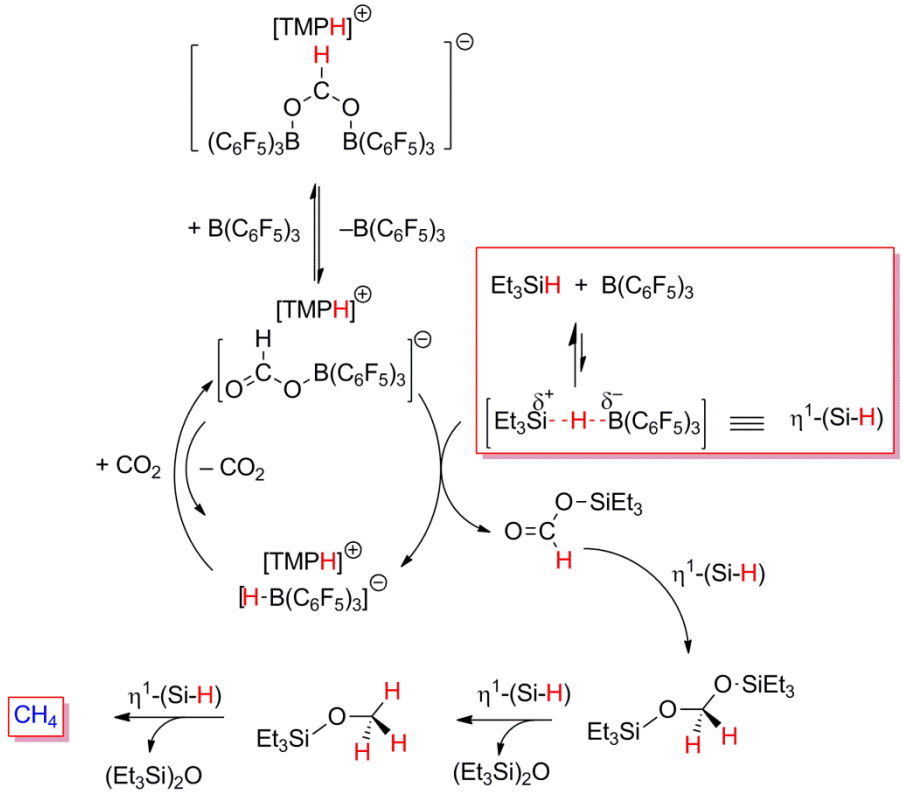

Figure 1.38. Deoxygenative hydrosiylation of CO_2 to CH_4 using $[TMPH][HB(C_6F_5)_3]$ and Et_3SiH.

Subsequent admission of CO_2 in the presence of Et_3SiH (18 equivalents) in C_6D_5Br at temperatures close to 60 ºC afforded the previously described formato borate $[TMPH][HC(O)OB(C_6F_5)_3]$. Under these conditions, ^1H and ^{19}F NMR spectroscopy showed no consumption of Et_3SiH. The strong oxophilicity of the boron unit is believed to prevent the appreciable formation of free $B(C_6F_5)_3$. Accordingly, when this reaction was performed under identical conditions but with an extra equivalent $B(C_6F_5)_3$, immediate formation of a highly reactive formylsilane $HC(O)OSiEt_3$ was observed alongside regeneration of $[TMPH][HB(C_6F_5)_3]$. Further monitoring of the reaction showed gradual consumption of the silane concomitant with the growth of resonances assigned to CH_4 and $(Et_3Si)_2O$. Interestingly, as the amount of Et_3SiH silane decreased, new species became observable in the ^1H and ^{19}F NMR spectra which were assigned to be the doubly activated formate intermediate $[TMPH]_2[H_2C(OB(C_6F_5)_3)_2]$. The equilibrium between these species and the *mono*formato borate provides a source of $B(C_6F_5)_3$ which, in the presence of Et_3SiH, forms the η^1-(Si–H) reductant. In the presence of silane neither the *bis* or *mono* formatoborate are observed, which suggests the rate determining step involves transfer of hydride from $[TMPH][HB(C_6F_5)_3]$ to CO_2. Upon addition of further silane and pressurisation with additional CO_2, a 'living' catalytic system was witnessed for the deoxygenative

hydrosilylation of CO_2. Since this process is free of H_2, the generation of $[TMPH][HB(C_6F_5)_3]$ was shown to occur *via* deprotonation of the zwitterionic $[TMP–C(O)O–B(C_6F_5)_3]$ by a further TMP equivalent (Figure 1.39).

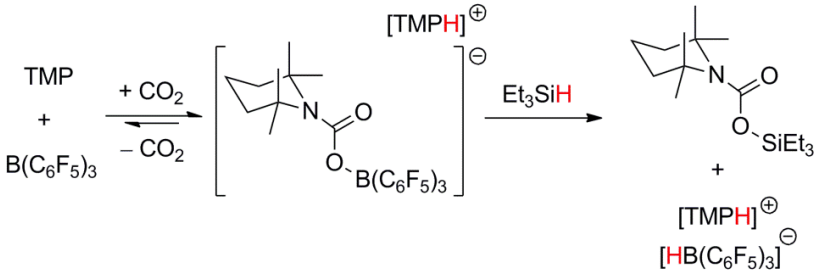

Figure 1.39. Formation of $[TMPH][HB(C_6F_5)_3]$ and the triethysilylcarbamate.

Evidently, silanes behave as substitutes for molecular H_2 with the formation of $(Et_3Si)_2O$ acting as a thermodynamic sink instead of H_2O. This permits hydosilylation to occur under lower temperatures (56 ºC) than reported for the hydrogenation of CO_2 to CH_3OH by Ashley *et al*. In light of these initial results, Piers *et al.* have developed systems which circumvent the rate limiting B–H insertion step through use of a more reactive transition metal $[Cp^*_2Sc]^+$ Lewis acid, which significantly activates CO_2 towards H^- acceptance.[51] In the presence of excess borane, this system was shown to be highly active for the hydrosilylation of CO_2 to CH_4 (Figure 1.40).

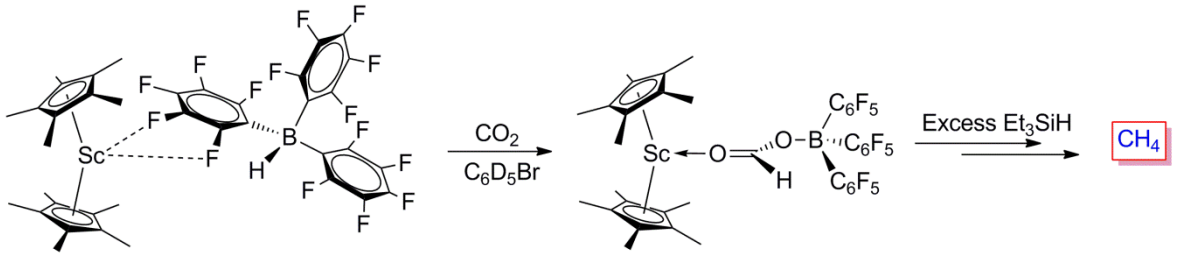

Figure 1.40. Hydrosilylation of CO_2 by $[Cp^*_2Sc][HB(C_6F_5)_3]$

1.10 Limitations of FLP-mediated transformations

Despite the advancements made in the field of FLP mediated catalysis, the range of Lewis acids which are suitable for the activation and hydrogenation of small molecules remain severely limited. The vast majority of the transformations detailed have employed strong organoborane Lewis acids which contain powerfully electron withdrawing perfluoroaryl groups. Though these Lewis acids are effective in hydrogenating a range of nitrogen based functional groups, the need for steric bulk about these substrates remains a serious limitation.

Strong binding by unhindered substrates has been illustrated to quench Lewis acidity and thereby inhibit catalytic reactivity. It is for the same reason that the hydrogenation of oxygen containing functionalities remains limited to a small number of stoichiometric examples. The formation of a strong B–O bond acts as a thermodynamic sink and has previously precluded catalytic turnover, with degradation of the catalyst occurring prior to dissociation. This is the case, for example, for the homogenous reduction of CO_2 to CH_3OH, in which H^+ attack occurs on the aryl ring (Figure 1.41)

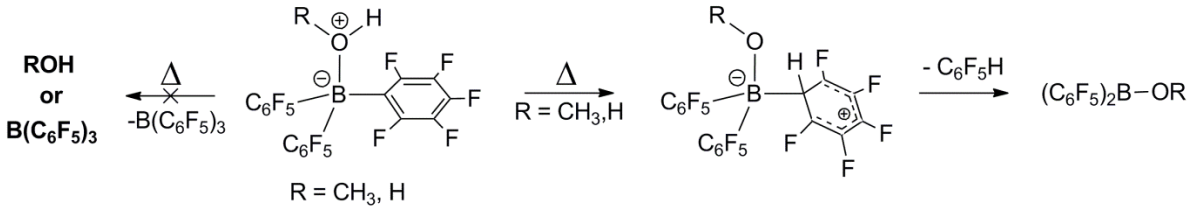

Figure 1.41. Thermolysis of $ROH{\cdot}B(C_6F_5)_3$ adducts *via* ipso proton attack on the C_6F_5 ring.

Methods to circumvent these issues and enhance the functional group tolerance of these systems have included enhancing the steric bulk of the pendant aryl ligands or the steric bulk of the substrate. The latter case has been achieved by incorporating an unhindered substrate into a large molecular cavity.[32]

Alternatively, silanes (a surrogate for molecular H_2) in combination with $B(C_6F_5)_3$ have been used to effect the hydrosilylation of oxygenated substrates. For example the η^1-(Si–H) $[R_3Si{\cdots}H{\cdots}B(C_6F_5)_3]$ moiety has been shown to catalyse the reductive hydrosilation of CO_2 and other oxygenated functionalities under relatively mild conditions although for current systems the starting silane is not generated from H_2. The resultant $(R_3Si)_2O$ byproduct behaves as a thermodynamic sink, and consequently regeneration of the Lewis acid 'R_3Si^+' component (protonation of Si–O) does not occur. The atom inefficiency impacts the attractiveness of this process.

Müller *et al.* have shown the generation of R_3SiH from R_3Si^+/PR_3 FLP systems (R = bulky aryl) to indeed be feasible, although currently these systems require considerable steric bulk on the silylium Lewis acid to prevent classical adduct formation and/or undesirable side reactions with the solvent or corresponding anion (Figure 1.42a).[52] The potent electrophilicity of these systems has been employed to heterolytically cleave H_2 and activate CO_2, although no reduction chemistry has been reported (Figure 1.42b). Silane hydride-donor abilities have been examined by Mayr and co-workers to roughly follow the electron donating ability of the pendant ligand.[53] For example, due to strong electron σ-donating effects from the alkyl

ligands, trialkylsilanes are more potent hydrides than triarylsilanes ($Ph_3SiH<Me_2PhSiH<<iPr_3SiH\sim Et_3SiH$). Thus it would be advantageous to also be able to synthesise R_3SiH (R = Et, *i*Pr) from dihydrogen.

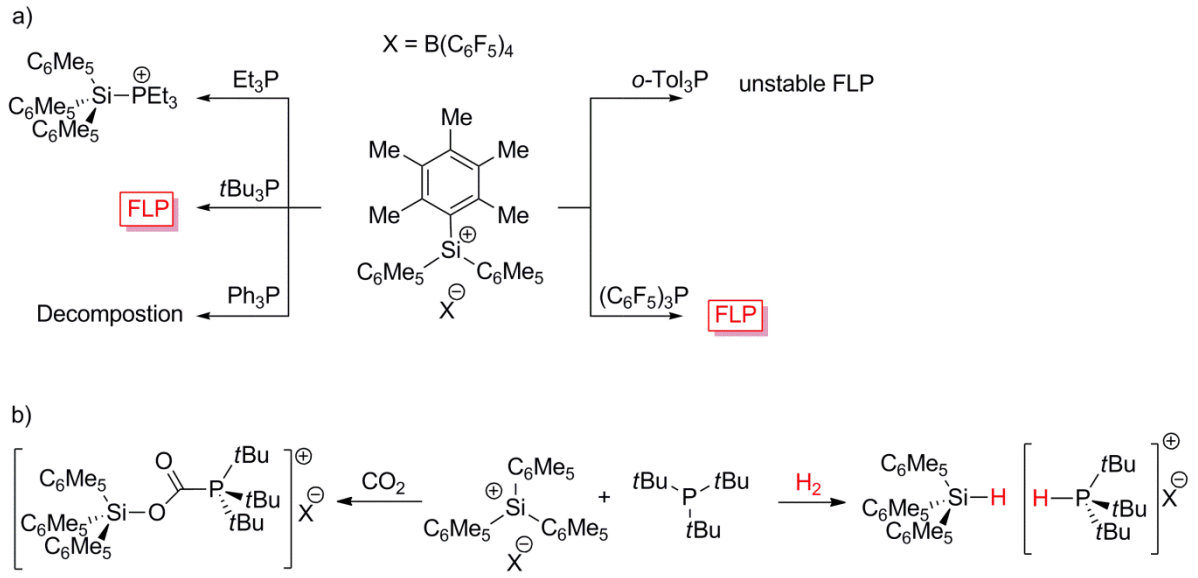

Figure 1.42. a) Reactivity of a $[(C_5Me_5)_3Si][B(C_6F_5)_4]$ silylium ion in the presence of different phosphines b) FLP style reactivity of $tBu_3P/[(C_5Me_5)_3Si][B(C_6F_5)_4]$ FLP in C_6D_6.

1.11 Thesis Aims

Remarkably, systematic modifications to the Lewis acid component of FLP systems have yet to be widely documented.[54] The majority of these changes have retained at least one strongly electron-withdrawing perflouroaryl group. To address this limitation the initial aim of this thesis was to examine Lewis acids which display steric and electronic properties that differ from $B(C_6F_5)_3$. It was hoped that these modifications might furnish Lewis acids which are robust in the presence of protic agents such as H_2O. A secondary aim was to investigate these new acids systems for their role in FLP chemistry paying particular attention to any modes of H_2 and CO_2 activation. Achievement of these aims may present viable alternatives to $B(C_6F_5)_3$ and a better understanding of the parameters involved in the reactivity of these systems.

1.12 References

[1] L. J. Hounjet, D. W. Stephan, *Org. Process Res. Dev.* **2014**, *18*, 385-391.
[2] (a) J. A. Osborn, F. H. Jardine, J. F. Young, G. Wilkinson, *J. Chem. Soc. A.* **1966**, 1711-1732; (b) M. A. Mercadante, C. B. Kelly, C. Lee, N. E. Leadbeater, *Org. Process Res. Dev.* **2012**, *16*, 1064-1068.

[3] L. Yang, Q. Pan, G. L. Rempel, *J. Supercrit. Fluids* **2012**, *68*, 104-112.
[4] (a) J. Chatt, L. A. Duncanson, *J. Chem. Soc.* **1953**, 2939-2947; (b) G. J. Kubas, *J. Organomet. Chem.* **2001**, *635*, 37-68.
[5] P. P. Power, *Nature* **2010**, *463*, 171-177.
[6] (a) V. Benghiat, Leiserow.L, G. M. J. Schmidt, *J. Chem. Soc* **1972**, 1769-&; (b) A. Sekiguchi, R. Kinjo, M. Ichinohe, *Science* **2004**, *305*, 1755-1757; (c) M. Stender, A. D. Phillips, R. J. Wright, P. P. Power, *Angew. Chem. Int. Ed.* **2002**, *41*, 1785-1787; (d) A. D. Phillips, R. J. Wright, M. M. Olmstead, P. P. Power, *J. Am. Chem. Soc.* **2002**, *124*, 5930-5931; (e) L. H. Pu, B. Twamley, P. P. Power, *J. Am. Chem. Soc.* **2000**, *122*, 3524-3525.
[7] P. P. Power, B. Rekken*, Vol. 26 Organometallic Compounds of Low-Coordinate Si, Ge, Sn and Pb: From Phantom Species to Stable Compounds* (Eds.: V. Y. Lee, A. Sekiguchi), Wiley Ltd., Chichester, **2010**, pp. 1-202. [8] G. H. Spikes, J. C. Fettinger, P. P. Power, *J. Am. Chem. Soc.* **2005**, *127*, 12232-12233.
[9] Y. Peng, B. D. Ellis, X. Wang, J. C. Fettinger, P. P. Power, *Science* **2009**, *325*, 1668-1670.
[10] G. D. Frey, V. Lavallo, B. Donnadieu, W. W. Schoeller, G. Bertrand, *Science* **2007**, *316*, 439-441.
[11] (a) Y. Peng, B. D. Ellis, X. Wang, P. P. Power, *J. Am. Chem. Soc.* **2008**, *130*, 12268-12269; (b) Y. Peng, M. Brynda, B. D. Ellis, J. C. Fettinger, E. Rivard, P. P. Power, *Chem. Commun.* **2008**, 6042-6044.
[12] (a) W. H. Harman, J. C. Peters, *J. Am. Chem. Soc.* **2012**, *134*, 5080-5082; (b) S. K. Podiyanachari, R. Froehlich, C. G. Daniliuc, J. L. Petersen, C. Mueck-Lichtenfeld, G. Kehr, G. Erker, *Angew. Chem. Int. Ed.* **2012**, *51*, 8830-8833.
[13] H. C. Brown, *J. Am. Chem. Soc.* **1942**, *64*, 325-329.
[14] G. C. Welch, R. R. S. Juan, J. D. Masuda, D. W. Stephan, *Science* **2006**, *314*, 1124-1126.
[15] G. C. Welch, D. W. Stephan, *J. Am. Chem. Soc.* **2007**, *129*, 1880-1881.
[16] (a) G. Erker, D. W. Stephan, Editors, *Frustrated Lewis Pairs I: Uncovering and Understanding. Top. Curr. Chem.*, Springer GmbH, Berlin, **2013**, pp. 1-350; (b) G. Erker, D. W. Stephan, *Frustrated Lewis Pairs II: Expanding The Scope. Top. Curr. Chem.*, Springer GmbH, Berlin, **2013**, pp. 1-317.
[17] G. J. Kubas, *Chem. Rev.* **2007**, *107*, 4152-4205.
[18] P. E. M. Siegbahn, J. W. Tye, M. B. Hall, *Chem. Rev.* **2007**, *107*, 4414-4435.
[19] T. A. Rokob, A. Hamza, A. Stirling, T. Soos, I. Papai, *Angew. Chem. Int. Ed.* **2008**, *47*, 2435-2438.
[20] S. Grimme, H. Kruse, L. Goerigk, G. Erker, *Angew. Chem. Int. Ed.* **2010**, *49*, 1402-1405.
[21] T. A. Rokob, I. Bako, A. Stirling, A. Hamza, I. Papai, *J. Am. Chem. Soc.* **2013**, *135*, 4425-4437.
[22] (a) S. J. Geier, D. W. Stephan, *J. Am. Chem. Soc.* **2009**, *131*, 3476-3477; (b) P. A. Chase, T. Jurca, D. W. Stephan, *Chem. Commun.* **2008**, 1701-1703.
[23] T. A. Rokob, A. Hamza, I. Papai, *J. Am. Chem. Soc.* **2009**, *131*, 10701-10710.
[24] L. Greb, S. Tussing, B. Schirmer, P. Ona-Burgos, K. Kaupmees, M. Lokov, I. Leito, S. Grimme, J. Paradies, *Chem. Sci.* **2013**, *4*, 2788-2796.
[25] M. Ullrich, A. J. Lough, D. W. Stephan, *Organometallics* **2010**, *29*, 3647-3654.
[26] (a) G. Kovacs, I. Papai, *Organometallics* **2006**, *25*, 820-825; (b) Z. B. Maksic, R. Vianello, *Pure Appl. Chem* **2007**, *79*, 1003-1021; (c) R. Vianello, Z. B. Maksic, *Inorg. Chem.* **2005**, *44*, 1095-1102.

[27] M. T. Mock, R. G. Potter, D. M. Camaioni, J. Li, W. G. Dougherty, W. S. Kassel, B. Twamley, D. L. DuBois, *J. Am. Chem. Soc.* **2009**, *131*, 14454-14465.
[28] (a) U. Mayer, V. Gutmann, W. Gerger, *Monatsh. Chem.* **1975**, *106*, 1235-1257; (b) M. A. Beckett, G. C. Strickland, J. R. Holland, K. S. Varma, *Polymer* **1996**, *37*, 4629-4631.
[29] P. A. Chase, A. L. Gille, T. M. Gilbert, D. W. Stephan, *Dalton Trans.* **2009**, 7179-7188.
[30] D. W. Stephan, S. Greenberg, T. W. Graham, P. Chase, J. J. Hastie, S. J. Geier, J. M. Farrell, C. C. Brown, Z. M. Heiden, G. C. Welch, M. Ullrich, *Inorg. Chem.* **2011**, *50*, 12338-12348.
[31] G. Eros, H. Mehdi, I. Papai, T. A. Rokob, P. Kiraly, G. Tarkanyi, T. Soos, *Angew. Chem., Int. Ed.* **2010**, *49*, 6559-6563.
[32] C. B. Caputo, K. Zhu, V. N. Vukotic, S. J. Loeb, D. W. Stephan, *Angew. Chem. Int. Ed.* **2013**, *52*, 960-963.
[33] L. J. Hounjet, C. Bannwarth, C. N. Garon, C. B. Caputo, S. Grimme, D. W. Stephan, *Angew. Chem. Int. Ed.* **2013**, *52*, 7492-7495.
[34] P. Spies, G. Erker, G. Kehr, K. Bergander, R. Froehlich, S. Grimme, D. W. Stephan, *Chem. Commun.* **2007**, 5072-5074.
[35] M. Lehmann, A. Schulz, A. Villinger, *Angew. Chem. Int. Ed.* **2009**, *48*, 7444-7447.
[36] (a) S. J. Connelly, W. Kaminsky, D. M. Heinekey, *Organometallics* **2013**, *32*, 7478-7481; (b) A. Schulz, A. Villinger, *Angew. Chem. Int. Ed.* **2012**, *51*, 4526-4528; (c) H. F. T. Klare, M. Oestreich, *Dalton Trans.* **2010**, *39*, 9176-9184.
[37] (a) R. M. Bullock, Editor, *Catalysis Without Precious Metals*, Wiley-VCH Verlag GmbH, Weinheim, **2010**, pp. 1-290; (b) J. Chojnowski, *Hydrosilylation. A Comprehensive Review on Recent Advances by Bogdan Marciniec, Hieronim Maciejewski, Cezary Pietraszuk, and Piotr Pawluc, Vol. 88*, Springer GmbH, Berlin, **2009**, pp. 1-408.
[38] (a) V. Gevorgyan, J. X. Liu, M. Rubin, S. Benson, Y. Yamamoto, *Tetrahedron Lett.* **1999**, *40*, 8919-8922; (b) V. Gevorgyan, M. Rubin, S. Benson, J. X. Liu, Y. Yamamoto, *J. Org. Chem.* **2000**, *65*, 6179-6186; (c) D. J. Parks, W. E. Piers, *J. Am. Chem. Soc.* **1996**, *118*, 9440-9441; (d) J. M. Blackwell, K. L. Foster, V. H. Beck, W. E. Piers, *J. Org. Chem.* **1999**, *64*, 4887-4892; (e) D. J. Parks, J. M. Blackwell, W. E. Piers, *J. Org. Chem.* **2000**, *65*, 3090-3098.
[39] S. Rendler, M. Oestreich, *Angew. Chem. Int. Ed.* **2008**, *47*, 5997-6000.
[40] (a) J. Yang, P. S. White, C. K. Schauer, M. Brookhart, *Angew. Chem. Int. Ed.* **2008**, *47*, 4141-4143; (b) T. Robert, M. Oestreich, *Angew. Chem. Int. Ed.* **2013**, *52*, 5216-5218.
[41] G. A. Olah, *Angew. Chem. Int. Ed.* **2005**, *44*, 2636-2639.
[42] G. J. Sunley, D. J. Watson, *Catalysis Today* **2000**, *58*, 293-307.
[43] C. M. Momming, E. Otten, G. Kehr, R. Froehlich, S. Grimme, D. W. Stephan, G. Erker, *Angew. Chem., Int. Ed.* **2009**, *48*, 6643-6646,.
[44] I. Peuser, R. C. Neu, X. Zhao, M. Ulrich, B. Schirmer, J. A. Tannert, G. Kehr, R. Froehlich, S. Grimme, G. Erker, D. W. Stephan, *Chem. Eur. J* **2011**, *17*, 9640-9650, .
[45] G. Menard, D. W. Stephan, *J. Am. Chem. Soc.* **2010**, *132*, 1796-1797.
[46] G. Menard, T. M. Gilbert, J. A. Hatnean, A. Kraft, I. Krossing, D. W. Stephan, *Organometallics* **2013**, *32*, 4416-4422.
[47] V. Sumerin, F. Schulz, M. Nieger, M. Leskela, T. Repo, B. Rieger, *Angew. Chem., Int. Ed.* **2008**, *47*, 6001-6003.
[48] A. E. Ashley, A. L. Thompson, D. O'Hare, *Angew. Chem., Int. Ed.* **2009**, *48*, 9839-9843.

[49] S. D. Tran, T. A. Tronic, W. Kaminsky, M. D. Heinekey, J. M. Mayer, *Inorg. Chim. Acta.* **2011**, *369*, 126-132.
[50] A. Berkefeld, W. E. Piers, M. Parvez, *J. Am. Chem. Soc.* **2010**, *132*, 10660-10661.
[51] A. Berkefeld, W. E. Piers, M. Parvez, L. Castro, L. Maron, O. Eisenstein, *Chemical Science* **2013**, *4*, 2152-2162.
[52] (a) M. Reissmann, A. Schafer, S. Jung, T. Müller, *Organometallics* **2013**, *32*, 6736-6744; (b) A. Schaefer, M. Reissmann, A. Schaefer, W. Saak, D. Haase, T. Müller, *Angew. Chem. Int. Ed.* **2011**, *50*, 12636-12638.
[53] H. Mayr, N. Basso, G. Hagen, *J. Am. Chem. Soc.* **1992**, *114*, 3060-3066.
[54] (a) H. Li, A. J. A. Aquino, D. B. Cordes, F. Hung-Low, W. L. Hase, C. Krempner, *J. Am. Chem. Soc.* **2013**, *135*, 16066-16069; (b) F. Bertini, V. Lyaskoyskyy, B. J. J. Timmer, F. J. J. de Kanter, M. Lutz, A. W. Ehlers, J. C. Slootweg, K. Lammertsma, *J. Am. Chem. Soc.* **2012**, *134*, 201-204; (c) J. M. Farrell, J. A. Hatnean, D. W. Stephan, *J. Am. Chem. Soc.* **2012**, *134*, 15728-15731.

CHAPTER TWO

Synthesis & Characterisation of Electron Deficient *Tris*arylboranes

2.1 Introduction

Although $B(C_6F_5)_3$ remains the archetypal Lewis acid in FLP chemistry, simple electronic and steric modifications have been reported which are shown to effect catalytic reactivity.[1] For example, $B(C_6F_5)_3$ is prone to nucleophilic aromatic substitution by phosphine bases at the *para*-carbons of the fluoroaryl rings (Figure 2.1).[2] This leads to the formation of phosphonium borate zwitterions which limit use of PR_3 bases in small molecule activation.

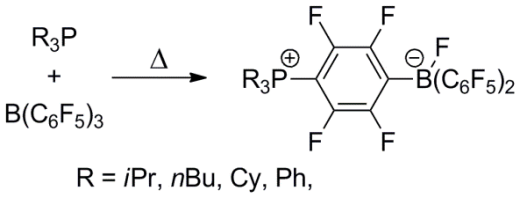

Figure 2.1. C–F activation of the flouroaryl rings of $B(C_6F_5)_3$ with various phosphine bases.

To avoid undesirable C–F activation, facile replacement of *para*-F for *para*-H affords $B(p\text{-}C_6F_4H)_3$, a Lewis acid which is comparable in Lewis acidity yet no longer subject to nucleophilic attack by phosphine bases.[1b] Consequently, this borane has been employed as a catalyst for hydrodesilylation of silylphosphines. [3] Alternatively, replacing the C_6F_5 group in $B(C_6F_5)_3$ with a chiral ligand has successfully effected the asymmetric hydrogenations of imines (Figure 2.2).[1d]

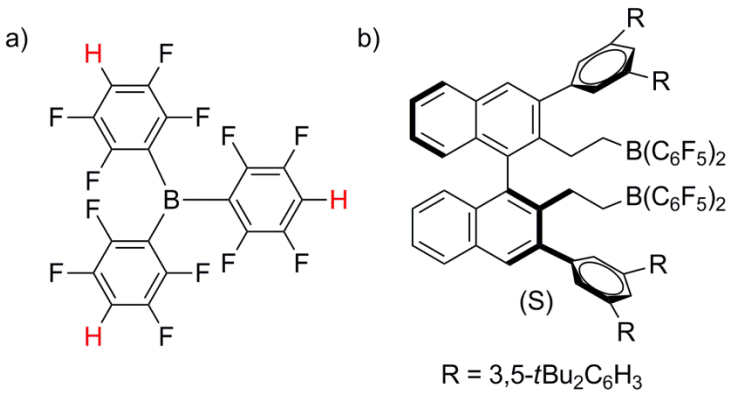

Figure 2.2. a) $B(C_6F_4H)_3$ used for the hydrodesilylation of silylphosphines b) A chiral C_6F_5-subsitutued borane prepared by Du *et al*. for enantioselective reduction of imines.

The overwhelming majority of these powerful boron Lewis acids derive their reactivity from the use of electron-withdrawing fluoroaryl ligands.[4] However, while these groups impart strong acidity at the acceptor site inductively due to the high electronegativity of F ($\chi_{Pauling}$ = 3.98),[5] mesomeric donation from the *ortho*- and *para*-F lone pairs leads to significant back donation from the π-system into the B acceptor orbital, which may partially attenuate the Lewis acidity. $B(C_6F_5)_3$ forms a tightly bound adduct with H_2O in which the acidity of the electron deficient borane weakens the O–H bond and thus renders it strongly Brønsted acidic and comparable to that of HCl (pK_a = 8.4 in CH_3CN).[6] This O–H activation, coupled with the π-basicity of the aromatic system, is reasoned to encourage H^+ attack upon the *ipso*-C_6F_5 position for hydroxylic adducts $ROH{\cdot}B(C_6F_5)_3$ (R = Me, H) (Figure 1.38) at elevated temperature (> 50 ºC). This concept was proposed by Ashley *et al*. for the FLP-mediated reductions of CO_2 to CH_3OH, in which protonolysis of $ROH{\cdot}B(C_6F_5)_3$ (R = Me, H) was reasoned to preclude dissociation and the formation of a catalytic cycle (Figure 1.41).[7]

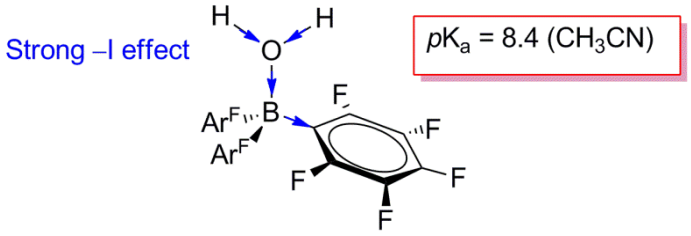

Figure 2.3. Strong activation of the O–H bond *via* –I effects of electron withdrawing C_6F_5 pendant on the borane.

The degree to which the π-electrons from aryl substituents donate electron density into the aromatic ring may be quantified using the Hammett equation.[8] This formula describes a linear free energy relationship between reaction rates and equilibrium constants for the ionisation of benzoic acid and derivatives containing various *meta*- and *para*- substituents (Figure 2.4). *Ortho*-substituents are not usually treated within this context due to possible competing steric effects.

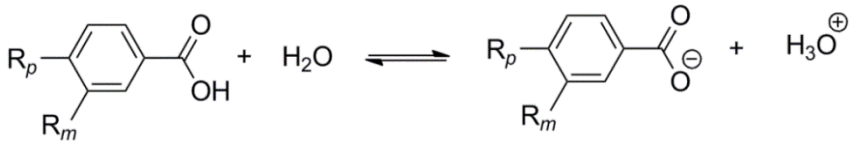

Figure 2.4. Ionisation of benzoic acid and derivates when $R_p/R_m \neq H$.

The basic form of the equation reads:

$$\log \frac{k}{k_0} = \rho\sigma$$

k = rate (or equilibrium) constant for a *meta*- or *para*-substituted aromatic compound

k_0 = rate (or equilibrium) constant for $PhCO_2H$

ρ = reaction constant (taken as unity for the ionization of $PhCO_2H$)

σ = constant for a given substituent (taken as unity for $PhCO_2H$)

Large positive σ values denote powerful electron-withdrawing groups, in the absence of steric effects. Trifluoromethyl substituents possess larger σ values than those of F substituents [σ_m: 0.430 (CF_3) *vs.* 0.337 (F); σ_p: 0.540 (CF_3) *vs.* 0.062 (F)]; the almost neutral value for the *para*-F is evidence for effective mesomeric donation of electron density from F to the aryl ring by dint of effective 2p-2p overlap (Figure 2.5). Accordingly, substitution of perfluoraryl for (trifluoromethyl)aryl substituents was envisaged to fulfil the dual purpose of retaining the strong Lewis acidity of the borane, whilst also deactivating the π-system towards protonation. Assuming the same mode of hydrolysis, this property should therefore favour water dissociation over H^+ attack on the aryl ring.

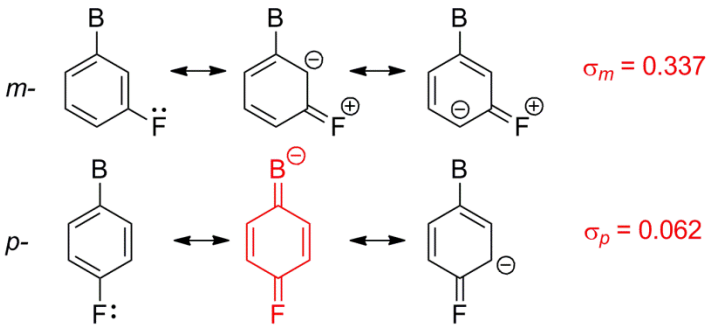

Figure 2.5. Canonical forms of the *meta* and *para*-fluorinated aryl boranes as π-donors.

2.2 Adventitious syntheses of *tris*[(3,5-trifluoromethyl)phenyl]borane

The *tetra*aryl borate anions $[B(C_6F_5)_4]^-$ and *tetrakis*[3,5-*bis*(trifluoromethyl)phenyl]borate, $[BArF_{24}]^-$, (Figure 2.6) have attracted widespread use as weakly-coordinating counterions to stabilise reactive cationic metal centres (e.g. in homogeneous olefin polymerisation).[9] Their high stability in acidic and oxidative conditions, relative to *tetra*phenylborate $[BPh_4]^-$, is attributed to the electron-withdrawing properties of their F-substituents (which lower aromatic π-basicity and hence susceptibility towards electrophilic B–C bond cleavage), and the high strength of their C–F bonds.[10]

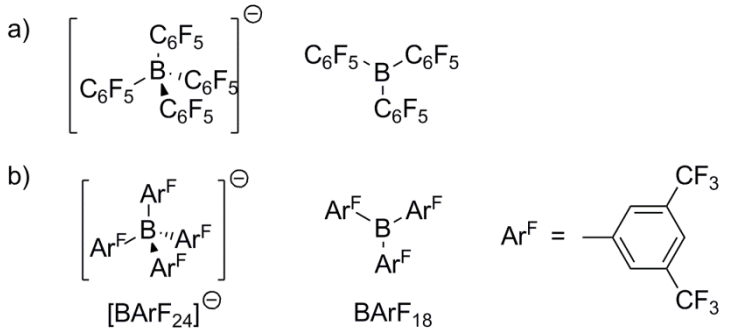

Figure 2.6. Commonly used fluorinated aryl borates and their 'parent' Lewis acid boranes.

Remarkably, in view of the rich chemistry developed for $B(C_6F_5)_3$[11] (which can be viewed as the Lewis acid 'parent' of $[B(C_6F_5)_4]^-$), the analogous *tris*[(3,5-trifluoromethyl)phenyl]borane ($BArF_{18}$) has only been generated *via* adventitious routes. The first, reported by Kubas *et al.,* detailed the decomposition of the $[BArF_{24}]^-$ anion by the electrophilic platinum complex *trans*-$[(Ph_3P)_2Pt(Me)(OEt_2)]^+$ while the second reported the formation of the pyridine adduct $C_5H_5N{\cdot}BArF_{18}$ *via* decomposition of a ferrocenyl-substituted silylium ion (Figure 2.7).[12] For the former only X-ray crystallographic data was reported, while for the latter ^1H, ^{19}F and ^{11}B solution NMR accompanied the crystallographic data.

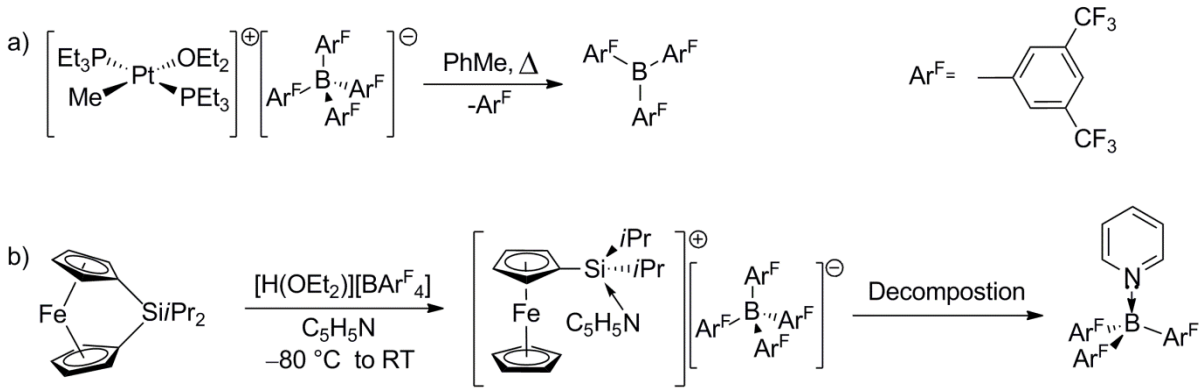

Figure 2.7. a) Decomposition of the $[BArF_{24}]^-$ anion by the electrophilic platinum complex *trans*-$[(Ph_3P)_2Pt(Me)(OEt_2)]^+$. A mixture of uncharacterised platinum complexes were formed upon decomposition.[12a] b) Formation of the pyridine adduct $C_5H_5N{\cdot}BArF_{18}$ *via* the pyridine-stabilized ferrocenyl-substituted silylium ion.[12b]

2.3 Synthesis of *tris*[3,5-*bis*(trifluoromethyl)phenyl)]borane (1)

*Tri*aryl boranes and *tetra*aryl borates are commonly synthesised from a metathesis reaction between a boron trihalide and an organolithium or Grignard reagent.[13] For example, $B(C_6F_5)_3$ is synthesised by nucleophilic addition of C_6F_5MgBr or C_6F_5Li to boron trihalides $BF_3{\cdot}OEt_2$ or BCl_3.[14] The use of C_6F_5Li requires caution in handling since it can become explosive

above –30 ºC. Similarly, Na[$BArF_{24}$] is synthesised *via* reaction of excess [3,5-*bis*(trifluoromethyl)phenyl]MgX (X = Cl, Br) with $NaBF_4$ or $BF_3{\cdot}OEt_2$,[10b,15] and it was reasoned that $BArF_{18}$ should be an intermediate *en route* to this borate anion. Until recently, synthesis of the Grignard reagent was achieved *via* direct reaction of Mg with a 3,5-*bis*(trifluoromethyl)phenyl halide which can explode exothermically due to further Mg insertion into one of the C–F bonds. Fortunately, Yakelis and Bergman have since devised a safe and convenient preparation which uses a Knöchel type metal-halogen exchange which hence avoids use of Mg metal.[16]

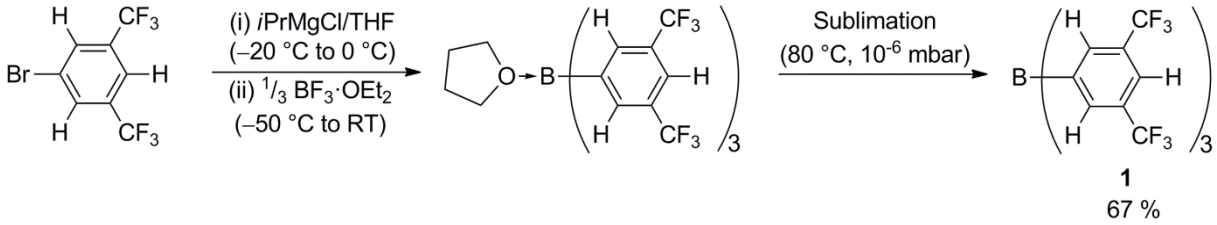

Figure 2.8. Synthesis of *tris*[3,5-*bis*(trifluoromethyl)phenyl]borane, (**1**).

Following this methodology (Figure 2.8) a multi-gram synthesis of $BArF_{18}$ (**1**) has been achieved for the first time. This has since been published in Dalton Transactions (see appendix).[17] The Grignard reagent was generated *via* metal-halogen exchange of *i*PrMgCl and 1-bromo-3,5-*bis*(trifluoromethyl)benzene in THF, which was then treated *in situ* with precisely $^1/_3$ equivalent $BF_3{\cdot}OEt_2$ (Figure 2.8). Facile work-up followed by high vacuum sublimation (80 ºC, 1 x 10^{-6} mbar) afforded *tris*[3,5-*bis*(trifluoromethyl)phenyl]borane (**1**, $BArF_{18}$) in good yield (67 %) as a white powder. The reaction solvent appeared to be important; Grignard formation can also be conducted in Et_2O, yet metathesis with $BF_3{\cdot}OEt_2$ led to formation of $[BArF_{24}]^-$ (shown by ^{11}B NMR spectroscopy, δ = –6.6 ppm, CD_2Cl_2). It is thought the use of THF may retard the competitive addition of a fourth Grignard equivalent by coordinating to **1** as it is formed in solution; indeed the sublimation step is required to remove THF from the moderately labile adduct **1**·THF, which is the actual product extracted immediately after the Grignard step, as evinced by ^{1}H, and ^{11}B NMR spectroscopy (Figure 2.9) (^{1}H NMR: δ = 1.95 (THF), 4.01 (THF), 7.84 (*o*-H, Ar^F), 7.87 ppm (*p*-H, Ar^F); ^{11}B NMR: δ = 11.3 ppm, $CDCl_3$). The ^{11}B NMR shift is downfield to that of $B(C_6F_5)_3{\cdot}$THF (^{11}B NMR: δ = 3.3 ppm) which perhaps suggests the greater lability of this adduct.[18]

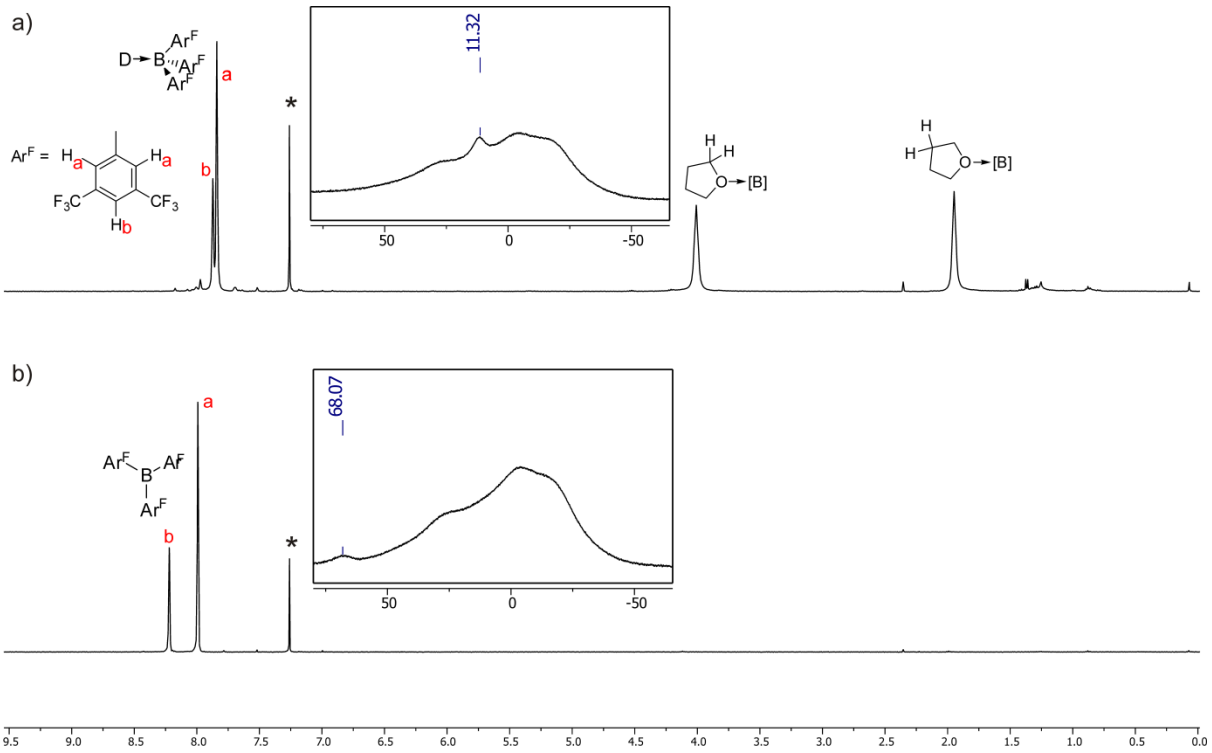

Figure 2.9. ^{1}H and ^{11}B NMR ($CDCl_3$) (insets) for a) **1**·THF and b) **1** post sublimation. A * denotes $CHCl_3$ solvent. Borosilicate probe displays broad background signal in the ^{11}B NMR spectra.

2.4 Characterisation of 1

1 was discovered to be insoluble in aliphatic hydrocarbons, moderately so in aromatic solvents yet displayed optimum solubility in CH_2Cl_2 or $CHCl_3$. This property contrasts with $B(C_6F_5)_3$ (soluble in most common non-donor media), and may be attributed to intermolecular H···F bond interactions between the *para* proton and CF_3 groups on neighbouring molecules in the solid-state for **1** (Figure 2.10); a distance of 2.54 Å was found upon crystallographic re-examination of the reported structure [sum of vdW radii, $r_w(F)$ + $r_w(H)$ = 2.67 Å].[12a,19]

For the first time, **1** has been fully characterised by ^{1}H, ^{13}C, ^{19}F and ^{11}B NMR spectroscopy; the ^{11}B NMR shift (δ = 68.1 ppm; CD_2Cl_2) is strongly indicative of a three-coordinate geometry in the solution phase and is noticeably deshielded in comparison with that found for $B(C_6F_5)_3$ (δ = 61.2 ppm; CD_2Cl_2). ^{11}B NMR shifts are composed of both paramagnetic (σ^p) and diamagnetic (σ^d) contributions, in which the greater electron withdrawing effect of 3,5-$(CF_3)_2C_6H_3$ aryl groups *vs.* the C_6F_5 groups found in $B(C_6F_5)_3$ may result in the increased deshielding. Elemental analysis, MS (EI) and IR (KBr) were all consistent with the formation of uncoordinated **1** (formula Unit: $C_{24}H_9BF_{18}$).

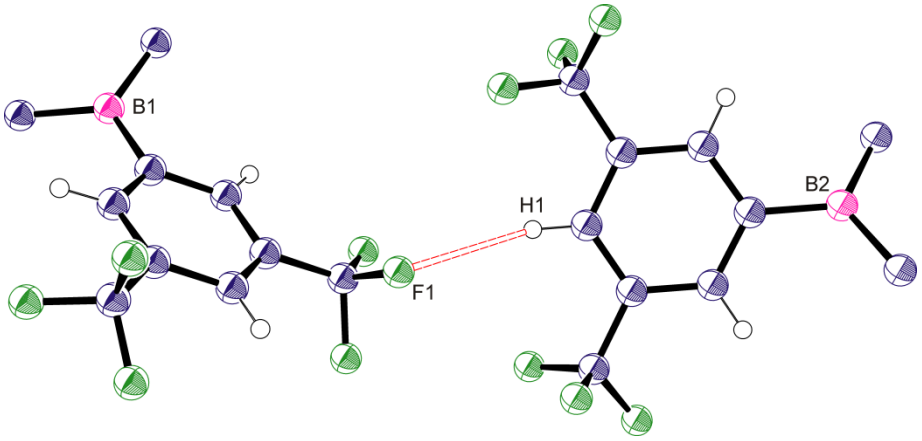

Figure 2.10. Intermolecular hydrogen bonding between the para proton and CF_3 group on neighbouring molecules of **1**. Selected H···F contact = 2.54 Å [sum of vdW radii, $r_w(F) + r_w(H) = 2.67$ Å]. For clarity only one phenyl ring for each borane is displayed. C atoms navy blue, B atoms pink, F atoms green and selected H atoms white.[12a]

In contrast to $B(C_6F_5)_3$ which is reported to be inert to pure oxygen at room temperature,[20] rapid decomposition of **1** was observed upon admission of dry O_2 to a CD_2Cl_2 solution (numerous unassignable resonances in the ^1H, ^{19}F and ^{11}B NMR spectra). Despite the strongly electron-withdrawing CF_3 groups in **1** (rationalised to contribute to the observed oxidative stability of the $[BArF_{24}]^-$ anion), it is plausible that the *ortho*-F substituents in $B(C_6F_5)_3$ are integral to suppressing reaction with O_2; the absence of this structural feature in **1** may therefore lead to the heightened reactivity observed for this trigonal borane.

2.5 Lewis acidity measurements of 1

A range of methods to assess relative Lewis acidity have been reported and are commonly based on spectroscopic techniques (IR, NMR).[21] For organoboranes, this typically comprises the Gutmann-Beckett[21d-e] and Childs[21a] methods which utilise the donor probes $Et_3P{=}O$ and *trans*-crotonaldehyde respectively (Figure 2.11). Both rely on the respective chemical shift differences ($\Delta\delta$) upon complexation of their respective probe to the Lewis acid, which is proportional to the Lewis acid strength of the acceptor site (Figure 2.11). In this regard, the Gutmann-Beckett method examines the change in ^{31}P NMR shift ($\Delta\delta$) of $Et_3P{=}O$,[21e,22] while the Childs is calculated from the downfield shift of the H_3 resonance of *trans*-crotonaldehyde.[21a]

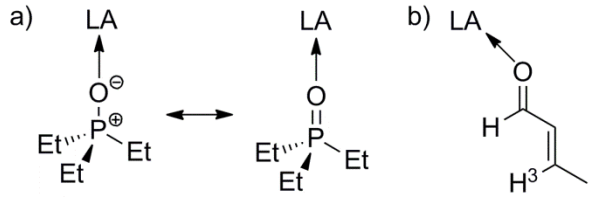

Figure 2.11. Donor-acceptor complexes formed in a) Gutmann-Beckett and b) Childs Lewis acidity tests.

Accordingly, **1** was found to coordinate both molecules. The results are tabulated below in Table 2.1 in which they are compared with those measured for $B(C_6F_5)_3$. Based upon the coordination of $Et_3P{=}O$, **1** displays a Lewis acidity *ca.* 6% greater than that for $B(C_6F_5)_3$, which contrasts markedly with the *ca.* 38% reduction observed employing the Childs method. A linear correlation is usually documented between methods,[2b] although an increasing number of boron systems are starting to oppose this trend.[1a,23] Notably, Britovsek *et al*. reported a non-linear trend for the series $B(C_6F_5)_{3-x}(OC_6F_5)_x$ (x = 1–3), where preference for $Et_3P{=}O$ binding over crotonaldehyde is observed as x increases.[23] This was rationalised using Pearson's Hard and Soft Acids and Bases (HSAB) principle where the covalent (softer) C=O bond is a preferable donor to $B(C_6F_5)_3$ compared with the more ionic (harder) P=O bond, favoured by $B(OC_6F_5)_3$.

Table 2.1. ^{31}P and ^{1}H NMR spectral data derived for Lewis acidity measurements of **1** and $B(C_6F_5)_3$ in CD_2Cl_2 at RT.

	Et_3PO		***trans*-Crotonaldeyde**	
Lewis Acid	^{31}P NMR /ppm	Δδ /ppm[a]	^{1}H NMR /ppm[a]	Δδ /ppm[b]
None	50.7	–	6.85	–
$B(C_6F_5)_3$	77.3	26.6	7.93	1.08
1	78.9	28.2	7.52	0.67

[a] $\Delta\delta = [Et_3P{=}O(\text{coordinated}) - Et_3P{=}O(CD_2Cl_2)]$. [b] $\Delta\delta = [H_3(\text{coordinated}) - H_3(CD_2Cl_2)]$

Since Lewis acidity is a composite of both steric and electronic factors at the acceptor site, it would be useful to compare the steric profile of **1** with $B(C_6F_5)_3$. However, as previously mentioned no solid-state structure of the latter has been reported. Fortunately the pyridine adducts, $C_5H_5N{\cdot}A$ (A = **1**, $B(C_6F_5)_3$), have been crystallographically characterised for both species, in which they have virtually identical B–N bond lengths (1.63 Å), permitting a valid comparison.[12b,24] Excision of the pyridine ligand followed by free volume calculations enabled a comparison of the sterics around the remaining pyramidalised borane fragments of **1** and $B(C_6F_5)_3$. These were performed by Dr Alexander J. W. Thom (Imperial College London) using Monte Carlo integrations (Figure 2.12, consult Chapter 5 for methodology).

The results showed that **1** is less hindered in the 2–4 Å region (i.e. that occupied by the pyridine molecule), as anticipated from the smaller size of the *ortho*-H in **1** relative to the *ortho*-F in $B(C_6F_5)_3$, which in conjunction with the discussed ^{11}B NMR spectroscopic data (an electronic probe at the B atom)[1a] support the Gutmann-Beckett assignment that **1** is more Lewis acidic than $B(C_6F_5)_3$.

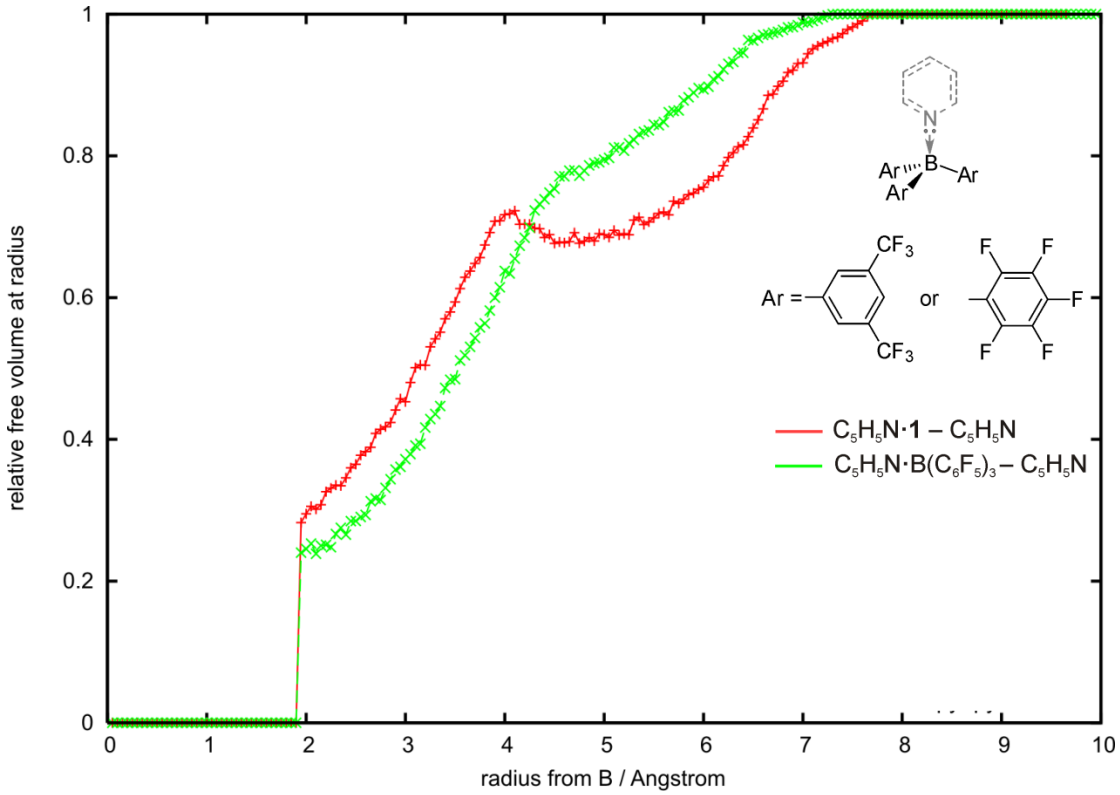

Figure 2.12. The relative free volume at a given radius from the boron centre for **1** and $B(C_6F_5)_3$ (defined as the percentage of a surface area of sphere of that radius centred on the boron not enclosed by the van der Waals surface).

The lower shift calculated for the Childs method would appear consistent with the HSAB principle as described by Britovsek *et al*. This notion appears logical for the series $B(C_6F_5)_{3-x}(OC_6F_5)_x$ (x = 1-3), where each subsequent B–O linkage has an increasing effect on the hardness of the boron centre, whereas for $B(C_6F_5)_3$ and **1**, electronic modification is remote *via* aryl substituent changes.

2.6 H_2 activation by 1/TMP FLP

In recent years, a range of Lewis bases from strongly basic carbanions[25] and carbenes[26] to the more common phosphines, amines and imines have been employed in FLP systems. For all these systems, the cumulative Lewis acid and base strength must be sufficiently strong to

permit the activation of small molecules (Figures 1.16 and 1.18). Although the mechanism of H_2 activation is still contested,[27] favourable free energy calculations for proton and hydride attachment to the Lewis base and Lewis acid are essential to overcome endothermic heterolytic H–H bond cleavage ($\Delta H^{\ddagger}$ = 432 kJ mol^{-1}).[28] A value of –65.2 kJ mol^{-1} was reported for the TMP/B(C_6F_5)$_3$ FLP system, which demonstrated irreversible activation at room temperature and standard pressure (1 atm).

Addition of **1** to TMP in CD_2Cl_2 (1:1) led to the formation of a FLP, as evidenced by unchanged resonances in the ^{1}H, ^{19}F and ^{11}B NMR spectra relative to the species in isolation. Subsequent admission of H_2 (1 atm) led to the rapid precipitation of a white solid, with ^{1}H NMR spectroscopy showing exactly half of the initial TMP to have remained in solution. In contrast, the ^{11}B NMR spectrum showed consumption of **1**, which indicated complete sequestration of the borane. Elemental analysis of the solid was consistent with the molecular formula unit (**1**)$_2$(TMP)(H_2) (**2**, Figure 2.13).

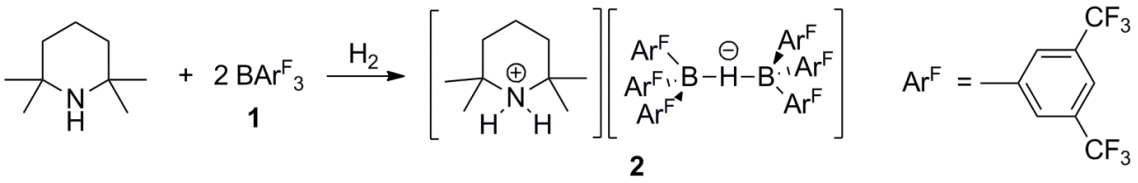

Figure 2.13. Generation of **2** from heterolytic activation of H_2 by **1** and TMP.

H_2 activation was also found to occur in Et_2O, which led to the generation of large single crystals suitable for study by X-Ray diffraction, that solved as the novel salt [TMPH][μ-H(BArF_{18})$_2$]·Et_2O (**2**·Et_2O; Figure 2.14). The anion geometry approximates to D_3 symmetry, and the bridging borohydride unit is close to linear (B$\hat{H}$B = 176.3°). The B–H bond lengths (1.40(3) and 1.42(3) Å) are similar to those for seen in Li[μ–H(BEt_3)$_2$] (1.376(6) Å)[29] yet distinct from [TMPH][H–B(C_6F_5)$_3$] (1.18 (2) Å);[30] the longer bonds reflect the electron-deficient B–H–B interactions (3-center-2-electron bond) relative to terminal B–H (2-center-2-electron bond).

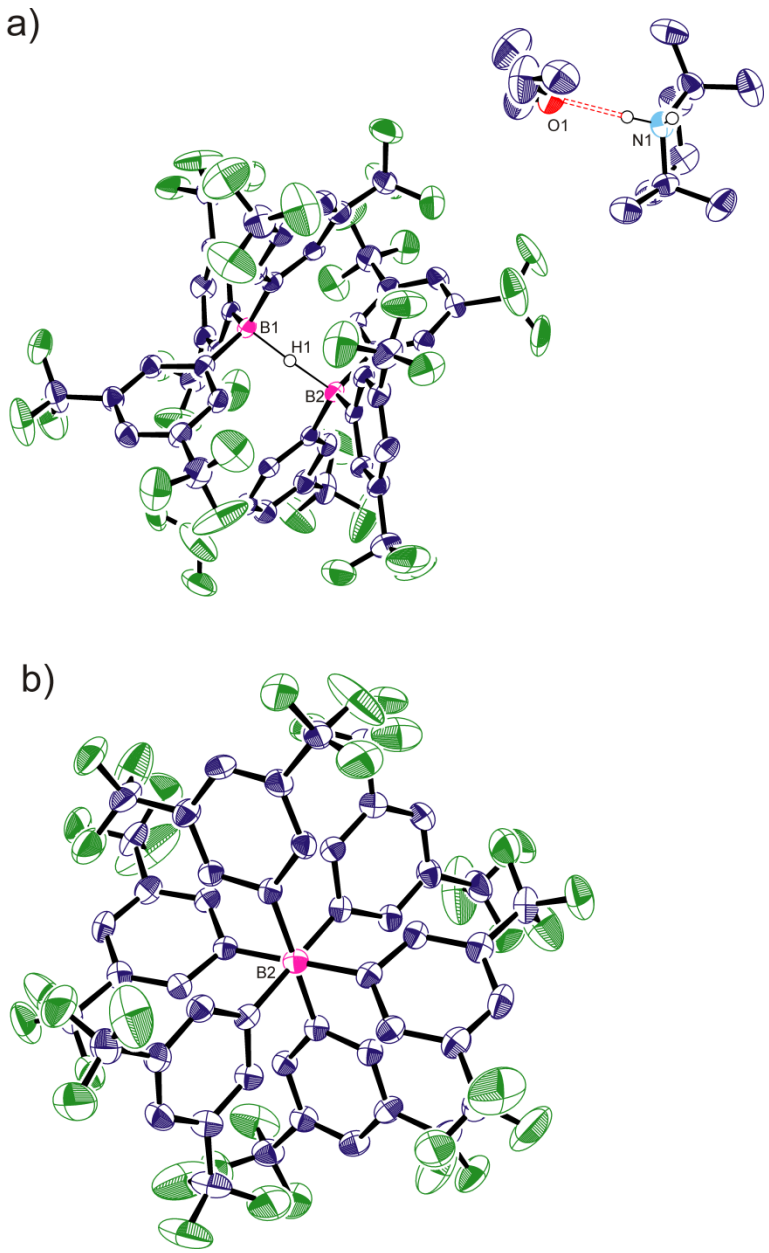

Figure 2.14. a) Ortep diagram of **2**·OEt_2. H atoms (except attached to B and N) have been removed for clarity; thermal ellipsoids are shown at 50 % probability. b) View showing staggered geometry along the B2–H1–B1 axis. C atoms navy blue, N atom sky blue, B atoms pink, F atoms green and displayed H atoms white. Thermal ellipsoids are shown at 50% probability. Selected bond lengths: B1–H1 = 1.40(3) Å, B2–H2 = 1.42(3) Å; H···O contact = 1.97 Å.

The aryl rings in **2**·OEt_2 adopt an almost staggered conformation (torsion angles 58.7–61.5°) about the B–H–B axis. The [TMPH] cation shows H-bonding to an Et_2O molecule with N···O and H···O separations of 2.869(4) and 1.97(5) Å respectively, and a N–H···O angle of *ca.* 178°. This was unusual since crystallographically characterised products from FLP-mediated H_2 cleavage have only demonstrated bridging dihydrogen (H···H) bonding interactions between the respective Lewis acid and Lewis base fragments (Figure 2.15).[31]

Thus, at the time of publication, this represented the first example of H_2 cleavage by an FLP to produce a bridging borohydride salt.

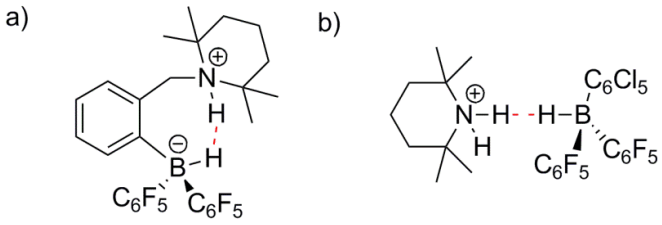

Figure 2.1. Crystallographically characterised products from H_2 activation which demonstrate dihydrogen bonds.[31]

Presumably, in the case of **2**·Et_2O, the potential to form a strong H···O contact leads to the ammonium ion binding preferentially to the neutral O atom of Et_2O. Furthermore, the only other example of arylborane-mediated H_2 activation in ethereal solvent was for the $HB(Fmes)_2$/DABCO FLP system [Fmes = 2,4,6-*tris*(trifluoromethyl)phenyl, DABCO = diazobicyclo[2.2.2]octane] (Figure 2.16).[32] Here, considerable steric protection about the B centre was reasoned to prevent solvent binding.

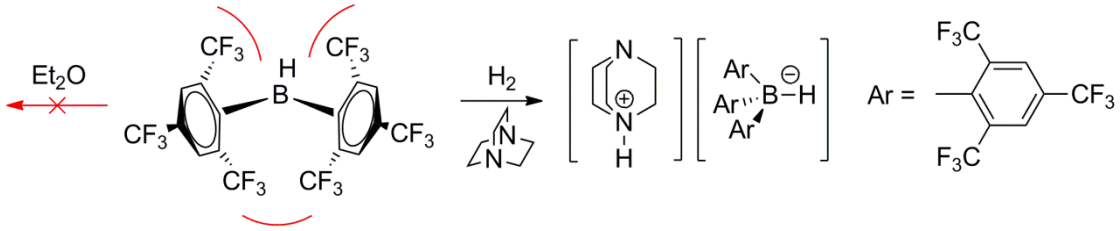

Figure 2.2. Heterolytic cleavage of H by a *bis*(2,4,6-*tris*(trifluoromethyl)phenyl)borane/DABCO FLP. The sterically bulky Fmes substituents inhibit Et_2O binding.

In contrast to $HB(Fmes)_2$, both **1** and $B(C_6F_5)_3$ coordinate Et_2O, as witnessed by ^{11}B NMR spectroscopy (δ = 18.7 and 7.4 ppm for **1**·OEt_2 and $B(C_6F_5)_3$·OEt_2 in C_6D_6); the **1**·OEt_2 the shift is intermediate between three and four coordinate boron. Since publication, Stephan *et al.* have shown combinations of $B(C_6F_5)_3/Et_2O$ to activate H_2 and effect the catalytic hydrogenation of 1,1-diphenylethylene (Figure 2.17).[33] In their study, the $B(C_6F_5)_3$·OEt_2 adduct is illustrated to be substantially labile and DFT calculations reveal a significant concentration of the FLP to be present in solution. Furthermore, upon H_2 cleavage, the $[Et_2O–H][H–B(C_6F_5)_3]$ product is reasoned to be stabilised by solvation, in which a second Et_2O molecule forms a strong hydrogen bond with the $[Et_2O–H]^+$ cation. In the context of these findings, it is plausible a similar mechanism is in operation for **1**/TMP; following H_2

activation, H^+ is shuttled from the $[Et_2O–H]^+$ cation (pK_a = –3.6 in H_2O) to the more basic TMP component (pK_a = 11.1 in H_2O) to yield **2**.[34]

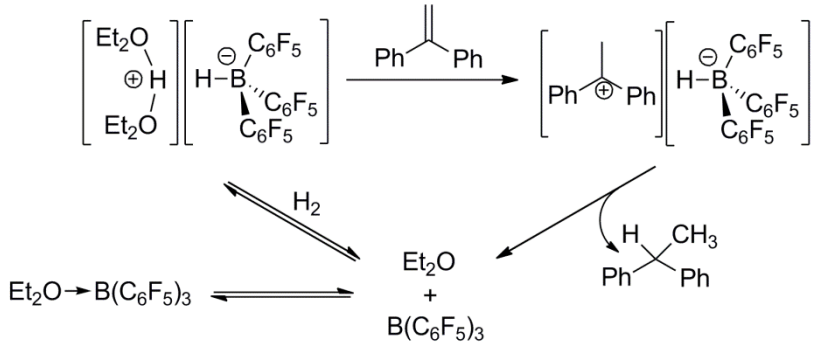

Figure 2.3. Proposed mechanism by Stephan *et al.* for the hydrogenation of 1,1-diphenylethylene by $Et_2O/B(C_6F_5)$ FLP system.[34]

The dissociation of **1**·OEt_2 to form an FLP system is analogous with the 2,6-lutidine/$B(C_6F_5)_3$ pair (lutidine = dimethylpyridine), which cleaves H_2 only upon dissociation of the weakly-bound classical adduct (Figure 2.18).[35] In light of these reports, **1**/TMP when dissolved in Et_2O may be considered as a system operating on the classical/frustrated Lewis pair borderline.

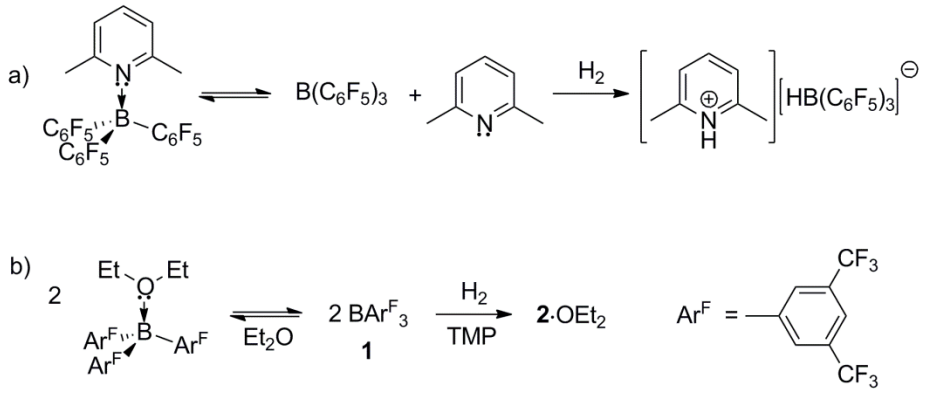

Figure 2.4. Examples of FLP systems operating on the classical/frustrated Lewis pair borderline a) classical and FLP reactions of 2,6-dimethylpyridine/$B(C_6F_5)_3$ b) Reversible Et_2O binding of **1**, permitting H_2 cleavage in ethereal solvent.

An unambiguous solution-phase assignment of **2** using NMR spectroscopy was hampered by the insolubility of the compound in most non-donor media (donor solvents were found incompatible with B–H–B unit due to sequestration of one of the $BArF_{18}$ fragments through solvent binding (*vide infra*); only using 1,2-difluorobenzene at 80°C [a solvent with a high dielectric constant (κ = 13.8 *vs.* 8.9 (CD_2Cl_2)) reported to dissolve poorly soluble ionic salts][36] were ^{1}H NMR resonances that correctly reproduced the **1**:TMP ratio in **2** obtained

(Figure 2.19). Despite this, no resonances associated with the bridging borohydride fragment B(μ-H)B were located in either the ^{1}H or ^{11}B NMR spectra. This property is reminiscent of the related $[(C_6F_5)_3B(\mu\text{-H})B(C_6F_5)_3]$ anion; here low temperature ^{1}H and ^{19}F NMR (< 183 K) provided means of identification, but with ^{11}B NMR unable to distinguish a B(μ-H)B environment.[37] IR or Raman spectroscopy of **2** and its deutero analogue, obtained from D_2 and TMP:**1** (1:2), also failed to unambiguously reveal a B–H(D) stretch.

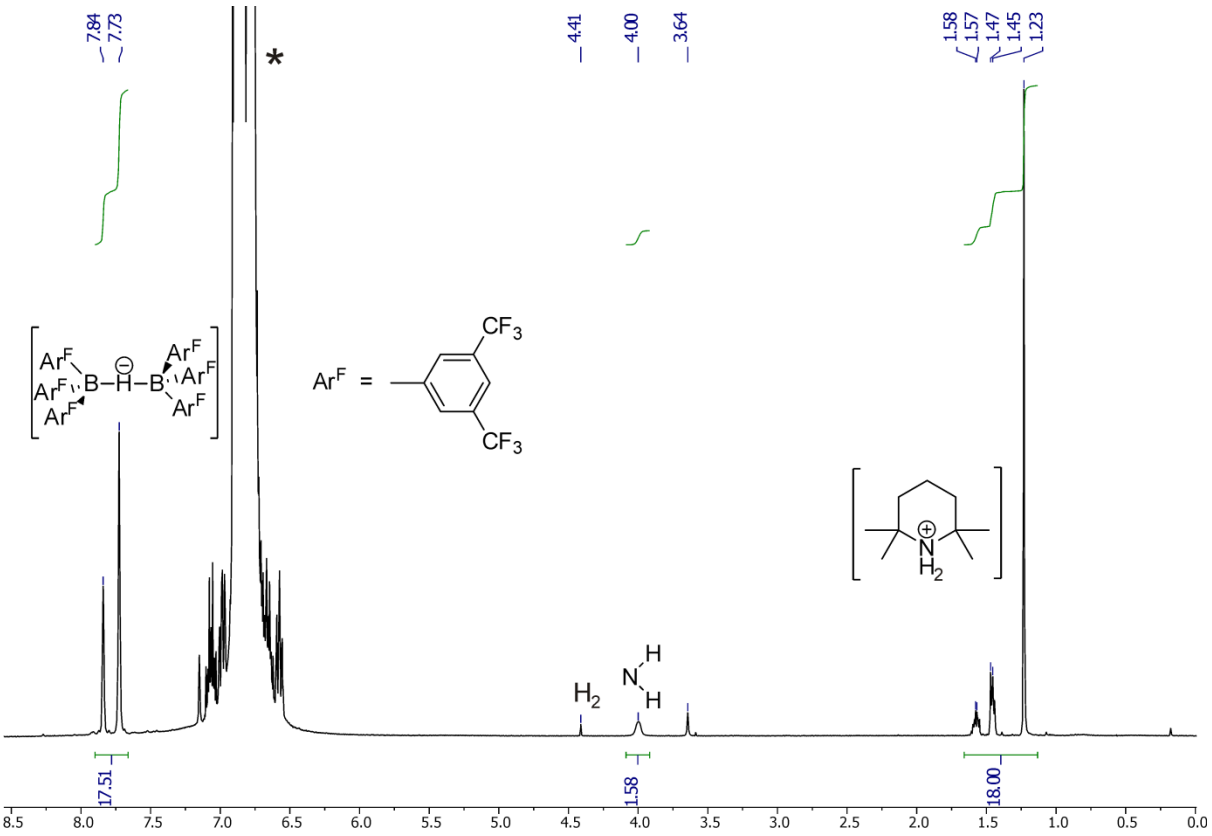

Figure 2.5. ^{1}H NMR for **2** in 1,2-difluorobenzene ($C_6H_4F_2$) at 80 ºC. Small quantities of H_2 evolved at this temperature, solvent signals (4,5-H positions referenced to δ = 6.75 ppm) denoted by *.

On the other hand, dissolution occurred readily in pyridine-d_5 to yield assignable ^{1}H (Figure 2.20), ^{19}F and ^{11}B NMR spectra, which corresponded to the species [**1**·pyridine-d_5], $[TMPH]^+$, and the borohydride anion $[\mathbf{1}\text{–H}]^-$ (1:1:1 ratio). The latter was cleanly resolved by a diagnostic terminal B*H* (1:1:1:1 quartet) in the ^{1}H NMR spectrum (δ = 4.53 ppm, $^{1}J(H,^{11}B)$ = 84 Hz, pyridine-d_5), accompanied by an intense doublet in the ^{11}B NMR spectrum (δ = –7.2 ppm, $^{1}J(^{11}B,H)$ = 84 Hz). This confirms the composition of **2**, and reveals the behaviour of the anion in donor media as both a source of terminal borohydride $[\mathbf{1}\text{–H}]^-$, and a labile equivalent of the Lewis acid **1**.

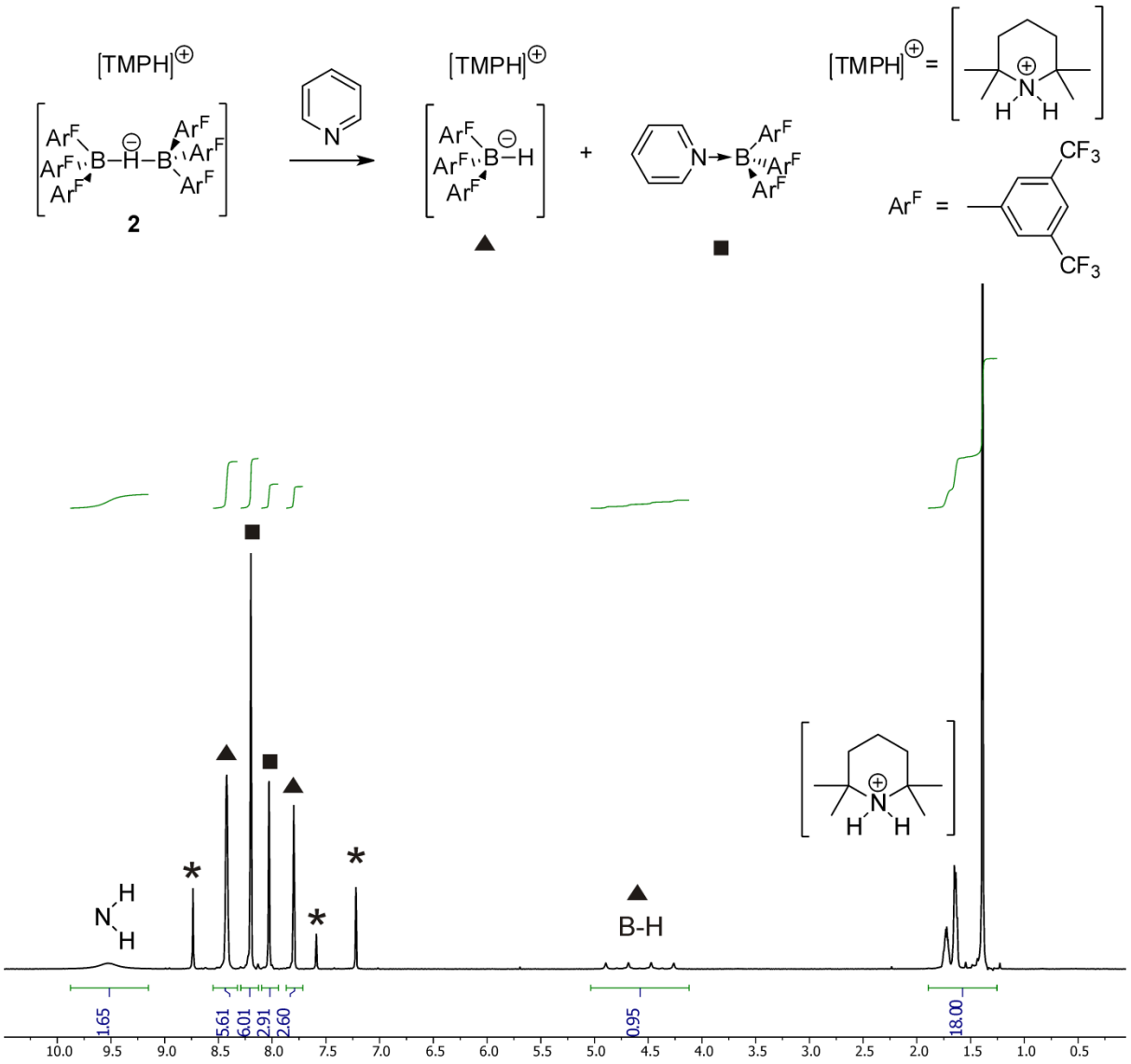

Figure 2.6. ^{1}H NMR spectrum of **2** (pyridine-d_5). Solvent peaks denoted by *, ▲ and ■ denote **1**·pyridine-d_5 and [**1**–H]$^-$ respectively.

2.7 Hydrolytic stability of 1

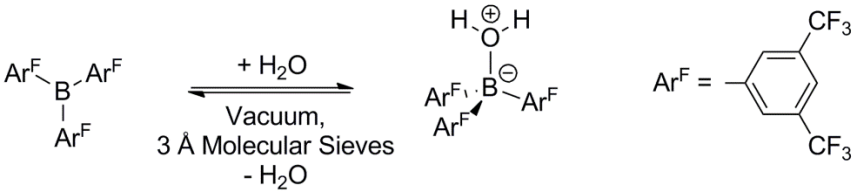

Figure 2.7. Reversible coordination of H_2O by **1**

Interestingly, H_2O was found to form the reversible dative complex **1**·OH_2; the donor can be removed under vacuum or through addition of 3 Å molecular sieves in CH_2Cl_2 solution. In contrast $B(C_6F_5)_3$ forms the tightly bound analogue $B(C_6F_5)_3$·OH_2 (Figure 2.21),[38] which contrasts with the Gutmann-Beckett assignment that **1** is the stronger Lewis acid. In light of

these observations it was hoped the electron withdrawing properties of the CF_3 groups may render the aryls less susceptible to H^+ attack for the species **1**·OH_2.

At room temperature aqua complexes of **1** and $B(C_6F_5)_3$ were intrinsically stable but at elevated temperatures (> 60 ºC) undergo protonolysis. This permitted an investigation into the relative rates of hydrolysis. At 60 ºC both complexes underwent protonolysis at an appreciably slow rate; only after 40 minutes were trace C_6F_5H or 1,3-$(CF_3)_2C_6H_4$ resonances observed. At 100 ºC, the products of protonolysis were identified within 5 minutes (Figure 2.22), in which the initial rate of decomposition (zero order for both) for **1** (2.5×10^{-5} M s^{-1}) was marginally greater than that for $B(C_6F_5)_3$ (1.9×10^{-5} M s^{-1}) (Figure 2.23).

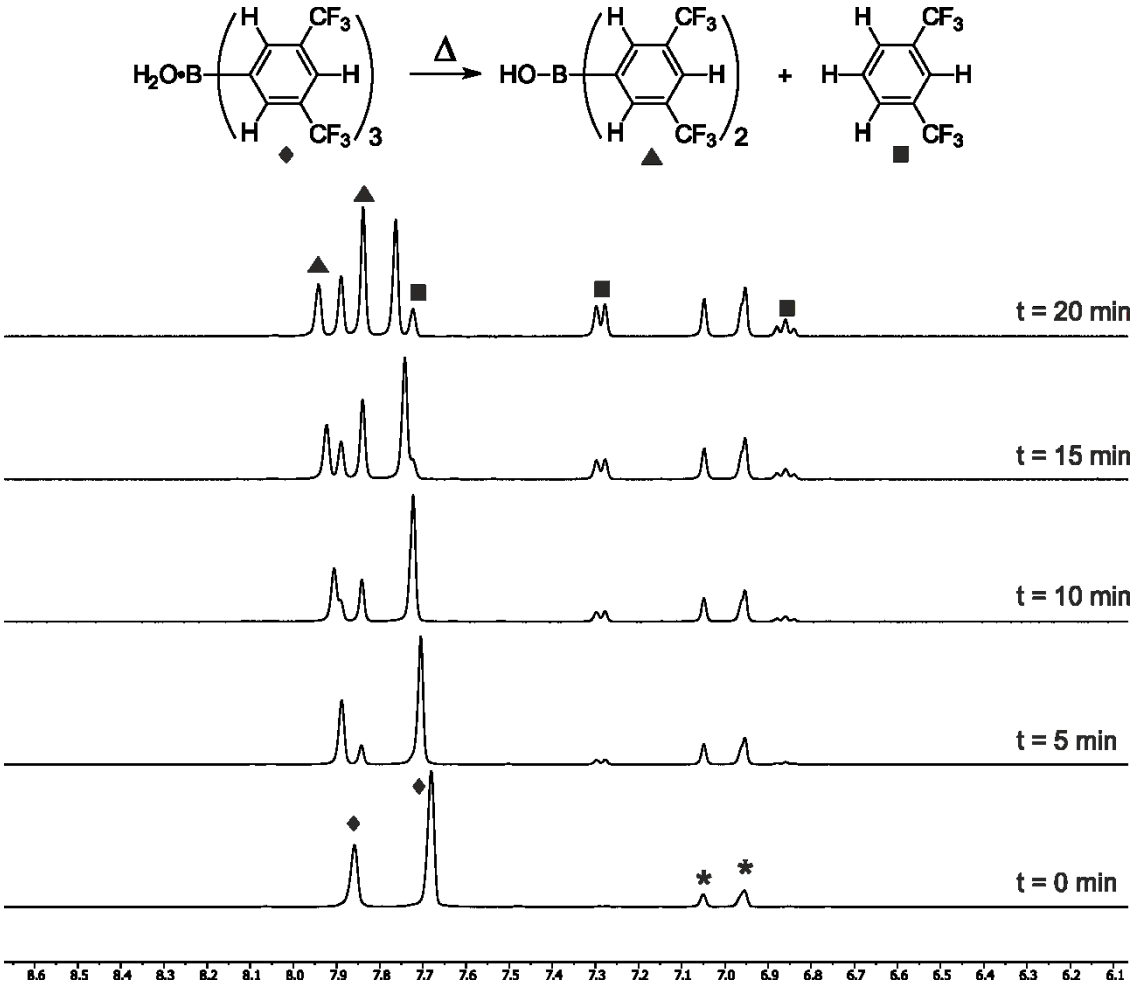

Figure 2.8. Selected ^{1}H NMR spectra for the decomposition of **1**·H_2O (♦) to 1,3-$(CF_3)_2C_6H_4$ (▲) and HO·B(3,5-$(CF_3)C_6H_2)_2$ (■) as a function of time at 100 °C. C_7D_8 solvent peaks denoted by *.

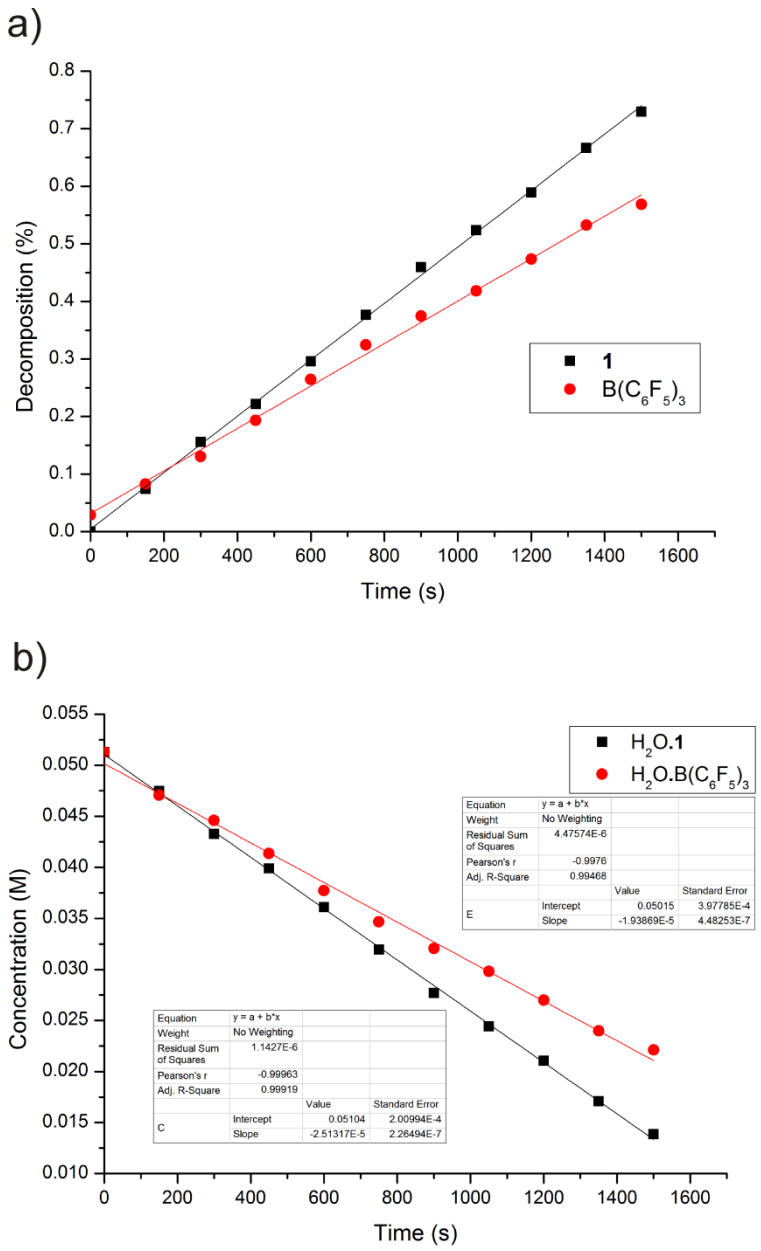

Figure 2.9. a) Decomposition plotted against time for the hydrolysis of H_2O·**1** and H_2O·$B(C_6F_5)_3$ at 100 ºC (2 runs for each complex). b) Concentration plotted against time for the initial rate of decomposition for H_2O·**1** and H_2O·$B(C_6F_5)_3$ at 100 ºC .

These findings clearly indicate the inclusion of two *meta*-CF_3 groups to be insufficient in deterring aryl cleavage. In other words, strong binding of H_2O for both **1** and $B(C_6F_5)_3$ weakens the O–H bond and renders it susceptible to attack by the *ipso*-C on the aryl rings. Therefore, the introduction of greater sterics about the boron centre is predicted to lengthen the B–O bond and favour facile dissociation over protonolysis. Accordingly, a bulkier *tris*aryl borane was sought which retained two powerfully electron withdrawing CF_3 substituents.

2.8 Synthesis and characterisation of *tris*[2,4-*bis*(trifluoromethyl)phenyl)]borane (3)

In 2003, Cornet and co-workers reported the unselective synthesis of *tris*[2,4-*bis*(trifluoromethyl)phenyl)]borane (**3**), from the metathesis of the organolithium precursor Li[2,4-$(CF_3)_3C_6H_4$] with BCl_3.[39] Examination of the spectral parameters revealed an ^{11}B NMR shift of 73.6 ppm ($CDCl_3$), which was reasoned to provide a reasonable probe into the electron density about the boron nucleus; the marginal upfield shift relative to **1** may coincide with the larger Hammett parameter for *p*-CF_3 relative to *m*-CF_3 ($\sigma_{p:}$ 0.540 *vs.* $\sigma_{m:}$ 0.430). Additionally, X-ray structural data for **3** showed a high degree of steric crowding, in which the three aryl groups exist in a propeller-like geometry. The average torsion angle (56.4º), defined as the angle between the best plane of the ring relative to the three carbons bonded to the boron centre, mirrors that of the sterically bulky trimesitylborane, $BMes_3$ (40-60º) (Mes = 2,4,6-trimethylphenyl).[40] Despite thorough spectroscopic and crystallographic characterisation of **3**, reactivity studies were not conducted, possibly due to the low synthetic yield (17 %). This involved non-selective lithiation of 1,3-*bis*(trifluoromethyl)benzene to afford Li[2,4-$(CF_3)_3C_6H_4$] and Li[2,6-$(CF_3)_3C_6H_4$], which afforded mono- and *bis*arylated boranes, B(2,6-$(CF_3)_2C_6H_3)Cl_2$ and B(2,6-$(CF_3)_2C_6H_3)_2F$, in addition to **3** (Figure 2.24). The presence of B(2,6-$(CF_3)_2C_6H_3)_2F$ is reasoned to form *via* Cl/F exchange during metathesis.

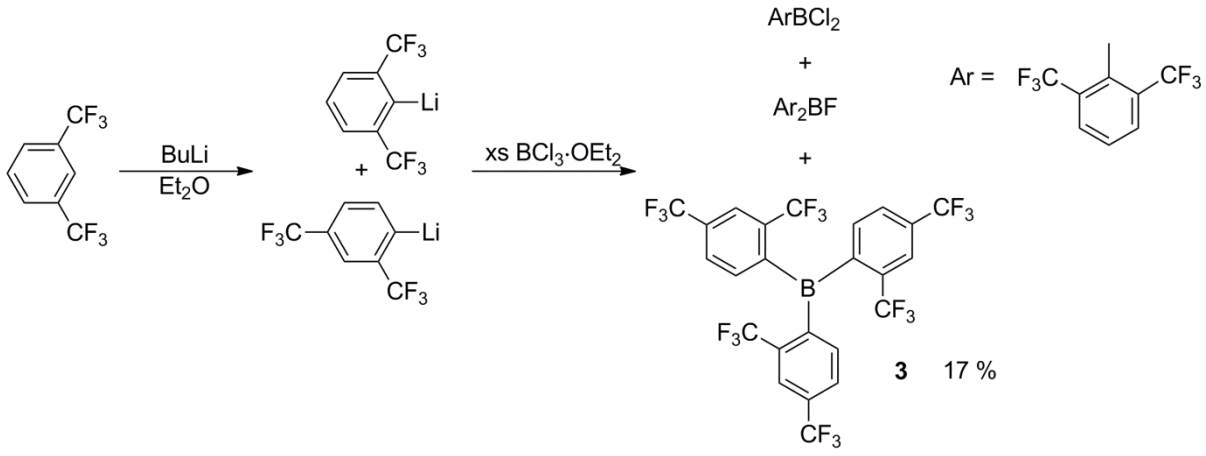

Figure 2.10. Pathway to **3** from lithiation of 1,3-*bis*(trifluoromethyl)benzene followed by metathesis with BCl_3·OEt_2. Yield **3**: 17%.

Accordingly, a new high yielding route to **3** was devised by facile substitution of the commericially available 1-bromo-2,4-*bis*(trifluoromethyl)benzene for 1,3-*bis*(trifluoromethyl)benzene, followed by lithiation and *in situ* addition of BCl_3 (3:1) (Figure 2.25). Expedient work up was facilitated by a high vacuum sublimation step (85 ºC, 1 x 10^{-6} mbar), to furnish **3** in excellent yield (90%). Conversely, **1** cannot be selectively generated

from organolithium precursor [3,5-*bis*(trifluoromethyl)phenyl]Li, rather the borate Li[BArF$_{24}$] is obtained from non-selective metathesis. The enhanced steric bulk of flanking *ortho* CF_3 substituents are believed to permit greater control in the metathesis reaction of **3**, where sterics strongly disfavour addition of a fourth aryl equivalent to the intermediate borane.

As found for **1**, compound **3** was practically insoluble in hydrocarbons, modestly soluble in aromatics, and readily soluble in CH_2Cl_2 or $CHCl_3$. Once again, these observations may be attributed to the intermolecular H···F bond interactions between the deshielded aromatic protons and the CF_3 substituents on neighbouring molecules. Upon re-examining the X-ray crystallography data for **3**, a distance of 2.60 Å was measured between the 5-H proton and the *ortho* CF_3 group of a neighbouring **3** [sum of vdW radii, r_w(F) + r_w(H) = 2.67 Å].[39]

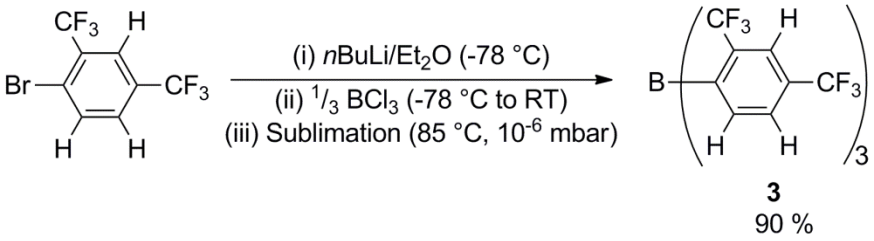

Figure 2.11. High yielding synthesis of *tris*[2,4-*bis*(trifluoromethyl)phenyl)]borane.

Whilst **1** was found to rapidly decompose upon admission of dry O_2, **3** was found to be inert; presumably the incorporation of three bulky CF_3 groups in the *ortho* position suppresses reactivity. Similarly, addition of H_2O to a toluene solution of **3** (1:1) resulted in no change to the ^{1}H, ^{19}F or ^{11}B NMR spectra. Even at elevated temperatures (> 100 ºC), **3** was found to be extremely robust; refluxing this toluene solution for several days showed no evidence for protonolysis by H_2O (Figure 2.26).

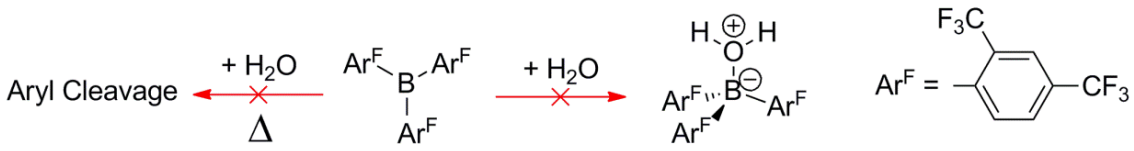

Figure 2.12. 3 resistant to H_2O complexation and protonolysis.

2.9 Lewis acidity measurements of 3

Complexation with **3** was not observed for either the Gutmann-Beckett or Child's methods. Seemingly, the sterics of the *ortho*-CF_3 substituent override the powerful electron

withdrawing effects of two CF_3 groups. Examination of the space-filling diagrams for the solid state structure of **3** *vs.* **1**, illustrate the marked screening of the boron acceptor site upon replacement of *ortho*-H with an *ortho*-CF_3 (Figure 2.27).

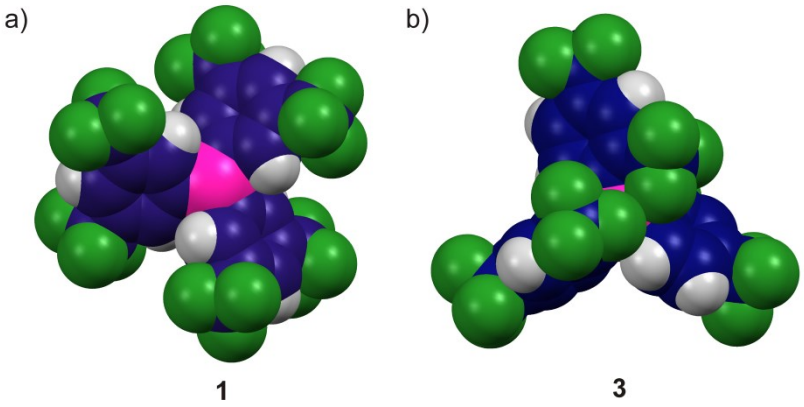

Figure 2.13. Space-filling diagram of a) **1** and b) **3;** C atoms blue, H atoms grey, F atoms green, and B atoms pink.

To garner a more accurate determination of the electron deficiency at the boron centre, the reduction potentials of **1** and **3** were explored. Previously, the reduction of the sterically bulky boranes $B(Mes)_3$ and $B(C_6Cl_5)_3$ to $[B(Mes)_3]^{\bullet-}$ and $[B(Mes)_3]^{\bullet-}$ respectively, led to minimal structural reorganisation of the trigonal planar environment upon electron transfer (X-ray structure determination).[1a,41] Consequently, the electrochemical potentials of boranes **1** and **3** may be seen as an approximate measure of their electrophilicity in the absence of steric effects.

2.10 Electrochemical studies of 1 and 3

In collaboration with the Wildgoose research group (UEA), the direct voltammetric reduction of compounds **1** and **3** in CH_2Cl_2 were examined at a macrodisk electrode using cyclic voltammetry (Figure 2.28). The weakly coordinating cation/anion combination $[n Bu_4N][B(C_6F_5)_4]$ was used as the electrolyte in which cyclic voltammograms were recorded at various scan rates (50-1000 mV/s for **1**; 25-1600 mV/s for **3**). A plot of the reductive peak current *vs* the square root of voltage scan rate was also constructed, in which a linear relationship is representative of a process operating under diffusion control (Figure 2.29).[42]

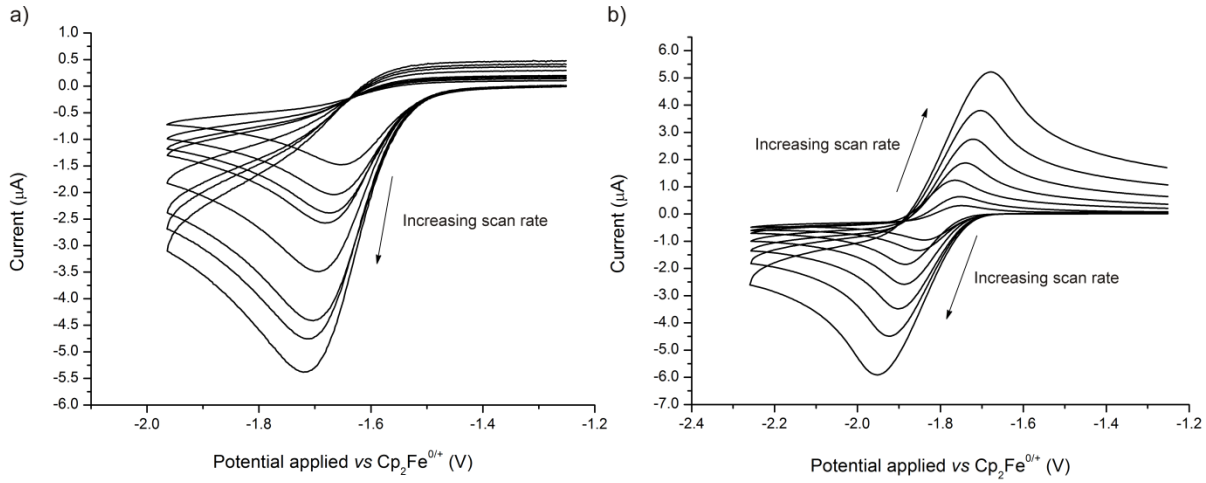

Figure 2.14. Overlaid cyclic voltammaograms recorded at scan rates of 50 to 1000 mV/s for **1** (a) and 25 to 16000 mV/s for **3** (b) (10 mM concentration).

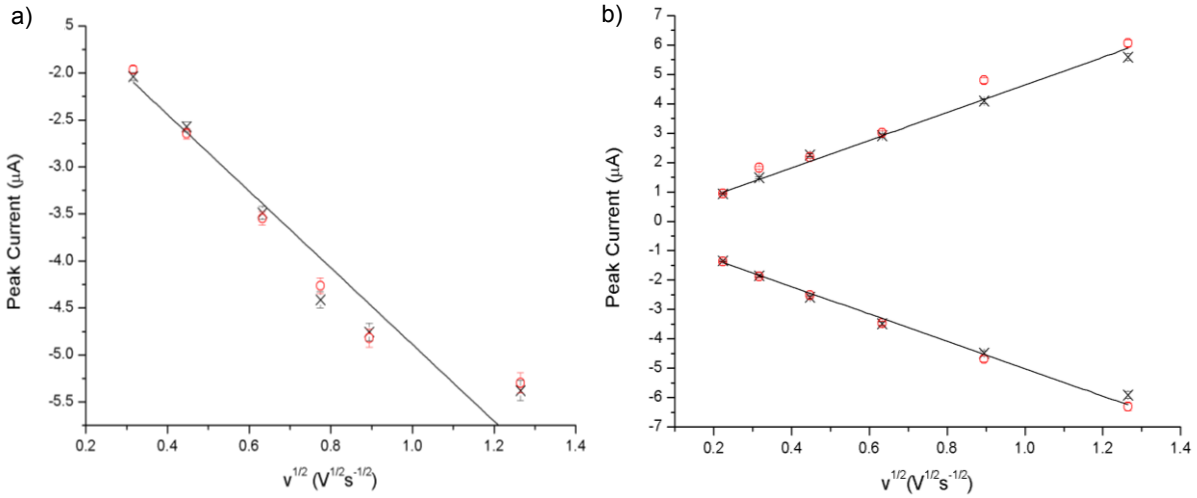

Figure 2.15. Plots of reductive peak current *vs* square-root of voltage scan rate for **1** (a) and **3** (b). x - experimental data, ○ - simulated data. 2 % error in peak current.

When the potential was scanned in the negative direction a single reduction peak was observed at –1.67 V and –1.89 V *vs* $Cp_2Fe^{0/+}$ (at 100 mV s^{-1}) for **1** and **3** respectively. In the case of **1**, the reduction wave appears to be irreversible with no oxidation wave witnessed upon reversal of the scan direction. As reported for the voltammetric reduction of $B(C_6F_5)_3$ and $B(C_6F_5)_{3-n}(Mes)_n$, this behaviour is consistent with an EC mechanism where "E" denotes a heterogenous electron transfer step and "C" denotes follow-up homogenous chemical step (Figure 2.30).[43] Upon formation of the radical anion at the electrode, homogenous follow up chemistry results in decomposition to yield redox inactive products. Over all scan rates the decomposition of **1** is perceived to occur in preference to that of re-oxidation. This

observation mirrors the findings of Wildgoose *et al.* for $B(C_6F_5)_3$ which, under low scan rates (< 100 mV s^{-1}), displayed only a reduction peak.[44] However, at faster scan rates a small oxidation wave was observed in which the kinetics of decomposition were eventually outrun on the voltammetric timescale. The products of decomposition were subsequently identified to be the result of solvolysis by the CH_2Cl_2 solvent in which $[HClB(C_6F_5)_2]^-$, $[Cl_2B(C_6F_5)_2]^-$ and $[ClB(C_6F_5)_3]^-$ were observed by ^1H and ^{11}B NMR spectroscopy. The similarity between $B(C_6F_5)_3$ and **1**, with regards to spectroscopic and reactivity studies, would suggest that **1** also decomposes *via* a similar solvent induced pathway.

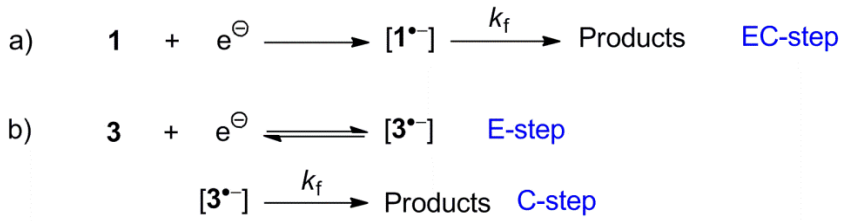

Figure 2.16. a) Postulated EC mechanism for reduction of **1** b) Quasi-reversible reduction of **3** (E-step). EC mechanism still active though at a considerably lower rate.

In the case of **3**, a quasi-reversible one-electron reduction (E step) is in operation in which the EC mechanism is active (ratio of oxidative to reductive current less than 1:1) at a considerably lower rate. In contrast to **1** and $B(C_6F_5)_3$, an oxidative wave is witnessed over all scan rates in which the kinetics of decomposition are progressively outrun as the scan rate increases.

Digital simulations of the experimentally observed cyclic voltammetric data enabled extraction of the kinetic and thermodynamic parameters. The thermodynamic standard potentials, E^o, of **1** and **3** (–1.61 (1) and –1.75 (1) V respectively) were comparable to those reported for $B(C_6F_5)_3$ (–1.75 (1) V), whilst the pseudo-first order rate constants for decomposition of radical anions ($\mathbf{1}^{\bullet-}$) and ($\mathbf{3}^{\bullet-}$) in CH_2Cl_2 were markedly different (10 (1) s^{-1} and 0.03 (1) s^{-1}) (Table 2.2). This difference reflects the increased shielding of the boron centred radical-anion upon introduction of an *ortho*-CF_3 substituent, and a similar buttressing effect has also been reported for the series $B(C_6F_5)_{3-n}(C_6Cl_5)_n$ (n = 1-3). Here, the larger size of *ortho* Cl substituents inhibited bimolecular decomposition pathways.[1a]

Table 2.2. Electrochemical parameters for the voltammetric reduction of **1** and **3**. Values in parentheses reflect estimated standard uncertainties.

	1	**3**
E_0/V *vs* $Cp_2Fe^{0/+}$ (V)	−1.61 (1)	−1.75 (1)
k_f (s^{-1})	10 (1)	0.03 (1)

These findings support the NMR spectral data and Lewis acidity measurements; CF_3 substituents impart a strong degree of electron deficiency on the boron centre, yet the three flanking *ortho* CF_3 substituents of **3** substantially shield the boron centre from decomposition pathways.

2.11 Reactivity of 3 with H_2

The electrochemical properties of **3**, coupled with contrasting Lewis acidity measurements, are strongly reminiscent of the electron-deficient *tris*(aryl)boranes, $B(C_6F_5)_{3-n}(C_6Cl_5)_n$ (n = 1-3), in which direct solution voltammetry suggested a concomitant increase of electrophilicity with each C_6Cl_5 group. The larger Hammett parameter for Cl *vs* F supported the notion that a C_6Cl_5 group is substantially more electron withdrawing than C_6F_5. In contrast, Gutmann-Beckett and Childs' methods illustrated a reduction in Lewis acidity, where the steric enhancement of each C_6Cl_5 group progressively discouraged complexation; the acceptor properties of $B(C_6Cl_5)_3$ could not be determined by either technique. In 2012, Gabbai and coworkers, intrigued by this lack of Lewis acidity, documented $B(C_6Cl_5)_3$, somewhat paradoxically, to be a potent Lewis acid with a preference for small donors such as fluoride and sterically non-restrictive organic Lewis bases.[45] $B(C_6Cl_5)_3$, upon combination with a phosphine base in THF, forms an FLP capable of H_2 activation at elevated temperature (90 ºC, 40-56 Hours) (Figure 2.31).[46] Evidently this Lewis acid, although possessing a strong degree of steric bulk, is not precluded from FLP style reactivity and therefore it is conceivable that **3**, in combination with a sterically bulky Lewis base, could activate H_2.

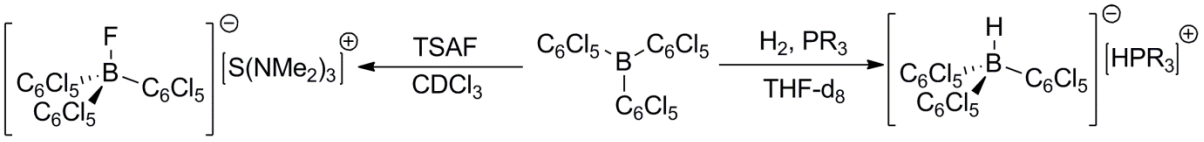

Figure 2.17. Fluoride abstraction by $B(C_6Cl_5)_3$ upon addition of TSAF (*tris*(dimethylamino)sulfonium difluorotrimethylsilicate; $[S(NMe_2)_3]^+[F_2Si(CH_3)_3]^-$), and H_2 activation by $B(C_6Cl_5)_3/PR_3$ FLP (R = Et, Cy, *n*Bu, *t*Bu and *p*Tol).

Combination of **3** with TMP (1:1) in CD_2Cl_2 generated an FLP, as evinced by unchanged resonances in ^1H, ^{19}F and ^{11}B NMR spectra relative to the species in isolation. Admission of H_2 (1 atm) at room temperature did not afford the products of H_2 cleavage, and accordingly CD_2Cl_2 was substituted for a higher boiling solvent (THF-d_8; b.p. 66ºC). Following H_2 admission, solutions were heated at 100 ºC for several days which once again displayed no evidence for H_2 cleavage. Likewise, substitution of TMP for a variety of phosphine bases gave an identical outcome. Finally, to test whether hydrido borate formation was indeed attainable, a solution of **3** was treated with the strong hydride donor $Li[HBEt_3]$ (1M in THF);[47] again no reaction of **3** was witnessed as evidenced by the ^{11}B NMR shift remaining unchanged (^{11}B = 73.6 ppm, $CDCl_3$). These findings reflect the inertness of **3** in which the bulk of the *ortho*-CF_3 renders the boron centre inaccessible to all donors tested.

2.12 Attempted synthesis of *tris*[3,4,5-*tris*(trifluoromethyl)phenyl)]borane; $BArF_{27}$

As a final investigation into the interplay between sterics and electronics the synthesis of a novel *tris*[3,4,5-tri(fluoromethyl)phenylated borane ($BArF_{27}$) was targeted. This borane would benefit not only from two *meta*-CF_3 substituents but more importantly through inclusion of a *para*-CF_3 group [$\sigma_{p:}$ 0.540 (CF_3) *vs*. 0.062 (F)]. Following successful synthesis a series of trifluoromethylphenyl substituted boranes would be achieved in which these permutations had been investigated for role in preventing protonolysis and permitting H_2 cleavage.

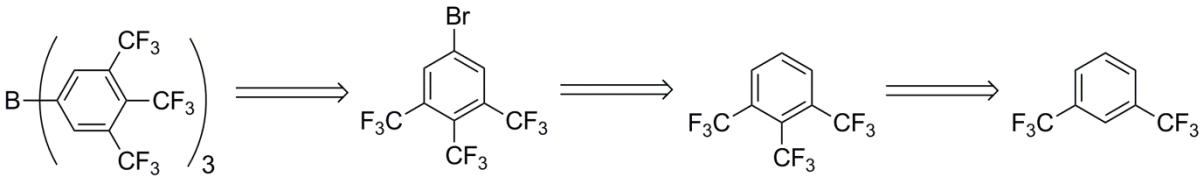

Figure 2.18. Retrosynthetic strategy for the synthesis of *tris*(trifluoromethyl)phenylated borane, **4**, from the bromo precursor.

Generation of the target borane was envisaged to occur *via* formation of an organolithium lithium or Grignard reagent from metal-halogen exchange with a 3,4,5-$(CF_3)_3C_6H_2Br$ precursor, followed by metathesis with BX_3 (Figure 2.32). A low-yielding synthesis of 3,4,5-$(CF_3)_3C_6H_2Br$ has been previously reported by Lukamanov and co-workers from the non-selective bromination of 1,2,3-*tris*(trifluoromethyl)benzene.[48] Here, a mixture of 1-bromo *tris*(trifluoromethyl)benzene and 1,5-dibromo-2,3,4-*tris*(trifluoromethyl)benzene were also obtained which, due to their similar boiling points, could not be separated (Figure 2.33).

Consequently, no data was provided for the characterisation of 3,4,5-$(CF_3)_3C_6H_2Br$. In addition, the 1,2,3-*tris*(trifluoromethyl)benzene starting material was generated under harsh conditions *via* a highly toxic fluorination of either 1,3-$(CO_2H)_2C_6H_3(CF_3)$ or 1,2,3-$(CO_2H)_3C_6H_3$ using SF_4, a highly corrosive gas which liberates toxic HF upon exposure to moisture (Figure 2.33).[49] An alternate, high yielding route to 3,4,5-$(CF_3)_3C_6H_2Br$ was therefore required which would avoid this hazardous step (Figure 2.34).

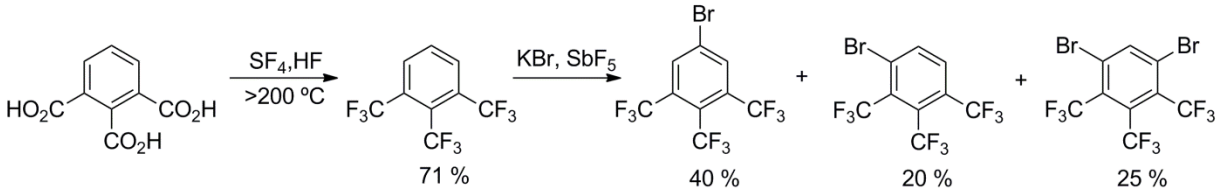

Figure 2.19. Reported synthetic procedure to **5**

A new facile synthesis was devised involving the initial generation of 2-iodo-1,3-*bis*(trifluoromethyl)benzene as described by Schlosser *et. al*.[50] In this reaction sequence a low temperature regioselective metallation of the commercially available 1,3-*bis*(trifluoromethyl)benzene is achieved with the extremely basic *n*BuLi/*t*BuOK (LIC-KOR) mixture which is presumed to contain a potent '*n*BuK' reagent that metalates at the most acidic position. Accordingly, electrophilic trapping with I_2 afforded 2-iodo-1,3-*bis*(trifluoromethyl)benzene (**4**) in high yield (80%).

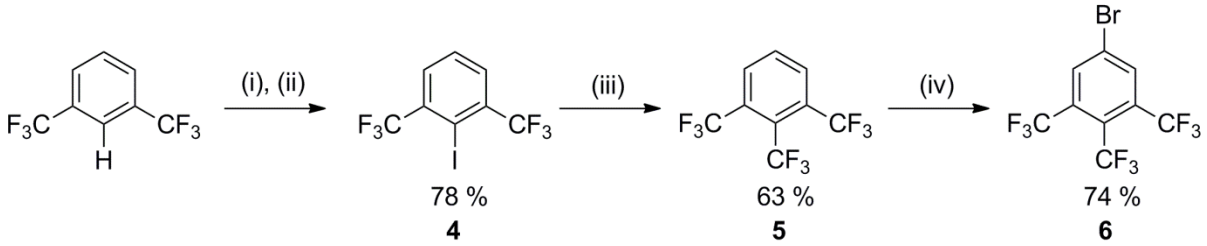

Figure 2.20. Synthesis of 3,4,5-$(CF_3)_3C_6H_2Br$ (**5**); (i) *n*BuLi, KO*t*Bu (LIC-KOR), THF/Et_2O (1:1), –78 ºC; (ii) I_2, –78 ºC to RT; (iii) CuBr, KF, CF_3SiMe_3, NMP (N-methyl-2-pyrrolidone), DMF, (–5 ºC to RT, 12 h); (iv) DBDMH (1,3-dibromo-5,5-dimethylhydantoin), H_2SO_4 (0ºC to RT, 12 h).

New methods to introduce trifluoromethyl groups onto organic substrates have developed apace due to the profound effect these groups have on the physical and chemical properties of organic molecules, such as improved metabolic stability and higher lipophilicity.[51] In 2007, Kolomeitsev and co-workers reported the convenient pertrifluoromethylation of hexaiodobenzene (C_6I_6) by use of pregenerated 'CF_3Cu' under mild reaction conditions.[52] In this strategy a solution stable 'CF_3Cu' species is formed from the reaction of Ruppert's reagent (CF_3SiMe_3) with basic KF and stabilised by N-methyl-2-pyrrolidone (NMP).

Gratifyingly, the reaction of **4** with 'CF_3Cu' afforded 1,2,3-*tris*(trifluoromethyl)benzene (**5**) in moderately good yield (63 %) following work up.

Dmowski and Maciejewska have reported a regioselective and quantitative bromination of the electron deficient 2,6-*bis*(trifluoromethyl)benzoic acid with 1,3-dibromo-5,5-dimethylhydantoin (DBDMH) to afford 4-bromo-2,6-*bis*(trifluoromethyl)benzoic acid (Figure 2.35).[53] CF_3 and CO_2H are comparable in their ability to draw substantial electron density away from the π-system [$\sigma_{p:}$ 0.540 (CF_3) *vs.* 0.450 (CO_2H)], and thus DBDMH, a particularly selective reagent for electron deficient aryl systems[54] was used. Here, the influence of two equivalent CF_3 substituents in the 2,6-position overrides the directing effects of the carboxylic acid to selectively brominate in the 4-position. Likewise, it was anticipated the two equivalent CF_3 substituents in **5** should favour the generation of 3,4,5-$(CF_3)_3C_6H_2Br$ over other isomers. In contrast to the non-regioselective bromination reported by Lukamanov, 3,4,5-$(CF_3)_3C_6H_2Br$ **6** was obtained cleanly in good yield (74 %) following bromination of **5** with DBDMH in H_2SO_4. **6** has been fully characterised by ^1H, ^{13}C and ^{19}F NMR spectroscopy. Notably, the considerably downfield shift of the *ortho*-protons (δ = 8.22 ppm, $CDCl_3$) support a highly electron deficient aryl ring.

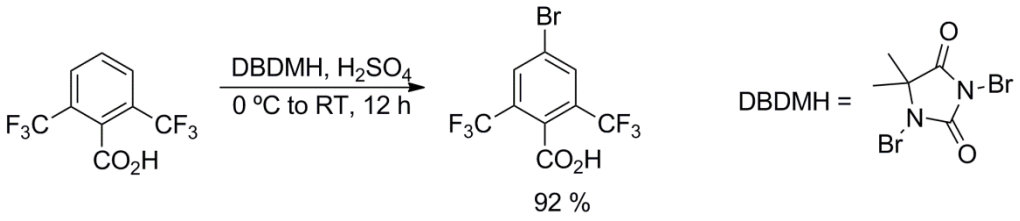

Figure 2.21. Bromination of *bis*(trifluoromethyl)benzoic acid with 1,3-dibromo-5,5-dimethylhydantoin (DBDMH).[53]

Upon acquiring key intermediate **6**, synthesis of $BArF_{27}$ was attempted in the same fashion as described for **3**; formation of the organolithium reagent *via* addition of *n*BuLi in Et_2O at –78 ºC, followed by rapid addition of BCl_3. However, employing this reagent led to the formation of borate Li[B(*n*Bu)$_4$] (^{11}B NMR: δ = –9.1 ppm, C_6D_6) concomitant with unassignable signals in the ^{19}F NMR spectra. Extensive modification to include *t*BuLi, higher temperatures (–78 ºC to RT), non-polar solvent (hexane) or prolonged reaction time (1-2 hours) failed to prevent formation of the alkylborate; attempts to trap the targeted Li[3,4,5-$(CF_3)_3C_6H_2$] reagent with TMSOTf were also ineffective. Presumably, Li[3,4,5-$(CF_3)_3C_6H_2$] formation is too slow to compete with residual *n*BuLi in the metathesis with BCl_3. Alternate routes involving a Knöchel type metal-halogen exchange in either Et_2O or THF followed by addition of $BF_3{\cdot}OEt_2$, were unable to deliver $BArF_{27}$; Attempts to generate the Grignard *via* metal-

halogen exchange using *i*PrMgCl afforded unexpectedly unreacted **6** as evidenced by resolvable ^{19}F and ^{1}H NMR signals (^{19}F NMR: δ = –57.4 [3,5-$(CF_3)_2$], –54.3 ppm [4-(CF_3)]; ^{1}H NMR: δ = 8.22 ppm, $CDCl_3$). In light of these findings the synthesis of novel electron deficient *tri*alkyl Lewis acids became the subject for future study.

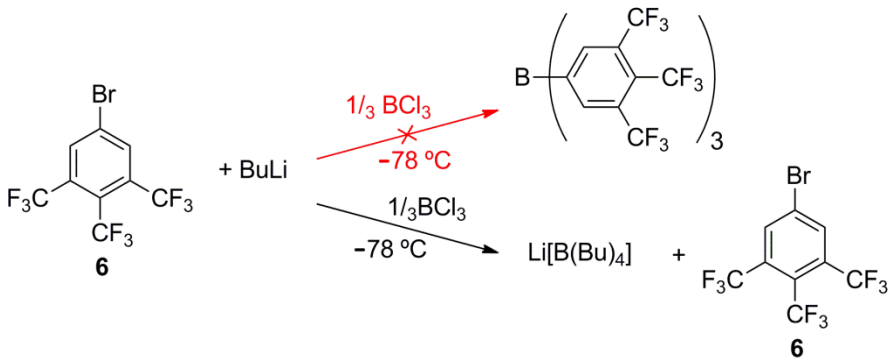

Figure 2.22. Attempted synthesis of **4**.

2.13 Conclusion

Like the ubiquitous perfluoroaryl rings, (trifluoromethyl)phenyl groups invoke considerable electrophilicity at the boron centre. In this regard, *tris*[3,5-*bis*(trifluoromethyl)phenyl]borane (**1**), has been synthesised on a practical scale for the first time. According to the Gutmann-Beckett method it is a more powerful Lewis acid than $B(C_6F_5)_3$, and yet reversibly forms the dative complex **1**·OH_2. In contrast to $B(C_6F_5)_3$·OH_2, H_2O can be removed from **1**·OH_2 under vacuum or through addition of 3 Å molecular sieves in CH_2Cl_2 solution. **1** forms a FLP in the presence of TMP which reacts rapidly with H_2 to form the anion [μ-$H(BArF_{18})_2]^-$, which has been crystallographically characterised. This is the first example of a bridging borohydride resulting from FLP-mediated H_2 heterolysis. Interestingly, this reaction also proceeds in Et_2O, and is believed to be an example of a system operating on the classical/frustrated Lewis pair borderline. However, degradation in the presence of H_2O occurs above 60 °C and is attributed to the strong Lewis acidity of **1**. These observations led to the convenient synthesis of *tris*[2,4-*bis*(trifluoromethyl)phenyl]borane (**3**) in which the installed *ortho*-CF_3 groups secure sufficient steric shielding to preclude H_2O binding.

Electrochemical studies reveal **1** and **3** to have a comparable electron affinity to $B(C_6F_5)_3$ in which the buttressing effect of **3** limits the decomposition of $\mathbf{3}^{\bullet-}$ *via* solvolysis. While electrochemistry provides a physio-chemical measure of the electron affinity of the boron acceptor site, it does not consider the steric cost of B sp^2-sp^3 rehybridisation upon donor acceptance. Consequently, while **1** retains the Lewis acidity necessary to undergo FLP

mediated H_2 cleavage, the severe steric congestion of **3** quenches all measurable Lewis acid and presumably the potential to undergo H_2 heterolysis.

Consequently, the synthesis of a novel *tris*[3,4,5-*tris*(trifluoromethyl)phenyl)]borane ($BArF_{27}$) was targeted. A high yielding route to the bromo precursor (**6**) was achieved which importantly avoids use of the hazardous fluorination chemistry which plagued previous attempts. Subsequent metathesis with a boron trihalide was not observed, the strong electron withdrawing power of three adjacent trifluoromethyl substituent is reasoned to render the lithium precursor poorly nucleophilic.

2.14 References

[1] (a) A. E. Ashley, T. J. Herrington, G. G. Wildgoose, H. Zaher, A. L. Thompson, N. H. Rees, T. Kraemer, D. O'Hare, *J. Am. Chem. Soc.* **2011**, *133*, 14727-14740; (b) M. Ullrich, A. J. Lough, D. W. Stephan, *Organometallics* **2010**, *29*, 3647-3654; (c) D. Chen, Y. Wang, J. Klankermayer, *Angew. Chem. Int. Ed.* **2010**, *49*, 9475-9478; (d) Y. Liu, H. Du, *J. Am. Chem. Soc.* **2013**, *135*, 6810-6813.

[2] (a) G. C. Welch, T. Holtrichter-Roessmann, D. W. Stephan, *Inorg. Chem.* **2008**, *47*, 1904-1906; (b) G. C. Welch, L. Cabrera, P. A. Chase, E. Hollink, J. D. Masuda, P. R. Wei, D. W. Stephan, *Dalton Trans.* **2007**, 3407-3414.

[3] K. Takeuchi, L. J. Hounjet, D. W. Stephan, *Organometallics* **2013**, *32*, 4469-4472.

[4] W. E. Piers, G. J. Irvine, V. C. Williams, *Eur. J. Inorg. Chem.* **2000**, 2131-2142.

[5] *CRC Handbook Of Chemistry and Physics, Internet Version* (Ed.: D. R. Lide), CRC Press, Boca Raton, FL, **2005**, pp. 1455.

[6] C. Bergquist, B. M. Bridgewater, C. J. Harlan, J. R. Norton, R. A. Friesner, G. Parkin, *J. Am. Chem. Soc.* **2000**, *122*, 10581-10590.

[7] A. E. Ashley, A. L. Thompson, D. O'Hare, *Angew. Chem. Int. Ed.* **2009**, *48*, 9839-9843.

[8] D. S. McDaniel, H. C. Brown, *J. Org. Chem.* **1958**, *23*, 420-427.

[9] I. Krossing, I. Raabe, *Angew. Chem. Int. Ed.* **2004**, *43*, 2066-2090.

[10] (a) H. Kobayashi, *J. Fluorine Chem.* **2000**, *105*, 201-203; (b) H. Nishida, N. Takada, M. Yoshimura, T. Sonoda, H. Kobayashi, *Bull. Chem. Soc. Jpn.* **1984**, *57*, 2600-2604.

[11] (a) G. Erker, *Dalton Trans.* **2005**, 1883-1890; (b) W. E. Piers, T. Chivers, *Chem. Soc. Rev.* **1997**, *26*, 345-354.

[12] (a) W. V. Konze, B. L. Scott, G. J. Kubas, *Chem. Commun.* **1999**, 1807-1808; (b) S. C. Bourke, M. J. MacLachlan, A. J. Lough, I. Manners, *Chem. Eur. J* **2005**, *11*, 1989-2000.

[13] C. Elschenbroich, A. Salzer, *Organometallics: A Concise Introduction, Second, Revised Edition*, Wiley-VCH Verlag GmbH, Weinheim, **1992**, pp. 1-508.

[14] A. G. Massey, A. J. Park, F. G. A. Stone, *Proc. Chem. Soc., London* **1963**, 212.

[15] (a) K. Fujiki, M. Kashiwagi, H. Miyamoto, A. Sonoda, J. Ichikawa, H. Kobayashi, T. Sonoda, *J. Fluorine Chem.* **1992**, *57*, 307-321; (b) M. Brookhart, B. Grant, A. F. Volpe, *Organometallics* **1992**, *11*, 3920-3922.

[16] N. A. Yakelis, R. G. Bergman, *Organometallics* **2005**, *24*, 3579-3581.

[17] T. J. Herrington, A. J. W. Thom, A. J. P. White, A. E. Ashley, *Dalton Trans.* **2012**, *41*, 9019-9022.

[18] C. Lorber, R. Choukroun, L. Vendier, *Organometallics* **2008**, *27*, 5017-5024.
[19] A. Bondi, *J. Phys. Chem.* **1964**, *68*, 441-451.
[20] A. G. Massey, A. J. Park, *J. Organomet. Chem.* **1966**, *5*, 218-225.
[21] (a) R. F. Childs, D. L. Mulholland, A. Nixon, *Can. J. Chem.* **1982**, *60*, 801-808; (b) M. F. Lappert, *J. Chem. Soc.* **1961**, 817-822; (c) M. F. Lappert, *J. Chem. Soc.* **1962**, 542-548; (d) U. Mayer, V. Gutmann, W. Gerger, *Monatsh. Chem.* **1975**, *106*, 1235-1257; (e) V. Gutmann, *Coord. Chem. Rev.* **1976**, *18*, 225-255.
[22] M. A. Beckett, G. C. Strickland, J. R. Holland, K. S. Varma, *Polymer* **1996**, *37*, 4629-4631.
[23] G. J. P. Britovsek, J. Ugolotti, A. J. P. White, *Organometallics* **2005**, *24*, 1685-1691.
[24] F. Focante, P. Mercandelli, A. Sironi, L. Resconi, *Coord. Chem. Rev.* **2006**, *250*, 170-188.
[25] H. Li, A. J. A. Aquino, D. B. Cordes, F. Hung-Low, W. L. Hase, C. Krempner, *J. Am. Chem. Soc.* **2013**, *135*, 16066-16069.
[26] (a) D. Holschumacher, T. Bannenberg, C. G. Hrib, P. G. Jones, M. Tamm, *Angew. Chem. Int. Ed.* **2008**, *47*, 7428-7432; (b) P. A. Chase, D. W. Stephan, *Angew. Chem. Int. Ed.* **2008**, *47*, 7433-7437; (c) E. L. Kolychev, T. Bannenberg, M. Freytag, C. G. Daniliuc, P. G. Jones, M. Tamm, *Chem. Eur. J.* **2012**, *18*, 16938-16946; (d) B. Ines, S. Holle, R. Goddard, M. Alcarazo, *Angew. Chem. Int. Ed.* **2010**, *49*, 8389-8391.
[27] T. A. Rokob, I. Bako, A. Stirling, A. Hamza, I. Papai, *J. Am. Chem. Soc.* **2013**, *135*, 4425-4437.
[28] T. A. Rokob, A. Hamza, I. Papai, *J. Am. Chem. Soc.* **2009**, *131*, 10701-10710.
[29] S. R. Boss, M. P. Coles, V. Eyre-Brook, F. Garcia, R. Haigh, P. B. Hitchcock, M. McPartlin, J. V. Morey, H. Naka, P. R. Raithby, H. A. Sparkes, C. W. Tate, A. E. H. Wheatley, *Dalton Trans.* **2006**, 5574-5582.
[30] V. Sumerin, F. Schulz, M. Nieger, M. Leskela, T. Repo, B. Rieger, *Angew. Chem., Int. Ed.* **2008**, *47*, 6001-6003.
[31] (a) H. Zaher, A. E. Ashley, M. Irwin, A. L. Thompson, M. J. Gutmann, T. Kraemer, D. O'Hare, *Chem. Commun.* **2013**, *49*, 9755-9757; (b) F. Schulz, V. Sumerin, S. Heikkinen, B. Pedersen, C. Wang, M. Atsumi, M. Leskela, T. Repo, P. Pyykko, W. Petry, B. Rieger, *J. Am. Chem. Soc.* **2011**, *133*, 20245-20257.
[32] Z. Lu, Z. Cheng, Z. Chen, L. Weng, Z. H. Li, H. Wang, *Angew. Chem., Int. Ed.* **2011**, *50*, 12227-12231.
[33] L. J. Hounjet, C. Bannwarth, C. N. Garon, C. B. Caputo, S. Grimme, D. W. Stephan, *Angew. Chem. Int. Ed.* **2013**, *52*, 7492-7495.
[34] (a) N. C. Deno, J. O. Turner, *J. Org. Chem.* **1966**, *31*, 1969-1970; (b) *CRC Handbook Of Chemistry and Physics, Internet Version* (Ed.: D. R. Lide), CRC Press, Boca Raton, FL, **2005**, pp. 1276-1286.
[35] S. J. Geier, D. W. Stephan, *J. Am. Chem. Soc.* **2009**, *131*, 3476-3477.
[36] T. R. O'Toole, J. N. Younathan, B. P. Sullivan, T. J. Meyer, *Inorg. Chem.* **1989**, *28*, 3923-3926.
[37] R. Gonzalez-Hernandez, J. Chai, R. Charles, O. Perez-Camacho, S. Kniajanski, S. Collins, *Organometallics* **2006**, *25*, 5366-5373.
[38] A. Y. Timoshkin, G. Frenking, *Organometallics* **2008**, *27*, 371-380.
[39] S. M. Cornet, K. B. Dillon, C. D. Entwistle, M. A. Fox, A. E. Goeta, H. P. Goodwin, T. B. Marder, A. L. Thompson, *Dalton Trans.* **2003**, 4395-4405.
[40] D. C. Bradley, I. S. Harding, A. D. Keefe, M. Motevalli, D. H. Zheng, *J. Chem. Soc* **1996**, 3931-3936.
[41] M. M. Olmstead, P. P. Power, *J. Am. Chem. Soc.* **1986**, *108*, 4235-4236.

[42] R. G. Compton, C. E. Banks, Editors, *Understanding Voltammetry, Second, Revised Edition*, Imperial College Press, London, **2007**, pp. 1-429.
[43] A. C. Testa, W. H. Reinmuth, *Anal. Chem.* **1961**, *33*, 1320-1324.
[44] E. J. Lawrence, V. S. Oganesyan, G. G. Wildgoose, A. E. Ashley, *Dalton Trans.* **2013**, *42*, 782-789.
[45] H. Zhao, J. H. Reibenspies, F. P. Gabbai, *Dalton Trans.* **2013**, *42*, 608-610.
[46] A. L. Travis, S. C. Binding, H. Zaher, T. A. Q. Arnold, J.-C. Buffet, D. O'Hare, *Dalton Trans.* **2013**, *42*, 2431-2437.
[47] H. C. Brown, Purdue Res. Found., Lafayette, IN, USA., **1979**, pp. 1-22.
[48] V. G. Lukmanov, L. A. Alekseeva, L. M. Yagupol'skii, *Zh. Org. Khim.* **1977**, *13*, 2129-2135.
[49] V. G. Lukmanov, L. A. Alekseeva, A. I. Burmakov, L. M. Yagupol'skii, *Zh. Org. Khim.* **1973**, *9*, 1019-1024.
[50] M. Schlosser, F. Mongin, J. Porwisiak, W. Dmowski, H. H. Buker, N. M. M. Nibbering, *Chem. Eur. J.* **1998**, *4*.
[51] O. A. Tomashenko, V. V. Grushin, *Chem. Rev.* **2011**, *111*, 4475-4521.
[52] A. Kutt, V. Movchun, T. Rodima, T. Dansauer, E. B. Rusanov, I. Leito, I. Kaljurand, J. Koppel, V. Pihl, I. Koppel, G. Ovsjannikov, L. Toom, M. Mishima, M. Medebielle, E. Lork, G.-V. Roeschenthaler, I. A. Koppel, A. A. Kolomeitsev, *J. Org. Chem.* **2008**, *73*, 2607-2620.
[53] W. Dmowski, K. Piasecka-Maciejewska, *Tetrahedron* **1998**, *54*.
[54] J. L. Leazer, R. Cvetovich, F. R. Tsay, U. Dolling, T. Vickery, D. Bachert, *J. Org. Chem.* **2003**, *68*, 3695-3698.

CHAPTER THREE

Synthesis & Characterisation of Electron Deficient *Tris*alkylboranes

3.1 Introduction

Trialkylboranes, such as BEt_3, are Lewis acids which are robust towards water and even strong mineral acids with the exception of HF.[1] The B-C bonds of BR_3 (R = alkyl) remain substantially robust in which hyperconjugation effects are observed between the C–H σ bonds and the empty boron p_z orbital.[2] These properties enable them to act as effective catalysts in aqueous based transformations such as radical cyclisation reactions of iodoacetals and iodoacetates,[3] in which protonolysis of BR_3 by alcohols and phenols requires temperatures in excess of 160 ºC. Conversely triarylboranes are activated towards electrophilic attack at the *ipso*-C of the aryl group. Furthermore the trialkylborohydrides $[HBR_3]^-$ are exceptionally powerful reducing agents which has led to their assignment as "superhydrides".[4] The reductions of hindered halides, epoxides, cyclic ethers, olefins, among others, are reported using these versatile agents.

Nonetheless, one of the crucial weaknesses of BR_3 is a perceived lack of Lewis acidity; Gutmann-Beckett measurements for BEt_3 (^{31}P (Δδ) = 11.6 ppm, C_6D_6) yield values less than half those observed for $B(C_6F_5)_3$ or BPh_3 [^{31}P (Δδ) = 29.8 and 23.6 ppm, C_6D_6)].[5] These observations translate experimentally; $B(C_6F_3)_3$ in combination with 2,6-dimethylpyridine forms a system capable of H_2 cleavage (Figure 2.16), while BEt_3 forms an inactive FLP.[6] The absence of H_2 reactivity here reflects a low cumulative acid-base strength.[7] In this regard, $[HBR_3]^-$ formation from H_2 remains limited to a small number of systems which utilise the transferring ability of a transition metal hydride or an exceptionally strong Lewis base. In 2006, Dubois reported a stepwise transition metal mediated process for generating $K[HBEt_3]$ from H_2, KO*t*Bu, and BEt_3.[8] Here, $HRh(dmpe)_2$ [dmpe = 1,2-*bis*(dimethylphosphinoethane)], generated from H_2 and $[Rh(dmpe)_2]^+$ in the presence of KO*t*Bu (pKa ~ 29 in DMSO),[9] possessed a thermodynamic hydride donor ability comparable to $Li[HBEt_3]$ (Figure 3.1).[10] Attempts to observe a one-pot conversion were hampered by strong adduct formation between BEt_3 and KO*t*Bu.

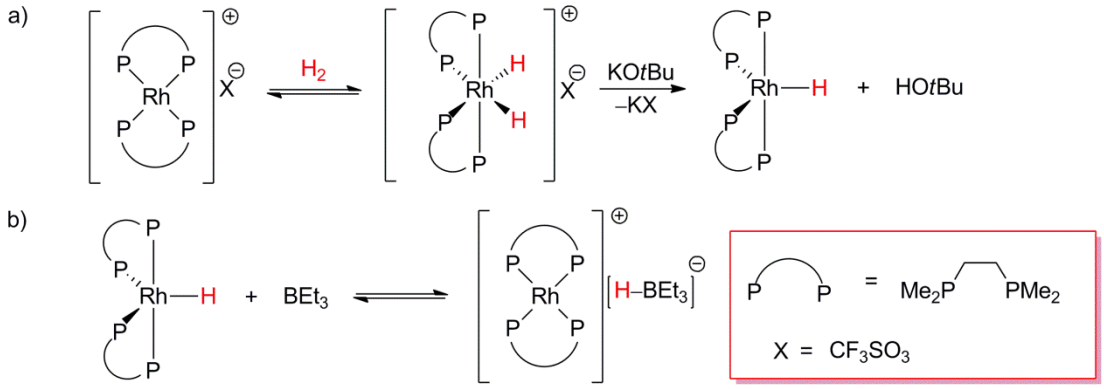

Figure 3.1. Stepwise (indirect) process for generating K[$HBEt_3$] from H_2 a) Oxidative addition of H_2 to form [$H_2Rh(dmpe)_2$][CF_3SO_3], followed by deprotonation to yield $HRh(dmpe)_2$ b) Hydride transfer from $HRh(dmpe)_2$ to BEt_3.

In 2010, Bercaw *et al.* reported the first metal-free system example which is capable of generating $[HBR_3]^-$ directly from H_2 cleavage.[11] Here the trialkylborane *t*$BuCH_2CH_2B(C_8H_{14})$ and strong phosphazene base *t*BuNP(pyrrolidinyl)$_3$ [*p*Ka ~ 28 in MeCN] form an FLP with sufficient cumulative Lewis acidity and basicity to favour cleavage. Lately, Krempner and coworkers have reported that BEt_3 in the presence of the highly basic zwitterionic carbanion $[C(SiMe_2OCH_2CH_2OMe)_3]Na$ (*p*Ka ~ 23 in DMSO) undergoes irreversible H_2 activation (Figure 3.2).[5b] Modification of trialkyl Lewis acids to include electron withdrawing substituents is unprecedented and, due to an enhanced Lewis acidity, would be expected to enable the use of weaker bases such as TMP and *t*Bu_3P in the FLP. Thus the design of electrophilic yet water stable trialkyl borane Lewis acids capable of H_2 cleavage were targeted. The results of this study are outlined in this chapter.

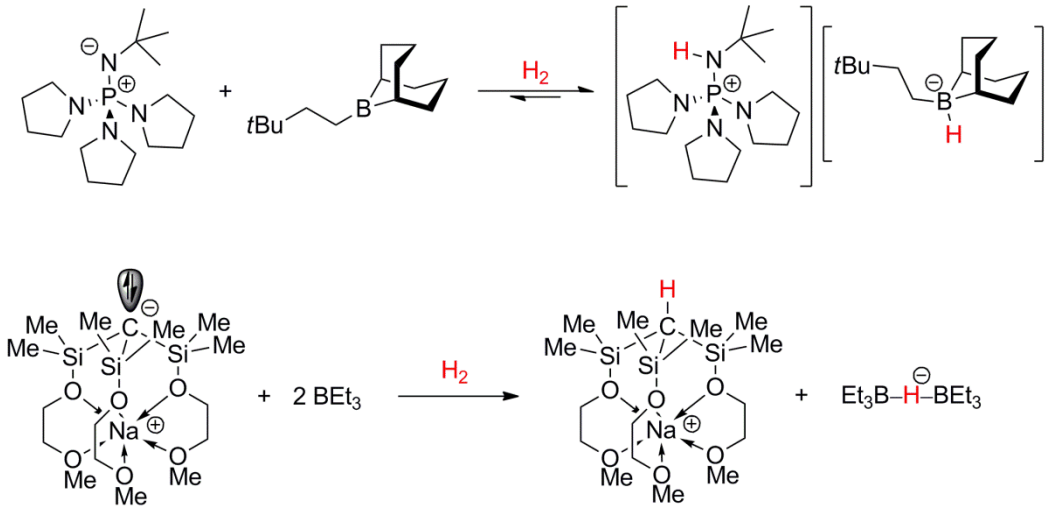

Figure 3.2. H_2 cleavage with a) *t*$BuCH_2CH_2B(C_8H_{14})$/*t*BuNP(pyrrolidinyl)$_3$ FLP and b) BEt_3/$[C(SiMe_2OCH_2CH_2OMe)_3]Na$ FLP.

3.2 *Tris*(fluoroalkyl)boranes

Perfluoroalkyl (R^F) ligands are known to dramatically affect the properties of their parent boron compounds (borates, amino boranes, amine-boranes, borane carbonyls) with respect to their non-fluorinated analogues. As discussed in Chapter 2, CF_3 substituents are comparable with Cl in their ability to remove electron density, while their effective steric demand is close to that of an *i*Pr substituent.[12] Uncoordinated *tris*(perfluoroalkyl)boranes of the type $B(C_nF_{2n+1})_3$ ($n \geq 1$) are yet to be reported; their propensity to undergo F^- abstraction has prohibited their isolation (*vide infra*).[12-13]

In contrast the tetrakis(trifluoromethyl)borate $[B(CF_3)_4]^-$ anion has been widely studied[14] and is synthesised from fluorination of the tetracyanoborate anion, $[B(CN)_4]^-$ with ClF_3 in anhydrous HF (Figure 3.3a).[15] $[B(CF_3)_4]^-$ forms stable salts with a variety of reactive cations e.g $[Co(CO)_5]^+$ and $[H(OEt_2)_2]^+$,[16] in which the intrinsic thermal, chemical and electrochemical stability of the B-CF_3 fragment has promoted application across a range of disciplines e.g. the trityl salt $[Ph_3C][B(CF_3)_4]$ may be employed as a cocatalyst for the Ziegler-Natta polymerisation of propylene.[16c]

Although $[B(CF_3)_4]^-$ is stable under reductive and oxidative conditions, this species will react with strong Brønsted or Lewis acids.[17] For instance, addition of H_2SO_4 to $K[B(CF_3)_4]^-$ results in its rapid conversion to a non-classical borane carbonyl $OC{\cdot}B(CF_3)_3$ (5σ-donation from CO only) (Figure 3.3b), which is reasoned mechanistically to proceed *via* a highly reactive $F_2C{=}B(CF_3)_3$ intermediate. Interestingly, the recorded IR ν(C=O) stretching band for $OC{\cdot}B(CF_3)_3$ (2269 cm^{-1})[17a] is the highest recorded for a borane carbonyl derivative and ascribed to the 'super' Lewis acidity of the parent borane, $B(CF_3)_3$.

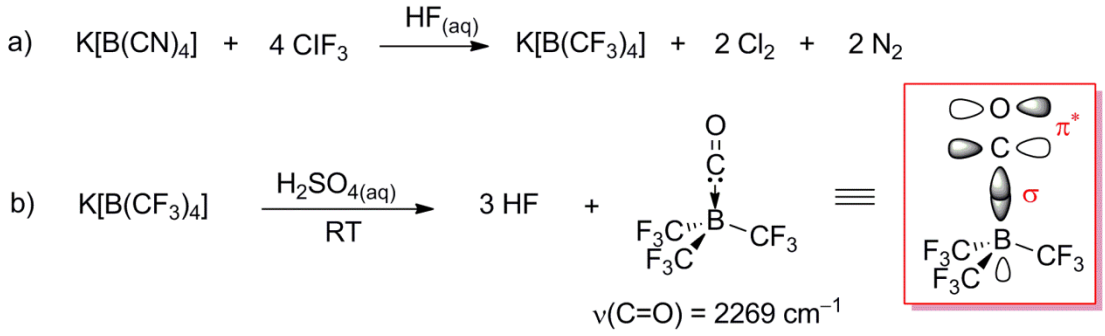

Figure 3.3. a) Synthesis of $[B(CF_3)_4]^-$ b) Generation of $OC{\cdot}B(CF_3)_3$

Under all investigated conditions (flash pyrolysis, matrix isolation techniques, etc), attempts to obtain direct experimental evidence for free $B(CF_3)_3$ from $OC{\cdot}B(CF_3)_3$ were unsuccessful;

mixtures containing BF_3 and non-branched perfluoroalkyldifluoroboranes $B(C_nF_{2n+1})F_2$ ($n \geq 2$) were obtained in preference.[18] Nevertheless, extensive experimental and theoretic studies by Willner and co-workers regarding the decomposition of $OC{\cdot}B(CF_3)_3$ favour initial dissociation of CO to yield the short lived $B(CF_3)_3$ borane. However, the inherent instability of this borane with respect to rearrangement of the B-C-F moiety is postulated to inhibit detection; a cascade of 1,2-fluoride shifts paired with perfluoroalkyl group migrations at the transient difluorocarbene complex afford a mixture of linear $B(C_nF_{2n+1})F_2$ ($n \geq 2$) (Figure 3.4). This rearrangement is initiated either by an *inter*molecular fluoride ion shift or *intra*molecular fluoride ion abstraction from one of the pendant CF_3 ligands. Follow-up studies on the analogous $OC{\cdot}B(C_2F_5)_3$ and $OC{\cdot}B(C_3F_7)_3$ complexes conclusively support these findings; CO dissociation is followed by rapid migration of α-fluorine.[19]

In contrast to the *tris*perfluoroalkyl boranes $B(C_nF_{2n+1})_3$, the monoperfluoroalkylfluoro boranes $B(C_nF_{2n+1})F_2$ ($n \geq 2$) are stable at room temperature. The fluoride affinity for these boranes provides a useful measure of their stability, in which F→B π donation from the pendant fluorines lowers their affinity (Table 3.1). However, $B(CF_3)F_2$ ($n = 1$) is unstable with respect to loss of CF_2 at RT, the activation barrier to isomerisation is half that calculated for the more stable $B(C_2F_5)F_2$.

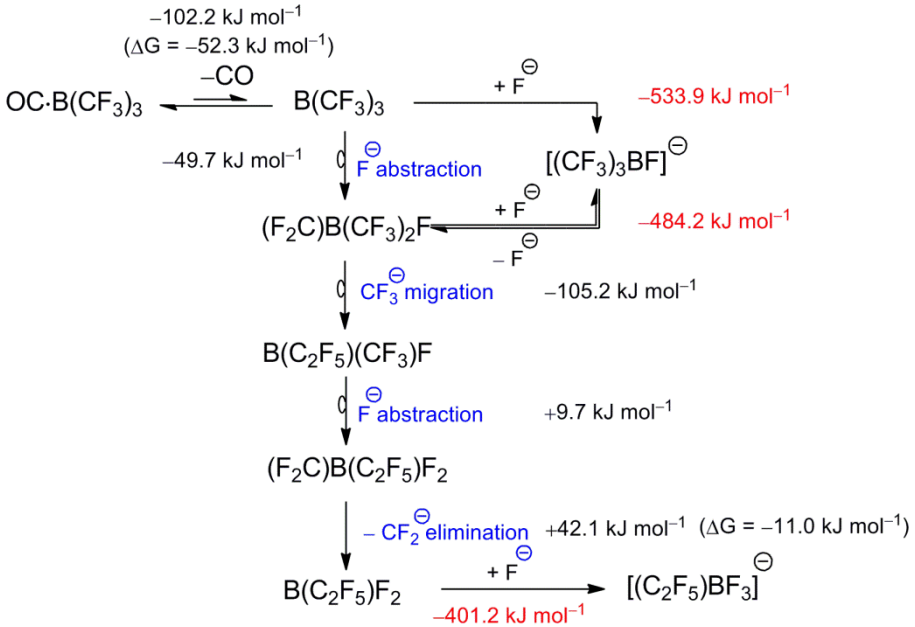

Figure 3.4. Postulated mechanism for the rearrangement of $OC{\cdot}B(CF_3)_3$ in anhydrous HF [ΔE(298 K)]. Energy: B3LYP/6-311+G(d). ZPC and thermal corrections: B3LYP/6-311G(d).[18]

In light of the instability of $B(CF_3)_3$, $OC{\cdot}B(CF_3)_3$ has become a useful synthon for the generation of boranes and borate ions which contain a '$B(CF_3)_3$' moeity. Nucleophiles may attack at the C atom of the carbonyl ligand to afford salts of the form $[B(CF_3)_3C(O)X]^-$ (X = F, Cl, Br, Me, OH, NH_2).[13] $[B(CF_3)_3CN]^-$ is synthesised via this route from the reaction of $OC{\cdot}B(CF_3)_3$ with $K[N(SiMe_3)_2]$; the recorded IR ν(C=N) stretch is the highest for a cyanoborate (2244 cm^{-1}), in support of the potent Lewis acidity of $B(CF_3)_3$.[20] For systems where the nucleophilic attack affords no stable addition product, displacement of the CO ligands may proceed *via* an S_N2 pathway resulting in species such as $B(CF_3)_3(XMe_2)$ (X = S, Se, Te).

Table 3.1. Calculated F^- affinity of selected perfluoroalkylboranes and BF_3. Energy: B3LYP/6-311+G(d). ZPC and thermal corrections: B3LYP/6-311G(d).[18]

	F^- Affinity	
	$\Delta H^‡$ (J mol^{-1} K^{-1})	**$\Delta G^‡$ (328K, kJ mol^{-1})**
BF_3	–332.2	–293.4
$B(CF_3)F_2$	–395.1	–349.5
$B(CF_3)_2F$	–463.3	–422.8
$B(CF_3)_3$	–536.4	–490.9
$B(C_2F_7)F_2$	–403.6	–362.1

3.3 $[HB(CF_3)_3]^-$

Caesium hydrido*tris*(trifluoromethyl)borate, $Cs[HB(CF_3)_3]$, remains the sole perfluoroalkylborohydride salt isolated to date, and is generated from an amino-borane complex.[21] The amino-borane complexes $R_2HN{\cdot}B(CF_3)_3$ (R= Et, Me), are accessible *via* the reaction sequence outlined in Figure 3.5.[22]

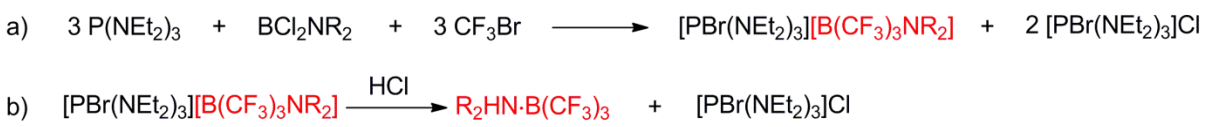

Figure 3.1. Synthesis of the aminoborane complexes $R_2HN{\cdot}B(CF_3)_3$ (R= Et, Me).

Of significance is the synthesis of $Et_2HN{\cdot}B(CF_3)_3$ which, under oxidative conditions, reacts with Br_2/KOH dissolved in H_2O to afford the ammonia complex $H_3N{\cdot}B(CF_3)_3$ (Figure 3.6);[23] the fate of the ethyl groups in this literature report was unknown. Subsequent, reaction of

$H_3N{\cdot}B(CF_3)_3$ with CsOH gave $Cs[B(CF_3)_3NH_2]$ which, upon addition of the aminating agent H_2NOSO_3H, yielded $Cs[HB(CF_3)_3]$ as the minor product (5 %).

This borohydride was highly stable at elevated temperature (300 ºC) and in concentrated HCl solutions, which is ascribed to the very low hydricity of the B–H unit due to the strong –I effects of the CF_3 substituents. Heating $Cs[HB(CF_3)_3]$ in D_2O, gave no evidence for H–D exchange as seen for $NaBH_4$,[24] although $Cs[HB(CF_3)_3]$ was reported to react with F_2, Cl_2 and Br_2 to furnish $[B(CF_3)_3X]^-$ (X = F, Cl, Br).[21] Decomposition, in the presence of aqua regia or anhydrous HF, was rationalised to proceed *via* formation of the highly reactive $B(CF_3)_3$ intermediate.[18]

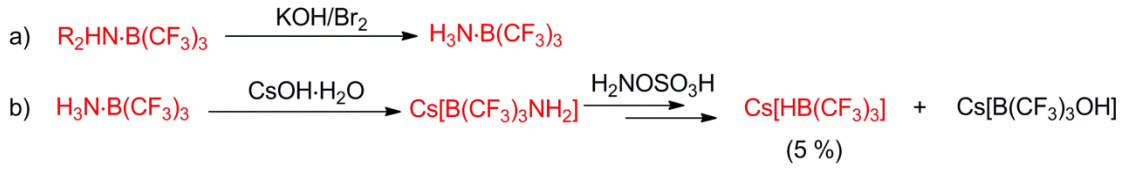

Figure 3.2. a) Synthesis of $H_3N{\cdot}B(CF_3)_3$ from the oxidation of $R_2HN{\cdot}B(CF_3)_3$ with KOH/Br_2 under aqueous conditions. b) Generation of $Cs[HB(CF_3)_3]$ starting from $Cs[B(CF_3)_3NH_2)]$ and H_2NOSO_3H. $Cs[B(CF_3)_3OH]$ identified as the major product (No yield reported).

Evidently, α-F atoms are incompatible with the formation of electron deficient *tris*alkylboranes. Enlightened by these observations, a *tris*fluoroalkylborane was targeted in which these groups were absent.

3.4 Fluoroorganometal reagents

The introduction of R^F groups onto Lewis acids (BCl_3, BBr_3, etc) has proven extremely challenging. Fluoroorganometal reagents R^FM possess much weaker carbon nuclephilicity than their alkyl counterparts, and therefore highly polar organometallic reagents (M = Mg, Li) are commonly employed to promote attack by the 'R^{F-}' synthon at the boron centre. In contrast to lithium alkyl derivatives, R^FLi reagents are thermally sensitive even at low temperatures. For example, CF_3Li has not been reported while higher analogues such as CF_3CF_2Li and $CF_3CF_2CF_2Li$ are stable only in ether-hexane mixtures kept below –70 ºC.[25] Furthermore, the perfluoroalkylating ability of these reagents $C_nF_{2n+1}Li$ (n > 2) is greatly determined by their mode of generation. For example, nC_3F_7I reacts with RLi (R = Me, Bu) to yield a poorly reactive complex $Li[(C_3F_7)_2I]$;[25c] the isolated salt does not react with $B(OMe)_3$ to yield $Li[B(C_3F_7)(OMe)_3]$, although poor yields of the borate were observed when the metallation was performed in *situ* with $B(OMe)_3$ (Figure 3.7a).[26] However, this approach

is incompatible with more potent electrophiles such as the boron trihalides BX_3 which would likely facilitate preferential attack of RLi (R = Me, Bu) over the weaker C_3F_7Li nucleophile. Alternatively, $Li[(C_3F_7)_2I]$ may be avoided altogether by use of *t*BuLi and the 1*H*-perfluoralkane C_3F_7H. Here, the more potent C_3F_7Li reagent afforded near quantitative conversion of $B(OMe)_3$ to $Li[B(C_3F_7)(OMe)_3]$ (Figure 3.7b).[26] In contrast to the capricious lithium compounds described, perfluoroalkyl magnesium reagents have been shown to demonstrate greater stability. For example, treatment of C_3F_7I with EtMgBr at –78 ºC in Et_2O furnished C_3F_7MgBr after a Knöchel type exchange which reacts quantitatively with $B(OMe_3)$ at –30 ºC to afford $[BrMg][B(C_3F_7)(OMe)_3]$. However, warming above this temperature resulted in decomposition to yield a mixture of $[BrMg][B(OMe)_4]$, $[BrMg][B(C_3F_7)(OMe)_3]$, and $B(C_3F_7)(OMe)_2$.[26]

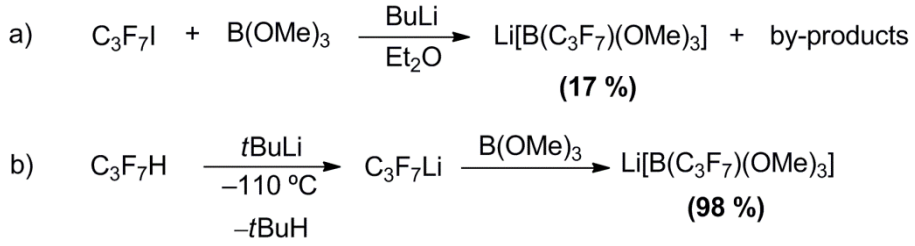

Figure 3.3. a) *In situ* generation of $Li[(C_3F_7)_2I]$ in the presence of $B(OMe)_3$ to yield $Li[B(C_3F_7)(OMe)_3]$ b) High yielding synthesis of $Li[B(C_3F_7)(OMe)_3]$ from generation of C_3F_7Li followed by sequential addition of $B(OMe)_3$.

3.5 Synthesis of 1,1,1,3,3,3-hexafluoropropyl iodide (7)

Clearly significant challenges surround the syntheses of a *tris*(fluoroalkyl)borane; the electron withdrawing effect of the fluoroalkyl groups severely limit the use of organometallic reagents with highly polar metals. The synthesis of *tris*(1,1,1,3,3,3-hexafluoroisopropyl)borane was envisaged to balance steric and electronic factors in which the power of two CF_3 substituents was reasoned to deliver potent electrophilicity at the boron centre *via* σ-electron withdrawing effects (Figure 3.8). Furthermore, syntheses of the 1,1,1,3,3,3-hexafluoropropyl halides C_3HF_6X (X = Br, I) have already been established and their existence as room temperature liquids (as opposed to the gases observed for lower homologues) was considered an important factor. Unfortunately 1,1,1,3,3,3-hexafluoropropane, although commercially available, is a gas at room temperature (b.p. –1.4 °C), strongly disfavours its use using standard laboratory techniques.

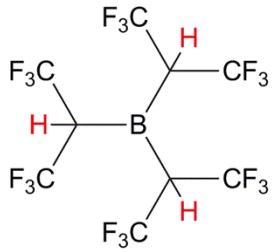

Figure 3.4. *Tris*(1,1,1,3,3,3-hexafluoroisopropyl)borane.

One established route to the hexafluoropropyl halides involves a simple bromination/iodination of the potassium salt of hexafluoroisobutyric acid.[27] This route, although simple, is limited by commercial availability of the acid which dictates synthesis from the highly toxic octafluoroisobutene.[28] To circumvent these issues, Hanack and Ullman have employed a simple nucleophilic substitution at the secondary carbon atom of nonafluorobutanesulfonate $C_3HF_6(OSO_2C_4F_9)$ (nonaflate) using NaI dissolved in acetylacetone.[29] Conveniently, this nonaflate could be prepared in CH_2Cl_2 from the reaction of hexafluoro-2-propanol with nonafluorobutanesulfonate fluoride and NEt_3 (Figure 3.9). Despite this relatively straightforward step, the final stage separation of the hexafluoropropyl iodide from the mother liquor became a major drawback. An exotic Spaltrohr distillation technique was detailed, which uses concentric grooved tubes to separate compounds with boiling points as close as 3 ºC.[30]

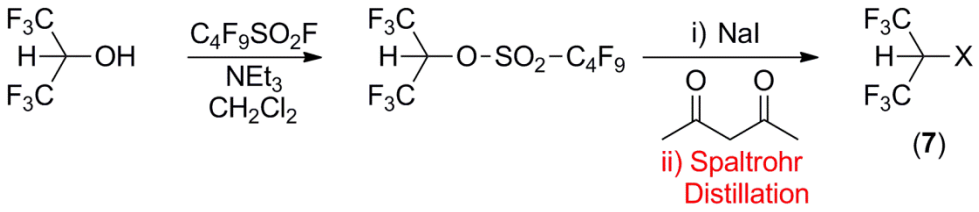

Figure 3.5. Synthesis of the hexafluoroisopropl halides *via* the reaction of the nonafluorobutanesulfonate $C_3HF_6(OSO_2C_4F_9)$ with NaI.

This specialised apparatus was not available, and attempts to substitute this technique with a cruder reduced pressure distillation was ineffective (in all instances, the hexafluoroisopropyl iodide could not be separated from the solvent). Acetylacetone is both a weak acid and electrophile which is reported to react with Grignard reagents to furnish *mono-* and *bis-*addition products.[31] Therefore this medium was incompatible with *in situ* generation of an organo metal salt from the fluoroalkyliodide. Recognising this issue, the reaction solvent was switched to benzene, a relatively inert aromatic which demonstrates limited reactivity with either *n*BuLi or *t*BuLi.[32]

Naturally, replacement of acetylacetone for this non-polar solvent led to insolubility of the NaI, however it was hoped elevated temperature (80 ºC) might promote heterogeneous reactivity. Disappointingly, nucleophilic substitution was not observed, and so NaI was substituted for the organic soluble tetrabutylammonium salt $[NBu_4]I$. Gratifyingly, an NMR scale reaction of the nonaflate with $[NBu_4]I$ in C_6D_6 furnished the hexafluoropropyl iodide, **7** and $[NBu_4][OSO_2C_4F_9]$ in complete conversion following six hours at 80 ºC (^{1}H NMR: δ = 3.42 ppm, $^3J_{HF}$ = 7 Hz; ^{19}F NMR: δ = 65.9 ppm, $^3J_{FH}$ = 7 Hz, C_6D_6). After scale up, difficulties arose with isolation of **7** from the aromatic and hydrocarbon soluble $[NBu_4][OSO_2C_4F_9]$ byproduct; several reduced pressure distillations afforded **7** as the major component although with significant amounts of $[NBu_4][OSO_2C_4F_9]$ impurity (Figure 3.10a).

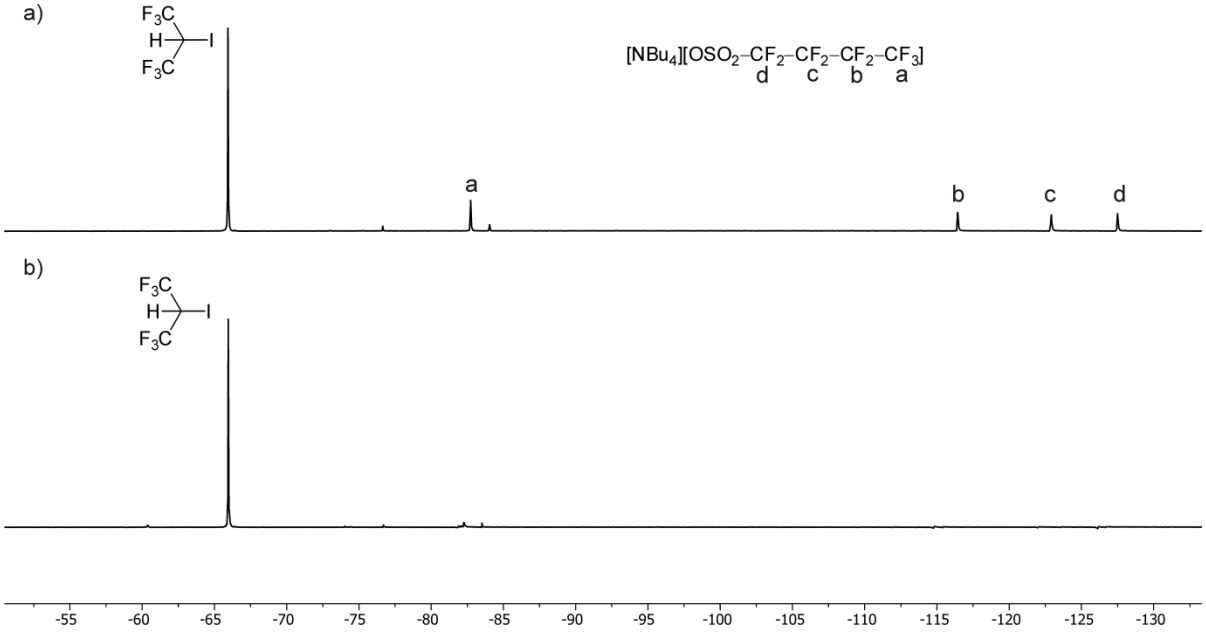

Figure 3.6. ^{19}F NMR spectra of **7** contaminated with $[NBu_4][OSO_2C_4F_9]$ (**a**) and free from such impurities employing a NaI/18-Crown-6 synthetic protocol (**b**).

18-crown-6 possess a high affinity for alkali metal ions, in particular K^+, and has been used to solubilise inorganic salts such as $K[MnO_4]$ in benzene.[33] The loss of ion pairing also leads to enhanced nucleophilicity, which might be expected to promote formation of **7**. Quantitative conversion to **7** was observed after heating solutions of the nonaflate with KI and 18-Crown-6 for a few hours at 80 ºC (Figure 3.10b). Advantageously, the $[K(18\text{-crown-6}][OSO_2C_4F_9]$ by-product could be precipitated with pentane (Figure 3.11). Follow up reduced pressure distillations could not separate **7** from C_6H_6 and therefore the concentration was determined *via* ^{19}F NMR integration against an internal $C_6Cl_5(CF_3)$ standard.

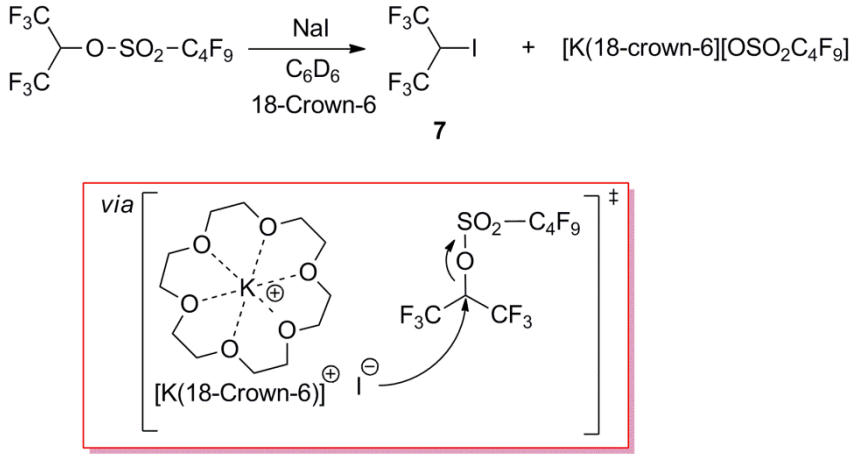

Figure 3.7. Modified preparation of **7** utilising 18-Crown-6 and KI.

3.6 Attempted synthesis of *tris*(1,1,1,3,3,3-hexafluoroisopropyl)borane

Taking into account the difficulties of adding perfluoroalkyl groups to electrophilic boranes, a range of halogen-metal exchange reactions were trialled in which the resultant mixtures were treated with BX_3 (X = F, Cl, Br). The treatment of **7** in Et_2O with *n*BuLi or *t*BuLi (< –80 ºC) led to the formation of $[B(nBu)_4]^-$ (^{11}B NMR: δ = –9.1 ppm), upon addition of $BF_3{\cdot}OEt_2$ or BX_3 (X = Cl, Br) B in which electrophilic trapping of the fluoroaryl lithium salt did not occur. Under all conditions, the warming of these solutions saw unassignable ^{19}F NMR signals in which lithiated **7** is anticipated to undergo decomposition *via* elimination of 1,1,1,3,3-pentafluoropropene and lithium fluoride (Figure 3.12).

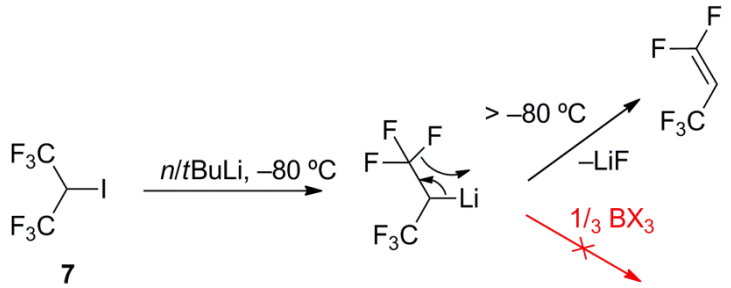

Figure 3.8. Decomposition of the lithium salt of **8** in preference to metathesis with BX_3

Modifications of this reaction procedure to include higher or lower temperatures and/or the introduction of a hexane co-solvent (as prescribed in other syntheses) were ineffective.[34] These findings appear commensurate with the instability of perfluoroalkyl lithium derivatives of the sort $C_nF_{2n+1}Li$ (n > 2), for which fast thermal decomposition occurs above –80 ºC. The products of decomposition for the very slowly forming perfluoroheptyllithium ($C_7F_{15}Li$) have been previously documented.[25c] Rapid β-elimination (> –80 ºC) yields a transient alkene

$C_5F_{11}CF{=}CF_2$ which in the presence of *n*BuLi is attacked to give *trans*-1-butyldecafluoro-1-heptene ($C_5F_{11}CF{=}CF_2C_4H_9$) (Figure 3.13). In the case of **8**, it would therefore appear reasonable to assume a similar decomposition pathway is in effect, in which hexafluoropropene reacts with *n*BuLi.

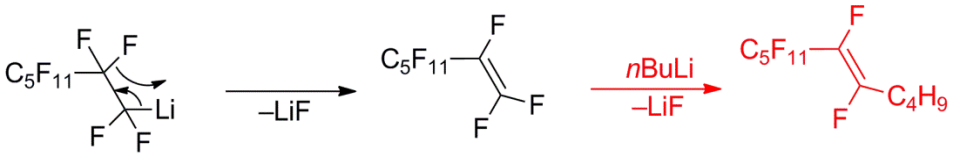

Figure 3.9. Decomposition of perfluoroheptyllithium ($C_7F_{15}Li$) into $C_5F_{11}CF{=}CF_2$. In the presence of excess RLi this olefin reportedly reacts to give ($C_5F_{11}CF{=}CF_2C_4H_9$).[25c]

Attempts to form the fluoroalkylborane *via* a Knöchel type metal-halogen exchange of **7** with *i*PrMgCl were also unproductive. Under various temperatures (–78ºC to RT), the addition of $BF_3{\cdot}OEt_2$ gave ^{19}F NMR signals of the starting material while the ^{11}B NMR spectrum displayed resonances associated with $BF_3{\cdot}OEt_2$ and B(*i*Pr$_3$) (^{11}B NMR: δ = 84 ppm, C_6D_6) . Thus, it was assumed the formation of the organo magnesium species was too slow to compete with the more nucleophilic *i*PrMgCl. Bubbles of gas, presumed to be $F_2C{=}C(CF_3)$ (b.p –21 ºC) were evolved when refluxing solutions of **7** in the presence of magnesium metal which was assumed to originate from facile β-elimination.

Since direct electrophilic substitution of the lithium and magnesium analogues of **7** failed to furnish the target borane, organozinc reagents were investigated. *Bis*perfluoroalkylzinc reagents and their solvates are considerably less reactive than their lithium and magnesium counterparts; the lower polarity of the R-M bond ($\chi_{Pauling}$ = 1.65) relative to Li ($\chi_{Pauling}$ = 0.98) or Mg ($\chi_{Pauling}$ = 1.32) greatly reduce their reactivity.[35] For example, heptafluoropropylzinc iodide stabilised by the strong donor dioxane does not react with aldehydes, ketones or non-fluorinated acyl chlorides.

However, when realising the room temperature stability of these species, the synthesis of $Zn(C_3F_6H)_2$ was investigated in which elevated temperature was hoped to promote metathesis. The reaction of perfluoroalkyl iodides in dioxane was previously reported to furnish a monoperfluoroalkylzinc compound while ligand exchange with $ZnEt_2$ afforded the *bis*-substituted perfluoroalkylzinc species (Figure 3.14).[36] In either strategy the resultant compounds were stabilised as solvates. For metathesis reactions of BX_3 with R–Zn, diminished polarity of the R–M bond may be offset through use of the strongly Lewis acidic BBr_3 (a stronger lewis acid than $BF_3{\cdot}OEt_2$ and BCl_3). However, the use of donors such as

dioxane or THF undergo are incomptable with BBr_3, undergoing C–O ether cleavage in its presence.[37] Thus, the synthesis of $Zn(C_3F_6H)_2$ was attempted *via* a ligand exchange reaction between **7** and $ZnEt_2$ performed in hexane at –78 ºC. Upon warming this solution, the ^{19}F NMR signal of **7** remained visible in which the ^1H NMR spectra displayed resonances associated with unreacted $ZnEt_2$ (^1H NMR: δ = 0.10 and 1.13 ppm, C_6D_6). Heating this solution overnight (60 ºC) led to multiple unassignable resonances in both the ^1H and ^{19}F NMR spectra. *In situ* addition of BBr_3 at temperatures of –78 ºC or higher produced no evidence for metathesis.

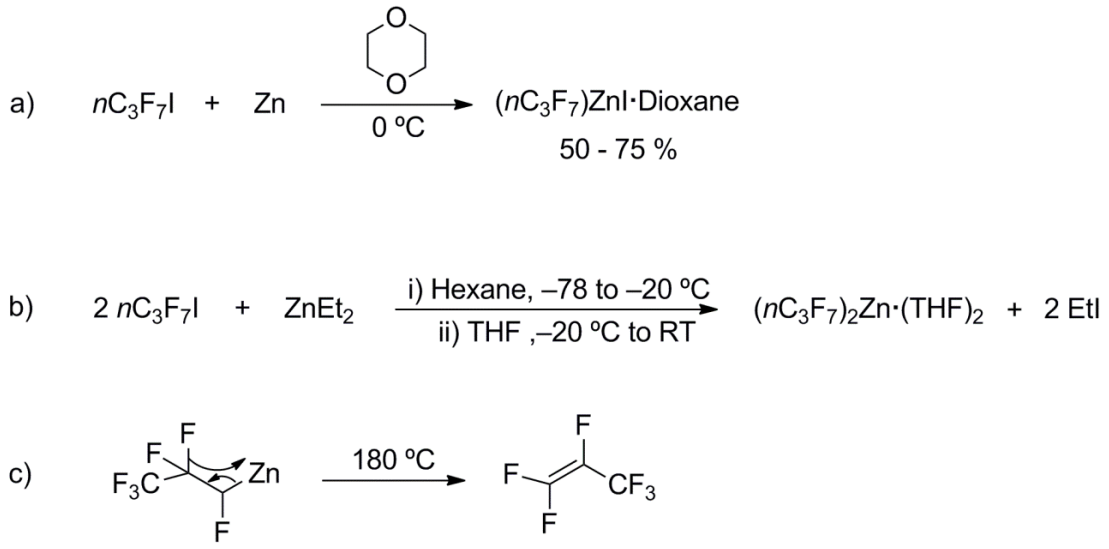

Figure 3.10. a) Synthesis of a monoperfluoroalkylzinc $(C_3F_7)ZnI$ stabilised in dioxane b) Metal halogen exchange of $ZnEt_2$ with C_3F_7I to form the *bis*perfluoroalkylzinc $(C_3F_7)_2Zn{\cdot}THF$ solvate. c) Greater thermal stability of the perfluoroalkyl ligand with respect to β- fluoride elimination.

In view of these exploits, **7** was perceived unattainable from the hexafluoroisopropyl halide precursor. Replacement of CF_3 for the more robust C_6F_5 aryl functionality became the target for the remainder of this chapter.

3.7 Synthesis of $B[CH(C_6F_5)_2]_3$

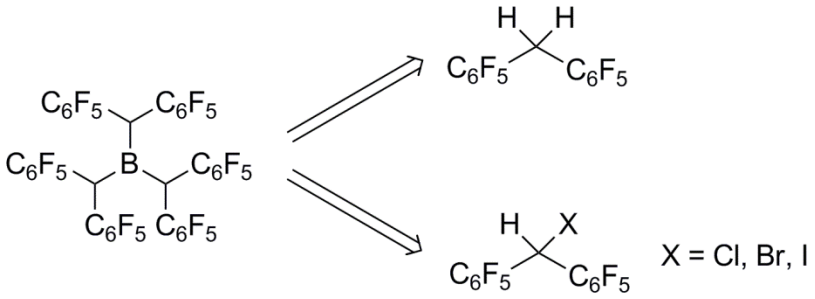

Figure 3.11. Retrosynthetic strategy for the synthesis of $B[CH(C_6F_5)_2]_3$

Retrosynthetic analyses (Figure 3.15) suggested $B[CH(C_6F_5)_2]_3$ to be accessible *via* deprotonation and metallation of *bis*(pentafluorophenyl)methane, or metal halogen exchange from the *bis*(pentafluorophenyl)methyl halide. For the former, a literature known Friedel-Crafts alkylation of pentafluorobenzene with CH_2Cl_2 in the presence of $AlCl_3$ furnishes *bis*(pentafluorophenyl)methane in good yield (76 % Figure 3.16a).[38] Although this one step preparation is straightforward, the high temperatures (150 ºC) and pressure (~50 atm) required lower its practicality. An alternative and relatively benign synthesis has exploited sulphone-stablised carbanions which react with fluorinated aromatic compounds to form diaryl-methyl sulphone derivatives.[39] Following treatment with aluminium amalgam, these derivatives were reduced to *bis*(pentafluorophenyl)methane, although in an unfavourable yield (18 %; Figure 3.16b).

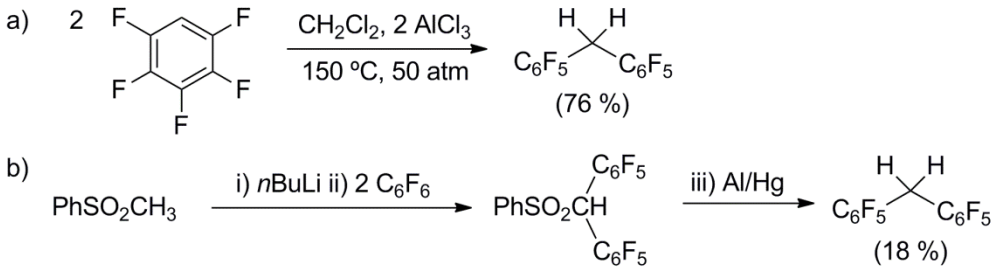

Figure 3.12. Synthesis of *bis*(pentafluorophenyl)methane *via* a) Friedel-Crafts alkylation of C_6F_5H[38] or b) sulphone stabilised carbanions.[39]

Accordingly a new higher yielding route to *bis*(pentafluorophenyl)methane was envisaged to proceed *via* generation of the literature-known decafluorobenzhydrol, which can be synthesised *via* addition of pentafluorophenyl magnesium bromide to ethylformate in Et_2O (Figure 3.17a).[40] Fry *et al.* have observed the reduction of benzophenones and benzhydrols by HI catalytically generated from a mixture of hypophosphorous acid (H_3PO_2) and I_2.[41]

Using an analogous route, the conversion of decafluorobenzhydrol to *bis*(pentafluorophenyl)methane (**8**; 74 %) was achieved after 3 days heating at 60 ºC (Figure 3.17b).

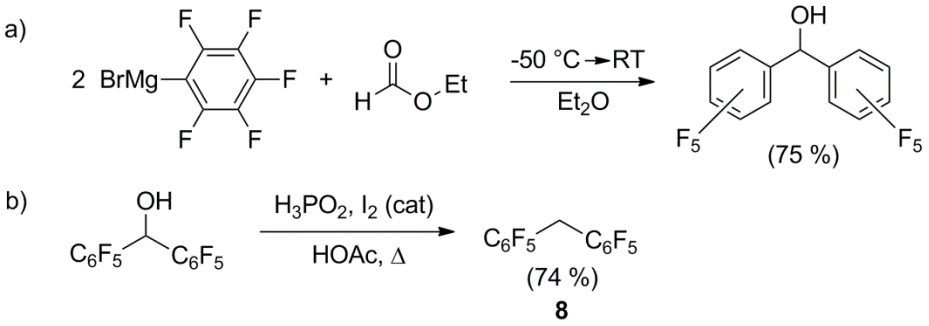

Figure 3.13. a) Synthesis of decafluorobenzahydrol from reaction of $BrMgC_6F_5$ and ethylformate in Et_2O.[40] b) Synthesis of **8**.

It was anticipated that metallation of **8** and subsequent addition to BX_3 should furnish the borane *via* a standard metathesis pathway. However, metallation of **8**, as described for **7,** presented an unusual challenge. Under various conditions generation of the lithium salt using *n*BuLi or *t*BuLi in Et_2O did not furnish the target borane following addition of BX_3 (X = F, Cl, Br); ^{19}F NMR and ^{11}B NMR spectra showed no evidence for B-C formation.

As described in Chapter 2 for the synthesis of 2-iodo-1,3-*bis*(trifluoromethyl)benzene (**4**), Schlosser *et al.* have developed powerfully basic LIC-KOR (*n*BuLi/*t*BuOK) mixtures, whose unprecedented reactivity delivers regioselective hydrogen/metal exchange for hydrocarbons in the low acidity range (*p*Ka 35-40).[42] Deprotonation of the arylalkanes toluene and diphenylmethane have previously furnished resonance-stabilised organometallic species with a characteristic vivid red colour. Given these reports, deprotonation of the weakly acidic C-H of **8** should be feasible; with the resultant anion stabilised by delocalisation onto the π-system of two powerfully electron withdrawing C_6F_5 substituents. Treatment of **8** with a LIC-KOR mixture dissolved in Et_2O yielded a similar red solution thus suggested formation of the potassium salt. At –78ºC, addition of BX_3 (X = Cl, Br) revealed no evidence of metathesis as exemplified by a silent ^{11}B NMR spectrum upon removal of the solvent and hence any unreacted BX_3. Warming solutions of the supposed $K[CH(C_6F_5)_2]$ salt with BX_3 led to the disappearance of the red solution concomitant with the formation of a white precipitate. Despite these promising observations, unassignable resonances were once again seen in the ^{19}F NMR alongside an ^{11}B NMR spectrum which revealed no boron environment.

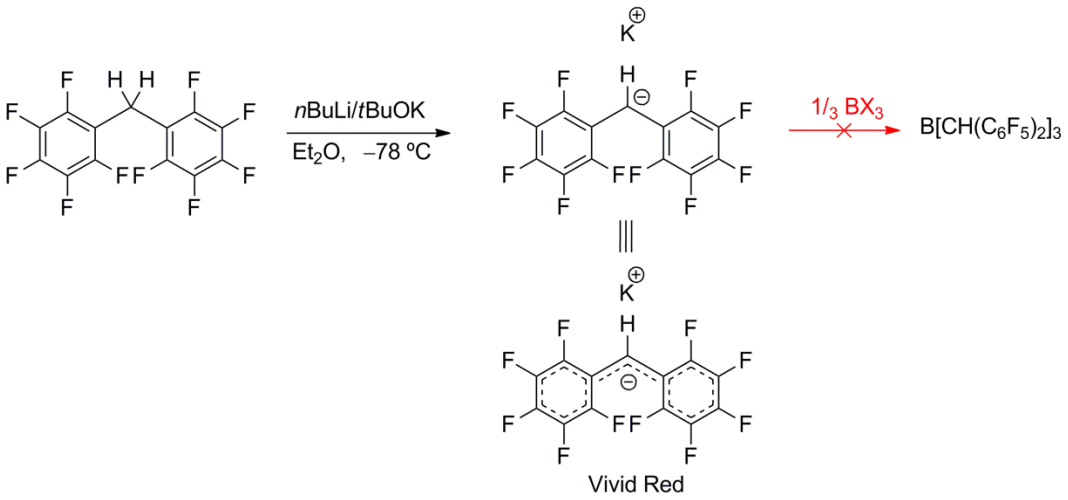

Figure 3.14. Formation of unreactive $K[CH(C_6F_5)_2]$, rendered poorly nuceleophilic by the adjacent C_6F_5 groups.

It was assumed deprotonation of $CH_2(C_6F_5)_2$ with LIC-KOR had occurred to yield $K[CH(C_6F_5)_2]$, since any unreacted *n*BuK would have formed $K[BBu_4]^-$. However the electron withdrawing effect of two C_6F_5 substituents apparently renders the organopotassium salt too poorly nucleophilic to react under reasonable conditions (Figure 3.18). This conclusion is supported by the failure of all attempts to trap this anion *in situ* with electrophilic Me_3SiCl. Upon warming, the potassium salt may α-eliminate KH to form a carbene which rapidly polymerises. Given the failure of the above protocol, a polar *bis*(pentafluorophenyl)methyl halide was targeted instead.

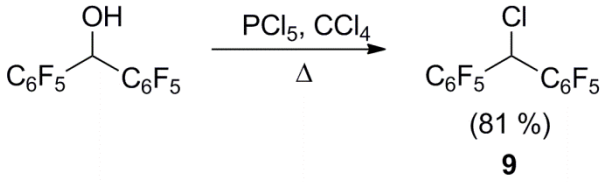

Figure 3.15. Synthesis of **9** *via* chloronation of decafluorobenzahydrol.

Vorozhtsov *et al.* have detailed the synthesis of *bis*(pentafluorophenyl)methyl chloride $(C_6F_5)_2CHCl$ *via* chlorination of decafluorobenzhydrol with PCl_5 dissolved in CCl_4 (Figure 3.19).[43] Gratifyingly, adaption of this procedure afforded $(C_6F_5)_2CHCl$ (**9**) in good yield (81 %) following a final vacuum distillation stage (^1H and ^{19}F NMR spectra are detailed in the Chapter 5). With this key intermediate in hand, the generation of the Grignard was achieved using a suspension of preactivated Mg powder in Et_2O. Addition of $BF_3{\cdot}OEt_2$ to this solution followed by overnight reflux led to a weak resonance at 80 ppm in the ^{11}B NMR spectrum. The ^{11}B NMR resonances for trialkyl boranes are observed typically within the 80-

90 ppm window (BEt_3 and B*i*Pr_3 display resonances in Et_2O at 86.6 and 84.1 ppm respectively).[44] EI mass spectrometry also revealed an ion peak at 1052 commensurate with the formula unit of $B[CH(C_6F_5)_2]_3$ ($C_{39}H_3BF_{30}$).

Brown *et al.* have reported a direct (and often cleaner) route to many triorganylboranes, *via* the *in situ* preparation of the Grignard in the presence of $BF_3{\cdot}OEt_2$.[44] Compared to the classical step-wise method, this procedure saved considerable time and prevents side reactions such as Wurtz coupling. Employing this methodology, a one pot synthesis was successfully performed which cleanly afforded $B[CH(C_6F_5)_2]_3$ (**10**) as a white microcrystalline solid in moderate yield (63 %; Figure 3.20). Here, decomposition of the organo magnesium reagent is believed to be outrun by rapid electrophilic trapping.

In contrast to boranes *tris*[3,5-*bis*(trifluoromethyl)phenyl)]borane (**1**) and *tris*[2,4-*bis*(trifluoromethyl)phenyl)]borane (**3**) which readily sublime at 80 ºC (1 x 10^{-6} mbar), the high molecular weight of **10** required temperatures in excess of 150 ºC for sublimation (10^{-6} mbar). **10** is moderately soluble in hydrocarbons, yet much more so in aromatics and chlorinated solvents. Interestingly, **10** does not bind donor solvents such as Et_2O, THF or pyridine as evinced by ^{11}B NMR, presumably due to the steric bulk of the $CH(C_6F_5)_2$ groups (*vide infra*).

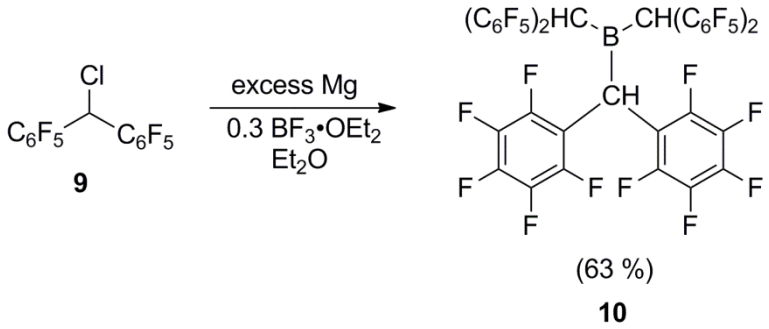

Figure 3.16. Synthesis of **10** from the *in situ* formation of $[(C_6F_5)_2CH]MgCl$ in the presence of $BF_3{\cdot}OEt_2$.

3.8 X-ray diffraction studies of $B[CH(C_6F_5)_2]_3$ (10)

Clear prisms of **10**·(toluene) were obtained from slow cooling of a saturated toluene solution to –30 ºC. Despite the prevalence of the B-C_6F_5 motif in a variety of Lewis acidic boranes, no structural data exist for a trigonal borane in which the electron withdrawing groups are all separated *via* alkyl linkages. Stephan *et al.* have reported a $CH_2(C_6F_5)$ fragment in a borane-oxy-borate formed from the reaction of tBu$_3$P/$B(C_6F_5)_3$ with syngas (CO/H_2) (Figure 3.21).[45]

However, this borane is electronically and sterically very different due to the B-O and pendant [B-(C_6F_5)$_3$] fragments.

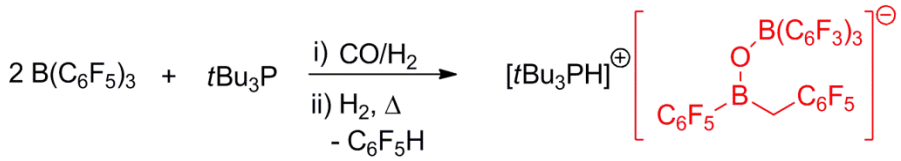

Figure 3.17. Generation of a borane-oxy-borate from the reaction of B(C_6F_3)$_3$/*t*Bu$_3$P FLP with syngas (CO/H_2) followed by heating under H_2.[45]

Compound **10** represents the first structurally characterised trialkyl borane where C_6F_5 groups were not proximal to the boron centre (Figure 3.22). As expected, the coordination about the boron centre is trigonal planar as evident from the near zero deviation of the central atom from the plane of the three pendant –CH(C_6F_5)$_2$ ligands (sum of CBC angles = 359.4º). Table 3.2 shows some selected bond lengths and torsion angles of **10**. The B-C bond lengths (range 1.595(4)–1.595(4) Å) are comparable to those reported for the sterically bulky *tri*cyclohexylborane (BCy$_3$) (range 1.5833(3)–1.5893(4) Å)[46] and *tris*tertbutylborane (B*t*Bu$_3$) (1.618(3) Å).[47]

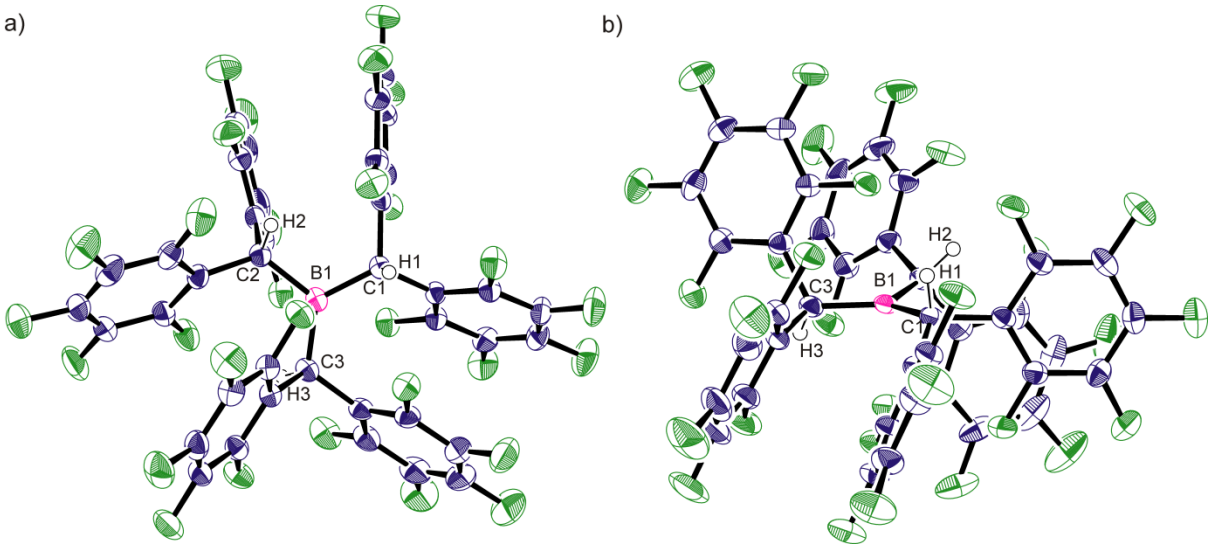

Figure 3.18. Diagram of **10**; thermal ellipsoids are shown at 50 % probability. a) Orthogonal and b) side views of **10**. C atoms navy blue, B atoms pink, F atoms green and H atoms white. For selected bond lengths see Table 3.2.

Table 3.2. Selected bond lengths and angles for **10.** Numbers in parentheses are estimated standard uncertainties (esu).

	10
B1-C1 (Å)	1.209(5)
B1-C2 (Å)	1.198(4)
B1-C3 (Å)	1.208(2)
Range H···F (Å)	2.264-2.499(4)
Range (C_6F_5)^(CH)BAr''$_2$ (deg)	62.3–89.6º

*Tris*arylboranes of the type $Ar_xB(C_6F_5)_{3-x}$ (Ar = C_6H_5, Mes, C_6Cl_5) display torsion angles (the angle between the best plane of C_3B and the aryl ring) within the range of 20-45º. The lowest energy conformation based upon minimisation of nonbonding interactions between the *ortho*-substituents of each ring is predicted to resemble a 'propeller' in which each C_6F_5^BAr'$_2$ ≈ 60º (Ar' = C_6F_5, C_6H_5, Mes, C_6Cl_5, B-C_6F_5). However, π-donation from the C_6F_5 rings into the vacant B *p*-orbital leads to a marked deviation in these angles. In the case of **10**, the C_6F_5 rings are no longer proximal to the B centre and so π-donation from the rings no longer participates. Thus, the average torsion angle should solely reflect the steric influence of crowding six C_6F_5 rings about the boron centre [Range (C_6F_5)^(CBAr''$_2$) (62.3-89.6º)] (Figure 3.23a). Upon adopting this configuration, **10** displays two protons above the C_3B plane and one proton below. The two protons which are projected above the plane are inequivalent; the angle from the best plane of their respective BCH unit and that of the C_3B plane yields values of 80.4º and 43.1º for H1 and H2 respectively (Figure 3.23b). Interestingly, these protons show evidence of H-bonding with one *ortho*-F of each aryl ring, with average F···H separations of 2.34 Å significantly less than the sum of vdW radii (r_w(F) + r_w(H) = 2.67 Å) (Figure 3.24). Similar contacts were witnessed upon re-examining the crystal structure for the structurally rigid boracyclopent-3-ene heterocycles formed from H_2 activation by an antiaromatic borole.[48] Here, the cis-3 isomer shows H···F separations of 2.55 and 2.32 Å between the *ortho*-Fs orientated c*is* to the two α-protons (Figure 3.25).

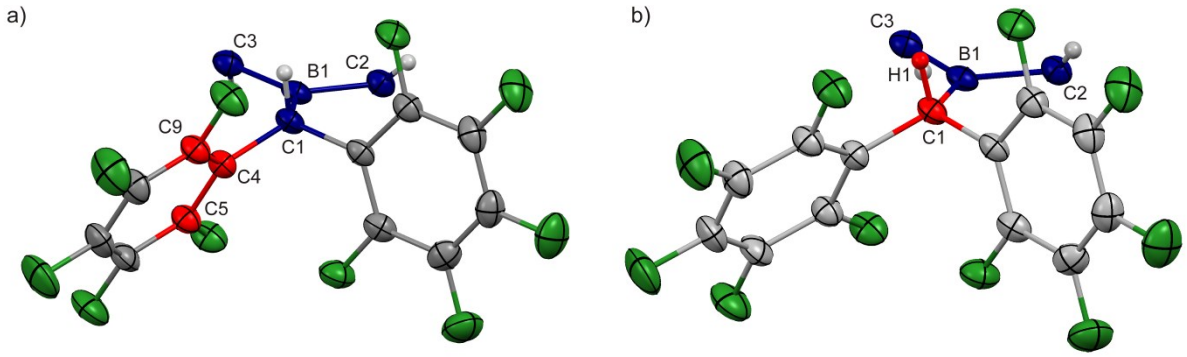

Figure 3.19. a) Method of calculation for the torsion angle for a C_6F_5 ring in **10** (C_6F_5)^(CBAr''$_2$) (Ar'' = $CH(C_6F_5)_2$) and defined as the angle between the plane of the aryl ring (red) and the C_3B unit (blue). b) Demonstration of the angle between the BCH unit (red) and that of the C_3B plane (blue). F atoms shown in green, and for clarity the C_6F_5 rings on C2 and C3 have been omitted for clairity.

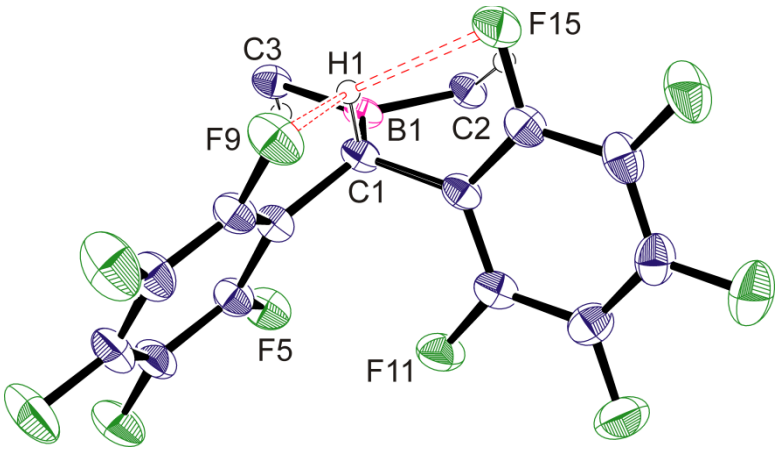

Figure 3.20. Diagram of **10** illustrating intramolecular hydrogen bonding between an *ortho*-F on each aryl ring and the neighbouring proton. Selected H···F contacts: H1···F9 = 2.32 Å, H1···F15 = 2.307 Å. C atoms navy blue, B atoms pink, F atoms green and H atoms white. Additional C_6F_5 groups removed for clarity.

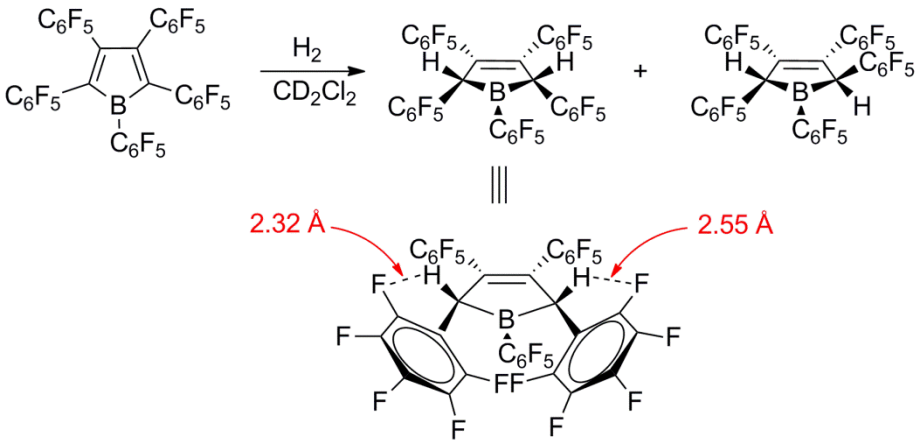

Figure 3.21. H_2 activation by an antiaromatic perfluoropentaphenylborole to form *cis* and *trans* isomers of the boracyclopent-3-ene heterocyles. F···H separations of 2.55 and 2.32 Å.[48]

3.9 NMR spectroscopy of 10

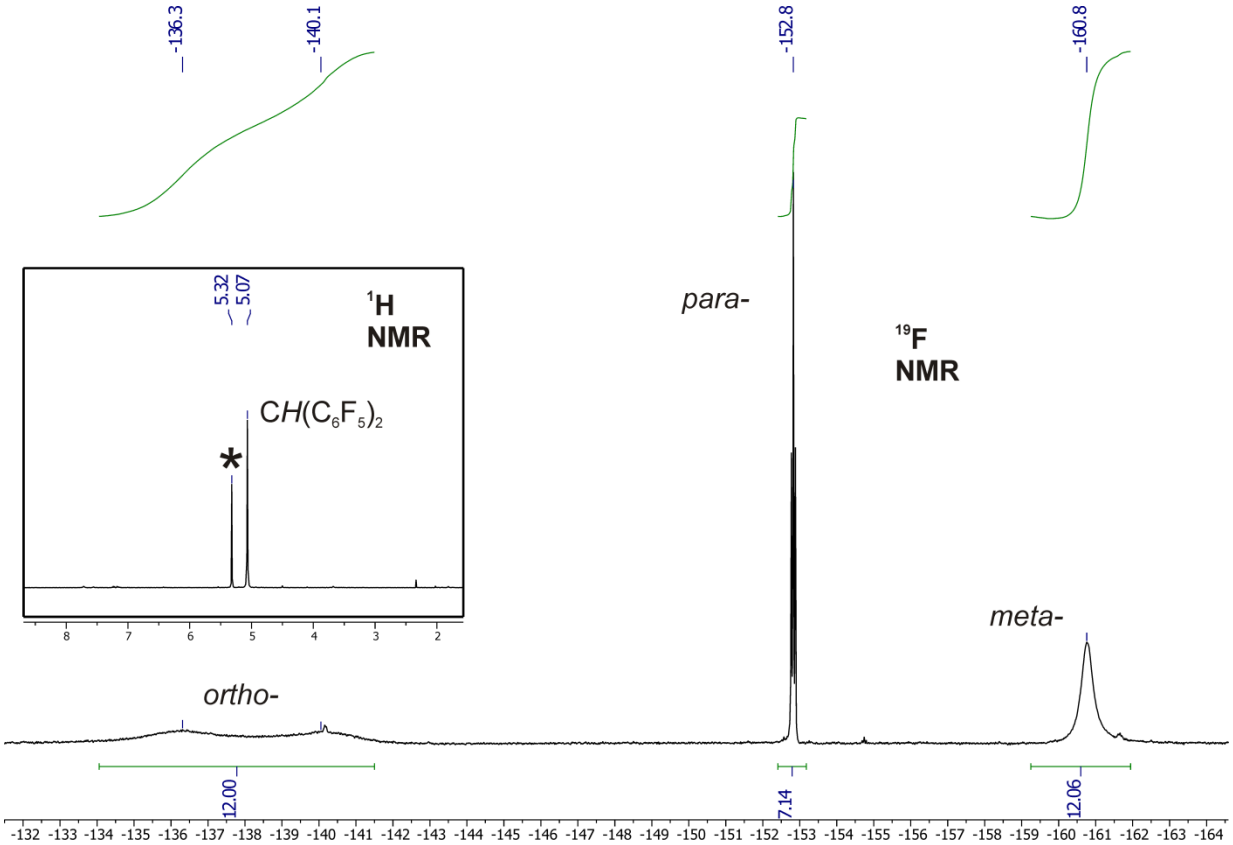

Figure 3.22. The room temperature ^{1}H and ^{19}F NMR of **10.** * denotes CH_2Cl_2 solvent.

10 was characterised by ^{1}H, ^{13}C, ^{19}F and ^{11}B NMR spectroscopy; the latter shift (80.3 ppm) is consistent with a three coordinate trialkyl borane. The ^{1}H NMR spectrum reveals a broad singlet at 5.07 ppm while the ^{19}F NMR spectrum consists of two broad signals for the *ortho*-fluorines, a broad resonance for the *meta*-fluorines, and a sharp triplet for the *para*-fluorines (Figure 3.26). These shifts support observations made in the solid state where restricted rotation about the C-(C_6F_5) bond leads to two chemically inequivalent *ortho*-F environments which are reasoned to be discrete on the ^{19}F NMR timescale (376.8 MHz) (inequivalence of the *meta*-F environments is not resolved, in which a broad shift is seen at –160.8 ppm). Interestingly, at elevated temperature (> 80 ºC) these *ortho*- resonances coalesce to afford a single environment in the ^{19}F NMR spectra (Figure 3.27) concomitant with a sharpened signal in the ^{1}H NMR. These findings are supportive of an ever increasing free rotation about the C–(C_6F_5) bond, which is assigned as Process **A** (Figure 3.29).

Conversely, cooling a solution of **10** led to the gradual resolution and sharpening of the *ortho*-fluorine environments in the ^{19}F NMR spectra in addition to the appearance of two very broad meta resonances. Here, a progressively slower rate of rotation about the C–(C_6F_5)

bond permits observation of the two inequivalent meta environments on the ^{19}F NMR timescale. Below –40 ºC, a new set of ^{19}F resonances appeared which were seen to reflect six *ortho*-F resonances (two superimposed) and six *meta*-F resonances (Figure 3.27) and indicative of restricted rotation about both the C-(C_6F_5) and B-C bonds (Process **A** & **B** combined; Figure 3.29). Thus, each $CH(C_6F_5)_2$ ligand is rendered inequivalent in which the *ortho* and *meta* fluorine resonances are split depending on their proximity or lack of to the C-H fragment. On the basis of this hypothesis it was surprising to see at low temperatures (< –50 ºC) the ^{1}H NMR spectrum to split from one broad resonance into two (and not three) broad environments (relative integration (2:1); Figure 2.28). This may be explained through aid of the solid state structure in which two hydrogen atoms are located above the C_3B plane and one below. These two protons are not completely identical as evidenced from the angle between the BCH and the C_3B planes, yet they present identical ^{1}H NMR shifts. It is assumed the modest differences in each ligand set are exaggerated at distances distant from the boron centre and therefore the ^{19}F NMR spectra reveals six, and not four, environments. The range in torsion angles (Δ = 27º) of the best plane of the rings relative to the C_3B plane may reflect these differences (range (C_6F_5)^(CH)BAr''$_2$ 62.3–89.6º).

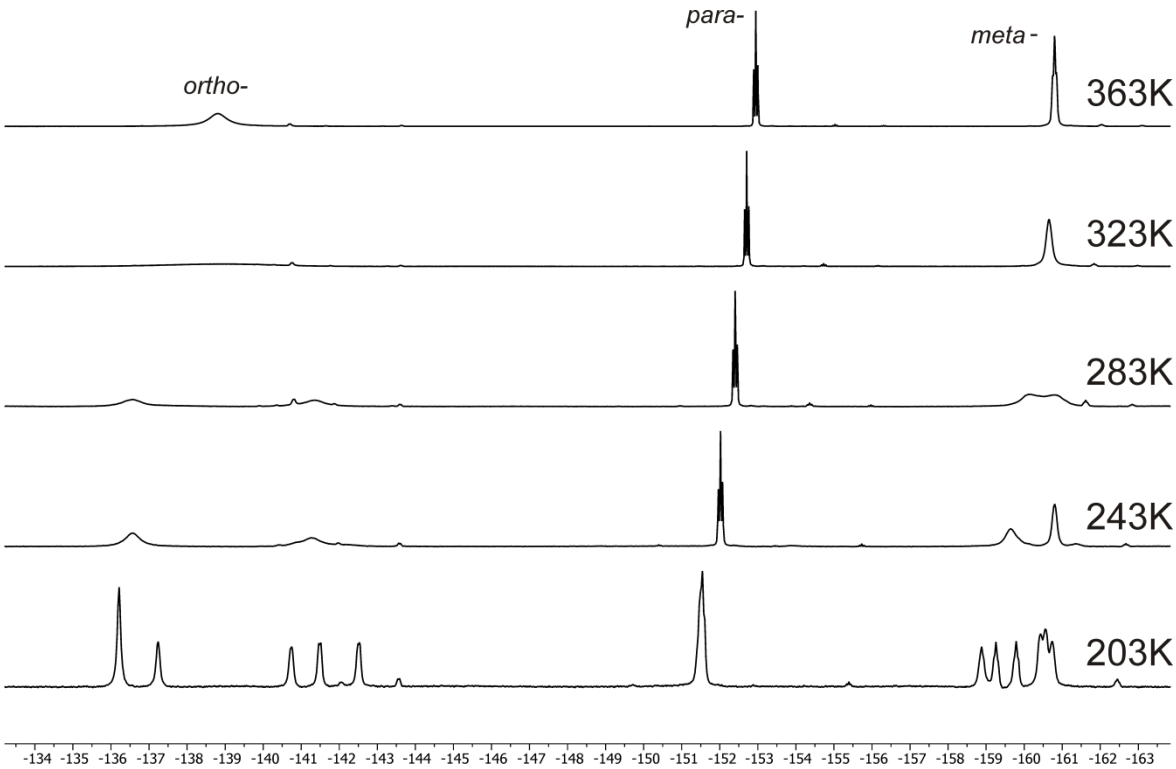

Figure 3.23. Variable temperature ^{19}F NMR spectroscopy of **10** dissolved in C_7D_8.

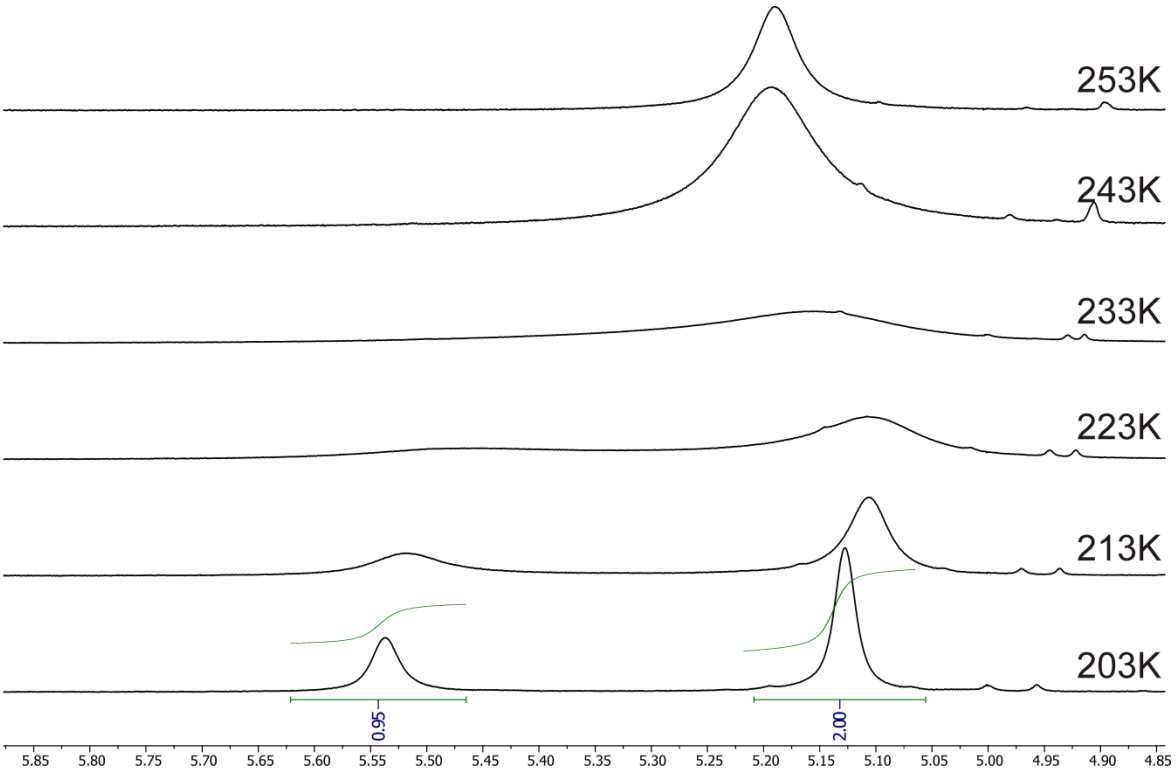

Figure 3.24. Variable temperature ^{1}H NMR spectroscopy of **10** dissolved in C_7D_8.

Restricted rotation around the B-C and B-O bonds of diarylboronic acids $(C_6F_5)_2BOR$ (R= H, C_6F_5) has been previously observed using ^{19}F VT NMR spectrscopy.[49] Line shape analysis of the ^{19}F NMR spectra as a function of temperature permitted extraction of the activation barriers for rotation. Analogous studies were therefore performed on **10** to yield rate constants and thermodynamic parameters for both processes, and the data is presented in Table 3.3. Eyring plots (see Appendix) permitted extraction of $\Delta H^{\ddagger}$, $\Delta S^{\ddagger}$ and $\Delta G^{\ddagger}$ parameters. Process **A** was examined over a 303-332 K temperature range while Process **B** was examined over 209-244 K. In the case of Process **B,** line shape analysis using the ^{1}H NMR spectra gave parameters commensurate with those obtained employing ^{19}F NMR. Accordingly, the activation barriers are reported at their respective coalescence temperatures of 313 and 228 K (T_c).

a) Process A: C–(C_6F_5) Rotation

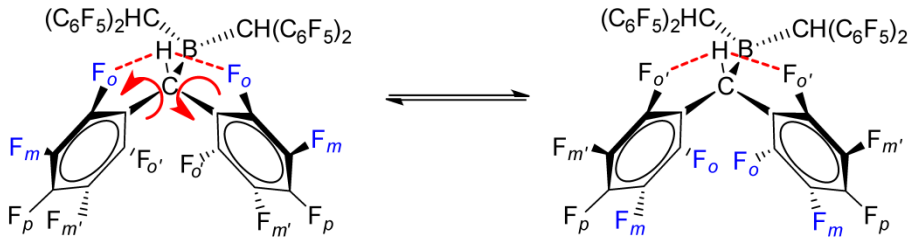

b) Process B: B–C Rotation

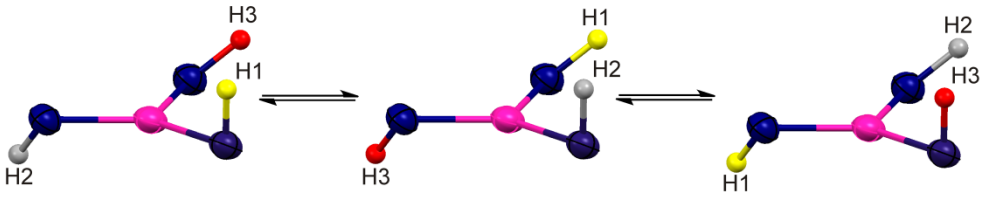

Figure 3.25. Degenerate exchange processes a) the two chemically inequivalent *ortho*-F of the C_6F_5 ring upon restricted C-C_6F_5 rotation. T_c = 313 K and b) the three inequivalent $CH_2(C_6F_5)_2$ ligands from restricted B-C rotation. Illustration based upon the configuration found in the crystal structure. T_c = 228 K. C_6F_5 groups for process **B** were emitted for clarity.

Table 3.3. Activation parameters determined by VT ^{19}F NMR (C_7D_8) for process **A** (range examined 303-332 K) and VT ^{19}F and ^{1}H NMR (C_7D_8) for process **B** (range examined 209-244 K).

NMR	Process (T_c)	$\Delta H^{\ddagger}$ (kJ mol^{-1})	$\Delta S^{\ddagger}$ (J mol^{-1} K^{-1})	$\Delta G^{\ddagger}$ (T_c, kJ mol^{-1})
^{19}F	**A (313 K)**	32.1(5)	-75(2)	55.5(4)
^{19}F	**B (228 K)**	28(2)	-84(10)	48(3)
^{1}H	**B (228 K)**	32(1)	-71(4)	48(1)

3.10 Lewis Acidity measurements

Both Gutmann-Beckett and Childs measures of Lewis acidity gave values of $\Delta\delta$ = 0 upon addition of each donor. Examination of the space fill diagram indicates severe steric shielding about the boron atom, with both sides of the C_3B plane extremely hindered (Figure 3.30). Interestingly, treatment of **10** with the superhydride Na[$HBEt_3$] in THF afforded a distinct hydride resonance in the ^{11}B NMR (δ = –14.4, THF-d_8), concomitant with new ^{1}H and ^{19}F resonances. This result demonstrated that **10**, unlike *tris*[2,4-*bis*(trifluoromethyl)phenyl)]borane (**3**), possesses sufficient Lewis acidity to accept H^-; the sterics of the larger Et_3P=O and *trans*-crotonaldehyde presumably prevent coordination.

Attempts to use electrochemistry as a probe for investigating electrophilicity in the absence of sterics were unsuccessful due to the ill-defined cyclic voltammograms obtained.

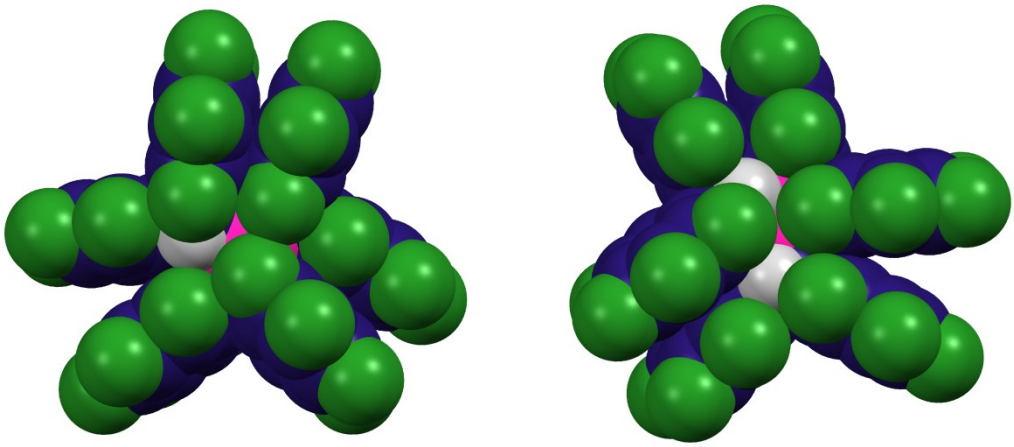

Figure 3.26. Space-fill diagrams of **10** from the perspective of both sides of the C_3B plane. C atoms blue, H atoms white, F atoms green, B atoms pink.

3.11 H_2 reactivity studies

Compound **10** does not bind ethereal solvents and is stable at elevated temperatures. In contrast, strong binding for the adduct $B(C_6F_5)_3$·THF quenches Lewis acidity and leads to solvent polymerisation upon heating above 60 ºC.[50] In contrast, $B(C_6Cl_5)_3$ like **10** demonstrates appreciable stability in THF solvent, and in analogous fashion does not coordinate Et_3P=O or *trans*-crotonaldehyde.[34b] Yet, this borane is capable of accepting small donors, in which O'Hare *et al.* recently reported a series of $R_3P/B(C_6Cl_5)_3$ FLPs (R = Et, Cy, *n*Bu, *t*Bu, *p*Tol) to activate H_2 in THF solvent. [51] In light of these observations addition of tBu_3P to **10** in THF led to the formation of a FLP which decomposed upon heating to 90 ºC (loss of characteristic resonances in ^1H, ^{19}F and ^{11}B NMR spectra and formation of a vivid red solution). Fluoroaryl boranes containing *para*-flourines are documented to undergo nuclecophilic attack, for example nBu_3P reacts with $B(C_6F_5)_3$ to yield the zwitterion $nBu_3P(C_6F_4)BF(C_6F_5)_2$ (Figure 2.1) with characteristic ^{31}P, ^{11}B and ^{19}F NMR shifts (^{31}P NMR: δ = 33.2 ppm; ^{11}B NMR: δ = –0.9 ppm; ^{19}F NMR: δ: –190 ppm (B–F), C_6D_5Br). [52] The spectral data for the decomposition of **10**/P*t*Bu$_3$ were supportive of zwitterion formation (Figure 3.31): in the ^{31}P NMR a new resonance at 49.8 ppm was consistent with P–C bond formation while the ^{11}B NMR spectra displayed a significant broad resonance at –14.0 ppm. The ^{19}F NMR was significantly more complicated, with five major resonances witnessed in addition to a minor peak observed upfield at –177.1 ppm, the latter assigned to B–F.

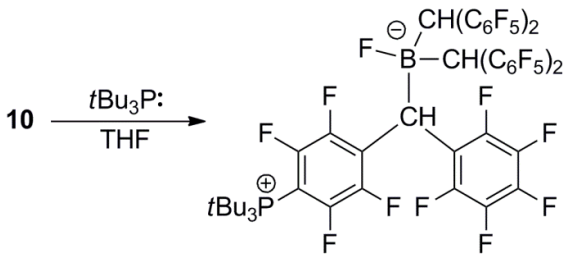

Figure 3.27. Formation of the zwitterion $(Bu_3P(C_6F_4)CH(C_6F_5)BF(CH(C_6F_5)_2$ from attack of tBu$_3$P.

Addition of TMP to **10** in THF led to the formation of an FLP as witnessed by no change to the ^{1}H, ^{19}F or ^{11}B NMR resonances. Importantly, heating this solution afforded no evidence for decomposition in either the ^{1}H, ^{19}F or ^{11}B NMR spectra. Encouragingly, H_2 activation slowly occurred upon heating THF solutions under H_2 (4 bar) to 90 ºC (Figure 3.32). Only after four days heating however, was complete consumption of the borane witnessed concomitant with new resonances in the ^{1}H, ^{19}F and ^{11}B NMR spectra assigned to be that of the borohydride salt [TMPH][HB(CH(C$_6$F$_5$)$_2$)$_3$]; **11**. As reported for the addition of Na[HBEt$_3$], the ^{11}B NMR spectra displayed a broad doublet at –14.5 (^{1}J(H,^{11}B) = 85 Hz) . The ^{19}F NMR spectrum was quite remarkable, the *ortho*-F environments practically flattened to the baseline while resonances for both the *meta*- and *para*-flourines were sharp. The difference in shift between the *para* and *meta* environments narrowed considerably upon formation of **11** from **10** [$\Delta\delta_{m,p}$ = 7.93 (**10**) and 3.38 ppm (**11**)] (Figure 3.33). Minor impurities were also observed in the ^{19}F environment but could not be identified. Notably, the ^{1}H NMR spectra correctly reproduced a 1:1 ratio of **10**:TMP ratio with a broad singlet at 6.05 ppm assigned for the CH(C$_6$F$_5$)$_2$ fragment. Despite this, a resonance could not be assigned to the [B–H] unit.

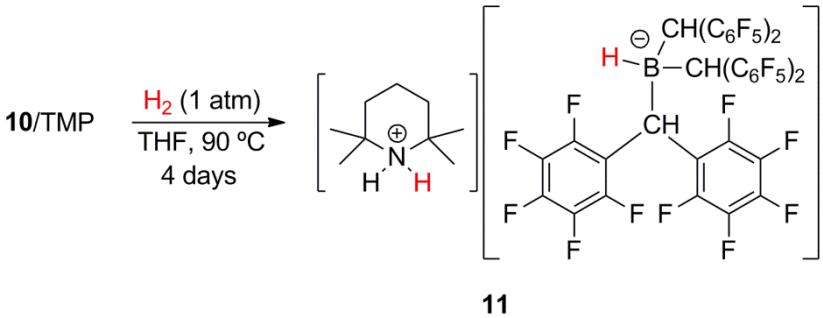

11

Figure 3.28. Generation of [TMPH][HB(CH(C$_6$F$_5$)$_2$)$_3$] from heterolytic H_2 activation by **10** and TMP

HRMS (ES+/ES–) (see appendix) was consistent with the formulation of **11** although attempts to grow crystals suitable for X-ray crystallography were unsuccessful. In all instances an amber oil was obtained.

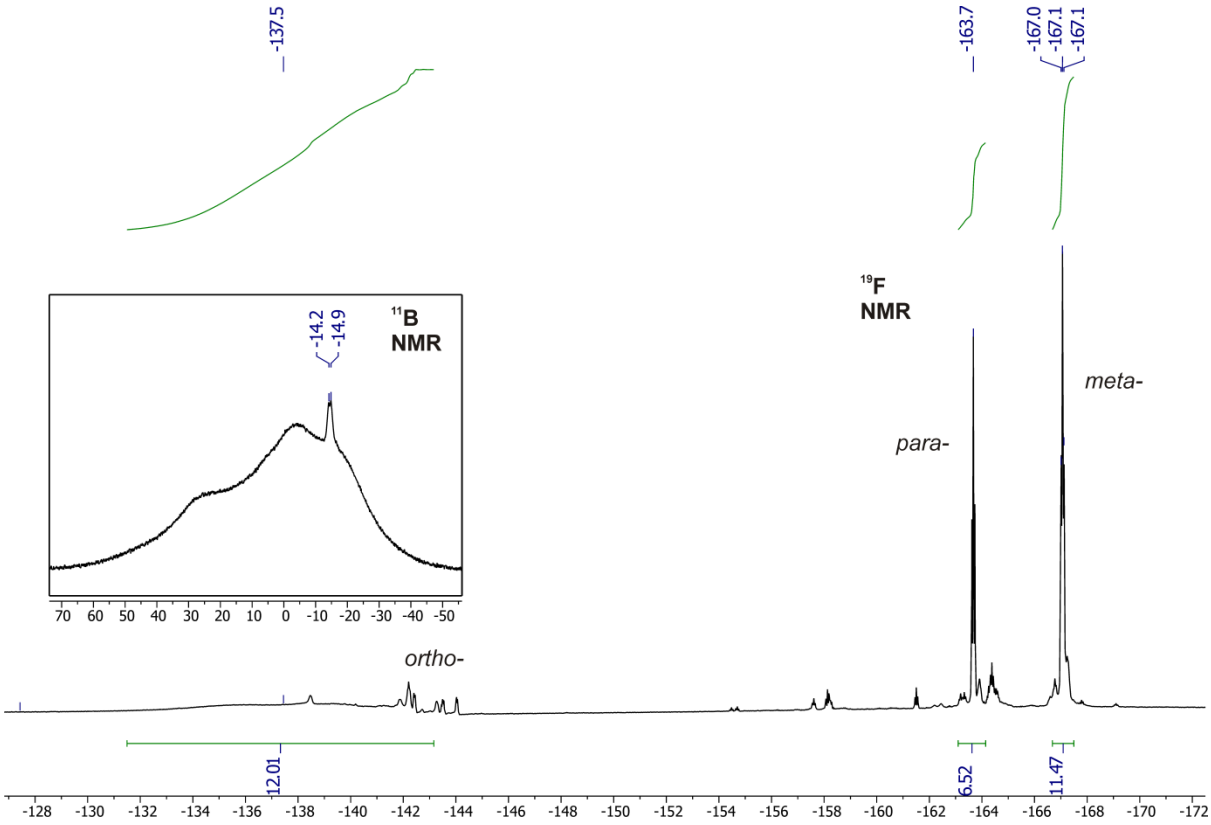

Figure 3.29. The room temperature ^{11}B and ^{19}F NMR of **11** (THF-d_8)

3.12 H_2O stability

Addition of H_2O to **10** led to B-C cleavage, with $CH_2(C_6F_5)_2$ (**8**) detected in the ^{1}H and ^{19}F NMR spectra in addition to a 'R_2B-O' unit (^{11}B NMR: δ = 49.0 ppm; ^{19}F NMR: δ –140.4, –154.1 and –161.3 ppm, C_7D_8) (Figure 3.34). At room temperature, the unhindered tribenzyl borane [$B(CH_2Ph)_3$], is hydrolysed by H_2O to form the borinic acid [$HOB(CH_2Ph)_2$] which may be attributed to its benzylic functionality.[53] Therefore in light of this report an analogous $HOB(CH(C_6F_5)_2)_2$ species was assigned. At elevated temperature (100 ºC) further B-C cleavage occurred, in which the ^{11}B NMR spectra showed disappearance of the resonance at 49.0 ppm concomitant with a new signal at 30.2 ppm in tandem with ^{19}F NMR revealing the loss of $HOB(CH(C_6F_5)_2)_2$, and the appearance of three new resonances (^{19}F NMR: δ = –141.0, –156.4 and –162.9 ppm, C_7D_8) and additional $CH_2(C_6F_5)_2$ (**8**). Integration of these environments relative to **8** (1:2) pointed to the formation of an 'RBO_2' unit. Boronic acids such as [$HOB(CH_2Ph)_2$] are reported to be thermally unstable towards dehydration at

elevated temperature and the formation of tricyclic boroxins, which therefore led to the assignment of this 'RBO$_2$' unit as [OBCH(C$_6$F$_5$)$_2$]$_3$.[54] Heating this species for an additional two hours in excess H$_2$O afforded the complete loss of 'RBO$_2$' resonances and the formation of an insoluble white solid; this dissolved in D$_2$O and was indentified as B(OH)$_3$ by its characteristic ^{11}B NMR resonance (19.3 ppm).[55] The marked lability of the B-C bonds was attributed to the benzylic functionality of the ring in which a benzylic intermediate is postulated (Figure 3.35).

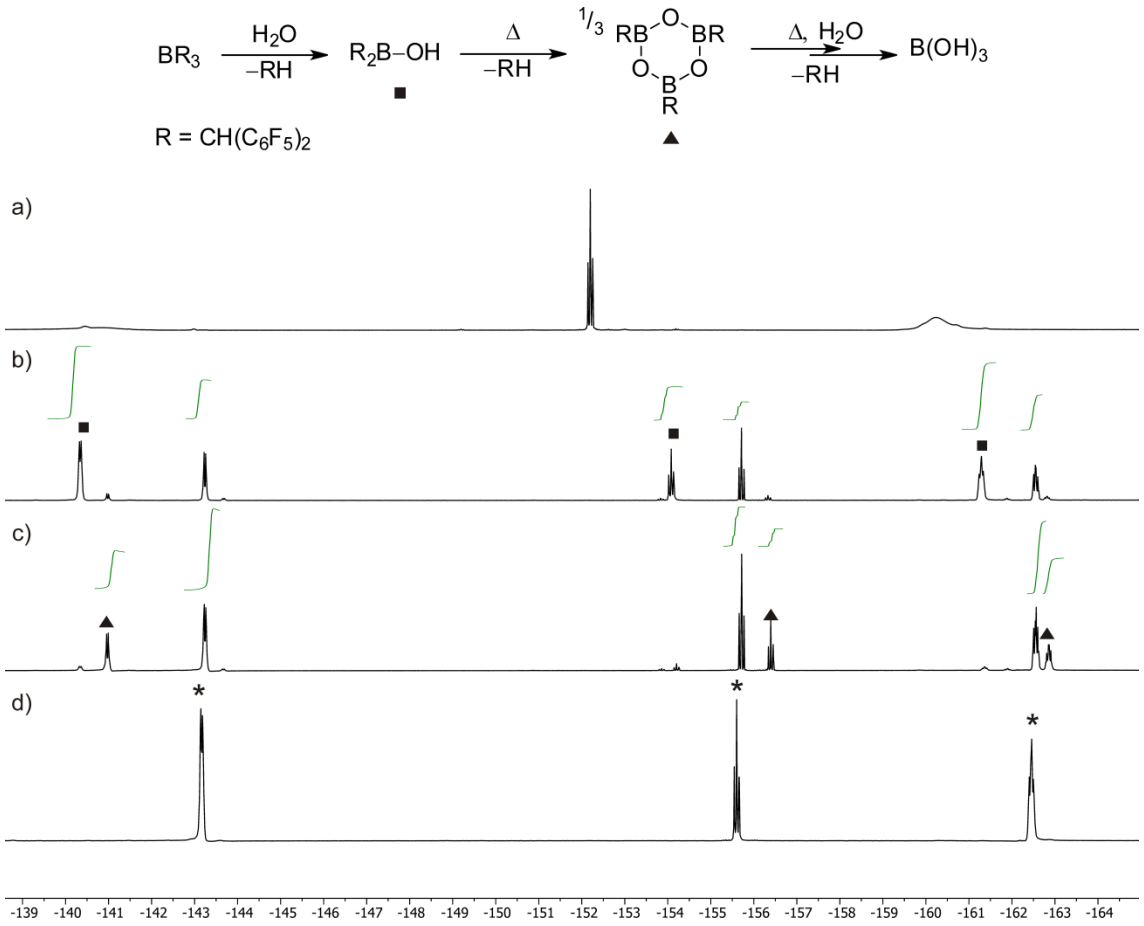

Figure 3.30. Stacked ^{19}F NMR spectra for the protonolysis of **10** a) **10** dissolved in C$_7$D$_8$ prior to H$_2$O addition b) RT addition of 1 equiv H$_2$O c) Following 10 minutes heating **10**/H$_2$O at 100 ºC d) Following 2 hours heating at 100 ºC. * denotes CH$_2$(C$_6$F$_5$)$_2$.

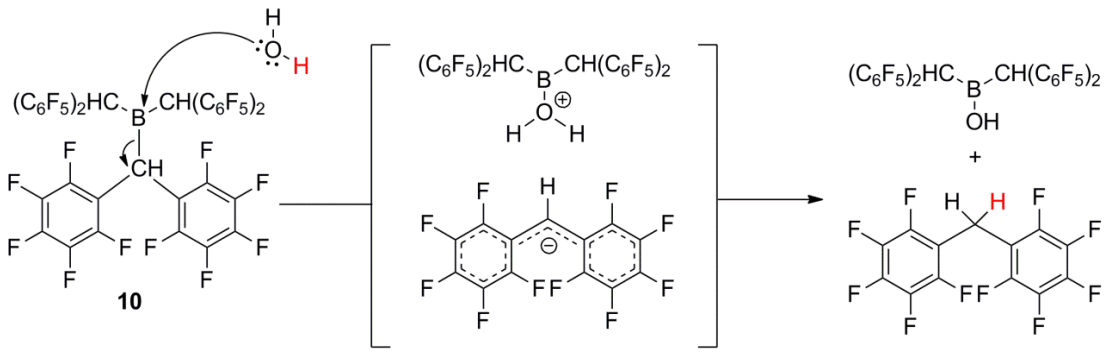

Figure 3.31. Formation of HOB[(CH(C$_6$F$_5$)$_2$]$_2$ from addition of H$_2$O to **10** at room temperature.

3.13 Conclusion

To employ the stability of B-C bonds towards hydrolysis, yet maintain sufficient electrophilicity at the boron centre to participate in facile H_2 cleavage, attempts were made to prepare a new series of fluoroalkylboranes. After considering the pitfalls of perfluoroalkyl ligands, which readily form carbenic intermediates *via* α-F elimination, the *tris*(1,1,1,3,3,3-hexafluoroisopropyl)borane was targeted. Unfortunately, and despite rigourous investigation, attempts to generate this species from a suitable halide precursor were unsuccessful. Under all circumstances, β-F elimination of the lithium precursor was believed to occur in preference to B-X metathesis. To circumvent these issues, an alkyl borane containing C_6F_5 groups was targeted in which the polar organometal precursors would be devoid of a readily labile leaving group. *In situ* preparation of the Grignard generation (from **9**) in the presence of $BF_3{\cdot}OEt_2$ furnished $B[CH(C_6F_5)_2]_3$ (**10**) in moderate yield after a final sublimation stage. Crystals grown in toluene provided the first example of an electron deficient trialkylborane which was discovered to display hydrogen bonding between an *ortho* fluorine on each aryl ring and the adjacent CH fragment. In the solution phase, restricted rotation about the CH-C_6F_5 axis afforded two *ortho* signals at room temperature while, upon heating, these signals were observed to coalesce. Conversely, cooling solutions to –70 ºC led to the appearance of six *ortho* and six *meta* signals. Here, it was reasoned that restricted rotation about both the C-C_6F_5 and B-C bonds removed the ligand degeneracy. VT NMR analysis allowed the kinetic and thermodynamic parameters to be derived for both processes.

Due to the bulk of the $CH(C_6F_5)_2$ ligands, both the Gutmann and Childs methods implied **10** to possess no Lewis acidity relative to BEt_3. However, combination of **10** with TMP led to the formation of an FLP which reacted slowly with H_2 in THF solvent and is the second report of a borane undergoing H_2 heterolysis in this strongly donating medium. Despite these encouraging results, degradation of **10** occurred readily upon addition of H_2O; full cleavage of the B-C bonds occurred after heating **10** for 2 hours at 100 ºC. It appears facile B-C cleavage is promoted by the benzylic functionality of the ligand set.

The bridgehead perfluorobicyclolithium reagents such as perfluorobicyclo[2,2,1]hept-1-yllithium are reported to be more stable to room temperature.[56] This stems from the formation of unfavourable high energy bridgehead alkenes or diradicals (Bredt's rule; Figure 3.36).[57] In future, this precursor may be worth exploring for the aim of generating a water stable triorgano borane.

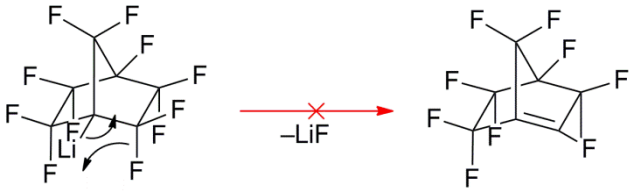

Figure 3.32. b) Disfavoured formation of high energy bridgehead alkenes or diradicals from the decomposition of perfluorobiclyclo[2.2.1]hept-1-lyllithium (Bredt's Rule).

3.14 References

[1] (a) H. C. Brown, K. J. Murray, *Tetrahedron* **1986**, *42*, 5497-5504; (b) R. Koster, K. L. Amen, H. Bellut, W. Fenzl, *Angew. Chem. Int. Ed.* **1971**, *10*, 748-&.

[2] B. Wrackmeyer, O. L. Tok, *Z. Naturforsch.* **2005**, *60*, 259-264.

[3] (a) H. Yorimitsu, T. Nakamura, H. Shinokubo, K. Oshima, *J. Org. Chem.* **1998**, *63*, 8604-8605; (b) H. Yorimitsu, T. Nakamura, H. Shinokubo, K. Oshima, K. Omoto, H. Fujimoto, *J. Am. Chem. Soc.* **2000**, *122*, 11041-11047.

[4] (a) H. C. Brown, S. C. Kim, S. Krishnamurthy, *J. Org. Chem.* **1980**, *45*, 1-12; (b) S. Krishnamurhy, *Aldrichim. Acta.* **1974**, *7*, 55-60; (c) H. C. Brown, Purdue Res. Found., Lafayette, IN, USA., **1979**, pp. 1-22.

[5] (a) A. Adamczyk-Wozniak, M. Jakubczyk, A. Sporzynski, G. Zukowska, *Inorg. Chem. Commun.* **2011**, *14*, 1753-1755; (b) H. Li, A. J. A. Aquino, D. B. Cordes, F. Hung-Low, W. L. Hase, C. Krempner, *J. Am. Chem. Soc.* **2013**, *135*, 16066-16069.

[6] S. J. Geier, D. W. Stephan, *J. Am. Chem. Soc.* **2009**, *131*, 3476-3477.

[7] T. A. Rokob, A. Hamza, I. Papai, *J. Am. Chem. Soc.* **2009**, *131*, 10701-10710.

[8] D. L. DuBois, D. M. Blake, A. Miedaner, C. J. Curtis, M. R. DuBois, J. A. Franz, J. C. Linehan, *Organometallics* **2006**, *25*, 4414-4419.

[9] E. M. Arnett, L. E. Small, *J. Am. Chem. Soc.* **1977**, *99*, 808-816.

[10] M. T. Mock, R. G. Potter, D. M. Camaioni, J. Li, W. G. Dougherty, W. S. Kassel, B. Twamley, D. L. DuBois, *J. Am. Chem. Soc.* **2009**, *131*, 14454-14465.

[11] A. J. M. Miller, J. A. Labinger, J. E. Bercaw, *J. Am. Chem. Soc.* **2010**, *132*, 3301-3303.

[12] G. Pawelke, H. Burger, *Coord. Chem. Rev.* **2001**, *215*, 243-266.

[13] M. Finze, E. Bernhardt, H. Willner, *Angew. Chem. Int. Ed.* **2007**, *46*, 9180-9196.

[14] (a) W. Beck, K. Sunkel, *Chem. Rev.* **1988**, *88*, 1405-1421; (b) S. H. Strauss, *Chem. Rev.* **1993**, *93*, 927-942; (c) I. Krossing, I. Raabe, *Angew. Chem., Int. Ed.* **2004**, *43*, 2066-2090; (d) C. A. Reed, *Acc. Chem. Res.* **1998**, *31*, 325-332.

[15] E. Bernhardt, G. Henkel, H. Willner, G. Pawelke, H. Burger, *Chem. Eur. J.* **2001**, *7*, 4696-4705.

[16] (a) E. Bernhardt, M. Finze, H. Willner, C. W. Lehmann, F. Aubke, *Angew. Chem. Int. Ed.* **2003**, *42*, 2077-2079; (b) E. Bernhardt, M. Finze, H. Willner, C. W. Lehmann, F. Aubke, *Chem. Eur. J.* **2006**, *12*, 8276-8283; (c) M. Finze, E. Bernhardt, M. Berkei, H. Willner, J. Hung, R. M. Waymouth, *Organometallics* **2005**, *24*, 5103-5109.

[17] (a) M. Finze, E. Bernhardt, A. Terheiden, M. Berkei, H. Willner, D. Christen, H. Oberhammer, F. Aubke, *J. Am. Chem. Soc.* **2002**, *124*, 15385-15398; (b) A. Terheiden, E. Bernhardt, H. Willner, F. Aubke, *Angew. Chem. Int. Ed.* **2002**, *41*, 799-801.

[18] M. Finze, E. Bernhardt, M. Zahres, H. Willner, *Inorg. Chem.* **2004**, *43*, 490-505.

[19] M. Gerken, G. Pawelke, E. Bernhardt, H. Willner, *Chem. Eur. J.* **2010**, *16*, 7527-7536.

[20] M. Finze, E. Bernhardt, H. Willner, C. W. Lehmann, *J. Am. Chem. Soc.* **2005**, *127*, 10712-10722.
[21] J. Geier, G. Pawelke, H. Willner, *Inorg. Chem.* **2006**, *45*, 6549-6554.
[22] (a) G. Pawelke, *J. Fluorine Chem.* **1989**, *42*, 429-433; (b) D. J. Brauer, H. Burger, F. Dorrenbach, B. Krumm, G. Pawelke, W. Weuter, *J. Organomet. Chem.* **1990**, *385*, 161-172.
[23] G. Pawelke, *J. Fluorine Chem.* **1995**, *73*, 51-55.
[24] I. A. Oxton, A. G. McInnes, J. A. Walter, *Can. J. Chem.* **1979**, *57*, 503-505.
[25] (a) H. Uno, H. Suzukib, *Synlett* **1993**, 91-96; (b) A. A. Kolomeitsev, A. A. Kadyrov, J. Szczepkowska-Sztolcman, M. Milewska, H. Koroniak, G. Bissky, J. A. Barten, G. V. Roschenthaler, *Tetrahedron Lett.* **2003**, *44*, 8273-8277; (c) P. Johncock, *J. Organomet. Chem.* **1969**, *19*, 257-265; (d) W. B. Farnham, J. C. Calabrese, *J. Am. Chem. Soc.* **1986**, *108*, 2449-2451.
[26] N. Y. Adonin, V. V. Bardin, H.-J. Frohn, *Z. Anorg. Allg. Chem.* **2007**, *633*, 647-652.
[27] B. L. Dyatkin, E. P. Mochalina, L. T. Lantseva, I. L. Knunyants, *Zh. Vses. Khim. O-va. im. D. I. Mendeleeva* **1965**, *10*, 469-470.
[28] D. C. England, C. G. Krespan, *J. Am. Chem. Soc.* **1966**, *88*, 5582-5587.
[29] M. Hanack, J. Ullmann, *J. Org. Chem.* **1989**, *54*, 1432-1435.
[30] R. J. Errington, *Advanced Practical Inorganic and Metalorganic Chemistry*, Blackie Academic & Professional, London, **1997**, pp. 1-296.
[31] (a) A. Barabas, A. T. Balaban, *Tetrahedron* **1971**, *27*, 5495-5503; (b) A. Chaney, M. J. Astle, *J. Org. Chem.* **1951**, *16*, 57-63; (c) E. P. Kohler, J. L. E. Erickson, *J. Am. Chem. Soc.* **1931**, *53*, 2301-2309.
[32] J. Clayden, *Organolithiums: Selectivity for Synthesis* Elsevier Science Ltd., Oxford, **2003**, pp. 1-362.
[33] (a) D. G. Lee, H. Karaman, *Can. J. Chem.* **1982**, *60*, 2456-2459; (b) F. L. Cook, C. W. Bowers, C. L. Liotta, *J. Org. Chem.* **1974**, *39*, 3416-3418; (c) C. L. Liotta, H. P. Harris, M. McDermott, T. Gonzalez, K. Smith, *Tetrahedron Lett.* **1974**, 2417-2420; (d) C. L. Liotta, H. P. Harris, *J. Am. Chem. Soc.* **1974**, *96*, 2250-2252.
[34] (a) M. D. Rausch, F. E. Tibbets, H. B. Gordon, *J. Organomet. Chem.* **1966**, *5*, 493-500; (b) A. E. Ashley, T. J. Herrington, G. G. Wildgoose, H. Zaher, A. L. Thompson, N. H. Rees, T. Kraemer, D. O'Hare, *J. Am. Chem. Soc.* **2011**, *133*, 14727-14740.
[35] (a) D. J. Burton, L. Lu, *Organofluorine Chemistry: Techniques and Synthons, Vol. 193*, 1997 ed. (Ed.: R. D. Chambers), Springer GmbH, Berlin, **1997**, pp. 45-89; (b) D. J. Burton, Z. Y. Yang, *Tetrahedron* **1992**, *48*, 189-275; (c) *CRC Handbook Of Chemistry and Physics, Internet Version* (Ed.: D. R. Lide), CRC Press, Boca Raton, FL, **2005**, pp. 1455.
[36] D. Naumann, C. Schorn, W. Tyrra, *Z. Anorg. Allg. Chem.* **1999**, *625*, 827-830.
[37] C. Sousa, P. J. Silva, *European Journal of Organic Chemistry* **2013**, *2013*, 5195-5199.
[38] W. F. Beckert, J. U. Lowe, *J. Org. Chem.* **1967**, *32*, 582-584.
[39] R. D. Chambers, M. Todd, *J. Fluorine Chem.* **1985**, *27*, 237-240.
[40] A. K. Barbour, M. W. Buxton, P. L. Coe, R. Stephens, J. C. Tatlow, *J. Chem. Soc.* **1961**, 808-817.
[41] M. Allukian, G. S. Han, L. Hicks, A. J. Fry, *Arkivoc* **2002**, 76-79.
[42] (a) M. Schlosser, S. Strunk, *Tetrahedron Lett.* **1984**, *25*, 741-744; (b) F. Leroux, M. Schlosser, E. Zohar, I. Marek, *Chemistry of Organolithium Compounds, Vol. 1* (Eds.: Z. Rappoport, I. Marek), Wiley, Chichester, **2004**, 435-493; (c) M. Schlosser, *Pure Appl. Chem* **1988**, *60*, 1627-1634; (d) Schlosse.M, J. Hartmann, *Angew. Chem. Int. Ed.* **1973**, *12*, 508-509; (e) M. Schlosser, *J. Organomet. Chem.* **1967**, *8*, 9-16.

[43] N. N. Vorozhtsov, Jr., V. A. Barkhash, S. A. Anichkina, *Dokl. Akad. Nauk SSSR* **1966**, *166*, 598-601.
[44] H. C. Brown, U. S. Racherla, *J. Org. Chem.* **1986**, *51*, 427-432.
[45] R. Dobrovetsky, D. W. Stephan, *J. Am. Chem. Soc.* **2013**, *135*, 4974-4977.
[46] M. Scheibitz, H. Li, J. Schnorr, A. S. Perucha, M. Bolte, H.-W. Lerner, F. Jaekle, M. Wagner, *J. Am. Chem. Soc.* **2009**, *131*, 16319-16329.
[47] A. R. Cowley, A. J. Downs, S. Marchant, V. A. Macrae, R. A. Taylor, *Organometallics* **2005**, *24*, 5702-5709.
[48] C. Fan, L. G. Mercier, W. E. Piers, H. M. Tuononen, M. Parvez, *J. Am. Chem. Soc.* **2010**, *132*, 9604-9606.
[49] (a) G. J. P. Britovsek, J. Ugolotti, A. J. P. White, *Organometallics* **2005**, *24*, 1685-1691; (b) T. Beringhelli, G. D'Alfonso, D. Donghi, D. Maggioni, P. Mercandelli, A. Sironi, *Organometallics* **2003**, *22*, 1588-1590.
[50] T. Chivers, G. Schatte, *Eur. J. Inorg. Chem.* **2003**, 3314-3317.
[51] (a) H. Zhao, J. H. Reibenspies, F. P. Gabbai, *Dalton Trans.* **2013**, *42*, 608-610; (b) A. L. Travis, S. C. Binding, H. Zaher, T. A. Q. Arnold, J.-C. Buffet, D. O'Hare, *Dalton Trans.* **2013**, *42*, 2431-2437.
[52] (a) G. C. Welch, L. Cabrera, P. A. Chase, E. Hollink, J. D. Masuda, P. R. Wei, D. W. Stephan, *Dalton Trans.* **2007**, 3407-3414; (b) G. C. Welch, T. Holtrichter-Roessmann, D. W. Stephan, *Inorg. Chem.* **2008**, *47*, 1904-1906.
[53] M. Zaidlewicz, J. Meller, *Science of Synthesis* **2004**, *6*, 921-943.
[54] (a) S. Korcek, G. B. Watts, K. U. Ingold, *J. Chem. Soc., Perkin Trans. 2* **1972**, 242-248; (b) A. L. Korich, P. M. Iovine, *Dalton Trans.* **2010**, *39*, 1423-1431.
[55] M. J. S. Dewar, R. Jones, *J. Am. Chem. Soc.* **1967**, *89*, 2408-2410.
[56] (a) W. B. Hollyhead, R. Stephens, J. C. Tatlow, W. T. Westwood, *Tetrahedron* **1969**, *25*, 1777-1783; (b) S. F. Campbell, J. M. Leach, R. Stephens, J. C. Tatlow, *J. Fluorine Chem.* **1971**, *1*, 85-101; (c) S. F. Campbell, R. Stephens, J. C. Tatlow, W. T. Westwood, *J. Fluorine Chem.* **1972**, *1*, 439-444.
[57] M. B. Smith, J. March, *March's Advanced Organic Chemistry: Reactions, Mechanisms, and Structure, 5th Edition*, Wiley-Blackwell, New Jersey, **2000**, pp. 1-2112

CHAPTER FOUR

Si-P Lewis Pairs: Classical Adducts Exhibiting 'Frustrated' Reactivity

4.1 Introduction

By far the most commonly used Lewis acids in FLP chemistry are organometallics of the Group 13 elements (e.g. R_3E; E= B or Al, R = electron-deficient organyl) in which congeners of the ubiquitous $B(C_6F_5)_3$ have retained their appeal. As shown by the Papai research group a cumulative Lewis acidity and basicity is required to effect H_2 cleavage, in which $B(C_6F_5)_3$ will activate H_2 upon the addition of moderately basic TMP and tBu$_3$P bases. Silylium ions (R_3Si^+) (R = alkyl, aryl) are isoelectronic with this class of compounds and, due to their potent electrophilicity, can be expected to undergo similar FLP reactivity when employed as the Lewis acid partner. [1] Modification of the pK_a of the base has already been demonstrated by Paradies to effect the reduction of electron-poor unsaturated substrates.[2] Therefore, the increased Lewis acidity of these ions may shift the reactivity spectrum towards weaker bases whose conjugate acidity remain capable protonating the robust Si-O [Bond Enthalpies ΔH : Si–O (453 kJ mol^{-1}) *vs* O–H (459 kJ mol^{-1})]; p*K*a ~ –1.5 ($Et_3SiOSiEt_3$)] formed during the reductive silylation of CO_2 and other oxygenated substrates.[3] Shephered *et al.* using UV spectroscopy have shown hexamethyldisiloxane ($Me_3SiOSiMe_3$) to be measurably protonated by the dye-4-chloro-2-nitroaniline (p*K*a ~ –1.0 in H_2O; Figure 4.1). Phenyl substituted siloxanes are weaker bases than their alkyl analogues in which IR studies have shown preferential hydrogen bonding of the phenyl rings to the conjugate acid rather than to the siloxane oxygen. Thus, these siloxanes are less favoured for incorporation into a catalytic cycle.

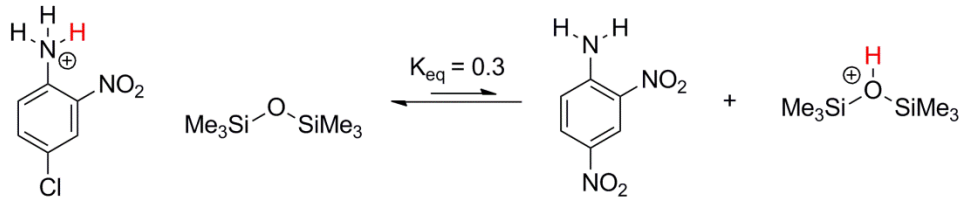

Figure 4.1. Protonation of $Me_3SiOSiMe_3$ by 4-chloro-2-nitroaniline (p*K*a ~ –1.0 in H_2O).

In contrast to the analogous R_3C^+, there are few reports for stable R_3Si^+ cations, which is ascribed to the difficulties in stabilising the diffuse 3*p* Si valence orbitals *via* either

hyperconjugation or π-conjugation.[4] Si–C bonds are typically 25% longer than those of C–C bonds which thus leads to a considerable diminishment in stabilising π-bonding interactions. This reduced tendency for stabilisation can explain, in part, their voracious affinity for nucleophiles; in the condensed phase even traditionally 'inert' arene solvents[5] and weakly coordinating anions (WCAs)[6] display interactions with the silicon centre. The findings of Ozerov *et al.* reflect this indiscriminate appetite for σ- and π- donors, with decomposition of even the robust $[B(C_6F_5)_4]^-$ anion observed, presumably *via* $[C_6F_5]^-$ abstraction or C–F activation.[7]

To disfavour side reactivity with either the WCA or solvent, Müller *et al.* have incorporated steric protection about the Si centre.[8] In this instance, bulky triarylsilylium compounds (Ar_3Si^+; Ar = $C_6H_{6-x}Me_x$, x = 3-5), in combination with a phosphine base (R_3P; R = alkyl, aryl), are shown to generate FLPs that engage in both H_2 cleavage and CO_2 sequestration. Nonetheless, eventual solution-phase decomposition of these FLPs under ambient conditions was observed, and attributed to the instability of Ar_3Si^+ in solution as evidenced by formation of protonated arene products (*vide infra*).[9]

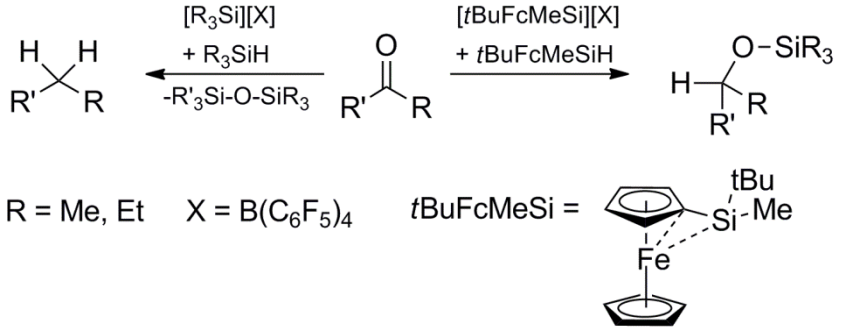

Figure 4.2. Selective hydrosilylation employing tamed silylium ions vs. 'untamed' R_3Si^+.

Alternatively, the voracious electrophilicity of the silylium centre may be mediated by incorporation of intramolecular donors which tame the potent reactivity and allow sufficient selectivity. In this respect, Oestereich and co-workers employed the ferrocene-stablised silylium ion $[(C_5H_5)Fe(C_5H_4Si\textit{t}BuMe)]^+$ to selectively and catalytically hydrosilylate various ketones to the corresponding alkyl/silyl ethers (RR'CH–O–SiR_3; R/R' = alkyl);[10] conversely the fully reduced alkanes R–CH_2–R' were isolated upon use of 'untamed' R_3Si^+ (Figure 4.2).[11] Although this system does not display FLP reactivity, the use of donors may provide a useful paradigm for future silicon based Lewis acids, which not only stabilise the silylium centre but are sufficiently basic to support FLP style reactivity.

In this regard, the following chapter details the synthesis and characterisation of *classical* phosphine adducts of the sterically unencumbered trialkylsilylium ions R_3Si^+ (R = Et, *i*Pr) in combination with the bulky base *t*Bu_3P. These systems demonstrate appreciable thermal stability, in which use of a Lewis base stabilises the otherwise highly reactive R_3Si^+ moiety, but remarkably, despite not being 'true' FLPs, are not precluded from H_2 and CO_2 activation.

4.2 Traditional routes to R_3Si^+

Traditional approaches for generating R_3Si^+ have centred around electrophilic abstraction of X^- from four coordinate R_3SiX (X = H, halide or oxyanion). Typically this has utilised the Barlett-Condon-Schneider (BCS) hydride transfer reaction (X = H), in which hydride delivery is driven by formation of a stronger C–H covalent bond (Figure 4.3).[12]

Figure 4.3. Generic Bartlett-Condon-Schneider (BCS) hydride transfer reaction for the generation of $[R_3Si]^+$. (R = alkyl, aryl)

This reaction, although expedient for conventional trialkylsilanes such as Me_3SiH and Et_3SiH, remains governed by kinetic factors, for example the high steric demands of bulky triarylsilanes such as trimesitylsilane (Mes_3SiH) demonstrate no reaction with $[Ph_3C][B(C_6F_5)_4]^-$.[13] Müller *et al.* have circumvented this problem through use of diaryl(methyl)silanes, which undergo a classic BCS hydride reaction prior to a rapid alkyl-aryl exchange which ultimately yields the targeted triarylsilylium ion and Me_3SiH (Figure 4.4).[8]

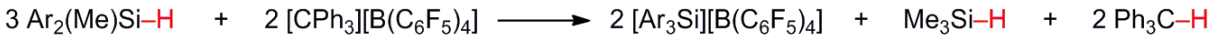

Figure 4.4. Synthesis of triarylsilylium ions from diaryl(methyl)silanes. Ar = pentamethyl (Pemp), 2,6-dimethylphenyl (Xylyl), 2,4,6-trisopropylphenyl (Tipp), 2,4,6-trimethylphenyl (Mes).

Alternatively, the generation of R_3Si^+ may proceed *via* the electrophilic abstraction of X^-. Performed in weakly polar solvents (e.g PhMe), this approach relies upon the formation of an insoluble halide or oxyanion salt of the electrophile (Ag^+, Na^+) which not only drives the reaction but facilitates facile separation. However, thermodynamic factors often limit this strategy, in which the interaction of R_3Si^+ with its corresponding anion leads to significant covalency. For example, AgBr precipitates from the reaction of *i*Pr_3SiBr and $AgClO_4$ in which the resultant *i*Pr_3Si^+ is coordinated to by the perchlorate anion. Switching $[ClO_4]^-$ for

the very weakly coordinating carborane anion $[CB_{11}H_6Br_6]^-$ leads to no reaction while mixing AgBr with iPr$_3$Si($CB_{11}H_6Br_6$) (the reverse) affords iPr$_3$SiBr (Figure 4.5).[1,14] Evidently, the formation of a Si–O bond provides a considerable driving force for the reaction of iPr$_3$SiBr with $AgClO_4$, although at the expense of a three-coordinate silicon centre. Here ^{37}Cl NMR line broadening experiments illustrated the silyl perchlorate to be significantly covalent.[15]

a) iPr$_3$SiBr + $AgClO_4$ $\xrightarrow{PhMe}$ iPr$_3$Si($OClO_3$) + $AgBr_{(s)}$

b) iPr$_3$SiBr + Ag($CB_{11}H_6Br_6$) $\xrightarrow{PhMe}$ iPr$_3$Si($CB_{11}H_6Br_6$) + $AgBr_{(s)}$

Figure 4.5. a) Halide abstraction upon treatment of iPr$_3$SiBr with $AgClO_4$. Reaction driven by Si–O formation. b) No reaction upon substitute of $[ClO_4]^-$ for weakly coordinating carborane $[CB_{11}H_6Br_6]^-$.

4.3 Anion and solvent considerations for the reactivity studies of R_3Si^+

The strength of the interaction between R_3Si^+ and its environment is dependent on the counterion and solvent employed in which ^{29}Si NMR spectroscopy provides a useful handle. True three-coordinate silylium ions are calculated to have ^{29}Si NMR shifts greater than 200 ppm while tetravalent silicon compounds exhibit shifts close to 0 ppm. For example the ^{29}Si $\{^1H\}$ shift of the sterically bulky $[Mes_3Si][B(C_6F_5)_4]$ is reported at 225.5 ppm (C_6D_6) in which the severe steric congestion of six *ortho*-methyl groups precludes nucleophilic attack at the silicon centre.[13] In contrast $[R_3Si][B(C_6F_5)_4]$ (R = Et, iPr) species are reported to display ^{29}Si $\{^1H\}$ NMR resonances at 92.3 to 107.5 ppm (C_7D_8) (*vide infra*),[16] and reflect coordination to the aromatic solvent.

The difficulties in characterisation and isolation of a 'free' R_3Si^+ species have been extensively studied in which the accessibility of the empty orbital at the silicon atom is difficult to restrain. Presently, truly non-coordinating anions are unknown, in which the weakly coordinating anions (WCAs) $[B(C_6F_5)_4]^-$ and $[CB_{11}H_6Br_6]^-$ are the most widely used. Their large size and buried delocalised charge interact minimally with R_3Si^+ (R = alkyl) to the extent where coordination becomes difficult to detect in the solution phase. These observations contrast with that for tetraaryl borate $[BArF_{24}]^-$, which readily undergoes fluoride abstraction in the presence of Me_3Si^+; the C(sp^3)–F hybridised bonds remain activated towards nucleophilic attack at the Si centre.

Despite the availability of minimally interacting anions, solvent binding has proven problematic. This has led Reed and co-workers to conclude that truly uncoordinated R_3Si^+ (R = Et, iPr) exist only in the gas phase.[17] Addition of $[Ph_3C][B(C_6F_5)_4]$ to neat R_3SiH forms

dimeric $[R_3Si(\mu\text{-}H)SiR_3]^+[B(C_6F_5)]^-$ [^{29}Si {^{1}H} (C_6D_5Cl): δ = 58 ppm (R = Et)], whilst stoichiometric addition, even in a non-nucleophilic solvent, affords $[R_3Si{\cdot}(Solvent)]^+$.[16,18] Silylated arenium ions (Figure 4.6) are formed when electron rich aromatics (e.g. toluene and benzene) are employed,[19] which subsequently behave as strong Brønsted acids[20] in the presence of hindered amine and phosphine bases such as N,N-diisopropylethylamine[21] (*p*Ka ~ 11 in H_2O)[22] and trimesitylphosphine[9] (*p*Ka for Ph_3P ~ 3 in H_2O).[23] Moreover, the benzene solvate $[Et_3Si{\cdot}C_6H_6]^+$ (^{29}Si {^{1}H} (C_6D_6): δ = 94 ppm) is advocated to protonate Et_3SiH and evolve H_2 gas.[24]

4.4 Synthesis of $[R_3Si–P\mathit{t}Bu_3]^+[B(C_6F_5)_4]^-$ [R = Et (12); R = *i*Pr (13)]

In light of the inherent acidity of the species $[R_3Si{\cdot}S]^+$ (S= C_6H_6, PhMe), these solvates were unsuitable for use in generating the 'R_3Si^+' moiety especially if handled in the presence of the basic $\mathit{t}Bu_3P$ (*p*Ka for $\mathit{t}Bu_3P$ ~ 11.4 in H_2O).[23] Beneficially, the relatively electron-poor chlorobenzene (PhCl), forms an intrinsically more inert adduct $[R_3Si{\cdot}ClPh]^+$. DFT calculations reveal a preference for solvent coordination *via* the chlorine lone pair over the aforementioned arenium ion structure (Figure 4.6).[18]

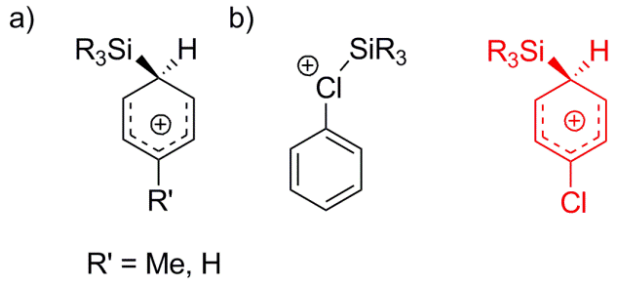

Figure 4.6. Solvent complexes $[R_3Si{\cdot}Solvent]^+$ (R = Et, *i*Pr; Solvent = C_6H_6, PhMe, PhCl); a) Silylated arenium ions of C_6H_6 and PhMe b) Chloronium ion formation as opposed to a chloroarenium ion formation (highlighted red) employing PhCl in the presence of R_3Si^+.[24]

Advantageously, addition of equimolar Et_3SiH to $[Et_3Si{\cdot}ClPh]^+$ does not liberate H_2 but rather led to a rapid exchange between $[Et_3Si{\cdot}ClPh]^+$, Et_3SiH and $[Et_3Si(\mu\text{-}H)SiEt_3]^+$ in which all three 'Et_3Si' species are in equilibrium; the observed ^{1}H chemical shift of '$Et_3Si–H$' is a weighted average of the free and bridging silane (Figure 4.7, the Si–H–Si fragment is displayed with a bent geometry to reflect that reported using X-Ray diffraction).[24] In light of these reports, electron poor aromatics, such as PhCl, were chosen as the preferred solvent for synthesis and solution phase studies for the target systems. It should be noted that these ions react readily with H_2O to form siloxanes $R_3Si–O–SiR_3$ and thus the following syntheses and

solution-phase studies required meticulous drying of solvents, and conducting reactions in Teflon® vials inside of a glovebox (consult Chapter 5 for further detail).

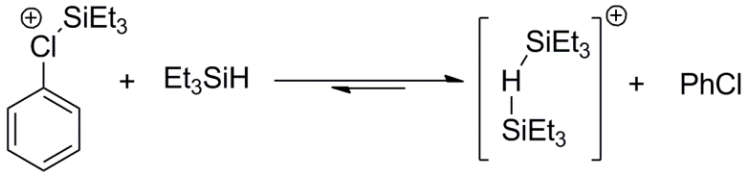

Figure 4.7. The equilibrium established between Et_3SiH, $[Et_3Si{\cdot}ClPh]$ and $[R_3Si(\mu\text{-}H)SiR_3]^+$.[24]

Treatment of excess R_3SiH (R = Et, *i*Pr) with $[Ph_3C][B(C_6F_5)_4]$ in PhCl afforded solutions of the silylium ion synthon 'R_3Si^+', stabilised as an equilibrium between the PhCl solvate $[R_3Si{\cdot}ClPh]^+$ and silane bridged cation $[R_3Si(\mu\text{-}H)SiR_3]^+$. Subsequent *in situ* reactions with tBu$_3$P saw immediate PhCl displacement to furnish the salts $[R_3Si{-}Pt\text{Bu}_3]^+[B(C_6F_5)_4]^-$ (R = Et, **12**; R= *i*Pr, **13**), which were precipitated with hexanes and recrystallised as white microcrystalline solids from PhCl in excellent yield (85% and 89% respectively) (Figure 4.8).

An alternative, silane-free route to **12** involves triflate abstraction from Et_3SiOTf by $LiB(C_6F_5)_4$, in the presence of tBu$_3$P (yield 71%). This reaction is driven by the formation of LiOTf which is insoluble in non-donor solvents. However, in PhCl metathesis afforded LiOTf as a fine suspension which necessitated tedious filtration techniques to ensure thorough separation of **12** [^{19}F NMR spectroscopy used to track the departed $[OTf]^-$ anion (^{19}F: δ = 78 ppm, C_6D_5Cl)]. Alternatively, metathesis in CH_2Cl_2 led to the rapid precipitation of LiOTf in which filtration afforded **12** in good yield (71 %).

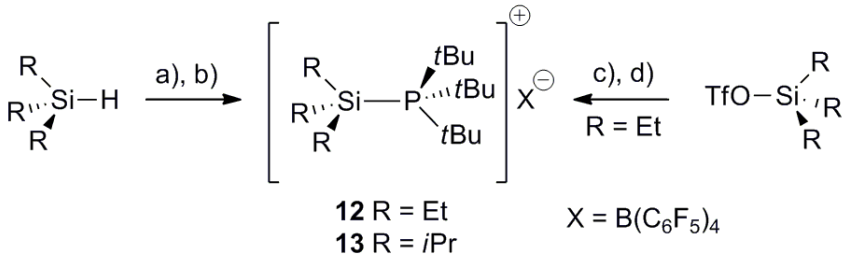

Figure 4.8. Synthesis of compounds **12** and **13**. Reagents and conditions: a) $[Ph_3C][B(C_6F_5)_4]$, PhCl, RT, –Ph_3CH; b) tBu$_3$P (yields 85% (**12**), 89% (**13**); c) $Li[B(C_6F_5)_4]$, CH_2Cl_2, RT, –LiOTf; d) tBu$_3$P (yield 71%).

An analogous protocol was applied for synthesis of the *i*Pr analogue **13**, in which a vivid red solution was witnessed upon addition of $LiB(C_6F_5)_4$ to iPr$_3$SiOTf. Work up gave an oily red material, in which the ^{1}H and ^{31}P NMR spectra gave unassignable signals, presumably as a result of side reactions with CH_2Cl_2 solvent. Upon replacement for the more inert PhCl,

precipitation of LiOTf was not observed, although three new environments were witnessed in the ^{31}P NMR spectrum; a minor resonance at 60.2 ppm, assigned to be the phosphonium impurity [*t*Bu$_3$PH]$^+$ from adventitious moisture present in the solvent, a small resonance at 57.3 ppm and a larger resonance at 56.0 ppm (Figure 4.10). Subsequently, the resonance at 56.0 ppm was found to be that of [*t*Bu$_3$P→Li][B(C$_6$F$_5$)$_4$] from addition of *t*Bu$_3$P to LiB(C$_6$F$_5$)$_4$ in the absence of *i*Pr$_3$SiOTf. Arguably, the preference for *t*Bu$_3$P coordination to Li$^+$ over *i*Pr$_3$Si$^+$ may be rationalised as a thermodynamic effect; the greater steric profile of an *i*Pr group compared with an Et substituent leads to a diminished Lewis acidity towards *t*Bu$_3$P (*i*Pr$_3$Si$^+$ relative to 'naked' Li$^+$). For this reason, and in contrast to the behaviour of Et$_3$Si$^+$, the *i*Pr$_3$Si$^+$ is deemed to preferentially coordinate the smaller and harder [OTf]$^-$ anion.

Following this observation, elevated temperature (> 50 ºC) was envisaged to force LiOTf formation. Heating a stoichiometric solution of *t*Bu$_3$P, LiB(C$_6$F$_5$)$_4$ and *i*Pr$_3$SiOTf at 50 ºC markedly enhanced the ^{31}P NMR resonance at 57.3 ppm [assigned as **13** (*vide infra*)] concomitant with a loss in intensity of [*t*Bu$_3$P→Li][B(C$_6$F$_5$)$_4$] (Figure 4.10). Although, full conversion was not witnessed irrespective of the temperature employed (50 - 100 ºC); presumably the solubility of LiOTf at this temperature established an equilibrium between [*t*Bu$_3$P→Li]$^+$ and **13** (Figure 4.9). Attempts to fractionally crystallise **13** *via* the slow diffusion of hexane onto a PhCl solution were unsuccessful, in which the resultant colourless plates were identified to be [*t*Bu$_3$P→Li][B(C$_6$F$_5$)$_4$] using X-ray crystallography (Figure 4.11).

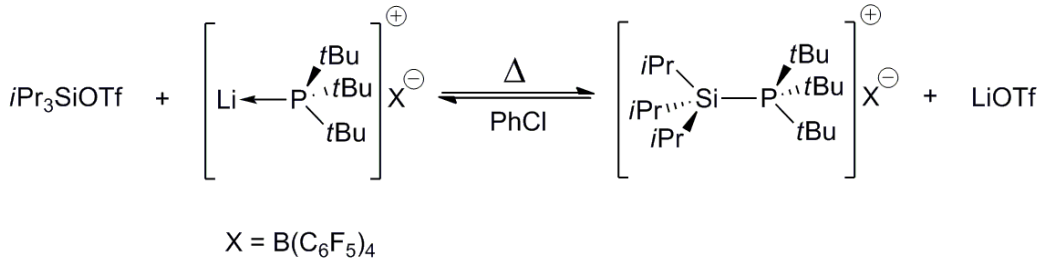

Figure 4.9. The equilibrium between [*t*Bu$_3$P→Li][B(C$_6$F$_5$)$_4$] and **13** established upon heating a solution of *t*Bu$_3$P, LiB(C$_6$F$_5$)$_4$ and *i*Pr$_3$SiOTf at 50 ºC.

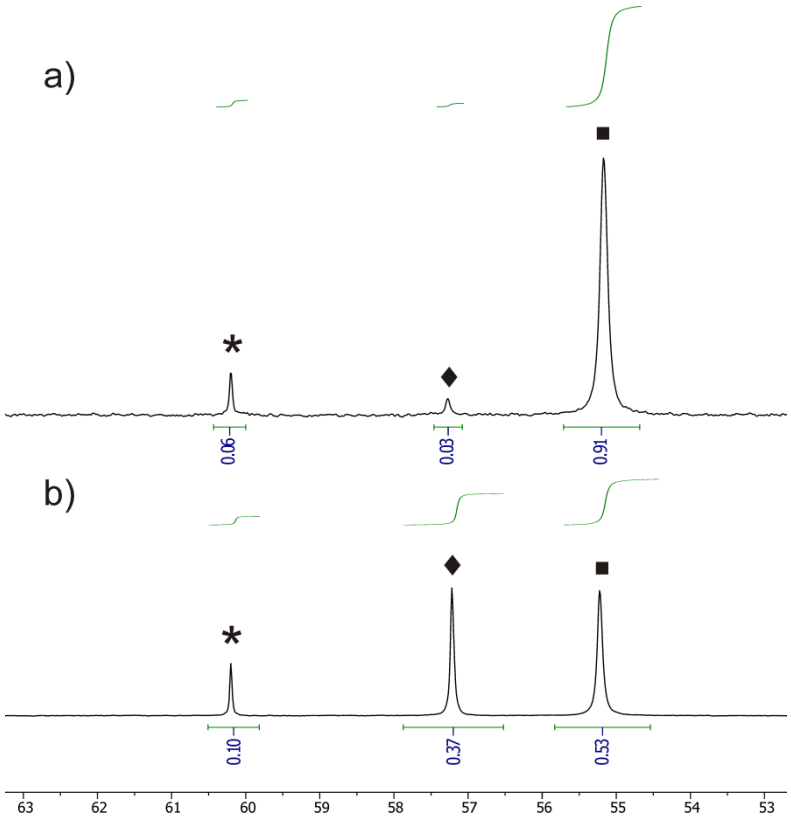

Figure 4.10. The ^{31}P {H} NMR spectra for a solution of tBu$_3$P, LiB(C$_6$F$_5$)$_4$ and iPr$_3$SiOTf. a) Prior to heating b) following 1 hour at 50 ºC. ♦ denotes **13**, ■ [tBu$_3$P→Li][B(C$_6$F$_5$)$_4$] and * the [tBu$_3$PH] impurity.

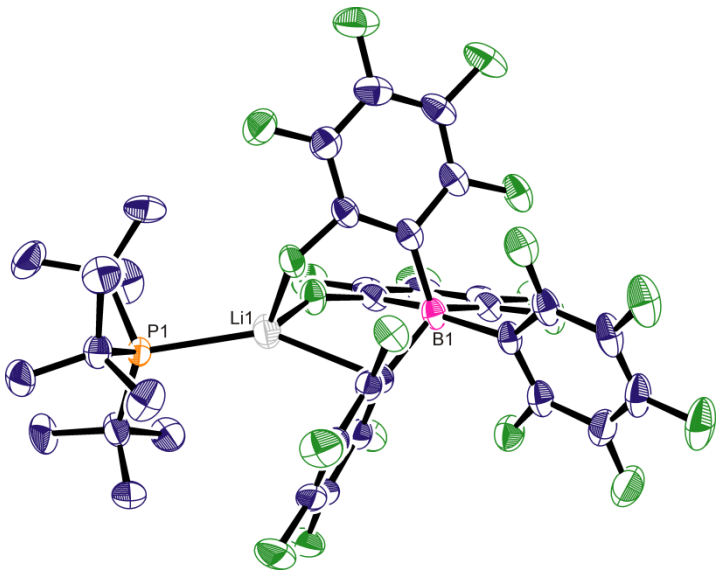

Figure 4.11. ORTEP plot of the X-ray structure of the asymmetric [tBu$_3$P→Li][B(C$_6$F$_5$)$_4$]. C atoms blue, P atom orange, B atom pink, F atoms green, Li atom grey, and Si atom light brown. H atoms have been removed for clarity, and thermal ellipsoids are shown at 50% probability.

Examination of the solid state structure illustrated tetracoordination about the lithium centre *via* the [B(C$_6$F$_5$)$_4$]$^-$ anion. The C···F contacts are unremarkable and comparable to those reported for the C$_6$H$_6$ and Et$_2$O solvates of Li[B(C$_6$F$_5$)$_4$].[25] Unusually, a short Li···C$_{ipso}$ contact

is observed (2.480(5) Å) which likely stems from a π-interaction of the C_6F_5 ring with the lithium centre. Therefore, **13** is best prepared using *i*Pr_3SiH and $[Ph_3C][B(C_6F_5)_4]$ in PhCl.

4.5 Characterisation of $[R_3Si–Pt Bu_3]^+[B(C_6F_5)_4]^-$ [R = Et (12); R = *i*Pr (13)]

Both **12** and **13** were characterised by HRMS (ES+/ES–), IR and elemental analysis. The IR spectra of **12** and **13** display no evidence for a 1900 cm^{-1} absorbance indicative of residual $[R_3Si–H–SiR_3][B(C_6F_5)_4]$,[17] and elemental analyses supported a silane free composition. Recrystallisation (–25 ºC) from PhCl (**12**) or PhF (**13**) produced large colourless plates suitable for single crystal X-ray diffraction (Figure 4.12 and Figure 4.13; see appendix for full structural details.

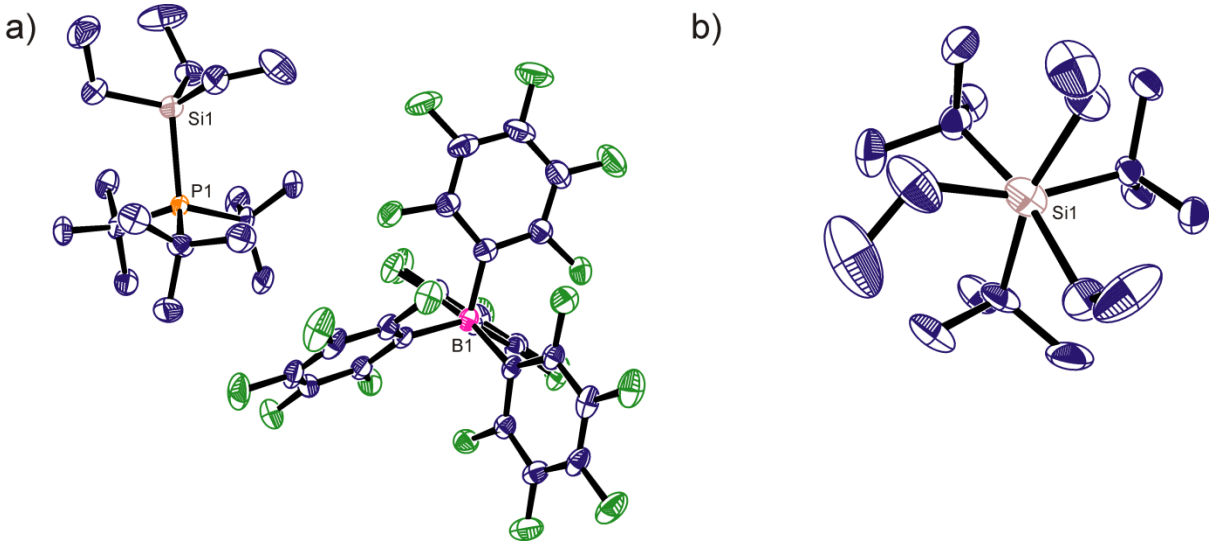

Figure 4.12. a) ORTEP plot of the X-ray structure of **12**. b) View along Si–P axis. $B(C_6F_4)_4^-$ anion removed for clarity. C atoms blue, P atom orange, B atom pink, F atoms green and Si atom light brown. H atoms have been removed for clarity, and thermal ellipsoids are shown at 50% probability. Selected bond length: Si1–P1 = 2.378(8) Å.

Both compounds contain cationic fragments derived from a donor-acceptor interaction between the $[R_3Si]^+$ moiety and *t*Bu_3P, as exemplified by the pyrimidalisation about the Si atom (*ca.* 0.60 Å deviation from best plane of the three C atoms in the C_3Si unit). The average C–Si–C bond angles of 109.9° and 111.4° are also much closer to the idealised tetrahedral angle (109.5°) than that found in *i*$Pr_3Si(CHB_{11}H_5Cl_6)$ (117.3°),[6] which possesses significant silylium character and hence approaches a trigonal geometry. $B(C_6F_5)_4^-$ anions are well separated from the cations, with no close Si to F contacts, and hence can be considered non-coordinating. However, the Si–P bond distances are rather long (2.378(8) Å and 2.484(3) Å for **12** and **13** respectively, and within the top 2% of those reported in the Cambridge

Structual Database (CSD). This may be attributed to the high degree of steric strain due to crowding between the organic groups along the Si–P axis, and is compared with $[PhMe_2Si–PtBu_3]^+[HB(C_6F_5)_3]^-$ (Si–P = 2.376(2) Å), which has been prepared from $PhMe_2SiH$ and the FLP system $tBu_3P/B(C_6F_5)_3$.[26]

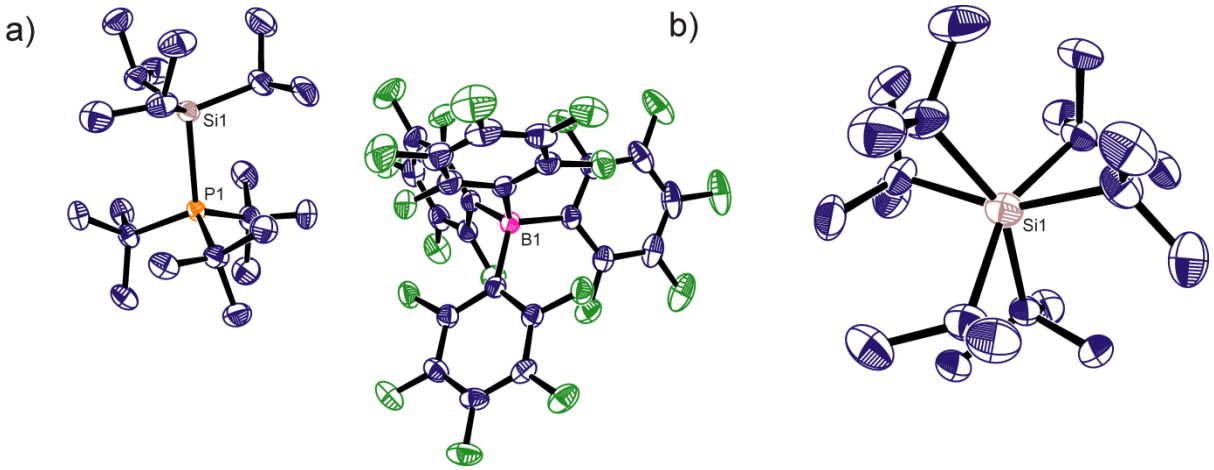

Figure 4.13. a) ORTEP plot of the X-ray structure of **13**. b) View along Si–P axis. $[B(C_6F_4)]^-$ anion removed for clarity. C atoms blue, P atom orange, B atom pink, F atoms green and Si atom light brown. H atoms have been removed for clarity, and thermal ellipsoids are shown at 50% probability. Selected bond length: Si1–P1 = 2.484(3) Å.

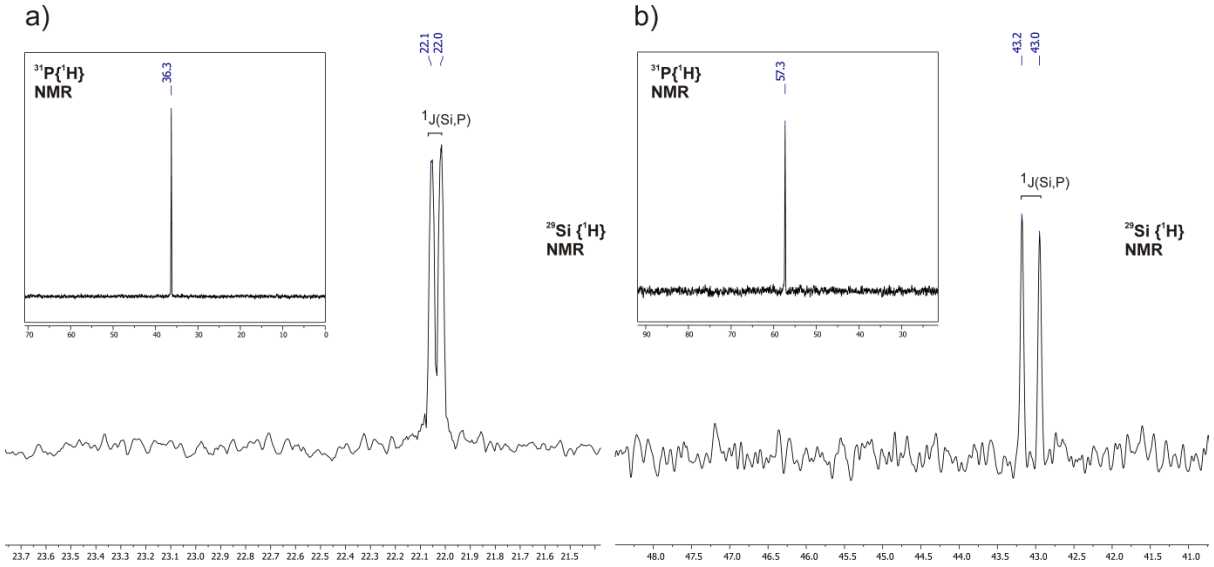

Figure 4.14. ^{31}P {H} and ^{29} Si {H} NMR spectrum of products (a) **12** and (b) **13**. ^1J(Si, P) = 4 Hz and 23 Hz respectively.

The room-temperature ^1H and ^{13}C NMR spectra (C_6D_5Cl) for both **12** and **13** are commensurate with the solid state structures, with the upfield ^{29}Si {^1H} resonances (δ = 22.0 and 43.1 ppm, ^1J(Si,P) = 4 and 23 Hz, respectively) revealing that the Si–P bond is intact in solution (Figure 4.14). However, these coupling constants are appreciably smaller than those

reported for $[(C_6Me_5)_3Si–PEt_3]^+[B(C_6F_5)_4]^-$[9] or zwitterionic $[Mes_2(SiPh_2H)P^+CH_2CH_2B^-H(C_6F_5)_2]$[27] ($^1J(Si,P)$ = 41.2 and 48.5 Hz, respectively), implying a weaker Si–P interaction. Interestingly the coupling constant for **12** is markedly smaller than that for **13** which is unexplained based upon the shorter Si–P bond witnessed in the solid state. The $^{31}P\{^1H\}$ NMR resonance for **13** (δ = 57.3 ppm) is noticeably closer to that seen for free tBu$_3$P (δ = 62.0 ppm) than for **12** (δ = 36.4 ppm), which correlates with a weaker bond between Si and P in **13** than in **12**, which might predispose greater reactivity. In accordance with this proposition, **13** reacted instantaneously with CD_2Cl_2 to give unassignable signals presumably from halide abstraction while in C_6H_6, iPr$_3$Si(C$_6$H$_5$) [^{1}H NMR: δ = 1.02 (d, [(C*H*$_3$)$_2$CH)]$_3$Si), 1.40 ppm (sept, [(CH$_3$)$_2$C*H*]$_3$Si)] and [tBu$_3$P–H][B(C$_6$F$_4$)] (^{1}H NMR: δ = 1.12 ppm; $^{31}P\{^1H\}$ NMR: δ = 60.2 ppm) were observed in solution. On the other hand, **12** was stable in both solvents (298 K).

12 and **13** proved to be highly reactive to even trace amounts of H_2O dissolved in PhCl to afford [tBu$_3$P–H][B(C$_6$F$_4$)] and R$_3$Si–O–SiR$_3$ (R=Et: ^{1}H NMR δ = 0.53 [((CH$_3$C*H*$_2$)$_3$Si)$_2$O], 0.94 ppm [((C*H*$_3$CH$_2$)$_3$Si)$_2$O]). Accordingly, the solution-phase studies required meticulous drying of deutero solvents and performing all NMR experiments in Teflon® inserts.

Table 5.1. Notable spectral data and yields for **12** and **13**

Compound	Yield (%)	Si–P (Å)	$\delta(^{31}P\{^1H\})$	$\delta(^{29}Si\{^1H\})$, ($^1J_{Si-P}$, Hz)
12	85	2.378(8)	36.4	22.0 (4)
13	89	2.484(3)	57.3	43.1 (23)

4.6 Dissociation studies

In order to investigate the possibility that **12** and **13** may dissociate to generate the FLP tBu$_3$P/R$_3$Si$^+$ reversibly in solution, variable temperature (VT) ^{31}P NMR studies were conducted over the range –40 to 100 °C (Ph$_3$P internal capillary reference). The ^{31}P resonances for both compounds move downfield as the temperature increases, yet reach only a maximum Δδ ≈ 6 ppm over the 140 K range, and free tBu$_3$P is never observed: a representative ^{31}P VT NMR spectrum of **13** is displayed in Figure 4.15. At low temperature the spectra show very broad resonances (^{31}P: δ = 33.6 and 54.5 ppm, –40 °C) which move progressively downfield (^{31}P: δ = 39.2 and 60.6 ppm, c.f. tBu$_3$P: δ = 65.0 ppm; both at 100 °C) and sharpen markedly; this behaviour might be consistent with a rapid equilibrium between [R$_3$Si–PtBu$_3$][B(C$_6$F$_5$)$_4$] and a small concentration of dissociated products. However,

addition of tBu$_3$P (1-10 eq.) to these solutions (100 °C) led to no discernible change in the line shape or chemical shift position of **12** and **13**; if a rapid exchange were indeed occurring, introduction of extraneous tBu$_3$P would be expected to lead to a significant perturbation of the ^{31}P NMR resonances. Additionally, a crossover experiment was performed on a mixture of **12** and **13** (100 °C, PhCl, 1:1), which was monitored through correlation (EXSY) of their corresponding ^{31}P resonances; again, no exchange could be detected.

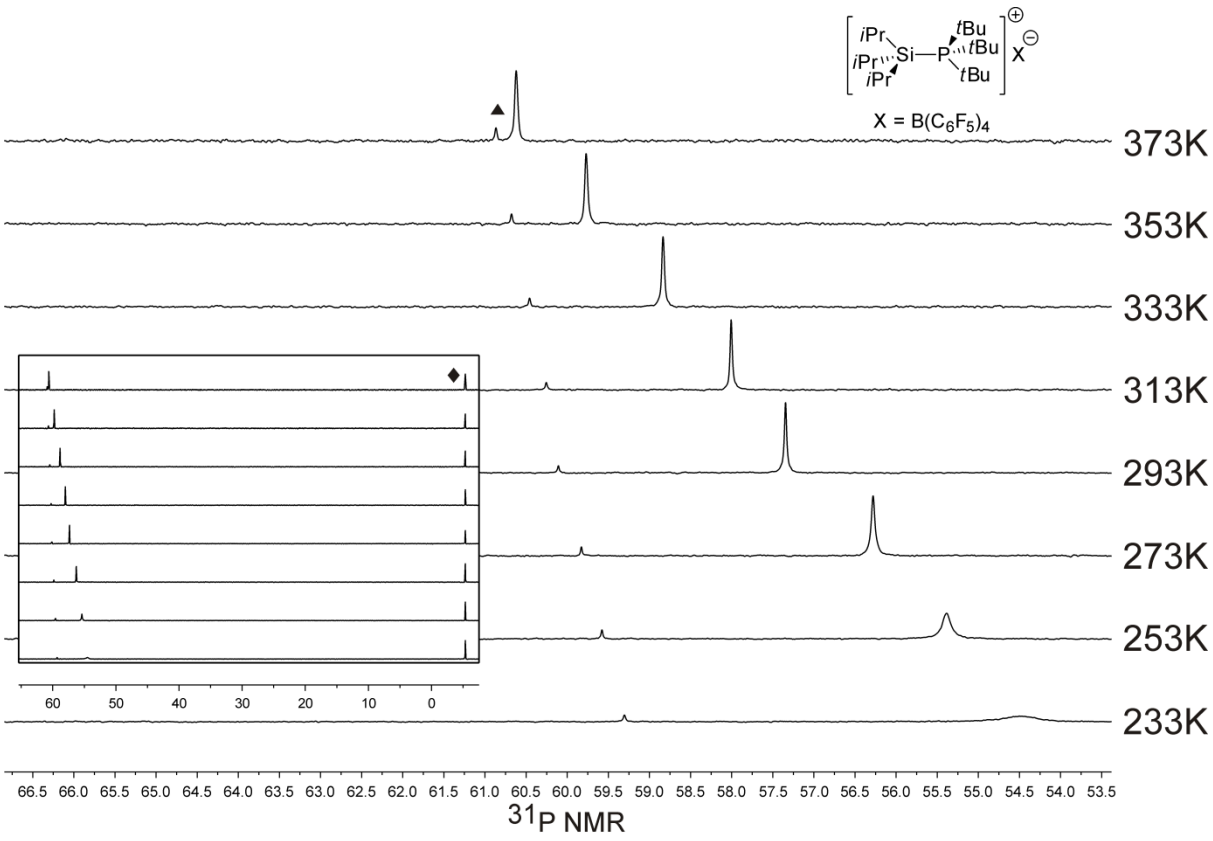

Figure 4.15. Variable temperature ^{31}P {^{1}H} NMR spectroscopy of **13** in C_6D_5Cl solvent. ▲ denotes trace [tBu$_3$PH][B(C$_6$F$_5$)$_4$] (due to adventitious H_2O). Resonances referenced to internal capillary (♦ denotes Ph_3P in C_6D_5Cl; δ = – 5.3 ppm).

Finally, the salts [R$_3$Si·ClPh]$^+$[B(C$_6$F$_5$)$_4$]$^-$ (R = Et, iPr) were isolated according to literature procedure in order to investigate their reactivity in the absence of added phosphine. As recently noted by Heinekey *et al*. these salts are not stable to long term storage in which the usually robust [B(C$_6$F$_5$)$_4$]$^-$ anion gradually decomposes. Accordingly, heating these species at 100 °C led to immediate decomposition of the [B(C$_6$F$_5$)$_4$]$^-$ anion [^{19}F NMR: δ = –166.1 ppm (*m*–CF), –162.4 ppm (*p*–CF), –131.6 ppm (*o*-CF)] to give a multitude of unassignable resonances. This implies that if dissociation of tBu$_3$P from either **12** or **13** occurs to generate R$_3$Si$^+$ or (more likely) [R$_3$Si·ClPh]$^+$, the instability of [B(C$_6$F$_5$)$_4$]$^-$ in the presence of the silylium ion would lead to extremely rapid decomposition of **12** and **13**. In contrast, **12** was

found robust in solution, even after heating PhCl solutions for several days at 100 ºC. In the case of **13,** trace decomposition (<5 %) occurred only after 24 hours of heating at 90 ºC. However, the borate anion remained robust in the ^{19}F NMR spectra in which the ^{1}H and ^{31}P solution demonstrated the formation of trace [tBu$_3$P–H][B(C$_6$F$_5$)$_4$] (^{1}H NMR: δ = 1.14 ppm; ^{31}P NMR: δ = 60.2 ppm) ($t_{½}$ = 120 hours). Attempts to identify the product of decomposition for the 'iPr$_3$Si' fragment employing ^{1}H, ^{29}Si and GC MS were unsuccessful. Collectively this data suggests that, even at elevated temperatures, the Si–P linkage for **12** and **13** remains surprisingly robust in solution.

4.7 Reactivity of 12 and 13 with H_2/D_2

In contrast to the results reported for the 'true' silylium FLPs, (C$_6$Me$_5$)$_3$Si$^+$/PR$_3$ (R = bulky alkyl/aryl; Mes, tBu, oTol, Cy, C$_6$Me$_5$) which underwent H_2 heterolysis after 30 minutes,[9] admission of H_2 (4 bar, 25 °C) to C$_6$D$_5$Cl solutions of either **12** or **13** led to no reaction. However, upon heating these solutions to 90-100 °C, complete consumption of **13** was observed**,** whilst only 50% in the case of **12**. For each experiment, the loss of the adduct in both ^{1}H and ^{31}P NMR spectra was concomitant with formation of the corresponding R$_3$Si–H (^{1}H NMR: δ = 3.76 (R = Et) and 3.43 (R = iPr) ppm) and phosphonium [tBu$_3$P–H]$^+$ (^{1}H NMR: δ = 4.17 ppm, ^{1}J(H,P) = 430 Hz; $^{31}P\{^{1}H\}$ NMR, δ = 60.3 ppm). Activation of H_2 by **12** was found to be much slower than **13**; only after 24 hours of heating at 100 ºC were appreciable Et$_3$Si–H resonances witnessed. Upon heating for an additional 4 days, the ^{31}P environment of **12** had diminished 50% relative to the newly formed [tBu$_3$P–H]$^+$, concomitant with an increase in the ^{1}H Et$_3$Si–*H* resonance. Prolonged reaction time (4 – 10 days) and/or higher reaction temperatures (100-140 ºC) afforded little or no improvement to the reported yield (50-53%, four runs at 100 ºC) (Figure 4.16). By comparison, **13**, following 8 hours heating at 90 ºC, was found to react more rapidly under a H_2 atmosphere and in almost quantitative yield (90-94%, four runs) (Figure 4.17). Reactions in dilute solution, such as those under H_2, invariably became exposed to trace amounts of H_2O, leading to [tBu$_3$PH][B(C$_6$F$_5$)$_4$] and (R$_3$Si)$_2$O (2:1). The yield for H_2 conversion was most reliably calculated *via* relative integration of ^{1}H NMR signals for the R$_3$Si-H resonance against that of tBu$_3$P-H (1:1 from H_2). Accordingly, hydrolysis produces twice the amount of phosphonium salt than the reaction with H_2, and accounts for the slightly sub-quantitative yields (90-94%) for the reaction of **13** with H_2.

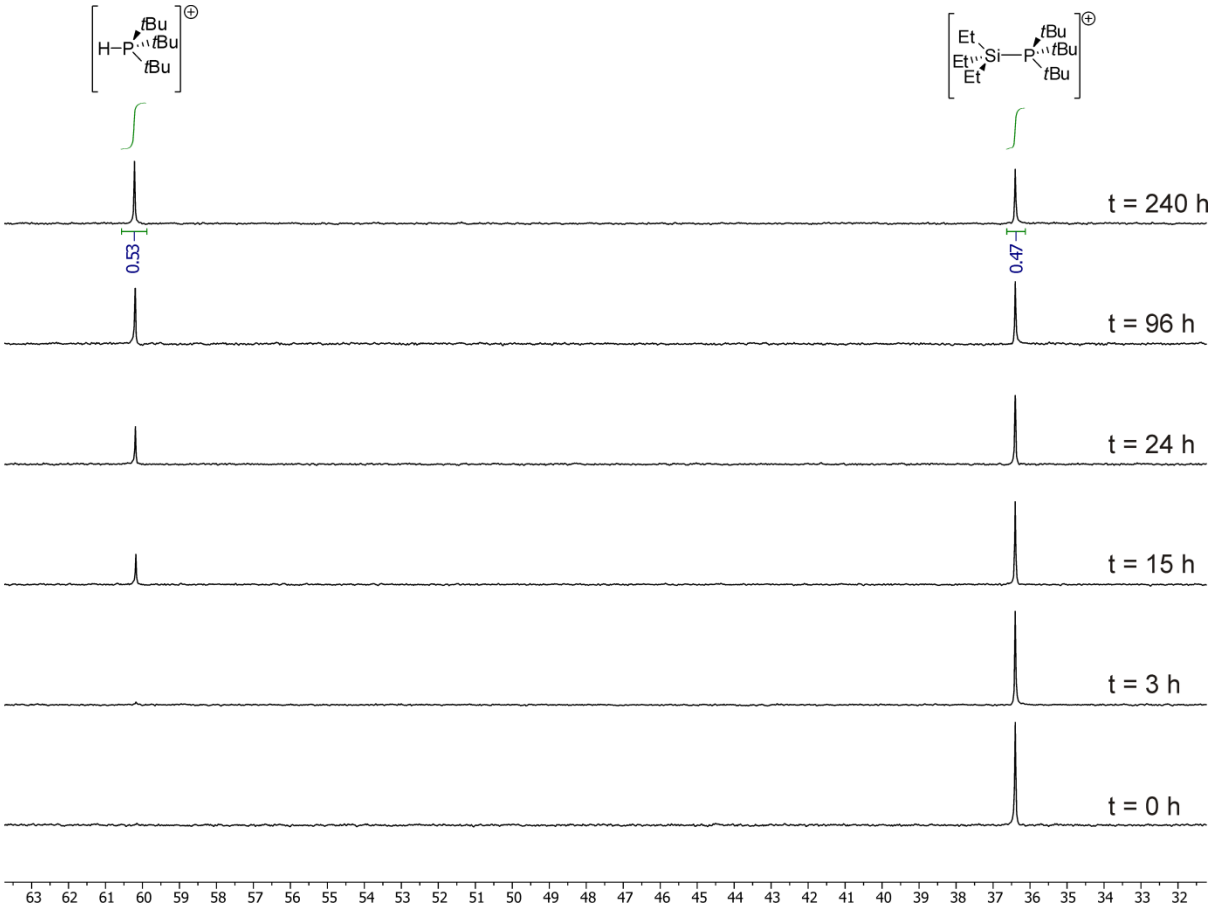

Figure 4.16. ^{31}P $\{^{1}H\}$ NMR spectra for the reaction of **12** with H_2 in PhCl solution at 100 ºC. After 10 days, ratio of the $[tBu_3P–H]^+$ to **12** is approximately 1:1 (*vide infra*).

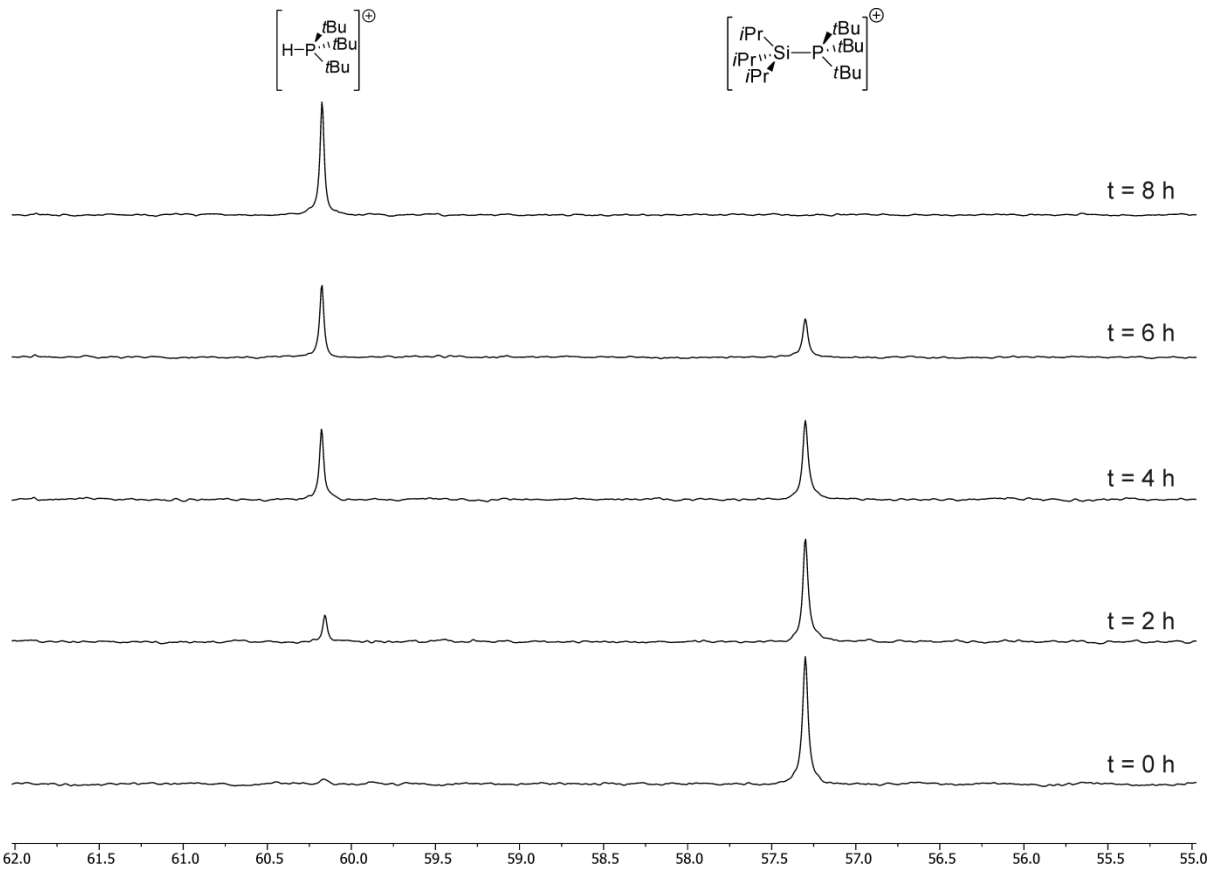

Figure 4.17. ^{31}P $\{^1H\}$ NMR spectra for the reaction of **13** with H_2 in PhCl solution at 90 ºC. Complete conversion of **13** within 8 hours heating.

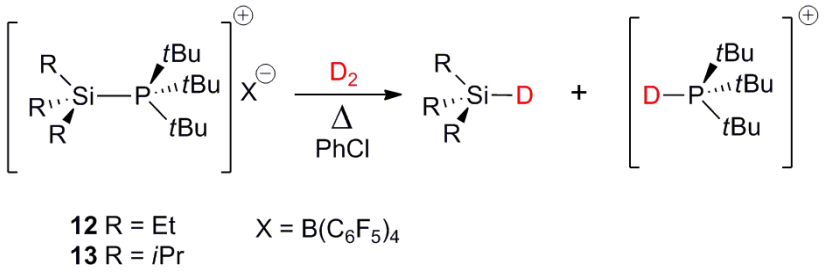

Figure 4.18. D_2 activation mediated by **12** and **13** heated at 100 and 90 ºC respectively. Conversion rates mirror those reported using H_2.

Conducting these experiments under D_2 atmosphere (PhCl solvent) gave the deuterated products $R_3Si–D$ and $[tBu_3P–D]^+$ (Figure 4.18), which were assigned using ^2H, ^{31}P $\{^1H\}$ and ^{29}Si $\{^1H\}$ NMR spectroscopy (Figures 4.19 and 4.20). Interestingly, the rate of activation for H_2/D_2 was comparable, hence a kinetic isotope effect was not observed. This may suggest dihydrogen cleavage is not the rate determining step. The ^{29}Si $\{^1H\}$ NMR spectra for each adduct displayed new upfield 1:1:1 triplets (δ = 0.1 (R = Et); 11.5 ppm (R = *i*Pr), in which the coupling constants were commensurate with $R_3Si–D$ formation ($^1J(Si,^2H)$ = 27 Hz). Likewise, the ^{31}P $\{^1H\}$ NMR spectra revealed identical 1:1:1 triplets (δ = 59.2 ppm, $^1J(P,^2H)$

= 67 Hz) indicative of $[t\text{Bu}_3\text{P–D}]^+$. ^{2}H NMR studies validated ^{31}P and ^{29}Si data, with a diagnostic doublet corresponding to $[t\text{Bu}_3\text{P–D}]^+$ (δ = 4.21 ppm, $^1J(^2H, P)$ = 67 Hz), in addition to a $R_3Si–D$ resonance [δ = 3.77 (R = Et) and 3.47 (R = *i*Pr)]. Satellites for the low abundance (*ca*. 5%) ^{29}Si were also resolved ($^1J(^2H, Si)$ = 27 Hz). Integration of the ^{1}H NMR signals for the $R_3Si–D$ resonance against that of $t\text{Bu}_3\text{P–D}$ showed a 1:1 ratio. The encouraging level of agreement between these spectra suggests that H_2/D_2 is the source of H atoms in the formally hydridic silane, and protic phosphonium ion. Furthermore, at completion, the ^{19}F and ^{11}B NMR spectra of these reactions presented resonances solely corresponding to the $[B(C_6F_5)_4]^-$ counterion, which implied a silylium-mediated decomposition of this anion had not occurred. Since neither $[H–B(C_6F_5)_3]^-$ nor $B(C_6F_5)_3$ species could be observed in solution, the possibility that H_2 cleavage involves the known $t\text{Bu}_3\text{P}/B(C_6F_5)_3$ FLP pathway may be confidently discounted.[26]

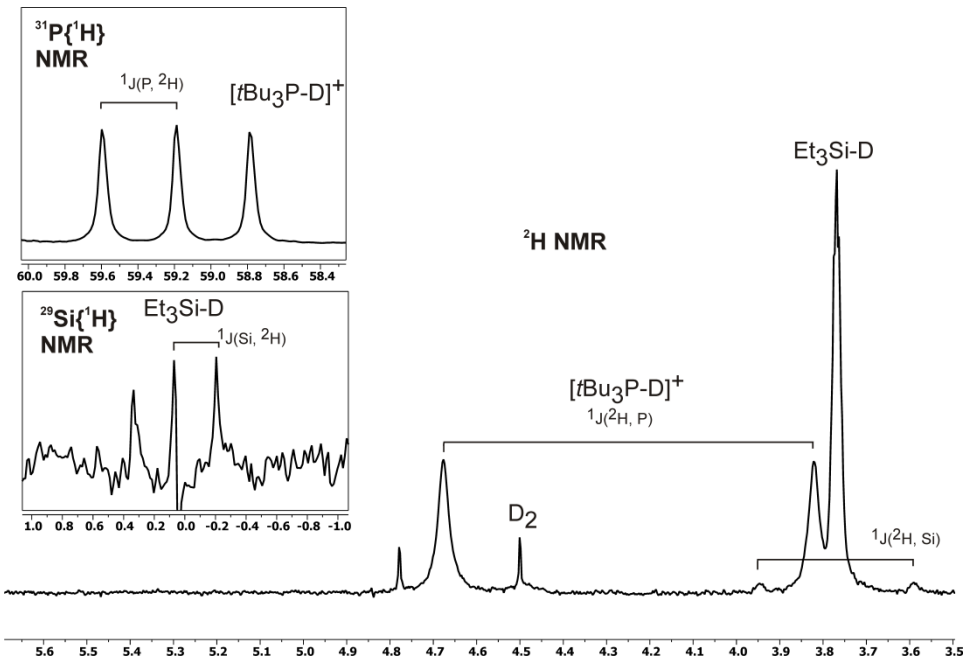

Figure 4.19. ^{2}H, ^{31}P {^{1}H} and ^{29}Si {^{1}H} NMR spectrum of products from reaction of **12** with D_2. $^1J(^2H, P)$ = 66 Hz and $^1J(Si, ^2H)$ = 27 Hz

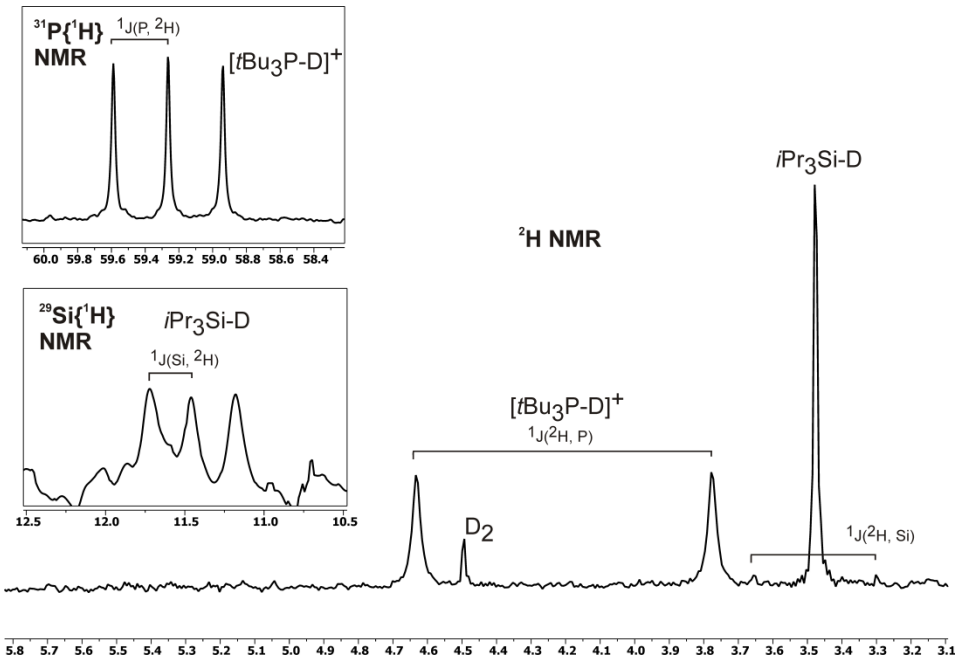

Figure 4.20. ^{2}H, ^{31}P $\{^{1}H\}$ and ^{29} Si NMR $\{^{1}H\}$ spectrum of products from reaction of **13** with D_2. $^{1}J(^{2}H, P) = 66$ Hz and $^{1}J(Si, ^{2}H) = 27$ Hz

Finally, as a control, solutions of $[R_3Si{\cdot}ClPh]^+[B(C_6F_5)_4]^-$ (R = Et, *i*Pr) were heated under H_2 atmosphere (4 bar), in which decomposition was observed to occur at the same rate as in the absence of H_2, with no R_3SiH formation. Based upon the described experiments, the role of these classical adducts in H_2 cleavage is strongly implied (Figure 4.21).

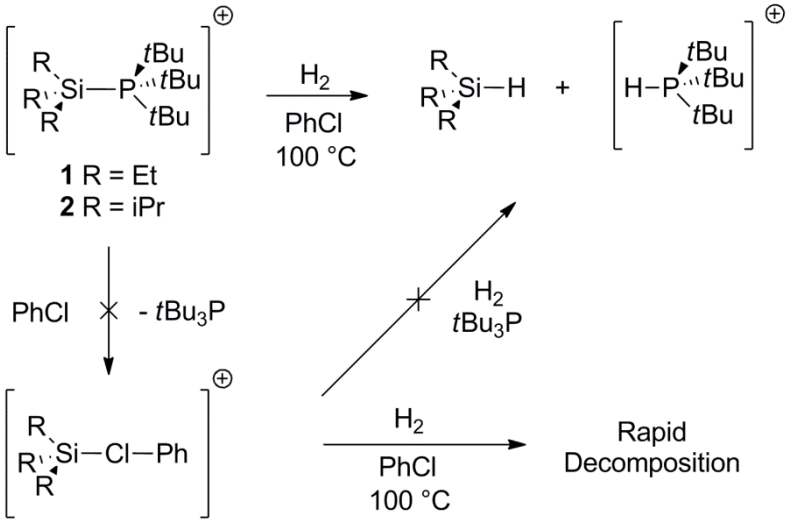

Figure 4.21. H_2 activation chemistry mediated by **12** and **13**, showing the absence of a 'true' FLP-mediated pathway. $B(C_6F_5)_4^-$ anions omitted for clarity.

As anticipated, the faster rate of H_2 heterolysis for **13** is in agreement with the weaker bond between Si and P; however the 50% conversion limit for **12** is surprising. FLP systems

containing a phosphine Lewis base can undergo highly reversible H_2 activations, even at temperatures as low as –80 ºC,[2b] and therefore the reactivity of **12**, although not a true FLP, might also be reversible. However, heating solutions of independently prepared [tBu$_3$P–H]$^+$[B(C$_6$F$_5$)$_4$]$^-$ with either Et$_3$SiH or iPr$_3$SiH (PhCl, 100°C, 60 hr) led to no reaction, demonstrating that the H_2 cleavage reaction is irreversible in both **12** and **13**. Furthermore, conducting the same experiments under D_2 did not produce any HD, which would be expected to form due to H/D scrambling.

Unfortunately a full kinetic study of **13** by ^{1}H NMR was hampered by the interaction of iPr$_3$SiH with **13**, which masks the actual amount of silane produced until the reaction is complete (i.e. complete conversion of **13**). This phenomenon has been noted for [R$_3$Si(μ-H)SiR$_3$][B(C$_6$F$_5$)$_4$] species,[17,24,28] wherein the silane proton is rendered invisible to ^{1}H NMR spectroscopy. In this light, it seemed plausible that a similar bridging silane interaction is in operation. This rationale may, in part, explain the unusual reactivity of **12**; the stronger hydride donor ability of Et$_3$SiH, relative to the sterically larger iPr$_3$SiH,[29] facilitates stronger coordination to the electrophilic Si centre which may thereby inhibit H_2 cleavage. Examination of the space-fill diagrams for solid state structures **12** and **13** reflect a considerably enhanced screening of the silicon centre upon replacement of Et substituents with iPr substituents (Figure 4.22). It is envisaged therefore that steric arguments may permit the stronger interaction of Et$_3$SiH with **12** than for iPr$_3$SiH with **13**.

In accordance with this hypothesis addition of stoichiometric Et$_3$SiH to **12**, prior to H_2 admission, markedly slowed H_2 cleavage following heating at 100 ºC. Even after heating for 10 days at 100 ºC, a yield of only 20% was determined by ^{31}P and ^{1}H NMR. In contrast, an analogous experiment employing iPr$_3$SiH and **13** afforded no perturbation in the recorded yield or rate. To investigate the possibility that the addition of Et$_3$SiH to **12** may establish an equilibrium with a bridging silane and tBu$_3$P (Figure 4.23), ^{31}P NMR studies were conducted at 100 ºC and RT (Ph$_3$P internal capilliary reference) in which Et$_3$SiH was added in varying concentrations. At both temperatures, the ^{31}P resonance for **12** moved marginally downfield upon addition of 1 equivalent Et$_3$SiH ($\Delta\delta$ = 0.03 ppm) and moved progressively further as the concentration increased ($\Delta\delta$ = 0.22 ppm at 100 equivalents) (Figure 4.24). Cooling these solutions to –40 ºC (m.p. PhCl = –45 ºC) did not yield separate resonances for **12** and tBu$_3$P, which suggests any equilibrium is too fast to be observed on the ^{31}P NMR timescale (^{31}P: 162.1 MHz).

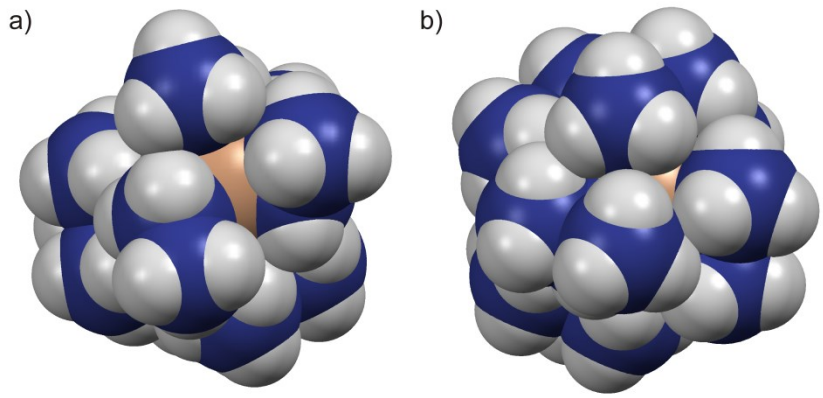

Figure 4.22. Space fill diagrams of a) **12** and b) **13**; C atoms blue, H atoms grey, Si atoms brown. $B(C_6F_5)_4^-$ anions omitted for clarity.

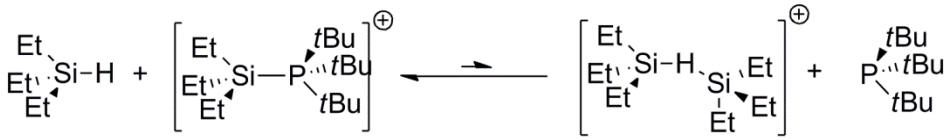

Figure 4.23. Proposed equilibrium between Et_3SiH, **12,** $Et_3Si–H–SiEt_3$ and tBu_3P

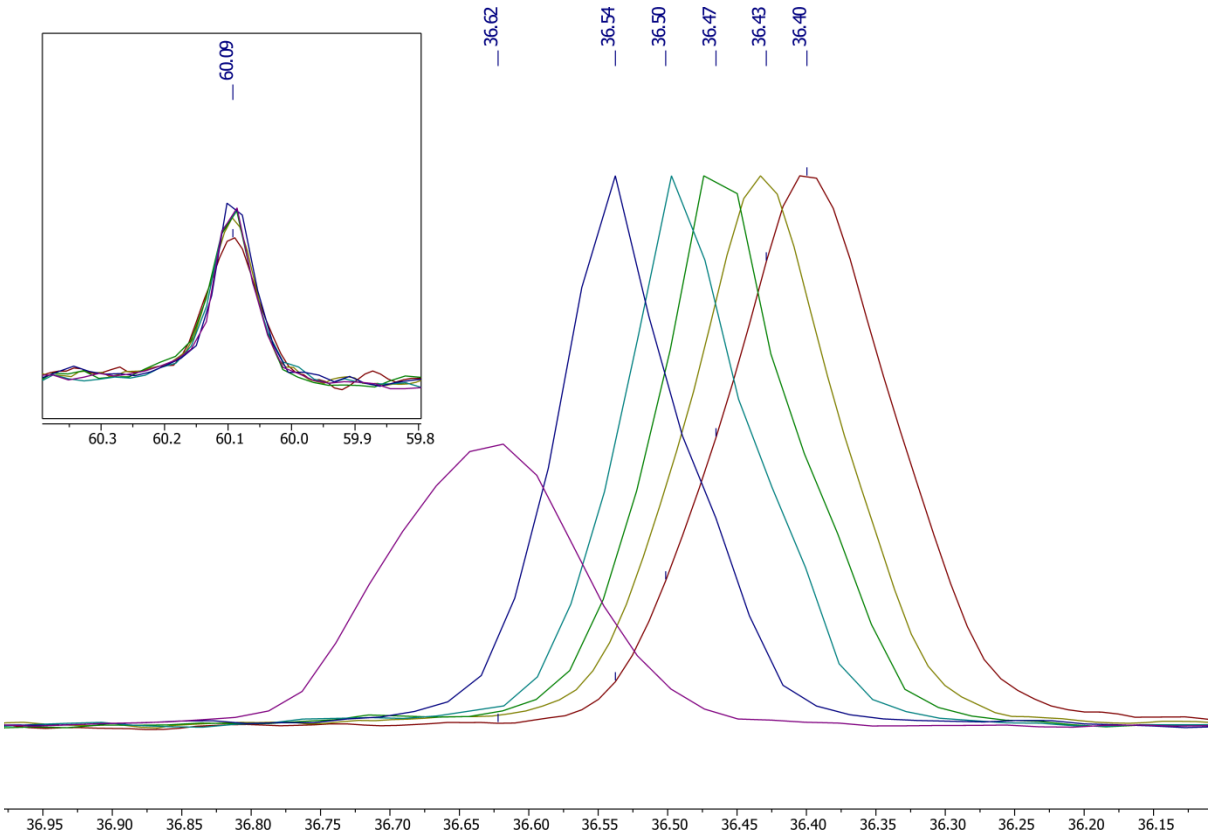

Figure 4.24. Superimposed $^{31}P\{^1H\}$ NMR spectra of **12** in the presence of varying Et_3SiH concentration: 0, 10, 20, 30, 50 and 100 equivalents; shift moves from right to left; $\Delta\delta = 0.22$ ppm using 100 equivalents at which point **12** begins to recrystallize from solution. Inset ^{31}P NMR spectra of residual $[tBu_3PH]^+$ whose shift is independent of Et_3SiH concentration.

4.8 CO_2 sequestration

In contrast to the expanding field of CO_2 fixation by FLP systems,[30] CO_2 insertion into main group bonds remains largely unexplored. A modest number of reports exist for insertion into P–N, As–N, Si–N and Si–P bonds, in which CO_2 uptake by neutral silylamides and disilylated phosphines are the most noteworthy (Figure 4.25).[31] The reactivity of these systems may be considered analogous to those of secondary or primary amines which, in aqueous solutions, form carbamates upon admission of CO_2.[32] Essentially the silylium centre can be considered a large proton,[33] which is transferred from the nitrogen or phosphorus to the carboxylate. In any case, the structure of these neutral systems differ strongly from the cationic Si–P adducts **12** and **13**, in which the phosphorus lone pair was found not to dissociate from the electrophilic Si centre.

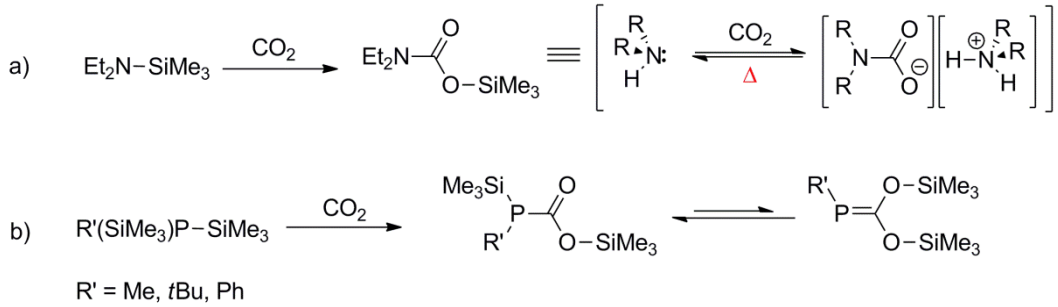

Figure 4.25. a) CO_2 insertion into the main group bond of silylamide Me_3SiNEt_2 (analogous to the related reactions of secondary and primary amines), b) CO_2 insertion into disiylated phoshphine $PR(SiMe_3)_2$ R = Me, *t*Bu, Ph

Interestingly, admission of $^{13}CO_2$ (1 atm, 25ºC) to C_6D_5Cl solutions of either **12** or **13** *via* a Toepler pump led to complete room temperature consumption of the adducts after 24 hours, with new ^{1}H, ^{13}C, ^{31}P and ^{29}Si NMR resonances (*vide infra*) indicative of $[tBu_3P–^{13}C(O)O–SiR_3][B(C_6F_5)_4]$ (R = Et, **14**; R = *i*Pr, **15**). These observations bore a strong resemblance to those reported for the 'true' silylium FLPs, $(C_6Me_5)_3Si^+/PR_3$ (R = *t*Bu, Cy) in which admission of CO_2 afforded the silylacylphosphonium ion $[R_3P–C(O)O–Si(C_6Me_5)_3][B(C_6F_5)_4]$.[9] However, unlike the $[tBu_3P–^{12}C(O)O–Si(C_6Me_5)_3][B(C_6F_5)_4]$ reported by Müller (Figure 4.28) which are only marginally stable at ambient conditions, **14** and **15** were found to be surprisingly stable for several days under ambient conditions.

Following scale up, and precipitation with hexane, salts **14** and **15** were obtained as white powders in excellent yield (81 % and 89 % respectively). Both compounds were characterised by HRMS (ES+/ES–), in which their ionic fragments were consistent with $[tBu_3P–^{13}C(O)O–SiR_3]^+$ and $[B(C_6F_5)_4]^–$. Recrystallisation from a PhCl solution layered with

hexane produced large colourless blocks suitable for X-Ray crystallography (Figure 4.27). To the author's knowledge, this represents the first example of an silylacylphosphonium characterised *via* this method; presumably the instability of [tBu$_3$P–C(O)O–Si(C$_6$Me$_5$)$_3$][B(C$_6$F$_5$)$_4$] prohibited isolation of X-ray quality crystals.

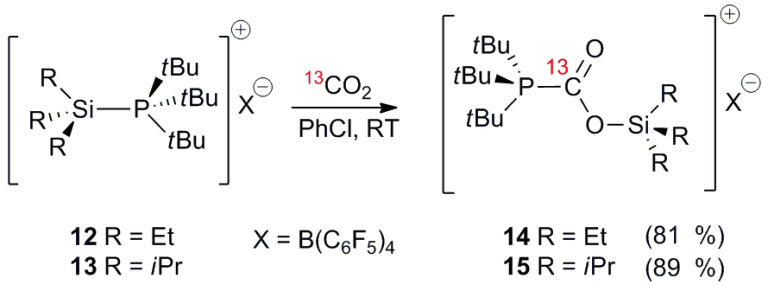

12 R = Et X = B(C$_6$F$_5$)$_4$ **14** R = Et (81 %)
13 R = *i*Pr **15** R = *i*Pr (89 %)

Figure 4.26. Synthesis of compounds **14** and **15** by $^{13}CO_2$ uptake.

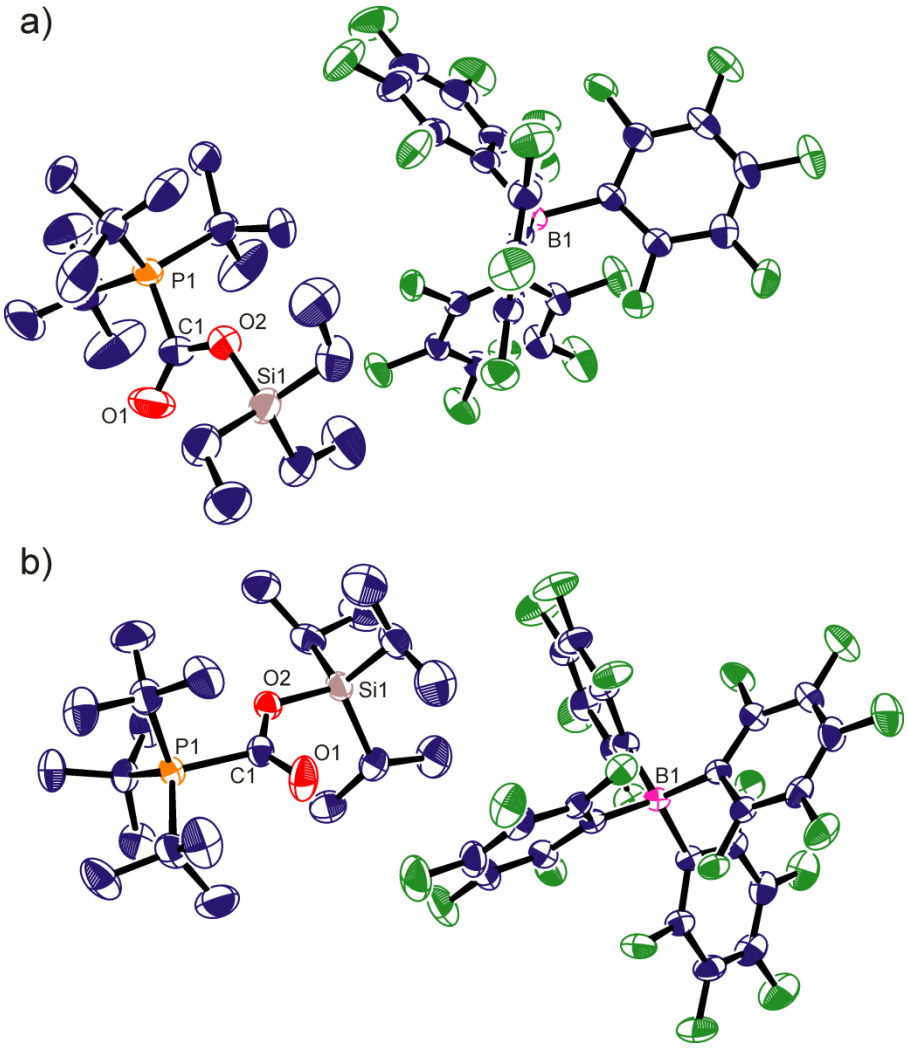

Figure 4.27. ORTEP plots of the X-ray structure of (a**) 14** and (b) **15**. C atoms blue, P atoms orange, B atoms pink, F atoms green, O atoms red and Si atoms light brown. H atoms have been removed for clarity, and thermal ellipsoids are shown at 50% probability. For selected bond lengths see Table 5.2

Table 5.2. Selected Bond Length for Compounds **14**, **15** and tBu$_3$P–C(O)O–B(C$_6$F$_5$)$_3$.

Compound	C=O Å	C–O Å	Si–O Å	P–C Å
14	1.209(5)	1.307(5)	1.734(3)	1.851(4)
15	1.198(4)	1.306(3)	1.747(2)	1.881(3)
***t* Bu$_3$P–C(O)O–B(C$_6$F$_5$)$_3$**	1.208(2)	1.299(1)	–	1.893(1)

The structural data for **14** and **15** were found to be in agreement with the formulated structures; both compounds contain a cationic fragment derived from CO_2 sequestration in which the phosphorus and silicon form a P–C and Si–O bond respectively. Once more, the $[B(C_6F_5)_4]^-$ anions can be said to be non-coordinating with no close Si to F contacts. The pyrimidalisation about the Si atom is slightly less than the parent adducts (*ca.* 0.50 Å deviation from best plane of the three C atoms of the C_3Si unit *vs*. 0.60 Å recorded for **12** and **13** respectively) with an average C–Si–C bond angle of 113.0º *vs.* those of 109.9º and 111.4º recorded for **12** and **13**. For either adduct the central carbon belonging to CO_2 displays a trigonal-planar geometry in which the sum of angles is equal to 360º. Both the C=O and C–O bond lengths are almost identical (1.198(4)/1.307(5) Å and 1.209(5)/1.306(3) Å for **14** and **15** respectively) which likely reflects a comparable degree of CO_2 activation; these parameters are akin to the zwitterionic betaine tBu$_3$P–C(O)O–B(C$_6$F$_5$)$_3$ (1.208(2)/1.299(1) Å) formed by Stephan and co-workers *via* CO_2 fixation employing the aforementioned tBu$_3$P/B(C$_6$F$_5$)$_3$ FLP system (Figure 4.28).[34] Additionally, the difference in Si–O bond lengths between **14** and **15** (Δ = 1.3 ppm) is considerably smaller than the Si–P bond length difference between **12** and **13** (Δ = 10.6 pm). This similarity is also seen between the P–C bond lengths (Δ = 3 pm). Presumably upon insertion, CO_2 (a molecule with limited steric profile) relieves the steric congestion about the Si–P axis to the extent where the steric effects of an Et *vs*. *i*Pr substituent become negligible. Measuring the internuclear distance between the Si and P atoms of **14** and **15** (i.e. the cavity size) support this hypothesis, in which near identical values of 4.338 Å and 4.392 Å are observed.

Table 5.3. Selected spectral data for Compounds **14**, **15,** tBu$_3$P(CO$_2$)Si(C$_6$Me$_5$) and tBu$_3$P(CO$_2$)B(C$_6$F$_5$)$_3$. [a] Values in ppm. [b] Values in cm^{-1}.

Compound	$\delta(^{31}P)$, ($^1J_{P\text{-}C}$, Hz)[a]	$\delta(^{29}Si)$[a]	$\delta(^{13}C)$, ($^1J_{C\text{-}P}$, Hz)[a]	ν (^{12}C=O)[b]
14	52.7 (87)	41	161.5 (87)	1710
15	53.4 (86)	38	162.0 (86)	1715
***t* Bu$_3$P(CO$_2$)Si(C$_6$Me$_5$)$_3$**	56.4 (88)	–0.3	159.6 (88)	1712
***t* Bu$_3$P(CO$_2$)B(C$_6$F$_5$)$_3$**	46.1	–	162 (93)	1696

The room temperature ^{1}H and ^{13}C NMR spectra (C_6D_5Cl) for **14** and **15** were once again commensurate with their solid state structures, in which ^{13}C NMR signals of the CO_2 fragment (δ = 161.5 and 162.0 ppm, $^{1}J(C,P)$ = 87 and 86 Hz, respectively) correlate very well with those reported for [*t*Bu_3P–C(O)O–Si(C_6Me_5)$_3$][B(C_6F_5)$_4$] (δ = 159.6 ppm $^{1}J(C,P)$ = 88 Hz).[9] As reflected in the solid state for the Si–O bond lengths of **14** and **15,** the ^{29}Si {^{1}H} resonances (δ = 41.0 and 38.1 ppm, Δδ = 2.9 ppm) are markedly closer than those reported for adducts **12** and **13** (δ = 22.0 and 43.1 ppm, Δδ = 21.1 ppm). Clearly, the steric variance between an Et and *i*Pr substituent has negligible impact upon insertion of a CO_2 molecule. The ^{31}P {^{1}H} NMR resonances of **14** and **15** are noticeably similar (δ = 52.7 and 53.4 ppm, $^{1}J(P,C)$ = 87 and 86 Hz, respectively) and comparable with [*t*Bu_3P–C(O)O–Si(C_6Me_5)$_3$][B(C_6F_5)$_4$] (δ = 56.4 ppm $^{1}J(C,P)$ = 88 Hz).

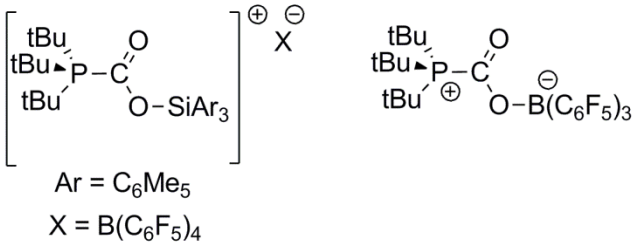

Figure 4.28. Reported acyl phoshphonium [*t*Bu_3P–C(O)O–Si(C_6Me_5)$_3$][B(C_6F_5)$_4$] and zwitterionic betaine *t*Bu_3P–C(O)O–B(C_6F_5)$_3$.[9,34]

The *ν*(^{13}C=O) IR stretches for **14** and **15** (1668 and 1673 cm^{-1}, respectively) were strongly similar and agree with the near identical C=O bond lengths seen in the solid state. Generation of ^{12}C–**14** and ^{12}C–**15** from $^{12}CO_2$ gave new IR ν(C=O) stretching bands (1710 cm^{-1} and 1715 cm^{-1}, respectively) which closely matched those of [*t*Bu_3P–C(O)O–Si(C_6Me_5)$_3$][B(C_6F_5)$_4$] (1712 cm^{-1}) and *t*Bu_3P(CO_2)B(C_6F_5)$_3$ (1696 cm^{-1}). This isotopic shift is in accordance with the calculated value assuming *ν* is solely influenced by a change in reduced mass (Figure 4.29). In consideration of all spectral parameters, **12** and **13** reflect a comparable degree of CO_2 activation.

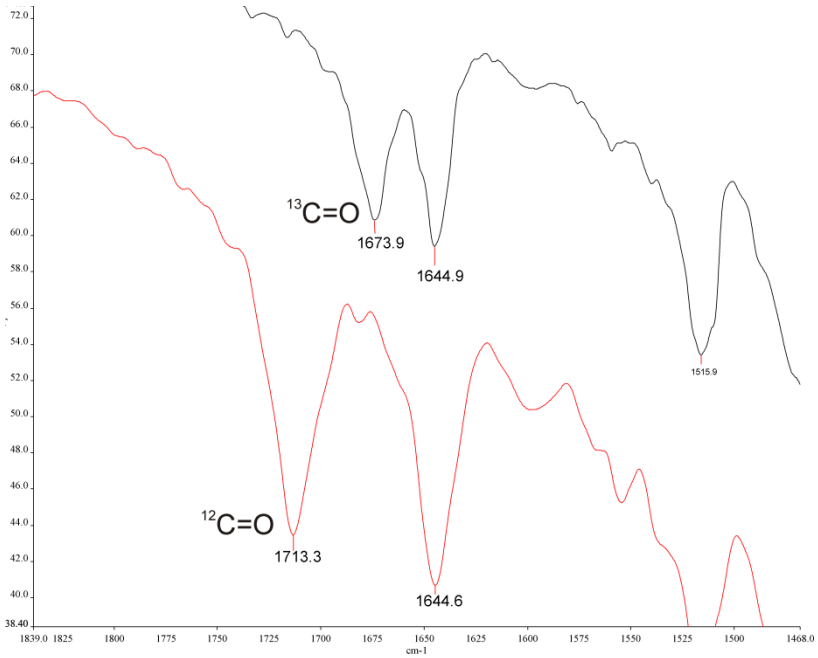

$$\text{Calculated: } \frac{\nu(^{12}\text{C=O})}{\nu(^{13}\text{C=O})} \approx \frac{\mu(^{13}\text{C=O})}{\mu(^{12}\text{C=O})} \approx 1.0227$$

Compound	ν (^{12}C=O)^a	ν (^{13}C=O)^a	ν (12C=O)/ν (13C=O)
14	1710	1668	1.0252
15	1715	1673	1.0251

Figure 4.29. (C=O) IR stretches for **14** and **15** from activation of $^{12}CO_2$ or $^{13}CO_2$. Isotopic shift compared with that calculated theoretically. ^{a} (KBr, cm^{-1}).

In contrast with [*t*Bu$_3$P–C(O)O–Si(C$_6$Me$_5$)$_3$][B(C$_6$F$_5$)$_4$], adducts **14** and **15** appeared thermally robust, withstanding temperatures as high as 80 ºC before slowly decomposing as demonstrated by formation of [*t*Bu$_3$P–H]$^+$ (20 %) after heating for 24 hours. Additionally, heating **14** and **15** in an NMR tube sealed under vacuum (60-100 ºC), yielded no free $^{13}CO_2$ in the ^{13}C NMR and showed no reformation of adducts **12** and **13** respectively, in the ^{31}P NMR spectra. Hence, CO_2 fixation must be irreversible.

4.9 Kinetic investigation of CO_2 uptake by 12 and 13

The reversibility and thermal instability of Müller's CO_2 adducts have previously inhibited extraction of the thermodynamic parameters for this process using solution phase techniques. Since **12** and **13** react cleanly with CO_2 to afford **14** and **15**, ^{31}P{^{1}H} NMR integral measurements (used as a proxy for product:substrate concentration) were exploited to determine the relative rates and activation parameters for CO_2 insertion. Therefore, to perform this study, solutions of **12** and **13** were prepared to a known concentration (0.06 M),

inserted into a Teflon lined Young's NMR tube, and exposed to a twenty fold excess of $^{13}CO_2$ (6 atm) administered with the aid of a Toepler pump (see Appendix for calculation). Subsequently, the NMR tubes were inserted into a NMR spectrometer, which was preheated to the desired temperature, and ^{31}P NMR spectra acquired at discrete time intervals (t_{diff} = 568s; Figure 4.30).

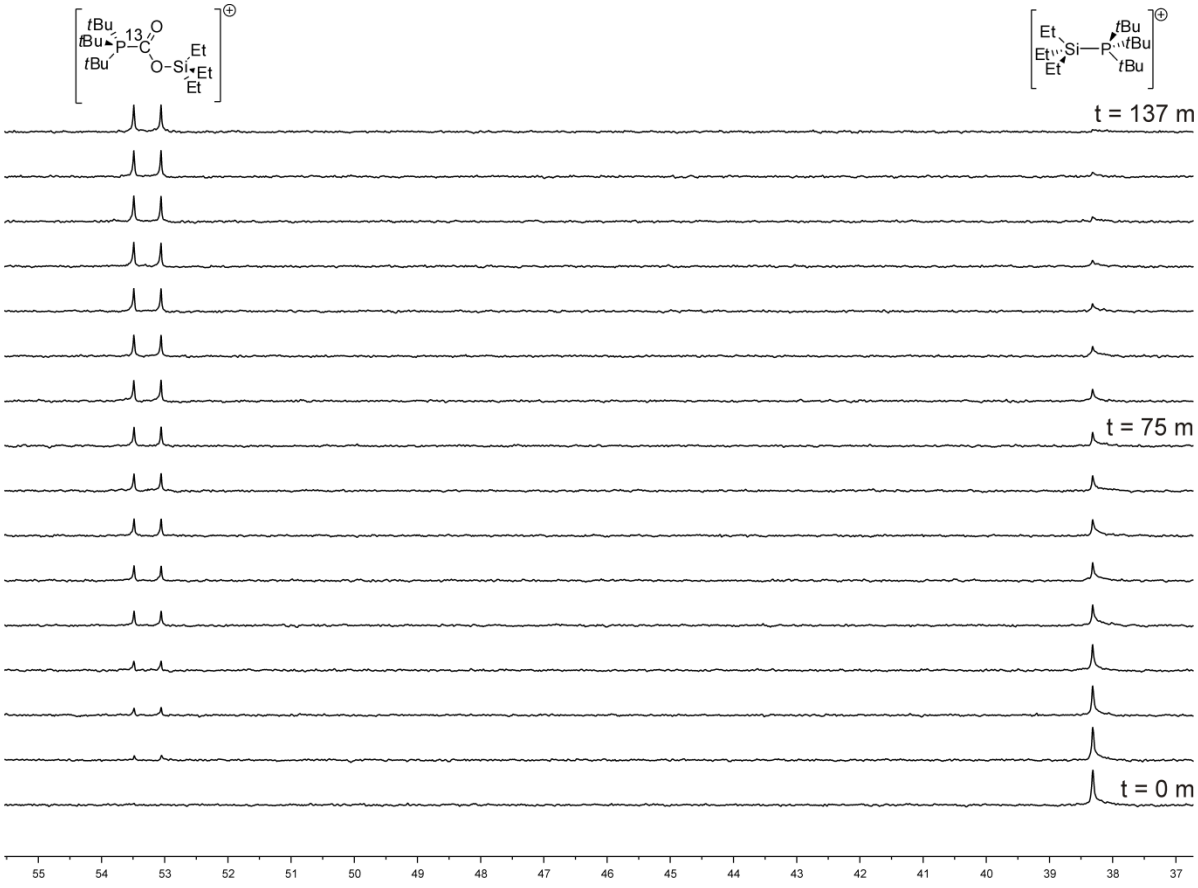

Figure 4.30. Stack plot of ^{31}P {^{1}H} NMR spectra at 55ºC from the reaction of **12** with CO_2 (5 atm, c.a. 0.6 M) to form **14.** Acquisitions taken every 568 seconds.

In a similar fashion to kinetic studies reported for CO_2 uptake using a Mes_3P/AlX_3 FLP system (X = Cl, Br, I),[35] NMR integration of substrates **12** and **13** vs. those of the formed products **14** and **15** displayed a pseudo first-order dependence, which enabled *qualitative* comparison of the reaction rate constants (k_{obs}) over a temperature range, in addition to *quantitative* analysis of the activation parameters ($\Delta H^{\ddagger}$, $\Delta S^{\ddagger}$ and $\Delta G^{\ddagger}$);[36] determination of k_{obs} over a 25 K temperature range permitted construction of an Eyring plot from which the parameters were extracted (Figure 4.32, Table 5.4).

Table 5.4. a) Rate constants for CO_2 activation employing **12** and **13** at temperatures 50 ºC, 55 ºC, 60 ºC and 65 ºC. b) Calculated activation parameters for CO_2 activation as determined by an Eyring Plot. Errors in parentheses.

a)

	Rate (10^4 k, s^{-1})	
Temp/C	**12**	**13**
50	0.63(2)	1.2(3)
55	1.2(1)	2.3(1)
60	2.2(2)	3.3(3)
65	3.9(3)	5.7(3)

b)

	$\Delta H^{\ddagger}$ (kJ mol^{-1})	$\Delta S^{\ddagger}$ (J mol^{-1} K^{-1})	$\Delta G^{\ddagger}$ (328K, kJ mol^{-1})
12	113(4)	22(12)	105(3)
13	101(5)	-11(16)	104(5)

As anticipated from the longer Si–P bond distance, the rate of CO_2 activation for **13** exceeded **12** at all temperatures, although at a far closer rate than that observed for H_2 cleavage (**12**: 4-10 days, 100 ºC; **13**: 8 Hours, 80 ºC). The larger $\Delta H^{\ddagger}$ for **12** relative to **13** (112.5(4) and 100.5(5) kJ mol^{-1}) is consistent with the stronger Si–P bond reported in the solid state, while the positive and negative $\Delta S^{\ddagger}$ values for **12** and **13** respectively remain somewhat puzzling and may be attributed to the appreciable error in these values. Nonetheless, the entropic contribution to $\Delta G^{\ddagger}$ is small relative to $\Delta H^{\ddagger}$, in which the reaction can be said to be dominated by the cost of breaking the Si–P bond. In addition, a reduction in CO_2 pressure led to a slower rate of reaction for both and corresponds with an overall second order dependence (Figure 4.31).

$$\text{Rate} = k\{[R_3Si\text{–}P\textit{t}Bu_3][B(C_6F_5)_4]\}\{CO_2\} \qquad R = Et\ (\mathbf{12}),\ \textit{i}Pr\ (\mathbf{13})$$

$$= k_{obs}\{[R_3Si\text{–}P\textit{t}Bu_3][B(C_6F_5)_4]\} \qquad \text{(high concentration } CO_2\text{)}$$

Figure 4.31. Order determination of CO_2 uptake employing **12** and **13**.

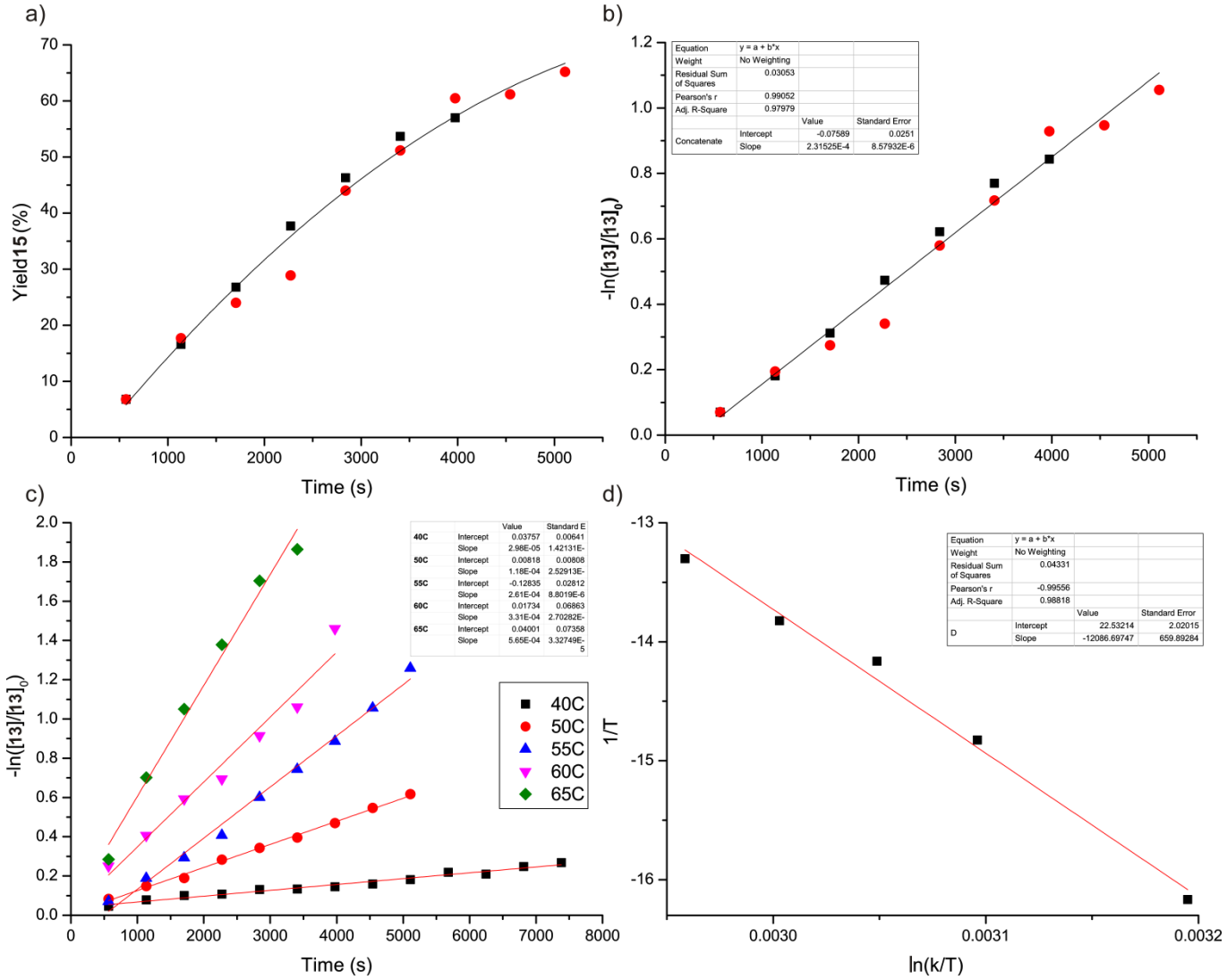

Figure 4.32. a) Yield (**15**) *vs.* time for CO_2 fixation (6 atm) employing **13** at 55 ºC (2 Runs). b) $-\ln([\mathbf{13}]/[\mathbf{13}_o])$ *vs* Time plot at 55 ºC for first order decay of **13** (2.3×10^{-4} s^{-1}) (2 runs, line represents best fit of two runs). c) $-\ln([C]/[C_o])$ *vs* Time plot for first order decay of **13** at temperatures 40 ºC (3.0×10^{-5} s^{-1}), 50 ºC (1.2×10^{-4} s^{-1}), 55 ºC (2.3×10^{-4} s^{-1}), 60 ºC (3.3×10^{-4} s^{-1}) and 65 ºC (5.7×10^{-4} s^{-1}). d) Eyring Plot (For parameters see Table 5.4)

4.10 *t*Bu$_3$P-mediated catalysis of CO_2 activation

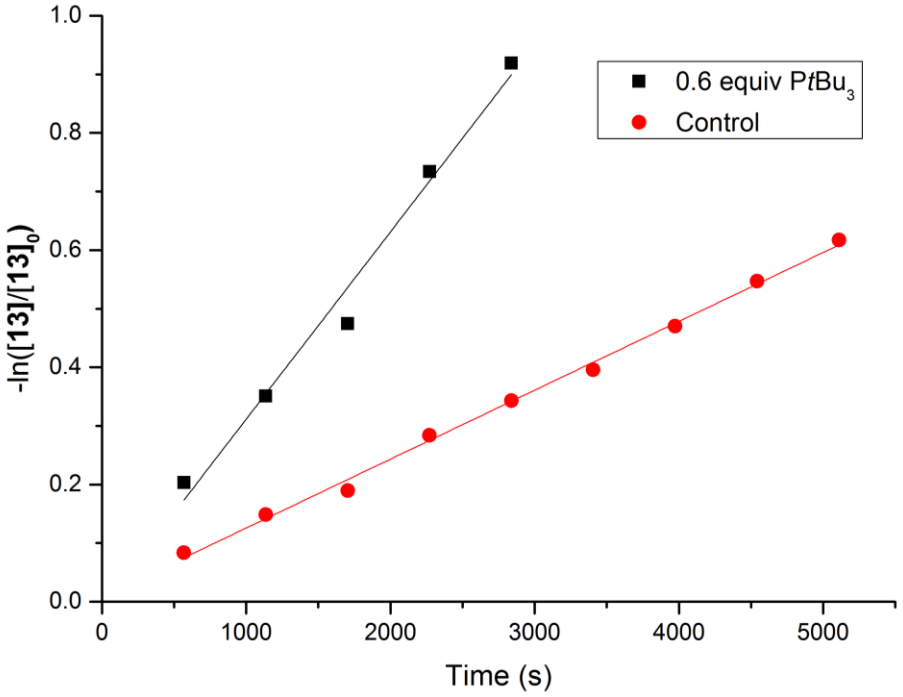

Figure 4.33. –ln(C/C$_o$) *vs* Time plot at 50 ºC for first order decay of **13**. Marked rate enhancement (~3 times) upon introducing 0.6 equivalents *t*Bu$_3$P to adduct **13** (black Line). Red line represents control**.** Respective rate constants (3.2 x 10^{-4} s^{-1} and 1.2 x 10^{-4} s^{-1}).

In order to explore the role of base in these transformations, addition of free *t*Bu$_3$P (~0.5 equivalents) to **12** or **13** led to an enhancement (2-3 times) in the rate of CO_2 uptake. (Figure 4.33). The concentration of free *t*Bu$_3$P remained unchanged over the duration of the reaction, nor did it influence the relative chemical shift or signal intensity of adducts **12** and **13**. While primary and secondary amines are reported to react with CO_2 to form carbamates, which are postulated to proceed *via* formation of a zwitterion intermediate (Figure 4.34), tertiary alkyl amines demonstrate no literature precedence.[32] Furthermore, primary, secondary and tertiary phosphines are not reported to react with CO_2. Accordingly, PhCl solutions of solely *t*Bu$_3$P showed no evidence for CO_2 activation by ^{13}C and ^{31}P NMR spectroscopy, even when heated under $^{13}CO_2$ atmosphere. Consequently, the reported rate enhancement is unlikely to stem from silylation of a zwitterionic *t*Bu$_3$P–CO_2 intermediate and supports literature precedence.[32]

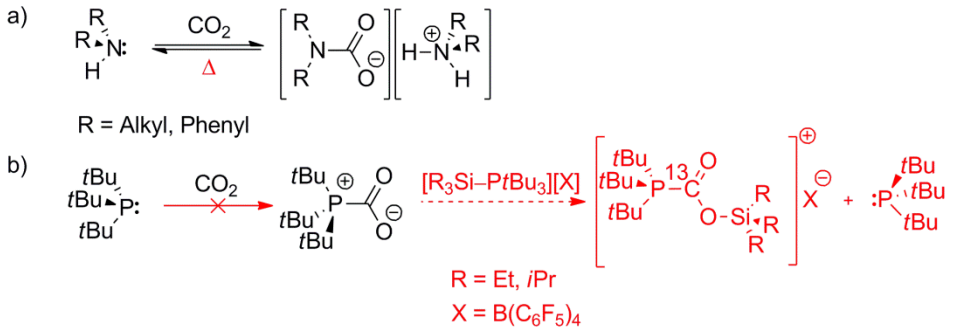

Figure 4.34. a) Reaction of a secondary amine with CO_2 to yield a carbamate which is postulated to have formed via a zwitterionic pathway. b) tBu$_3$P shown to be inert in the presence of CO_2. Hence, the formation of a zwitterionic intermediate is unlikely

To garner greater mechanistic insight, the concentration of tBu$_3$P at 50 ºC was varied, revealing a first order dependence at concentrations below 15 mol %. (Figure 4.35). At higher concentrations, the effect on rate becomes considerably less dramatic, which lends support towards the phosphine's role as an active catalyst.

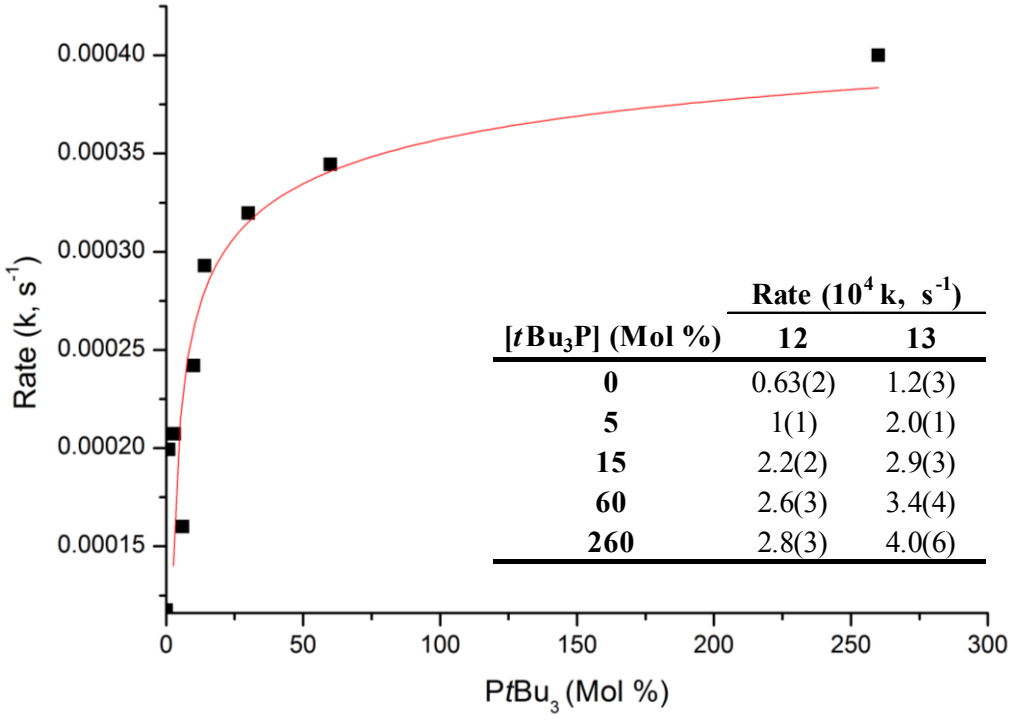

	Rate (10^4 k, s^{-1})	
[tBu$_3$P] (Mol %)	**12**	**13**
0	0.63(2)	1.2(3)
5	1(1)	2.0(1)
15	2.2(2)	2.9(3)
60	2.6(3)	3.4(4)
260	2.8(3)	4.0(6)

Figure 4.35. Effect of tBu$_3$P concentration upon the rate of CO_2 uptake by **13** (20 mg, 0.06 M). Curve generated from a logarithmic fit. Table inset: selected rates for **12** and **13** upon varying [tBu$_3$P].

No change was observed to the ^{31}P NMR spectra upon addition of tBu$_3$P to adducts **12** and **13** which demonstrates that the bulky tBu$_3$P is unable to interact with the $[R_3Si–PtBu_3]^+$ cation. The Et and iPr substituents provide a strong degree of steric protection about the Si atom, particularly in the case of **13**, which therefore blocks close approach of the sterically

cumbersome tBu$_3$P (Figure 4.22). Using DFT calculations Müller has previously proposed that CO_2 interacts with the silyl arenium ion $[R_3Si{\cdot}ClPh]^+$ (R = Et, iPr) (Figure 4.36).[18] Here it was envisaged a pre-equilibrium between the silylchloronium ion and a silylated CO_2 complex enhances the electrophilicity of the central carbon and thus favours nucleophilic attack by R_3SiH (R = Et and iPr), leading to hydrosilylation of the CO_2 molecule. Thus, a similar coordination effect may be operative for **12** and **13**.

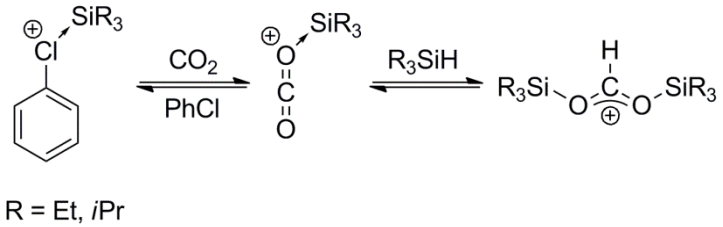

Figure 4.36. Proposed mechanism for the reduction of CO_2 by Müller.

4.11 Computational calculations for CO_2 activation by 12 and 13

In order to probe the mechanism for CO_2 activation, and to examine the role of free tBu$_3$P, DFT calculations were performed on adduct **13** by the Hunt research group (consult Chapter 5 for methodology). This represents the first time DFT studies have been performed on CO_2 activation by silylium/phosphine Lewis pair. The results of these computational calculations (M06-2X/6-31G(d,p)) for the phosphorous, silicon, carbon and oxygen atoms and 4-31G(d,p) basis set for all periphery atoms are presented in Figures 4.37-4.41 and pertinent bond lengths in Table 5.5 and 5.6. Owing to the inherent computation complexity, calculations omit any explicit solvent molecules and $[B(C_6F_5)_4]^-$.

In the absence of free tBu$_3$P molecule, two CO_2 molecules were found to participate along the reaction coordinate (Figure 4.37). To distinguish between the interacting CO_2 molecules the participating oxygen on each are denoted O^X and O^Y. In total three intermediates (**A-C**) and two transition states ($\mathbf{TS_{AB}}$ and $\mathbf{TS_{CD}}$) were located. In the presence of CO_2, **13** is found to exist in equilibrium with **A**, whereby one CO_2 molecule interacts with the silicon centre from the reverse side to the Si–P bond (S_N2 like), *via* a weak donation from the oxygen lone pair (O^X); this exerts negligible influence on the Si–P interaction (Table 5.5), as judged by the almost identical Si–P bond length found in the X-ray structure. While this coordination results in almost negligible enthalpic stabilisation of **A**, the entropic cost associated with the increased ordering renders **A** marginally less stable than **13**. Direct Si–O bond formation proceeds associatively through $\mathbf{TS_{AB}}$ which approximates to a trigonal

bipyrimidal geometry about the Si atom, as revealed by the average P–Si–$CHMe_2$ bond angle (92.0º) and nearly linear P–Si–O^X (175.0º) moiety, this large structural rearrangement of the *i*Pr substituents results in a significant energy barrier (ΔG = 80.19 kJ mol^{-1}). Subsequently, this process is accompanied by Si–O^X bond formation and substantial elongation of the Si–P bond (Table 5.5), resulting in intermediate **B**. This Si···P length (5.03 Å) is substantially greater than van der Waals radii of the elements (3.90 Å).[37] The prior coordination of CO_2 thus bears similarity with that reported by Müller.

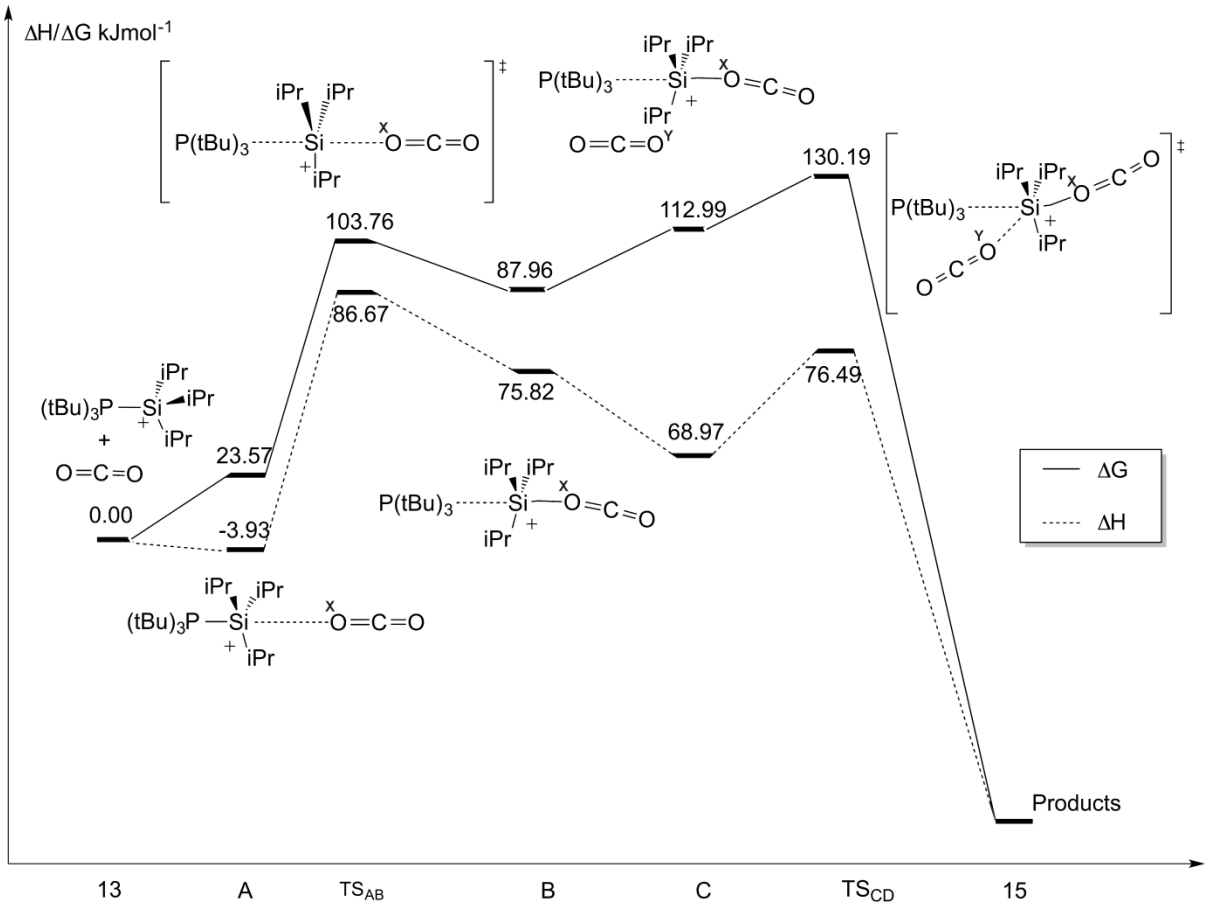

Figure 4.37. Relative energy profile of CO_2 activation by **13**.

Table 5.5. Pertinent interatomic distances corresponding to selective intermediates and transition states for the conversion of **13** to **15** in the absence of free tBu_3P

Bond lengths	Si···P (Å)	Si···O^X (Å)	Si···O^Y (Å)	P···C (Å)
13	2.49	-	-	-
A	2.48	3.84	-	-
TS_{AB}	4.32	2.51	-	-
B	5.03	2.07	-	-
C	5.07	2.06	4.72	5.25
TS_{CD}	5.38	2.09	3.52	4.39

Due to the increased Si···P length in **B**, the incipient 'cavity' now permits approach of the second CO_2 molecule which leads to a large decrease in entropy as a consequence of increased ordering ($\Delta\Delta G$ = 25.03 kJ mol^{-1}). CO_2 insertion proceeds *via* $\mathbf{TS_{CD}}$ in which the ligands twist away from the cavity to permit CO_2 insertion (Figure 4.38). Despite the large geometric reorganisation in the TS, only a modest increase in enthalpy is associated ($\Delta\Delta H$ = 7.52 kJ mol^{-1}) and is presumably diminished by the favourable Si···O^{Y} interaction (3.52 Å). Interestingly $\mathbf{TS_{CD}}$ shows the Si–O^{X} bond to remain strongly intact (2.09 Å). Attempts to compute the relative energy of the final intermediates and product along this reaction coordinate remain ongoing. It would appear the major energy cost of this process is the formation of **B** from **A** ($\Delta\Delta H$ = 90.6 kJ mol^{-1}, $\Delta\Delta G$ = 80.19 kJ mol^{-1} (298 K), in which this activation barrier is within error of those parameters determined experimentally ($\Delta H^{\ddagger}$ = 100.5 kJ mol^{-1}; $\Delta G^{\ddagger}$ = 103.7 kJ mol^{-1} (298 K).

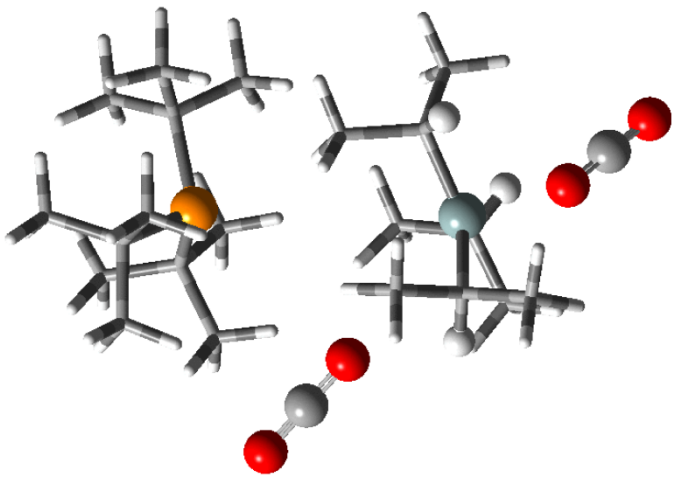

Figure 4.38. $\mathbf{TS_{CD}}$ showing insertion of a second CO_2 molecule into the cavity through aid of ligand twisting.

The relative ^{31}P NMR shift or signal intensity of adduct **13** was shown not to change upon addition of tBu$_3$P. Thus, it would seem possible that this free equivalent, in combination with **13**, may behave analogously to an FLP. Previous DFT calculations upon the 'tethered' FLP $(Me_3C_6H_2)_2PCH_2CH_2B(C_6F_5)_3$ showed CO_2 activation to proceed *via* a synchronous concerted transition state.[34] Parallel methodology was therefore applied for the CO_2 activation by tBu$_3$P/**13**. Under this treatment, two intermediates (**E** and **F**) and one transition state ($\mathbf{TS_{EF}}$) were located along the reaction coordinate (Figure 4.39). The energy cost for this process between **E** and **F** was practically identical to that calculated in the absence of tBu$_3$P [$\Delta\Delta G$ = 79.60 kJ mol^{-1} *vs* 80.19 kJ mol^{-1}, 298 K]. Therefore this pathway is incommensurate

with experimental findings and efforts were directed towards a stepwise route, which gratifyingly was calculated to proceed *via* a low energy pathway.

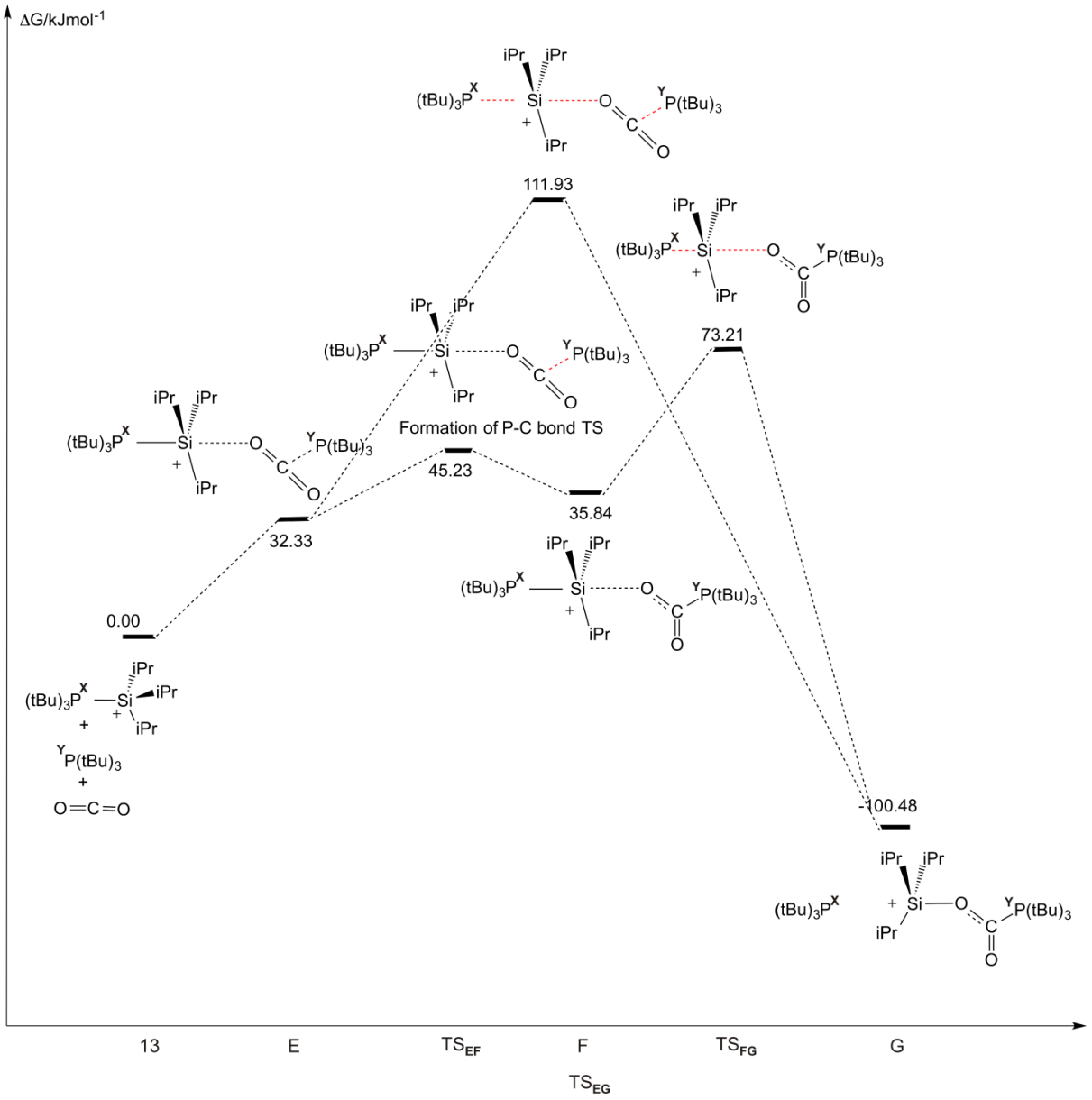

Figure 4.39. Relative energy profile of CO_2 by additional tBu$_3$P and **13**. Two pathways illustrated, a synchronous concerted mechanism (top; $\Delta\Delta G$ = 79.60 kJ mol^{-1}, 298 K) *vs.* a stepwise activation $\Delta\Delta G$ = 34.37 kJ mol^{-1}, 298 K).

Calculations for this stepwise mechanism, displayed two intermediates (**E** and **F**) and two transition states (**TS$_{EF}$** and **TS$_{EF}$**) (Figure 4.40). For convenience, the phosphorus bound to the silicon is denoted P^{X} and the phosphorus belonging to free tBu$_3$P is denoted P^{Y}. In the presence of CO_2, tBu$_3$P/**13** was found to exist in equilibrium with **E** whereby the oxygen of the CO_2 molecule interacts with the silicon centre (much like that found for **A**), concomitant with an interaction between the free phosphorus lone pair (P^{Y}) and the electrophilic carbon of

CO_2. The P^Y···C interaction is slightly less than the sum of the van der Waals radii (3.39 Å) in which the Si···O interaction exerts negligible influence on Si–P bond length found in the X-ray structure. While this coordination results in the considerable enthalpic stabilisation of **E** (ΔH = –49.97 kJ mol^{-1}) the entropic cost associated with preorganising free tBu$_3$P and CO_2 renders **E** less stable overall than tBu$_3$P/**13**. Direct P^Y–C bond (Table 5.6) formation with CO_2 proceed associatively through $\mathbf{TS_{EF}}$ in which the geometry about the Si fragment remains pseudo tetrahedral. The average P–Si–CHMe$_2$ bond angle (114.7º) best reflects this observation, in which a modest energy barrier is seen (ΔG = 12.90 kJ mol^{-1}).

Table 5.6. Pertinent interatomic distances corresponding to selective intermediates and transition states for the stepwise conversion of **13** to **15** in the presence of free tBu$_3$P

Bond lengths	**Si···P^X (Å)**	**Si···O (Å)**	**P^Y···C (Å)**
***t*Bu$_3$P/13**	2.49	-	-
E	2.48	3.82	3.18
TS_{EF}	2.48	3.63	2.53
F	2.49	3.92	1.95
TS_{FG}	3.37	2.67	1.93
G	5.3	1.79	1.89

Intermediate **F** presents a P^Y–C bond distance of 1.95 Å (Table 5.6) much akin to the tBu$_3$P–C(O)O–Si distance found in the X-ray structure of **15** (1.88 Å). The Si–P^X bond distance remains unchanged (2.49 Å) in which the Si···O contact still remains substantially extended (3.92 Å) [sum of the van der Waal radii (3.35 A)]. Interestingly, this would suggest the formation of a zwitterionic intermediate along the reaction coordinate, which is in contrast to experimental observations and literature precedent.

Ensuing Si–O bond formation proceeds *via* $\mathbf{TS_{FG}}$, whereby the Si–P^X bond weakens as the Si–O bond forms to generate [iPr$_3$Si–^{Y}PtBu$_3$]$^+$ and free tBu$_3P^X$ (Figure 4.41). This large structural rearrangement is enthalpically costly ($\Delta\Delta H$ = 44.91 kJ mol^{-1}) but is partially offset by the entropic gain from forming free tBu$_3P^X$ ($\Delta\Delta G$ = 34.37 kJ mol^{-1}, 298 K). The product **G**, demonstrates an extended Si···P^X bond distance and tBu$_3P^Y$, which was formally bound to the Si in **13**, can be said to be dissociated.

As for the calculations without free tBu$_3$P, Si–O bond formation (the step crucial for Si–P bond elongation) remains the major energy cost for this process. The energy barrier associated with the formation of **G** ($\Delta\Delta G$ = 34.37 kJ mol^{-1}, 298K) is less than half that

calculated for the formation of **B** ($\Delta\Delta G$ = 80.2 kJ mol^{-1}, 298 K). This pathway would therefore appear logical in the face of experimental observations.

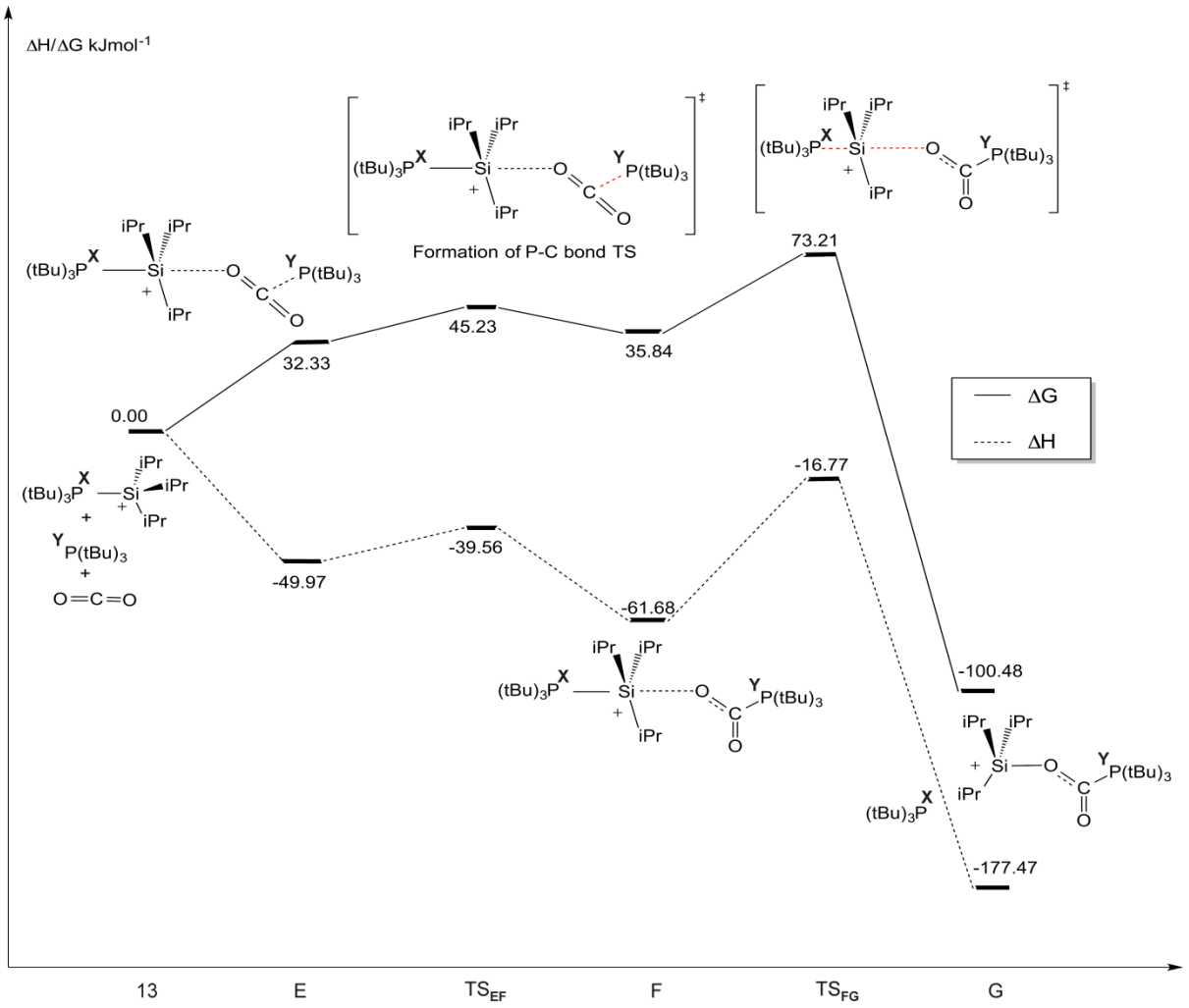

Figure 4.40. Relative energy profile of CO_2 by additional tBu$_3$P and **13** for stepwise activation of CO_2.

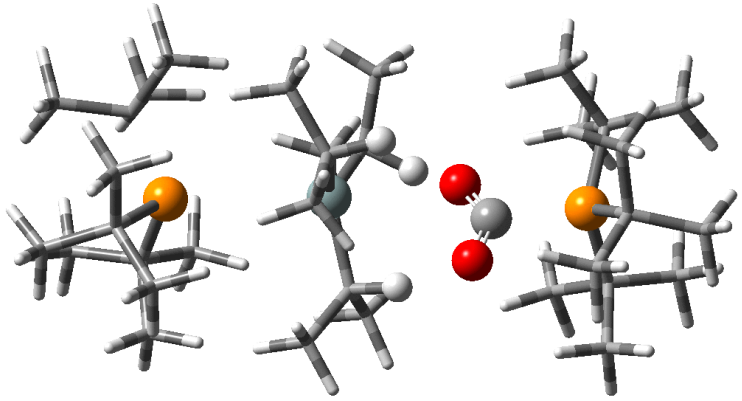

Figure 4.41. TS$_{FG}$, showing weakening of Si–P^X concomitant with Si–O bond formation

4.12 Effect of free *t*Bu$_3$P on H$_2$ activation

In light of experimental and theoretical insights for CO_2 activation, the role of free *t*Bu$_3$P in H_2 heterolysis was investigated. In contrast, added *t*Bu$_3$P was found to attenuate H_2 cleavage with both the yield and rate of H_2 cleavage impaired. For example, PhCl solutions of **13** loaded with 50 and 100 mol % free *t*Bu$_3$P took 16 and 24 hours respectively for full conversion to [*t*Bu$_3$P–H][B(C$_6$F$_5$)]$_4$ by ^{31}P NMR spectroscopy. Integration of the *i*Pr$_3$Si–H signal relative to [*t*Bu$_3$PH]$^+$[B(C$_6$F$_5$)$_4$]$^-$ in the ^{1}H NMR afforded a 40 % yield which was considerably lower than the 90% recorded in the absence of *t*Bu$_3$P. This marked rate reversal is suggestive of an alternative mechanistic pathway. As evinced by DFT calculations, the polarity of the C=O bond facilitates stepwise P–C and Si–O bond formation, a prerequisite for Si–P elongation. It is therefore likely the non-polar H_2 molecule is activated *via* a different pathway, which may involve substituted Si–P bond lengthening (hence the higher temperatures required for heterolysis) since H_2 attack at Si is enthalpically less favourable than by CO_2 assistance [ΔH: Si–O (453 kJ mol^{-1}) *vs* Si–H (318 kJ mol^{-1})].

4.13 Conclusion

The classical phosphine Lewis adducts **12** and **13** have been synthesised from the sterically unencumbered silylium ions R$_3$Si$^+$ (R = Et, *i*Pr) on a multigram scale. X-Ray diffraction studies reveal the Si–P bond distances to be substantially lengthened compared to those reported previously, although are considerably robust in solution; dissociation studies performed on both adducts illustrated no evidence for phosphine dissociation. Interestingly, the products of H_2 cleavage, R$_3$Si–H and [*t*Bu$_3$P–H][B(C$_6$F$_5$)$_4$], are formed upon heating these solutions in the presence of H_2. Follow up D_2 studies advocate an irreversible process in which the stronger hydride donor, Et$_3$SiH, inhibits H_2 cleavage in **12.** Interestingly, CO_2 irreversibly inserts into the Si–P bond of **12** and **13** at RT to afford the silylacylphosphonium adducts **14** and **15**. These systems were appreciably more stable which allowed for the first crystallographic characterisation of a silylacylphosphonium. Subsequently, the activation parameters for CO_2 uptake were experimentally investigated which revealed $\Delta G^{\ddagger}$ (105.4 and 104.0 respectively at 328 K) values dominated by the large $\Delta H^{\ddagger}$ term (105.4 and 104.0 respectively), attributable to the strong Si–P bond. The addition of *t*Bu$_3$P led to a marked improvement in the rate of CO_2 activation, and from examining the impact on rate as a function of concentration, may be considered a catalyst.

DFT calculations on **13** were found to support measurements made experimentally. In the absence of free tBu$_3$P, two CO_2 molecules participated in the formation of **15** from **13** which proceeds *via* initial Si–O bond formation. A low energy pathway for CO_2 activation by tBu$_3$P/**13** was discovered in which P–C and Si–O bond formation occur stepwise, and not concerted as determined by Stephan *et al.* for the described P/B FLP systems.

Overall these findings open up the possibility that other donor-acceptor species of heavier p-block elements bearing electrophilic moieties could be feasible candidates for H_2 activation, having been previously overlooked because they were not part of a genuine FLP system. Follow up investigations should likely focus on the hydrogenation capability of these systems, particularly in catalysis.

4.14 References

[1] C. A. Reed, *Acc. Chem. Res.* **1998**, *31*, 325-332.

[2] (a) L. Greb, P. Ona-Burgos, B. Schirmer, S. Grimme, D. W. Stephan, J. Paradies, *Angew. Chem. Int. Ed.* **2012**, *51*, 10164-10168; (b) L. Greb, S. Tussing, B. Schirmer, P. Ona-Burgos, K. Kaupmees, M. Lokov, I. Leito, S. Grimme, J. Paradies, *Chem. Sci.* **2013**, *4*, 2788-2796.

[3] (a) B. D. Shepherd, *J. Am. Chem. Soc.* **1991**, *113*, 5581-5583; (b) *CRC Handbook Of Chemistry and Physics, Internet Version* (Ed.: D. R. Lide), CRC Press, Boca Raton, FL, **2005**, pp. 1276-1286.

[4] A. Schulz, A. Villinger, *Angew. Chem. Int. Ed.* **2012**, *51*, 4526-4528.

[5] J. B. Lambert, S. H. Zhang, C. L. Stern, J. C. Huffman, *Science* **1993**, *260*, 1917-1918.

[6] Z. W. Xie, J. Manning, R. W. Reed, R. Mathur, P. D. W. Boyd, A. Benesi, C. A. Reed, *J. Am. Chem. Soc.* **1996**, *118*, 2922-2928.

[7] M. F. Ibad, P. Langer, A. Schulz, A. Villinger, *J. Am. Chem. Soc.* **2011**, *133*, 21016-21027.

[8] A. Schaefer, M. Reissmann, A. Schaefer, W. Saak, D. Haase, T. Müller, *Angew. Chem. Int. Ed.* **2011**, *50*, 12636-12638.

[9] M. Reissmann, A. Schafer, S. Jung, T. Müller, *Organometallics* **2013**, *32*, 6736-6744.

[10] K. Muether, M. Oestreich, *Chem. Commun.* **2011**, *47*, 334-336.

[11] M. Kira, T. Hino, H. Sakurai, *Chem. Lett.* **1992**, 555-558.

[12] P. D. Bartlett, F. E. Condon, A. Schneider, *J. Am. Chem. Soc.* **1944**, *66*, 1531-1539.

[13] J. B. Lambert, Y. Zhao, *Angew. Chem. Int. Ed.* **1997**, *36*, 400-401.

[14] D. J. Liston, Y. J. Lee, W. R. Scheidt, C. A. Reed, *J. Am. Chem. Soc.* **1989**, *111*, 6643-6648.

[15] J. B. Lambert, W. Schilf, *J. Am. Chem. Soc.* **1988**, *110*, 6364-6367.

[16] J. B. Lambert, S. Z. Zhang, S. M. Ciro, *Organometallics* **1994**, *13*, 2430-2443.

[17] M. Nava, C. A. Reed, *Organometallics* **2011**, *30*, 4798-4800.

[18] A. Schaefer, W. Saak, D. Haase, T. Müller, *Angew. Chem. Int. Ed.* **2012**, *51*, 2981-2984.

[19] (a) T. Müller, *Adv. Organomet. Chem., Vol. 53* (Eds.: R. West, A. F. Hill), **2005**, pp. 155-215; (b) H. F. T. Klare, M. Oestreich, *Dalton Trans.* **2010**, *39*, 9176-9184.

[20] A. Schaefer, W. Saak, D. Haase, T. Müller, *Chem. Eur. J.* **2009**, *15*, 3945-3950.
[21] G. A. Olah, T. Bach, G. K. S. Prakash, *J. Org. Chem.* **1989**, *54*, 3770-3771.
[22] D. D. Perrin, *Dissociation Constants of Organic Bases in Aqueous Solution*, Buttersworth, London, **1972**, pp. 1-452.
[23] T. Allman, R. G. Goel, *Can. J. Chem.* **1982**, *60*, 716-722.
[24] S. J. Connelly, W. Kaminsky, D. M. Heinekey, *Organometallics* **2013**, *32*, 7478-7481.
[25] (a) M. Bolte, I. Ruderfer, T. Müller, *Acta Cryst. E* **2005**, *61*, M1581-M1582; (b) M. Kuprat, M. Lehmann, A. Schulz, A. Villinger, *Organometallics* **2010**, *29*, 1421-1427.
[26] G. C. Welch, D. W. Stephan, *J. Am. Chem. Soc.* **2007**, *129*, 1880-1881.
[27] W. Nie, H. F. T. Klare, M. Oestreich, R. Froehlich, G. Kehr, G. Erker, *Z. Naturforsch.* **2012**, *67*, 987-994.
[28] S. P. Hoffmann, T. Kato, F. S. Tham, C. A. Reed, *Chem. Commun.* **2006**, 767-769.
[29] H. Mayr, N. Basso, G. Hagen, *J. Am. Chem. Soc.* **1992**, *114*, 3060-3066.
[30] G. Erker, D. W. Stephan, *Frustrated Lewis Pairs II: Expanding The Scope. Top. Curr. Chem.*, Springer GmbH, Berlin, **2013**, pp. 1-317.
[31] (a) G. Oertel, H. Malz, H. Holtschmidt, *Chem. Ber.* **1964**, *97*, 891; (b) I. Kwat, L. V. Griend, W. A. Whitla, R. G. Cavell, *J. Am. Chem. Soc.* **1977**, *99*, 7379-7380; (c) R. Appel, B. Laubach, M. Siray, *Tetrahedron Lett.* **1984**, *25*, 4447-4448.
[32] P. D. Vaidya, E. Y. Kenig, *Chem. Eng. Technol.* **2007**, *30*, 1467-1474.
[33] M. Lehmann, A. Schulz, A. Villinger, *Angew. Chem. Int. Ed.* **2009**, *48*, 7444-7447.
[34] C. M. Momming, E. Otten, G. Kehr, R. Frohlich, S. Grimme, D. W. Stephan, G. Erker, *Angew. Chem., Int. Ed.* **2009**, *48*, 6643-6646.
[35] G. Menard, D. W. Stephan, *J. Am. Chem. Soc.* **2010**, *132*, 1796-1797.
[36] D. G. Blackmond, *Angew. Chem. Int. Ed.* **2005**, *44*, 4302-4320.
[37] A. Bondi, *J. Phys. Chem.* **1964**, *68*, 441-451.

CHAPTER FIVE

Experimental Details & Characterising Data

5.1 General procedure

Unless stated otherwise, all reactions and compounds were manipulated under N_2 using either a MBraun Labmaster DP glovebox or using standard Schlenk line techniques on a dual manifold vacuum/inert gas line. For the manipulation of moisture sensitive compounds, all glassware was heated to 170 °C before use. Solvents and solutions were transferred using a positive pressure of nitrogen through stainless steel or Teflon cannulae, or via plastic syringes for volumes less than 20 ml. Filtrations were performed using either glassware containing sintered glass frits or modified stainless steel cannulae fitted with glass microfibre filters.

Reaction solvents (pentane, hexane, toluene, CH_2Cl_2) were dried using an Innovative Technology Pure Solv SPS-400, whereas Et_2O and THF were distilled from purple Na/benzophenone diketyl; all except CH_2Cl_2 and THF were stored over K-mirrored ampoules. PhCl (anhydrous) and PhF (anhydrous) were thoroughly dried and distilled over CaH_2. CCl_4 was used as received (Sigma-Aldrich, 99.5%)

Deuterated NMR solvents were dried and freeze-thaw degassed over the appropriate drying agent: CD_2Cl_2, $CDCl_3$, Pyridine-d_5 and THF-d_8 (activated 3 Å molecular sieves); PhCl-d_5 (CaH_2); C_6D_6 and C_7D_8 (K). With the exception of PhCl-d_5 (ABCR), all were purchased from Goss Scientific (99.8 % D respectively).

H_2 (5.5 Research Grade BOC) and CO_2 (5.0 Research Grade BOC) were dried *via* passage through WA-500 OMX and WA-500 Sunarc drying columns respectively, both of which were purchased from Matheson NANOCHEM®. D_2 (99.9% Cambridge Isotope Laboratories). D_2 was dried *via* passage through a Supelpure-O® Oxygen/Moisture Trap.

5.2 Elemental analyses

Elemental analyses were conducted by Mr. S. Boyer of the London Metropolitan University.

5.3 Mass spectrometry

High resolution mass spectrometry samples (HRMS; EI & ESI) were recorded by Dr L. Haigh using either a Micromass Autospec Premier or a Micromass LCT Premier spectrometer.

5.4 NMR spectroscopy

NMR spectra were recorded using Bruker AV-400 (400 MHz) and AV-500 (500 MHz) spectrometers. Chemical shifts, δ, are reported in parts per million (ppm). ^{1}H and $^{13}C\{^{1}H\}$ chemical shifts are given relative to Me_4Si and referenced internally to the residual proton shift of the deuterated solvent employed. ^{11}B, ^{19}F, $^{31}P\{^{1}H\}$ and $^{29}Si\{^{1}H\}$ chemical shifts were referenced externally to $BF_3{\cdot}OEt_2$, $CFCl_3$, 85% $H_3PO_{4(aq)}$ and Me_4Si, respectively. For Chapter 4, all samples were prepared inside the glovebox using NMR tubes fitted with Teflon® inserts and J. Young valves. In preparation for quantitative ^{1}H and ^{31}P NMR data, T_1 measurements were determined using an inverse-recovery experiment ($[t\text{Bu}_3\text{PH}]^+$ = 3.2 s and **13** = 10 s). $^{31}P\{^{1}H\}$ NMR spectra were measured using an inverse gated acquisition with a relaxation delay of 70 s and excitation pulse of 30° (to avoid nOe build-up). The sweep width of 400 ppm (190 to –210 ppm) was acquired using 64K data points, resulting in an acquisition time of 0.51 s. Shorter relaxation delays were found to deliver a higher relative phosphonium to adduct ratio in both ^{1}H and $^{31}P\{^{1}H\}$ NMR experiments, which was attributed to a positive NOE from the phosphonium proton.

5.5 IR Spectroscopy

IR spectra were recorded on a Perkin Elmer GX FT-IR spectrometer (range 4000-400 cm^{-1}, resolution 0.5 cm^{-1}) using KBr pellets. For all air sensitive samples the sample was finely ground with KBr and then transferred to a loaded die within the glovebox. Outside of the glovebox, this sample was rapidly pressed into a pellet, and the spectra recorded immediately afterwards.

5.6 Electrochemistry

All electrochemical experiments were performed using either an PGSTAT 302N computer-controlled potentiostat (Metrohm). Cyclic voltammetry (CV) was performed using a three-electrode configuration consisting of a glassy carbon macrodisk working electrode (GCE) (nominal diameter of 3 mm; BASi, Indiana, USA) combined with a Pt wire counter electrode (99.99 %; GoodFellow, Cambridge, UK) and an Ag wire pseudoreference electrode (99.99 %; GoodFellow, Cambridge, UK). The GCE was polished between experiments using successive grades of diamond paste slurries from 3.0 to 0.1 μm (Kemet, Maidstone, UK). The electrodes were briefly sonicated in distilled water and rinsed with ethanol between each polishing step, to remove any adhered microparticles. The electrodes were then dried in an oven at 100 °C to remove any residual traces of water. The Ag wire pseudoreference electrodes were calibrated to the ferrocene/ferrocenium couple in CH_2Cl_2 at the end of each run to allow for any drift in potential, following IUPAC recommendations.[1] All electrochemical measurements were performed at ambient temperatures under an inert N_2 atmosphere in CH_2Cl_2 containing 0.05 $[n\text{Bu}_4\text{N}][\text{B}(\text{C}_6\text{F}_5)_4]$ as the supporting electrolyte. All electrochemical measurements were iR-compensated to within 80 ± 5 % of the solution uncompensated resistance.

5.7 X-Ray crystallography

Single crystal X-Ray Diffraction data were collected and refined by Dr Andrew J. P. White of Imperial College London. Crystals were mounted on a glass fibre using perfluoropolyether oil and mounted in a stream of N_2 at 150 K using an Oxford Diffraction Xcalibur unit.

5.8 Assessment of Lewis acidity

Assessment of Lewis acidity using the Gutmann-Beckett method followed a method described by D.W. Stephan *et al*. which used an excess of Lewis acid to Et_3PO (3:1) dissolved in CD_2Cl_2.[2] To accurately record Δδ, the solution was placed in an NMR tube along with a sealed reference capillary containing uncoordinated Et_3PO dissolved in CD_2Cl_2. The $^{31}P\ \{^1H\}$ NMR shifts were recorded at 298 K. The Childs method was performed as described by Childs *et al*;[3] Lewis acid and *trans*-crotonaldehyde were mixed in a 1:1 ratio and placed in an NMR tube where the ^1H NMR chemical shift of the H_3 proton of crotonaldehyde was recorded.

5.9 General procedure for H_2/D_2 activation experiments of 12 and 13

Reactions in dilute solution, such as those under H_2, invariably become exposed to trace amounts of H_2O (especially as an impurity in H_2 gas), leading to $[t\text{Bu}_3\text{PH}]^+[\text{B}(\text{C}_6\text{F}_5)_4]^-$ and $(i\text{Pr}_3\text{Si})_2\text{O}$ (2:1); hydrolysis thus produces twice the amount of phosphonium salt than the reaction with H_2.

Inside a glove-box, 20mg (0.02 mmol) of **12/13** was dissolved in C_6D_5Cl and transferred to a J. Young sealed NMR tube containing a Teflon® insert. The solution was then measured by both $^{31}P\{^1H\}$ and ^1H NMR to confirm the integrity of the adduct relative to any $t\text{Bu}_3\text{P}–H^+$ impurity, which would result from partial hydrolysis. The solution was degassed once using the freeze-thaw method and sealed under 1 bar pressure of H_2 at 77 K (to ensure reproducible pressures all tubes were immersed in liquid N_2 to a control depth of 10 cm and backfilled for 10 s); this results in an equivalent internal NMR tube pressure of 4 bar at room temperature. $^{31}P\{^1H\}$ and ^1H NMR spectra of the solution were subsequently recorded again to ascertain the contribution from adventitious moisture (from H_2 gas) to the $t\text{Bu}_3\text{P}–H^+$ signal. The tube was then immersed in an oil bath (control depth 10 cm) and heated at 90°C. Reaction was complete after 8 hours, as judged by $^{31}P\{^1H\}$ and ^1H NMR spectroscopy. The yield for H_2 conversion is most reliably calculated *via* relative integration of ^1H NMR signals for the $i\text{Pr}_3\text{SiH}$ resonance against that of $t\text{Bu}_3\text{PH}$ (1:1 from H_2). This experiment was repeated a further 3 times to give a H_2 cleavage yield of 50-53 % (**12**) 90–94% (**13**), calculated on the basis of the starting adduct.

5.10 Kinetic studies

5.10.1 Protonolysis of $1\cdot OH_2$ and $B(C_6F_5)_3\cdot OH_2$

For each complex, a stock solution of borane dissolved in toluene (C_7D_8, 0.05 M), was prepared. H_2O was subsequently administered by means of a microlitre syringe and a known volume extracted (0.6 ml), added to a J. Young sealed NMR tube, and thereafter inserted into a NMR spectrometer set at the desired temperature. Acquisitions were taken every 2 minutes 30 seconds and the initial rate was determined *via* ^1H and ^{19}F NMR integrations of the complex relative to the resonances of the aryl cleavage products.

5.10.2 Variable temperature line shape analysis of 10

The sample was run by Dr Nick Rees of the University of Oxford. The spectra were run on a Varian Unity-plus with an 11.75 Tesla magnet; the ^{1}H NMR were recorded at 499.9MHz and ^{19}F at 490.3MHz. The rates were extracted from line shape simulations performed using gNMR (version 5.10) P. H. M. Budzelaar. See appendix for Eyring plots.

5.10.3 Procedure for calculating activation parameters of 12/13 with $^{13}CO_2$.

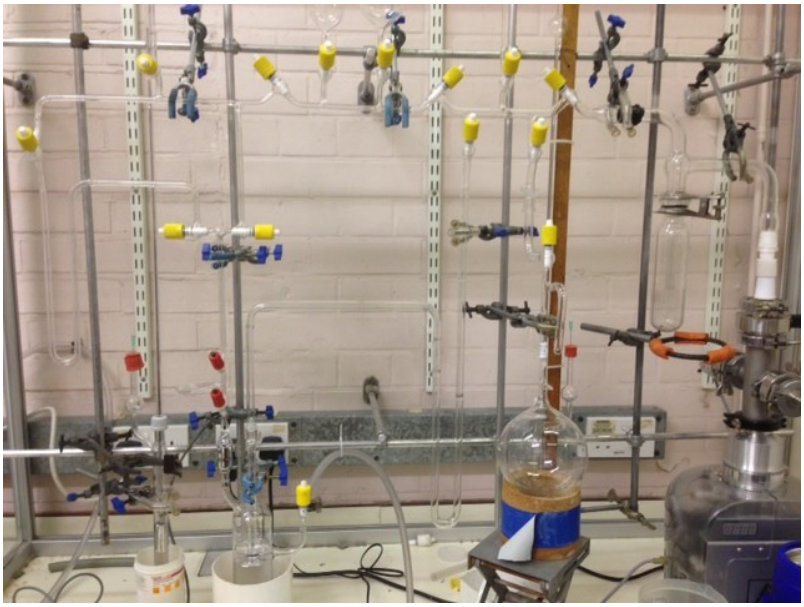

Figure 5.1 Toepler Pump

Following the same guidance as stated for the H_2/D_2 experiments, 20mg (0.02 mmol) of **12/13** was dissolved in C_6D_5Cl and transferred to a J. Young sealed NMR tube containing a Teflon® insert. The solution was examined by both $^{31}P\{^{1}H\}$ and ^{1}H NMR to confirm the integrity of the adduct relative to any tBu$_3$P–H^+ impurity, which would result from partial hydrolysis. With the aid of a Toepler line, the NMR solution was degassed once using the freeze-thaw method; $^{13}CO_2$ admitted to the tube and the solution allowed to warm (see appendix for calculation). To ensure adequate diffusion of CO_2 from the head space into solution, the tube was allowed to stand for 15 minutes, before being inserted into the NMR spectrometer preheated to the corresponding temperature. Due to the direct conversion of [tBu$_3$P–SiR$_3$][B(C$_6$F$_5$)$_4$] into [tBu$_3$P–^{13}CO$_2$–SiR$_3$][B(C$_6$F$_5$)$_4$] (R = Et, iPr) over the course of the reaction, the relative signal integration of the $^{31}P\{^{1}H\}$ NMR environments was used as means of determining the relative concentration of product to starting material. Each run was

repeated twice for each adduct at each temperature and mean data reported in the tables below. Data analysis was performed using OriginPro®. For both **12** and **13** the rate of CO_2 activation was found to be pseudo first order; the rate constants were calculated from a linearized plot of $\ln[C/C_o]$ vs t. Thermodynamic parameters ($\Delta H^{\ddagger}$, $\Delta S^{\ddagger}$ and $\Delta G^{\ddagger}$) were determined *via* an Eyring plot.

5.11 Computational details

5.11.1 Chapter 2

Calculations were performed by Dr Alexander J. W. Thom of Imperial College, London *via* Monte Carlo integration with 10000 samples per radius. The estimates of standard error for each point was < 0.005. Beginning with crystal structures for the tetrahedral pyridine adducts $C_5H_5N{\cdot}A$ (A = $B(C_6F_5)_3$, **1**; see main text for references) the pyridine was excised, leaving a pyramidal A structural residue. Using the van der Waals radii of Bondi,[5] and, for Boron, Martina *et al.*,[6] the van der Waals surface of each pyramidal A was constructed. The relative free volume at a given radius from the boron was defined as the percentage of a surface area of sphere of that radius centred on the boron which was not enclosed by the van der Waals surface, and was calculated by a Monte Carlo integration.

5.11.2 Chapter 4:

Calculations were performed using the Gaussian 09 software suite.[7] Geometry optimisations were performed, without symmetry constraints, using the M06-2X density functional in conjunction with the 6-31G(d,p) basis set for the phosphorous, silicon and carbon dioxide atoms and 4-31G(d,p) basis set for all peripheral atoms.[8] This initial low level calculation was chosen to provide a rough estimate of the energies and structures. The M06-2X functional has been shown to produce accurate thermodynamic data in related frustrated Lewis pair systems and is corrected for long distance interactions.[9] Frequency analysis was performed for all stationary points following structure optimisation. This confirmed the nature of the intermediate as either a minimum (no imaginary frequency) or a transition state (only one imaginary frequency). Intrinsic reaction coordinate (IRC) calculations were used to connect transition states and minima located on the potential energy surface allowing a full energy profile of the reaction to be constructed.[10] GaussView 5.0.9 was to visualise structures, charges and molecular orbitals.[11]

5.12 Commercially supplied chemicals

Acetic acid (99.7 %), *n*BuLi (2.5 M in hexanes), BCl_3 (1.0 M in hexanes), $BF_3{\cdot}OEt_2$ (99.9 %), CF_3SiMe_3 (> 99 %), 18-Crown-6 (99 %), CuBr (99.9 %), 1,3-dibromo-5,5-dimethylhydantoin (DBDMH) (98 %), Et_3SiH (99 %), Et_3SiOTf (99 %), Et_3PO (97 %), Iodine (99.9 %), KF (99 %, spray-dried), KI (99.5 %), Mg powder (20-230 mesh, 98 %), *i*PrMgCl (2.0 M in THF), iPr_3SiH (99 %), PCl_5 (> 98 %), 1-bromo-3,5-*bis*(trifluoromethyl)benzene (99.9 %), 2,2,6,6-tetramethylpiperidine (> 99 %), *trans*-crotonaldehyde (> 99 %), were purchased from Sigma Aldrich. 1-bromo-2,4-*bis*(trifluoromethyl)benzene (99.9 %) purchased from Fluorochem, and H_3PO_2 (50 % H_2O solution) purchased from VWR. All were used as received.

5.13 Literature preparations

The following compounds were synthesised according to published procedures: $B(C_6F_5)_3$,[12] 2-iodo-1,3-*bis*(trifluoromethyl)benzene (**4**),[13] decafluorobenzhydrol,[14] nonafluorobutanesulfonate,[15] $LiB(C_6F_5)$,[16] tBu_3P,[17] and $[Ph_3C][B(C_6F_5)_4]$.[18]

5.14 Experimental details for Chapter 2

5.14.1. Synthesis of *tris*[(3,5-trifluoromethyl)phenyl]borane [$BArF_{18}$; (1)]

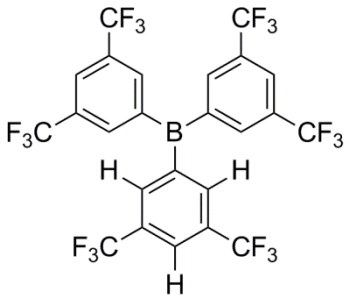

*i*PrMgCl (10.7 ml, 21.4 mmol, 2.0 M in Et_2O) was added slowly to a Schlenk flask charged with a −20 °C stirred solution of 1-bromo-3,5-*bis*(trifluoromethyl)benzene (6.00 g, 3.5 ml, 20.5 mmol) in THF (100 ml). Over 30 minutes the solution was allowed to warm to 0 °C before being cooled to −50 °C, whereupon $BF_3{\cdot}OEt_2$ (0.97 g, 0.84 ml, 6.8 mmol) was added drop wise using a syringe. The contents were warmed over the course of an hour, and volatiles removed under vacuum. The amber oil was extracted using a toluene/pentane mixture (1:1, 3 x 50 ml) and removed under vacuum. The off-white solid was sublimed at 80 °C under high vacuum (1 x 10^{-6} mbar) to produce $BArF_{18}$ as a white powder (2.88 g, 67%,

4.4 mmol). Recrystallization using a minimum quantity of toluene at 100 °C, which is filtered and slow cooled to room temperature, produced an analytical sample.

^{1}H NMR (400.4 MHz, CD_2Cl_2, 25 ºC) δ: 8.02 (s, 6H, *p*-CH), 8.24 (s, 3H, *o*-CH).
^{13}C{^{1}H} NMR (100.6 MHz, CD_2Cl_2, 25 ºC) δ: 123.7 (q, $^{1}J_{CF}$ = 273 Hz, CF_3), 127.0 (sep, $^{3}J_{CF}$ = 3 Hz, *p*-CH), 132.2 (q, $^{2}J_{CF}$ = 33 Hz, *m*-*C*(CF_3)), 138.3 (br, *o*-CH), 142.8 (br, B-C).
^{19}F NMR (376.8 MHz, CD_2Cl_2, 25 ºC) δ: –63.4 (s, CF_3).
^{11}B NMR (128.4 MHz, CD_2Cl_2, 25 ºC) δ: 67.2 (s, br).
HRMS (EI, m/z): for $BC_{24}F_{18}H_9$ Calcd: 650.0510. Found: 650.0510.
IR (KBr, cm^{-1}): 1615 (m), 1607 (m), 1385 (m), 1283 (s), 1227 (s), 1169 (s), 1127 (s), 909 (m), 844 (w), 720 (m), 709 (w), 683 (m), 657 (m).
Anal. Calcd. for $C_{24}H_9BF_{18}$: C 44.34; H 1.40; N 0.00. Found: C 44.22; H 1.29; N 0.00.

5.14.2. Synthesis of [TMPH][μ-H(BArF$_{18}$)$_2$] (2)

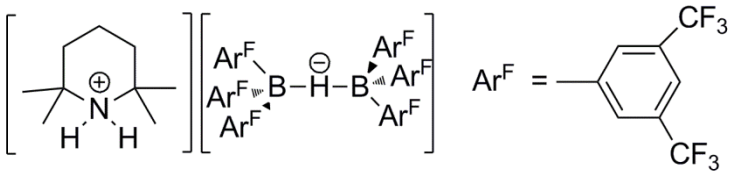

A 100 ml Rotaflo ampoule, equipped with stirrer bar, was charged with $BArF_{18}$ (0.5 g, 0.77 mmol) and TMP (0.07 ml, 0.41 mmol) inside a glovebox. The contents were transferred to a Schlenk line and CH_2Cl_2 (50 ml) added. The mixture was degassed using a freeze-thaw method and sealed under H_2 (1 atm). After 4 hours, a flocculent white solid had precipitated at which point the solution was decanted off. The powder was washed with pentane (2 x 20 ml) and then dried. Yield 0.44 g (0.30 mmol, 79 %).

^{1}H NMR (400.4 MHz, $C_6H_4F_2$, 80 ºC) δ: 1.23 (s, 12H, NC(CH_3)$_2$$CH_2$), 1.45 (m, 4H, NC($CH_3$)$_2CH_2$), 1.57 (m, 2H, NC($CH_3$)$CH_2CH_2$), 4.00 (s, 2H, NH_2), 4.41 (s, H_2)*, 7.73 (s, 12H, *p*-CH), 7.84 (s, 6H, *o*-CH). Hydride not observed.
^{19}F NMR (376.8 MHz, $C_6H_4F_2$, 80 ºC) δ: –63.7 ppm.
IR (KBr, cm^{-1}): 1616 (w), 1365 (m), 1279 (s), 1165 (m), 1126 (m), 900 (m), 841 (w), 710 (m), 682 (s), 649 (s). **Anal. Calcd**. for $C_{24}H_9BF_{18}$: C 47.42; H 2.72; N 0.97. Found: C 47.37; H 2.63; N 1.01.

* H_2 evolved at this temperature. Repeating this reaction in Et_2O (in the absence of stirring) provided a large crop of single crystals suitable for X-ray diffraction of **2**.Et_2O.

5.14.3. Synthesis of *tris*[2,4-*bis*(trifluoromethyl)phenyl)]borane (3)

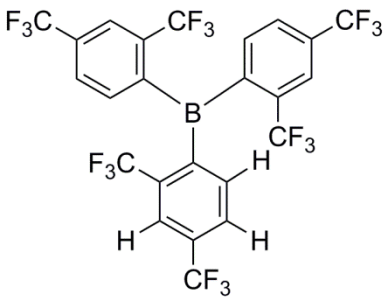

This compound was synthesised by modification of a literature procedure.[19] Bromo-2,4-*bis*(trifluoromethyl)benzene (2.00 g. 1.16 ml, 6.83 mmol) and Et_2O (100 ml) were added to a Schlenk flask. The solution was then cooled to –78 ºC and, with the aid of rapid stirring, *n*BuLi (2.87 ml, 7.17 mmol, 2.5 M in hexanes), was added slowly by means of a syringe. Following one hour of stirring, BCl_3 (2.28 ml, 2.28 mmol, 1 M in hexanes) was syringed into the amber solution and the mixture permitted to warm to room temperature. Under vacuum, the volatiles were removed and the off white residue extracted with CH_2Cl_2 (3 x 25 ml) and filtered through Celite®. CH_2Cl_2 was removed under vacuum and, following a high vacuum sublimation step (1 x 10^{-6} mbar) at 85 ºC, a pure white solid was obtained. Yield 1.33 g (2.04 mmol, 90%).

^{1}H NMR (400.4 MHz, CD_2Cl_2, 25 ºC) δ: 7.46 (d, 3H, $^3J_{HH}$ = 8 Hz, *o*-CH), 7.87 (d, 3H, $^3J_{HH}$ = 8 Hz, *m*-CH), 8.06 (s, 3H, *m*-CH).

^{13}C{^{1}H} NMR (100.6 MHz, CD_2Cl_2, 25 ºC) δ: 123.6 (q, $^1J_{CF}$ = 273 Hz, CF_3), 123.6 (sept, $^3J_{CF}$ = 3 Hz, *m*-CH), 123.9 (q, $^1J_{CF}$ = 273 Hz, CF_3), 127.9 (q, $^3J_{CF}$ = 3 Hz, *m*-CH), 133.7 (q, $^2J_{CF}$ = 34 Hz, $C(CF_3)$), 134.2 (q, $^2J_{CF}$ = 34 Hz, $C(CF_3)$), 135.9 (s, *o*-CH), 144.2 (br, B–C).

^{19}F NMR (376.8 MHz, CD_2Cl_2, 25 ºC) δ: –56.6 (s, *o*-$C(CF_3)$), –63.8 (s, *p*-$C(CF_3)$).

^{11}B NMR (128.4 MHz, CD_2Cl_2, 25 ºC) δ: 74.0 (s, br).

HRMS (EI, m/z): for $BC_{24}F_{18}H_9$ Calcd: 650.0510. Found: 650.0491.

Anal. Calcd. for $C_{24}H_9BF_{18}$: C 44.34; H 1.40; N 0.00. Found: C 44.48; H 1.47; N 0.00.

5.14.4. Synthesis of 1,2,3-*tris*(trifluoromethyl)benzene (5)

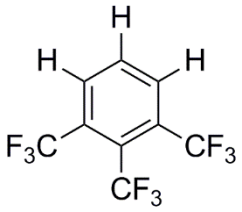

This synthesis was adapted from the previously reported syntheses of pentakis(trifluoromethyl)chlorobenzene ($C_6(CF_3)_5Cl$) *via* the pertrifluoromethylation of pentaiodochlorobenzene (C_6I_5Cl).[20] To a Schlenk flask charged with CuBr (6.46 g, 45.0 mmol) was added 50 ml anhydrous DMF. The flask was then later cooled to –5 ºC in an ethanol/water bath (50:50) fitted with a cooling probe, and CF_3SiMe_3 (5.33 g, 5.54 ml, 37.5 mmol) added. KF (1.91 g, 37.5 mmol) was then added as a suspension in –5 ºC cooled DMF (20 ml) and the resultant 'CF_3Cu' stabilised with NMP (4.7 ml). To this vivid green suspension was added 2-iodo-1,3-*bis*(trifluoromethyl)benzene (10.2 g. 30 mmol) which was followed by additional NMP (19 ml). Overnight, the contents were allowed to warm gradually to RT, by which time the green suspension had transformed into a tan slurry. In air, water was added (30 ml) and, with the aid of a seperatory funnel, the organics extracted with diethyl ether (3 x 50 ml). Using a rotary evaporator, the ether was removed under vacuum and the colourless oil extracted with pentane (3 x 50 ml). The organics were washed with water, dried over Na_2SO_4 and filtered through silica. After removal of the pentane, a fluid colourless oil (**5**) was obtained following distillation at 100 ºC (30 mbar). Yield 5.3 g (18.8 mmol, 63 %).

^{1}H NMR (400.4 MHz, $CDCl_3$, 25 ºC) δ: 7.87 (t, 1H, $^3J_{HH}$ = 8 Hz), 8.13 (d, 2H, $^3J_{HH}$ = 8 Hz).
^{13}C{^{1}H} NMR (125.8 MHz, $CDCl_3$, 25 ºC) δ: 121.8 (q, $^1J_{CF}$ = 276 Hz, 2-CF_3)), 122.7 (q, $^1J_{CF}$ = 274 Hz, 1,3-CF_3)), 128.1 (q, $^2J_{CF}$ = 36 Hz, 2-*C*(CF_3)), 131.2 (qq, $^2J_{CF}$ = 34 Hz, $^3J_{CF}$ = 2 Hz, 1,3-*C*(CF_3)), 131.7 (q, $^3J_{CF}$ = 6 Hz, 4,6-CH), 132.4 (s, 5-CH).
^{19}F NMR (376.8 MHz, $CDCl_3$, 25 ºC) δ: –57.7 (q, $^5J_{FF}$ = 16 Hz, 1,3-CF_3), –54.8 (sept, $^5J_{FF}$ = 16 Hz, 2-CF_3).
HRMS (EI, m/z): for $C_9H_3F_9$ Calcd: 282.0091. Found: 282.0083

5.14.5. Synthesis of 1-bromo-3,4,5-*tris*(trifluoromethyl)benzene (6)

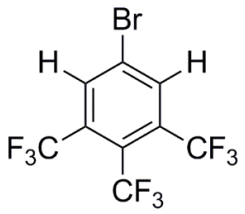

This synthesis was adapted from a literature procedure.[21] To a 100 ml RBF was added 1,3-dibromo-5,5-dimethylhydantoin (DBDMH) (3.34 g, 11.7 mmol) and H_2SO_4 (20 ml) and the contents stirred until the DBDMH dissolved. The solution was cooled to 0 ºC and **5** added (3.30 g, 11.7 mmol). The flask was sealed with Nescofilm® and the suspensions stirred for 3 hours at 0 ºC. Following warming to room temperature, the contents were poured over ice water, and decolourised with a saturated $Na_2S_2O_3$ solution. Afterwards, the organics were extracted with pentane (3 x 50 ml), dried over Na_2SO_4 before being filtered through a frit. The pentane was removed under vacuum to yield a glassy solid which melts above room temperature. Yield 3.31 g (74 %, 9.2 mmol); m.p. (26-28 ºC).

^{1}H NMR (400.4 MHz, $CDCl_3$, 25 ºC) δ: 8.22 (s, 2,6-CH).
^{13}C{^{1}H} NMR (100.6 MHz, $CDCl_3$, 25 ºC) δ: 121.6 (q, $^1J_{CF}$ = 276 Hz, 4-CF_3)), 121.9 (q, $^1J_{CF}$ = 276 Hz, 3,5-CF_3)), 127.0 (q, $^2J_{CF}$ = 36 Hz, 4-*C*(CF_3)), 127.2 (s, C-Br), 132.7 (q, $^2J_{CF}$ = 34 Hz, 3,5-*C*(CF_3)), 134.9 (q, $^3J_{CF}$ = 6 Hz, 2,6-CH).
^{19}F NMR (376.8 MHz, $CDCl_3$, 25 ºC) δ: –57.8 (q, $^5J_{FF}$ = 16 Hz, 3,5-CF_3), –54.8 (sept, , $^5J_{FF}$ = 16 Hz, 4-CF_3).
HRMS (EI, m/z): for $C_9H_2BrF_9$. Calcd: 359.9196. Found: 359.9195

5.14.6. Assessment of Lewis acidity

Gutmann Beckett in CD_2Cl_2. *$^{31}P\{^1H\}$ NMR:* $Et_3P{=}O$ reference capillary: δ = 50.7. $(Et_3P{=}O){\cdot}B(C_6F_5)_3$ reference adduct: δ = 77.3 ppm. Reference shift: $\Delta\delta$ = 26.6. $(Et_3P{=}O){\cdot}BArF_{18}$ adduct: δ = 78.9. Shift: $\Delta\delta$ = 28.2. Lewis-acidity relative to $B(C_6F_5)_3$: 106.0%. *$^{11}B\{^1H\}$ NMR (adduct)*: $(Et_3P{=}O){\cdot}B(C_6F_5)_3$ reference adduct: δ = – 2.5 ppm. $(Et_3P{=}O){\cdot}BArF_{18}$ adduct: δ = + 4.3 ppm. *$^{31}P\{^1H\}$ NMR:* $Et_3P{=}O$ reference capillary: δ = 50.7. $(Et_3P{=}O){\cdot}B(C_6F_5)_3$ reference adduct: δ = 77.3 ppm. Reference shift: $\Delta\delta$ = 26.6.

Childs in CD_2Cl_2 at 298K. ^{1}H NMR: H_3C-CH=CH-CHO reference δ = 6.85 (m, 1H, *H-3*). (H_3C-CH=CH-CHO)-$B(C_6F_5)_3$ reference adduct: δ = 7.93 (m, 1H, *H-3*). Reference shift $\Delta\delta$ = 1.08. (H_3C-CH=CH-CHO)-$BArF_{18}$ adduct: δ = 7.52 (m, 1H, *H-3*). Shift: $\Delta\delta$ = 0.67. Lewis-acidity relative to $B(C_6F_5)_3$: 62.0%. *$^{11}B\{^1H\}$ NMR (adduct)*: (H_3C-CH=CH-CHO)-$B(C_6F_5)_3$ reference adduct: δ = 3.4. (H_3C-CH=CH-CHO)-$BArF_{18}$ adduct: δ = 10.7.

5.15 Experimental details for Chapter 3

5.15.1. Synthesis of 1,1,1,3,3,3-hexafluoropropyl iodide (7)

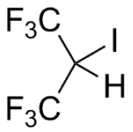

1,1,1,3,3,3-hexafluoropropyl iodide may be synthesised from a known literature procedure, requiring use of a Spaltrohr distillation technique.[15] A new synthesis is described which uses standard laboratory techniques. To 100 ml Rotaflo ampoule was added nonafluorobutanesulfonate $C_3HF_6(OSO_2C_4F_9)$ (6.5 g, 14.4 mmol), excess potassium iodide (9.6 g, 57.9 mmol), 18-Crown-6 (3.8 g, 14.4 mmol) and C_6H_6 (30 ml). The contents were sealed and then stirred at 80 ºC for 6 hours. Upon cooling to room temperature, the contents were siphoned into a 250 ml Schlenk flask and the [K(18-crown-6][$OSO_2C_4F_9$] by-product precipitated *via* the addition of pentane (30 ml). The pentane was removed under reduced pressure and the concentration of 1,1,1,3,3,3-hexafluoropropyl iodide (**7**) determined *via* ^{19}F NMR against a $C_6Cl_5(CF_3)$ reference. Yield 3.51 g (12.6 mmol, 87 %; based upon integration against an internal standard of $C_6Cl_5(CF_3)_3$ (5 mg in 0.5 ml))

^{1}H NMR (400.4 MHz, C_6D_6, 25 ºC) δ: 3.44 (sept, $^3J_{HF}$ = 7 Hz)
^{19}F NMR (376.8 MHz, C_6D_6, 25 ºC) δ: –66.0 (d, $^3J_{FH}$ = 7 Hz)

5.15.2. Synthesis of *bis*(pentafluorophenyl)methane (8)

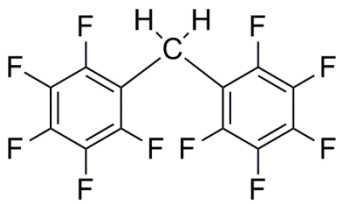

This was adapted from a report by Fry *et al.* for the reduction of various benzephenones and benzhydrols by hypophosphorus acid (H_3PO_2) and I_2.[22] In air, decafluorobenzhydrol (2.5 g, 6.9 mmol), iodine (1.74 g, 6.9 mmol), H_3PO_2 (50 % H_2O solution; 0.8 ml, 7.6 mmol) and acetic acid (40 ml) were added to an RBF fitted with a condenser. The solution was subsequently heated at 60 ºC for three days. Subsequently the solution was cooled to room temperature, diluted with H_2O (50 ml) and extracted with Et_2O (3 x 40 ml). The volatiles were removed to yield *bis*(pentafluorophenyl)methane (**8**) as a fluffy white solid (1.69 g, 4.9 mmol, 71%).

^{1}H NMR (400.4 MHz, $CDCl_3$, 25 ºC) δ: 4.01 (s, C*H*$_2$(C_6F_5)$_2$).
^{19}F NMR (376.8 MHz, $CDCl_3$, 25 ºC) δ: –161.8 (m, *m*-CF), –155.0 (t, $^3J_{FF}$ = 21 Hz, *p*-CF), –142.3 (d, $^3J_{FF}$ = 14 Hz, *o*-CF).

5.15.3. Synthesis of *bis*(pentafluorophenyl)methyl chloride (9)

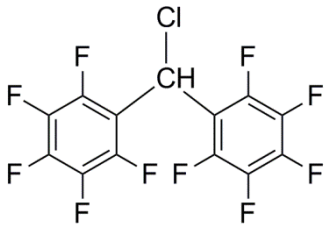

This was adapted from an imprecise literature procedure reported iby Vorozhtsov *et al.* In air, a 500 ml RBF fitted with condenser was charged decafluorobenzahydrol (4.83 g, 13.3 mmol) and PCl_5 (2.76 g, 13.3 mmol). CCl_4 (50 ml) was added and the solution refluxed for 4 hours. Once the contents had cooled to room temperature, the flask was transferred to a rotary evaporator and the volatiles removed to yield an oily yellow residue. This oil was extracted with pentane (3 x 50 ml), dried over anhydrous Na_2SO_4 and subsequently filtered through a frit. The volatiles were once again removed with aid of a rotary evaporator. A final distillation under full vacuum at 90 ºC (1 x 10^{-2} mbar), afforded an analytically pure colourless oil. The sample was stored over 4 Å molecular sieves. Yield 4.10 g (10.7 mmol, 81 %).

^{1}H NMR (400.4 MHz, $CDCl_3$, 25 ºC) δ: 6.61 (s, C*H*Cl(C_6F_5)$_2$).

^{19}F NMR (376.8 MHz, $CDCl_3$, 25 ºC) δ: –160.5 (m, *m*-CF), –151.2 (t, $^3J_{FF}$ = 21 Hz, *p*-CF), –139.2 (d, $^3J_{FF}$ = 14 Hz, *o*-CF).

5.15.4. Synthesis of *tris*[(*bis*pentafluorophenyl)methyl]borane (10)

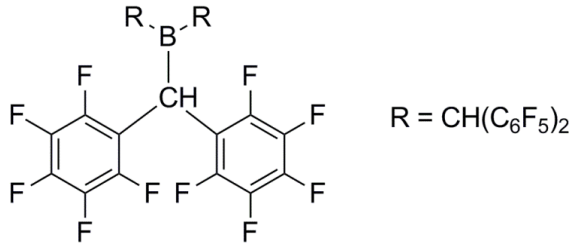

A 250 ml RBF fitted with condenser was charged with magnesium powder (1.93 g, 79.4 mmol) and Et_2O (50 ml). The magnesium surface was activated with trace iodine (0.1 g), and $BF_3{\cdot}OEt_2$ (0.39 ml, 3.17 mmol) and chloro(*bis*pentafluorophenyl)methane (3.80 g, 7.60 ml, 9.93 mmol) subsequently added by means of a syringe. The solution was boiled under reflux for 12 hours, in which the suspension visibly darkened. The contents were cooled to room temperature, the solvent siphoned off by means of a cannula and the pale yellow solution filtered through Celite®. The solvent was stripped under vacuum to yield a tan solid. Extraction with hot toluene (3 x 50 ml; 80 ºC) followed by recrystallization at –30 ºC afforded an off white solid. A final sublimation step (150 ºC; 1 x 10^{-6} mbar) afforded **10** as a white powder (2.10 g, 63 %, 2.00 mmol). Crystals suitable for X-Ray diffraction were grown from a saturated toluene solution cooled to –30 ºC.

^{1}H NMR (400.4 MHz, CD_2Cl_2, 25 ºC) δ: 5.07 (s, B-C*H*$(C_6F_5)_2$).

^{13}C{^{1}H} NMR (100.6 MHz, CD_2Cl_2, 25 ºC) δ: 28.8 (s, B-*C*H$(C_6F_5)_2$), 112.2 (t, $^2J_{CF}$ = 17 Hz, B-CH*C*$(CF)_2$), 137.9 (dm, $^1J_{CF}$ = 254 Hz, *m*-CF), 141.2 (dm, $^1J_{CF}$ = 257 Hz, *p*-CF) 145.1 (dm, $^1J_{CF}$ = 248 Hz, *o*-CF).

^{19}F NMR (376.8 MHz, CD_2Cl_2, 25 ºC) δ: –167.1 (m, 12F, *m*-CF), –163.7 (t, 6F, $^3J_{FF}$ = 20 Hz, *p*-CF), –137.5 (br, 12F, *o*-CF). Impurities at –164.4, –161.5, –157.6, –144.1, –143.1, –143.5, –143.3, –142.5, –138.5 (< 5 %)

^{11}B NMR (128.4 MHz, CD_2Cl_2, 25 ºC) δ: 80.3 (s, br).

IR (KBr, cm^{-1}): 1655 (m), 1525 (s), 1500 (s), 1427 (w), 1301 (w), 1222 (m), 1161 (w), 1131 (m), 1115 (m), 1080 (m), 1055 (m), 1005 (s), 972 (s), 913 (m), 896 (w).

Anal. Calcd. for $C_{39}H_3BF_{30}$: C 44.52; H 0.29; N 0.00. Found: C 44.42; H 0.29; N 0.00.

5.15.5. Synthesis of [TMPH][HB[CH(C_6F_5)$_2$]$_3$] (11)

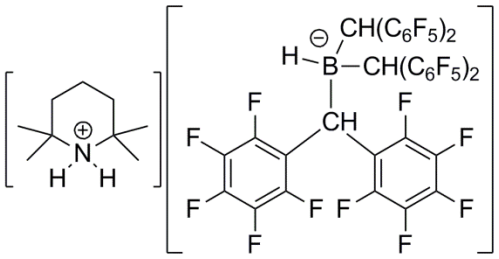

Inside a glovebox, a 100 ml Rotaflo ampoule, equipped with stirrer bar, was charged with TMP (0.03 ml, 0.17 mmol) and **10** (0.15 g, 0.14 mmol). The contents were transferred to a Schlenk line and THF (20 ml) added. The mixture was degassed using a freeze-thaw method and sealed under H_2 (1 atm). After 4 days of heating at 90 ºC, the solution was left to cool and washed with pentane. The resultant amber oil proved difficult to purify in which recrystallisation in chlorobenzene (slow cooled to –30 ºC) marginally improved the sample quality. Yield 0.1 g (0.08 mmol, 60 %).

^{1}H NMR (400.4 MHz, THF-d_8, 25 ºC) δ: 0.97 (s, 12H, NC(C*H*$_3$)$_2$CH$_2$), 1.12 (m, 4H, NC(CH$_3$)$_2$C*H*$_2$), 1.35 (m, 2H, NC(CH$_3$)CH$_2$C*H*$_2$), δ: 6.04 (br, 3H, B-C*H*(C_6F_5)$_2$). 7.90 (s, 2H, NH$_2$).

^{13}C{^{1}H} NMR (100.6 MHz, THF-d_8, 25 ºC) δ: 14.4 (s, NC(*C*H$_3$)$_2$CH$_2$), 23.0 (s, NC(CH$_3$)CH$_2$*C*H$_2$), 35.1 (s, NC(CH$_3$)$_2$*C*H$_2$), δ: 38.5 (s, B-*C*H(C_6F_5)$_2$), 122.0 (t, $^2J_{CF}$ = 17 Hz, B-CH*C*(CF)$_2$), 137.8 (dm, $^1J_{CF}$ = 248 Hz, *m*-CF), 138.4 (dm, $^1J_{CF}$ = 248 Hz, *p*-CF) 146.8 (dm, $^1J_{CF}$ = 248 Hz, *o*-CF).

^{19}F NMR (376.8 MHz, CD_2Cl_2, 25 ºC) δ: –137.3 (br, 12F, *m*-CF), –153.3 (t, 6F, $^3J_{FF}$ = 21 Hz, *p*-CF), –140.7 (br, 6F, *o*-CF), –136.8 (br, 6F, *o*-CF).

^{11}B NMR (128.4 MHz, CD_2Cl_2, 25 ºC) δ: –14.5 (d, $^1J_{BH}$ = 85 Hz, B–H).

HRMS (ES+, *m*/z): for $[C_9H_{20}N]^+$ Calcd: 142.1596 Found: 142.1592

HRMS (ES–, *m*/z): for $[C_{39}H_4BF_3]^-$ Calcd: 1052.9927 Found: 1052.9921

5.16 Experimental details for Chapter 4

The sensitivity towards protic media meant all manipulations were performed inside a glove box under inert atmosphere. To prevent protonation from glassware, all reactions were performed in Teflon® vials (Figure 5.1) with NMR experiments recorded in tubes containing

Teflon® inserts (Norell NMR-100-520D), except those requiring a glass capillary insert for referencing ^{31}P NMR spectra (e.g. Ph_3P/C_6D_5Cl).

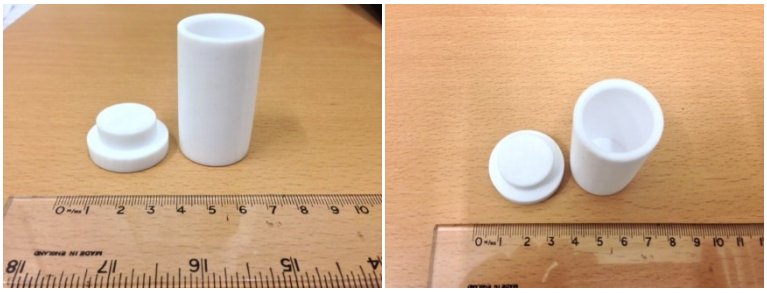

Figure 5.1. Side and top views of Teflon® vials used in the synthesis of **12** and **13**.

5.16.1. Synthesis of [*t*Bu$_3$P→SiEt$_3$][B(C$_6$F$_5$)$_4$] (12)

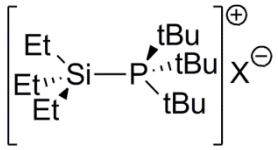

X = B(C$_6$F$_5$)$_4$

Inside a glovebox, a Teflon vial® was charged with *t*Bu$_3$P (0.145 g, 0.72 mmol) and Et$_3$SiOTf (0.195 g, 0.74 mmol) dissolved in CH_2Cl_2 (2 ml). To this solution LiB(C$_6$F$_5$)$_4$ (0.492 g, 0.72 mmol) was added and a fine suspension of LiOTf appeared following 5 minutes of stirring. This by-product was meticulously separated from the mother liquor *via* filtration through a sintered frit and again through a Teflon filter. A white precipitate of **12** was instantly observed after addition of hexane (3 ml) to the colourless clear solution. The resultant solid was left to settle, the supernatant decanted and the white powder washed further with hexane (2 x 3 ml). Recrystallization using a minimum quantity of chlorobenzene, cooled to –30 ºC, afforded an analytically pure sample once washed with hexane (2 x 5 ml) and dried in *vacuo* (0.505 g, 71%, 1.06 mmol). Crystals suitable for X-Ray analysis were grown by slow cooling a PhCl solution to –30 ºC within a glove-box freezer.

^{1}H NMR (400.4 MHz, C_6D_5Cl, 25 ºC) δ: 0.85 (s, 6H, $(CH_3CH_2)_3Si$), 0.85 (s, 9H, $(CH_3CH_2)_3Si$), 1.07 (d, $^3J_{PH}$ = 14 Hz, 27H, $[(CH_3)_3C]_3P$).

^{13}C{^{1}H} NMR (125.8 MHz, C_6D_5Cl, 25 ºC) δ: 8.1 (m, $(CH_3CH_2)_3Si$), 8.1 (m, $(CH_3CH_2)_3Si$), 30.6 (br s, $[(CH_3)_3C]_3P$), 40.5 (d, $^1J_{CP}$ = 15 Hz, $[(CH_3)_3C]_3P$), 136.8 (dm, $^1J_{CF}$ = 239 Hz, *m*-CF), 138.7 (dm, $^1J_{CF}$ = 244 Hz, *p*-CF), 148.9 (dm, $^1J_{CF}$ = 242 Hz, *o*-CF).

^{31}P{^{1}H} NMR (162.1 MHz, C_6D_5Cl, 25 ºC) δ: 36.3 (s).

^{29}Si{^{1}H} NMR (99.4 MHz, C_6D_5Cl, 25 ºC) δ: 22.0 (d, $^{1}J_{SiP}$ = 4 Hz).

^{19}F NMR (376.8 MHz, C_6D_5Cl, 25 ºC) δ: –166.1 (m, $B(C_6F_5)_4$, *m*–CF), –162.4 (t, $B(C_6F_5)_4$, $^{3}J_{FF}$ = 21 Hz, *p*–CF), –131.6 (d, $B(C_6F_5)_4$, $^{3}J_{FF}$ = 17 Hz, *o*–CF).

IR (KBr, cm^{-1}): 1645 (s), 1516 (s), 1463 (s), 1401 (w), 1377 (m), 1276 (m), 1164 (w), 1085 (s), 980 (s).

HRMS (ES+, *m*/*z*): for $[C_{18}H_{43}SiP]^{+}$ Calcd: 318.2872 Found: 318.2877.

HRMS (ES–, *m*/*z*): for $[BHC_{24}F_{20}]^{-}$ Calcd: 679.9852 Found: 679.9857.

Anal Calcd. for $C_{42}H_{42}BF_{20}PSi$: C, 50.62; H, 4.25. Found: C, 50.51; H, 4.38.

5.16.2. Synthesis of [*t*Bu$_3$P→Si*i*Pr$_3$][B(C$_6$F$_5$)$_4$] (13)

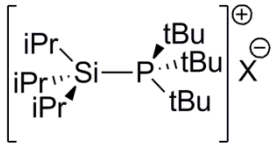

X = $B(C_6F_5)_4$

Inside a glove-box, 1.6 equivalents *i*Pr$_3$SiH (0.110 g, 0.69 mmol) were added to a Teflon® vial containing a stirred orange slurry of $[Ph_3C][B(C_6F_5)_4]$ (0.400 g, 0.43 mmol) in PhCl (2 ml), at room temperature. Over 5 minutes the solution decolourised, at which point 1.2 equivalents *t*Bu$_3$P (0.105 g, 0.52 mmol) were added. After the solution was stirred for an additional 5 minutes, addition of hexane (3 ml) led to formation of a white precipitate. The solid was left to settle and the supernatant siphoned off *via* syringe. To guarantee removal of trace *t*Bu$_3$P and Ph_3CH, the solid was washed thoroughly with hexane (3 x 10 ml), and dried under vacuum to yield a white powder. Recrystallization of this product from PhCl (–25 ºC) produced microcrystalline **13**, which was washed with hexane (2 x 3 ml) and dried *in vacuo* (0.400 g, 89 %, 0.39 mmol). Crystals suitable for X-ray crystallography were grown by cooling a concentrated PhF solution, from room temperature to –25 ºC, within a glove-box freezer.

^{1}H NMR (400.4 MHz, C_6D_5Cl, 25 ºC) δ: 1.01 (d, $^{3}J_{HH}$ = 6 Hz, 18H, $[(CH_3)_2CH)]_3Si$), 1.13 (d, $^{3}J_{HP}$ = 14 Hz, 27H, $[(CH_3)_3C]_3P$), 1.40 (m, 3H, $[(CH_3)_2CH]_3Si$).

^{13}C{^{1}H} NMR (125.8 MHz, C_6D_5Cl, 25 ºC) δ: 17.0 (d, $^{2}J_{CP}$ = 7 Hz, $[(CH_3)_2CH]_3Si$–P; d, $^{1}J_{C^{29}Si}$ (ca. 5%) = 50 Hz, $[(CH_3)_2CH]_3{}^{29}Si$–P), 20.4 (s, $[(CH_3)_2CH]_3Si$–P), 31.7 (br s, $[(CH_3)_3C]_3P$), 41.1 (d, $^{1}J_{CP}$ = 10 Hz, $[(CH_3)_3C]_3P$), 136.8 (dm, $B(C_6F_5)_4$, $^{1}J_{CF}$ = 240 Hz,

m-CF), 138.8 (dm, $B(C_6F_5)_4$, $^1J_{CF}$ = 235 Hz, *p*-CF), 148.9 (dm, $B(C_6F_5)_4$, $^1J_{CF}$ = 240 Hz, *o*-CF). **$^{31}P\{^1H\}$ NMR** (162.1 MHz, C_6D_5Cl, 25 ºC) δ: 57.3 (s).

$^{29}Si\{^1H\}$ NMR (99.4 MHz, C_6D_5Cl, 25 ºC) δ: 43.1 (d, $^1J_{SiP}$ = 23 Hz).

^{19}F NMR (376.8 MHz, C_6D_5Cl, 25 ºC) δ: –166.1 (m, $B(C_6F_5)_4$, *m*–CF), –162.3 (t, $B(C_6F_5)_4$, $^3J_{FF}$ = 21 Hz, *p*–CF), –131.6 (d, $B(C_6F_5)_4$, $^3J_{FF}$ = 17 Hz, *o*–CF).

IR (KBr, cm^{-1}): 1645 (s), 1515 (s), 1463 (s), 1402 (s), 1376 (s), 1329 (w), 1276 (s), 1163 (s), 1086 (s), 1024 (m), 980 (s).

HRMS (ES+, *m*/z): for $[C_{21}H_{49}SiP]^+$ Calcd: 360.3341 Found: 360.3344.

HRMS (ES–, *m*/z): for $[BHC_{24}F_{20}]^-$ Calcd: 679.9852 Found: 679.9854.

Anal Calcd. for $C_{45}H_{48}BF_{20}PSi$: C, 52.03; H, 4.66. Found: C, 51.84; H, 4.47.

5.16.3. Synthesis of $[tBu_3P–^{13}C(O)O–SiEt_3][B(C_6F_5)_4]$ (14)

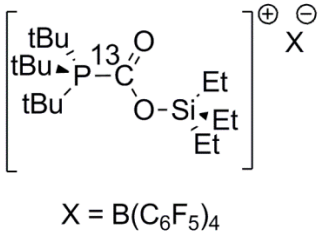

Inside a glove-box, 200 mg (0.20 mmol) of **12** was dissolved in C_6D_5Cl (2 ml) and transferred to a J. Young sealed ampoule. With the aid of a Toepler line, the solution was degassed once using the freeze-thaw method and sealed at 77 K under 1 bar pressure $^{13}CO_2$. The ampoule was left to slowly warm to RT and heated overnight at 60 °C. An aliquot was taken to ensure complete consumption of the adduct, and upon verification, the ampoule transferred to the inside of a glovebox. The solution was extracted *via* syringe and transferred to a Teflon® vial. A white precipitate formed upon addition of hexane and the solid was further washed with hexane (3 x 10ml). Recrystallization of this product from PhCl (–25 ºC) produced a white microcrystalline solid. Yield 170 mg (81 %, 0.16 mmol) Crystals suitable for NMR analysis were grown *via* a PhCl/Hexane layer.

^1H NMR (400.4 MHz, C_6D_5Cl, 25 ºC) δ: 0.65 (q, $^3J_{HH}$ = 8 Hz, 6H, $(CH_3CH_2)_3Si$], 0.83 (q, $^3J_{HH}$ = 8 Hz, 9H, $(CH_3CH_2)_3Si$], 1.18 (d, $^3J_{HP}$ = 15 Hz, 27H, $[(CH_3)_3C]_3P$).

$^{13}C\{^1H\}$ NMR (125.8 MHz, C_6D_5Cl, 25 ºC) δ: 4.3 (s, $(CH_3CH_2)_3Si$; d, $^1J_{C^{29}Si}$ (ca. 5%) = 59 Hz, $(CH_3CH_2)_3{}^{29}Si$), 6.1 (s, $(CH_3CH_2)_3Si$), 29.5 (br s, $[(CH_3)_3C]_3P$), 40.8 (d, $^1J_{CP}$ = 18 Hz,

$[(CH_3)_3C]_3P$), 136.8 (dm, $^1J_{CF}$ = 238 Hz, *m*-CF), 138.7 (dm, $^1J_{CF}$ = 240 Hz, *p*-CF), 148.9 (dm, $^1J_{CF}$ = 242 Hz, *o*-CF), 161.5 (d, $^1J_{CP}$ = 87 Hz, $[(CH_3)_3C]_3P–^{13}C(O)O–$).

$^{31}P\{^1H\}$ NMR (162.1 MHz, C_6D_5Cl, 25 ºC) δ: 52.7 (d, $^1J_{PC}$ = 87 Hz).

$^{29}Si\{^1H\}$ NMR (99.4 MHz, C_6D_5Cl, 25 ºC) δ: 41.0 (dd, $^2J_{Si}{}^{13}{}_C$ = 4 Hz, $^3J_{SiP}$ = 1 Hz).

^{19}F NMR (376.8 MHz, C_6D_5Cl, 25 ºC) δ: –166.1 (m, $B(C_6F_5)_4$, *m*–CF), –162.3 (t, $B(C_6F_5)_4$, $^3J_{FF}$ = 21 Hz, *p*–CF), –131.6 (d, $B(C_6F_5)_4$, $^3J_{FF}$ = 17 Hz, *o*–CF).

IR (KBr, cm^{-1}): 1668 (s, ^{13}C=O), 1644 (s), 1516 (s), 1464 (s), 1403 (m), 1382 (m), 1274 (m), 1210 (m), 1168 (m), 1087 (s), 980 (s).

HRMS (ES+, *m*/z): for $[^{12}C_{18}H_{42}{}^{13}CO_2SiP]^+$ Calcd: 362.2725 Found: 362.2718.

HRMS (ES–, *m*/z): for $[BC_{24}F_{20}]^-$ Calcd: 678.9774 Found: 678.9742.

**c.a.* 5 % based upon ^1H NMR integration *vs*. [tBu$_3$P–$^{13}CO_2$–SiEt$_3$]; δ: 0.97 (d, $^3J_{HP}$ = 16 Hz, $[(CH_3)_3C]_3P$)

5.16.4. Synthesis of [*t*Bu$_3$P–^{12}C(O)O–SiEt$_3$][B(C$_6$F$_5$)$_4$] (^{12}C-14)

Following the procedure outline for S5, 200 mg (0.20 mmol) of **12** was dissolved in C_6D_5Cl (2 ml) and transferred to a J. Young sealed ampoule and attached to a Schlenk line. The solution was degassed once using the freeze-thaw method and sealed at 195 K under 1 bar pressure $^{12}CO_2$. The ampoule was left to slowly warm to RT and heated overnight at 60 °C. A white crystalline solid was obtained following an identical workup as described for **14**. Yield 135 mg (65 %, 0.13 mmol).

^1H NMR (400.4 MHz, C_6D_5Cl, 25 ºC) δ: 0.65 (q, $^3J_{HH}$ = 8 Hz, 6H, $(CH_3CH_2)_3Si$], 0.82 (q, $^3J_{HH}$ = 8 Hz, 9H, $(CH_3CH_2)_3Si$], 1.18 (d, $^3J_{HP}$ = 15 Hz, 27H, $[(CH_3)_3C]_3P$).

$^{31}P\{^1H\}$ NMR (162.1 MHz, C_6D_5Cl, 25 ºC) δ: 52.4 (s).

IR (KBr, cm^{-1}): 1710 (s, ^{12}C=O), 1645 (s), 1515 (s), 1456 (s), 1403 (m), 1382 (m), 1274 (m), 1225 (m), 1172 (m), 1087 (s), 981 (s).

5.16.5. Synthesis of [*t*Bu$_3$P–^{13}C(O)O–Si*i*Pr$_3$][B(C$_6$F$_5$)$_4$] (15)

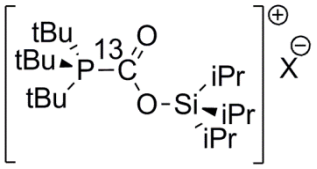

X = $B(C_6F_5)_4$

Following the procedure outlined for **14**, 200 mg (0.19 mmol) of **13** yielded 185 mg (89 % 0.17 mmol) of [*t*Bu$_3$P(^{13}CO$_2$)Si*i*Pr$_3$][B(C$_6$F$_5$)$_4$] (**15**) as a white microcrystalline solid.

^{1}H NMR (400.4 MHz, C_6D_5Cl, 25 ºC) δ: 0.92 (d, $^3J_{HH}$ = 7 Hz, 18H, [(C*H*$_3$)$_2$CH)]$_3$Si), 1.12 (sept, $^3J_{HH}$ = 7 Hz, 3H, [(CH$_3$)$_2$C*H*]$_3$Si), 1.21 (d, $^3J_{HP}$ = 15 Hz, 27H, [(C*H*$_3$)$_3$C]$_3$P).
^{13}C{^{1}H} NMR (125.8 MHz, C_6D_5Cl, 25 ºC) δ: 12.1 (s, [(CH$_3$)$_2$*C*H]$_3$Si; d, $^1J_{C^{29}Si}$ (ca. 5%) = 59 Hz, [(CH$_3$)$_2$*C*H]$_3^{29}$Si), 17.3 (s, [(*C*H$_3$)$_2$CH]$_3$Si–P), 29.7 (br s, [(*C*H$_3$)$_3$C]$_3$P), 40.9 (d, $^1J_{CP}$ = 18 Hz, [(CH$_3$)$_3$*C*]$_3$P), 136.8 (dm, B(C$_6$F$_5$)$_4$, $^1J_{CF}$ = 240 Hz, *m*-CF), 138.7 (dm, B(C$_6$F$_5$)$_4$, $^1J_{CF}$ = 235 Hz, *p*-CF), 148.9 (dm, B(C$_6$F$_5$)$_4$, $^1J_{CF}$ = 240 Hz, *o*-CF). 162.0 (d, $^1J_{CP}$ = 86 Hz, [(CH$_3$)$_3$C]$_3$P–^{13}C(O)O–).
^{31}P{^{1}H} NMR (162.1 MHz, C_6D_5Cl, 25 ºC) δ: 53.4 (d, $^1J_{PC}$ = 86 Hz).
^{29}Si{^{1}H} NMR (99.4 MHz, C_6D_5Cl, 25 ºC) δ: 38.1 (d, $^2J_{Si^{13}C}$ = 4 Hz).
^{19}F NMR (376.8 MHz, C_6D_5Cl, 25 ºC) δ: –166.1 (m, B(C$_6$F$_5$)$_4$, *m*–CF), –162.3 (t, B(C$_6$F$_5$)$_4$, $^3J_{FF}$ = 21 Hz, *p*–CF), –131.6 (d, B(C$_6$F$_5$)$_4$, $^3J_{FF}$ = 17 Hz, *o*–CF).
IR (KBr, cm^{-1}): 1673 (s, ^{13}C=O), 1644 (s), 1516 (s), 1459 (s), 1402 (w), 1381 (m), 1278 (m), 1207 (m), 1167 (m), 1085 (s), 981 (s).
HRMS (ES+, *m*/z): for [^{12}C$_{21}$H$_{48}$^{13}CO$_2$SiP]$^+$ Calcd: 404.3195 Found: 404.3200.
HRMS (ES–, *m*/z): for [BC$_{24}$F$_{20}$]$^-$ Calcd: 678.9774 Found: 678.9742.

5.15.6 Synthesis of [*t*Bu$_3$P–^{12}C(O)O–Si*i*Pr$_3$][B(C$_6$F$_5$)$_4$] (^{12}C-15)

Following the procedure outline for **^{12}C-14**, 200mg (0.20 mmol) of **13** was dissolved in C_6D_5Cl (2 ml) and transferred to a J. Young sealed ampoule and attached to a Schlenk line. The solution was degassed once using the freeze-thaw method and sealed at 195 K under 1 bar pressure $^{12}CO_2$. The ampoule was left to slowly warm to RT and heated overnight at 60°C. Following work-up a white crystalline solid was obtained. Yield 131 mg (65%, 0.12 mmol).

^{1}H NMR (400.4 MHz, C_6D_5Cl, 25 ºC) δ: 0.92 (d, $^3J_{HH}$ = 7 Hz, 18H, [(C*H*$_3$)$_2$CH)]$_3$Si), 1.12 (sept, $^3J_{HH}$ = 7 Hz, 3H, [(CH$_3$)$_2$C*H*]$_3$Si), 1.21 (d, $^3J_{HP}$ = 15 Hz, 27H, [(C*H*$_3$)$_3$C]$_3$P).
^{31}P{^{1}H} NMR (162.1 MHz, C_6D_5Cl, 25 ºC) δ: 53.4 (s).
IR (KBr, cm^{-1}): 1715 (s, ^{12}C=O), 1645 (s), 1516 (s), 1459 (s), 1402 (w), 1382 (m), 1277 (m), 1222 (m), 1171 (m), 1087 (s), 980 (s).

5.17 References

[1] G. Gritzner, J. Kuta, *Electrochimica Acta* **1984**, *29*, 869-873.

[2] G. C. Welch, L. Cabrera, P. A. Chase, E. Hollink, J. D. Masuda, P. R. Wei, D. W. Stephan, *Dalton Trans.* **2007**, 3407-3414.

[3] R. F. Childs, D. L. Mulholland, A. Nixon, *Can. J. Chem.* **1982**, *60*, 801-808.

[4] P. H. M. Budzelaar, gNMR (Version 5.10), Adept Scientific, Letchworth Garden City, U.K.

[5] A. Bondi, *J. Phys. Chem.* **1964**, *68*, 441-451.

[6] M. Mantina, A. C. Chamberlin, R. Valero, C. J. Cramer, D. G. Truhlar, *J. Phys. Chem A.* **2009**, *113*, 5806-5812.

[7] G. W. T. M. J. Frisch, H. B. Schlegel, G. E. Scuseria, M. A. Robb, J. R. Cheeseman, G. Scalmani, V. Barone, B. Mennucci, G. A. Petersson, H. Nakatsuji, M. Caricato, X. Li, H. P. Hratchian, A. F. Izmaylov, J. Bloino, G. Zheng, J. L. Sonnenberg, M. Hada, M. Ehara, K. Toyota, R. Fukuda, J. Hasegawa, M. Ishida, T. Nakajima, Y. Honda, O. Kitao, H. Nakai, T. Vreven, J. A. Montgomery, Jr., J. E. Peralta, F. Ogliaro, M. Bearpark, J. J. Heyd, E. Brothers, K. N. Kudin, V. N. Staroverov, R. Kobayashi, J. Normand, K. Raghavachari, A. Rendell, J. C. Burant, S. S. Iyengar, J. Tomasi, M. Cossi, N. Rega, J. M. Millam, M. Klene, J. E. Knox, J. B. Cross, V. Bakken, C. Adamo, J. Jaramillo, R. Gomperts, R. E. Stratmann, O. Yazyev, A. J. Austin, R. Cammi, C. Pomelli, J. W. Ochterski, R. L. Martin, K. Morokuma, V. G. Zakrzewski, G. A. Voth, P. Salvador, J. J. Dannenberg, S. Dapprich, A. D. Daniels, Ö. Farkas, J. B. Foresman, J. V. Ortiz, J. Cioslowski, D. J. Fox, Gaussian 09, Revision B.01, Gaussian, Inc., Wallingford CT, **2009**.

[8] Y. Zhao, D. G. Truhlar, *Theor. Chem. Acc.* **2008**, *120*, 215-241.

[9] S. Schirmer, S. Grimme, *Frustrated Lewis Pairs I: Uncovering and Understanding. Top. Curr. Chem.* (Eds.: G. Erker, D. W. Stephan), Springer GmbH, Berlin, **2013**, pp. 213-230.

[10] (a) K. Fukui, *Acc. Chem. Res* **1981**, *14*, 363; (b) H. P. Hratchian, H. B. Schlegal, *Theory and Applications of Computational Chemistry: The First 40 Years* (Eds.: C. E. Dykstra, G. Frenking, K. S. Kim, G. Scuseria), Elsevier, Amsterdam, **2005**, pp. 195-259.

[11] T. K. R. Dennington, J. Millam, GaussView, Version 5, Semichem Inc., Shawnee Mission KS, **2009**.

[12] S. J. Lancaster, ChemSpider SyntheticPages, http://cssp.chemspider.com/215, **2003**.

[13] M. Schlosser, F. Mongin, J. Porwisiak, W. Dmowski, H. H. Buker, N. M. M. Nibbering, *Chem. Eur. J.* **1998**, *4*.

[14] A. K. Barbour, M. W. Buxton, P. L. Coe, R. Stephens, J. C. Tatlow, *J. Chem. Soc.* **1961**, 808-817.

[15] M. Hanack, J. Ullmann, *J. Org. Chem.* **1989**, *54*, 1432-1435.

[16] M. Kuprat, M. Lehmann, A. Schulz, A. Villinger, *Organometallics* **2010**, *29*, 1421-1427.

[17] R. C. Srivastava, *J. Chem. Res* **1985**, 330-331.

[18] M. Lehmann, A. Schulz, A. Villinger, *Angew. Chem. Int. Ed.* **2009**, *48*, 7444-7447.

[19] S. M. Cornet, K. B. Dillon, C. D. Entwistle, M. A. Fox, A. E. Goeta, H. P. Goodwin, T. B. Marder, A. L. Thompson, *Dalton Trans.* **2003**, 4395-4405.

[20] A. Kutt, V. Movchun, T. Rodima, T. Dansauer, E. B. Rusanov, I. Leito, I. Kaljurand, J. Koppel, V. Pihl, I. Koppel, G. Ovsjannikov, L. Toom, M. Mishima, M. Medebielle, E. Lork, G.-V. Roeschenthaler, I. A. Koppel, A. A. Kolomeitsev, *J. Org. Chem.* **2008**, *73*, 2607-2620.

[21] V. G. Lukmanov, L. A. Alekseeva, A. I. Burmakov, L. M. Yagupol'skii, *Zh. Org. Khim.* **1973**, *9*, 1019-1024.
[22] M. Allukian, G. S. Han, L. Hicks, A. J. Fry, *Arkivoc* **2002**, 76-79.

APPENDIX

HRMS for 11

(ES– m/z) for $C_{39}H_4BF_{30}$

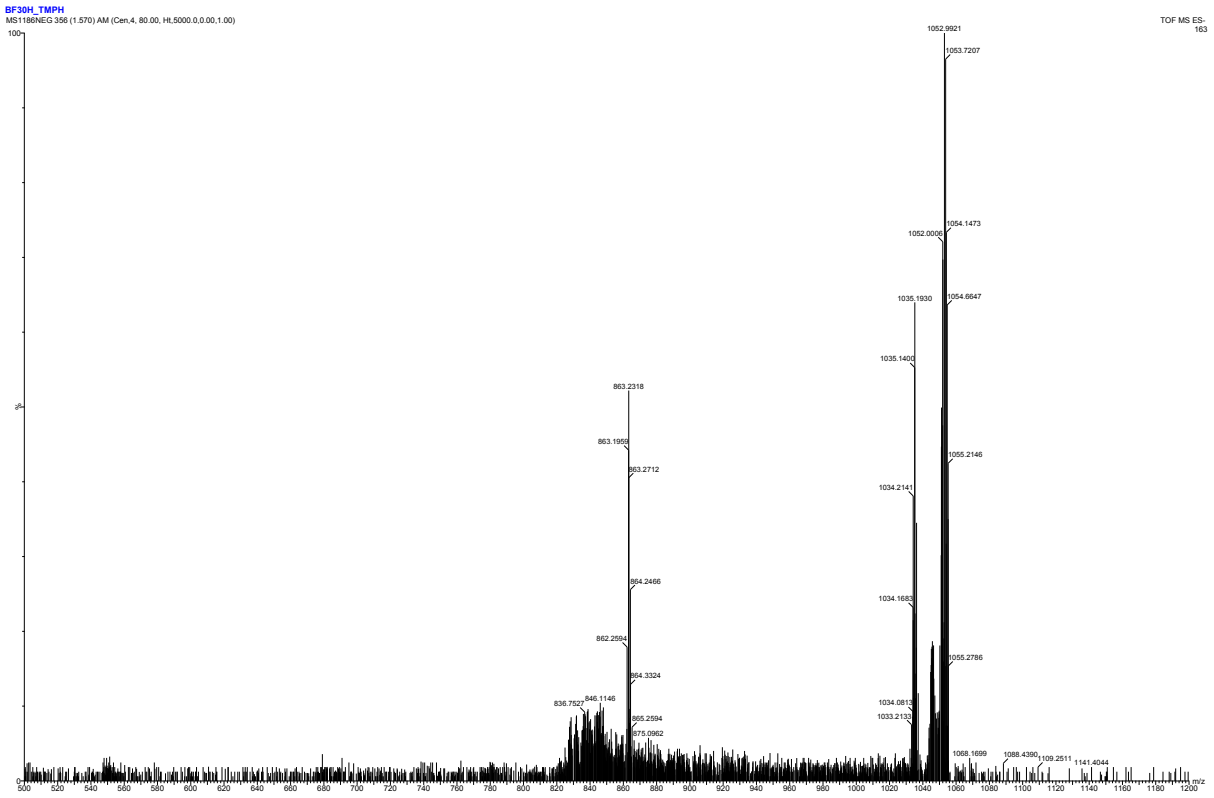

(ES– m/z) for $C_{39}H_4BF_{30}$

Monoisotopic Mass, Even Electron Ions

461 formula(e) evaluated with 1 results within limits (all results (up to 1000) for each mass)

Elements Used:

C: 39-39 H: 0-200 N: 0-10 O: 0-20 Na: 0-1 F: 30-30 11B: 1-1

Minimum:				-1.5			
Maximum:		5.0	10.0	50.0			
Mass	Calc. Mass	mDa	PPM	DBE	i-FIT	i-FIT (Norm)	Formula
1052.9921	1052.9927	-0.6	-0.6	23.5	107.7	0.0	C39 H4 F30 11B

(ES+ m/z) for $C_9H_{20}N$

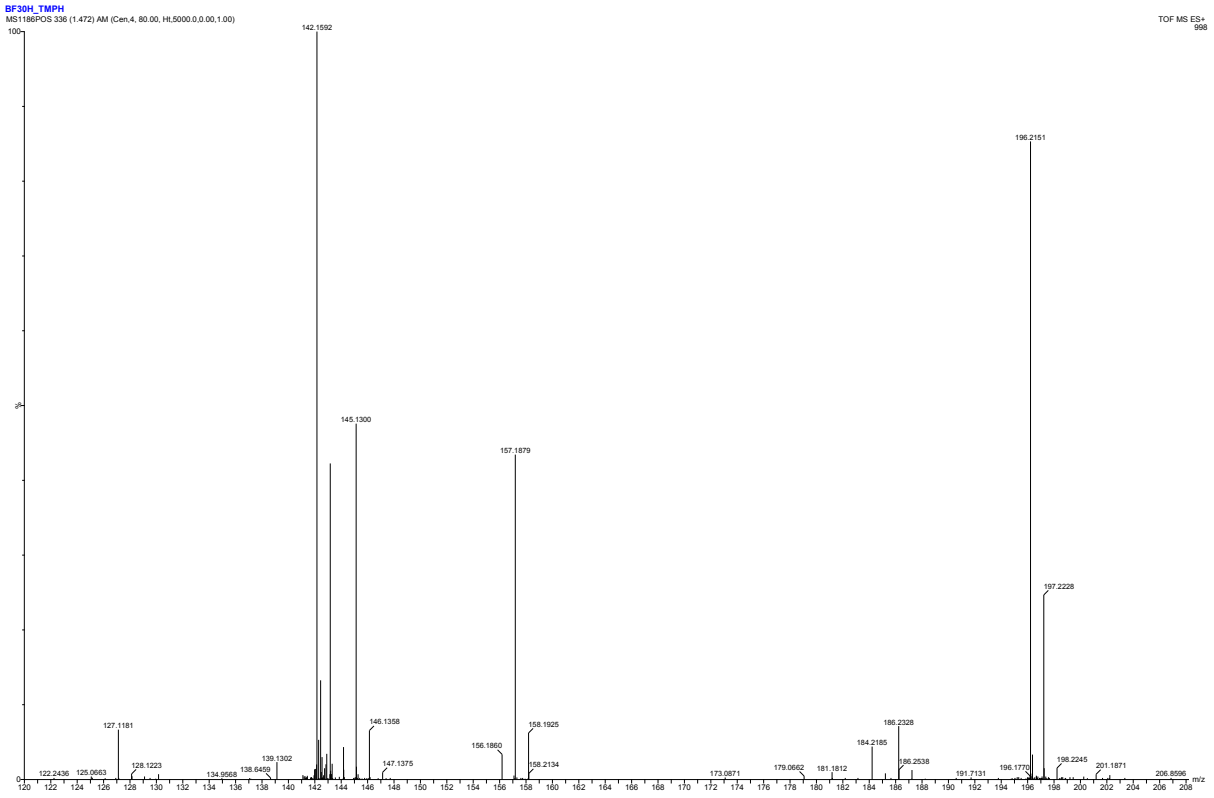

Elemental Composition Report

Single Mass Analysis

Tolerance = 10.0 PPM / DBE: min = -1.5, max = 50.0

Element prediction: Off

Number of isotope peaks used for i-FIT = 3

Monoisotopic Mass, Even Electron Ions

94 formula(e) evaluated with 1 results within limits (all results (up to 1000) for each mass)

Elements Used:

C: 9-9 H: 0-200 N: 0-10 O: 0-20 Na: 0-1

Minimum:				-1.5			
Maximum:		5.0	10.0	50.0			
Mass	Calc. Mass	mDa	PPM	DBE	i-FIT	i-FIT (Norm)	Formula
142.1592	142.1596	-0.4	-2.8	0.5	130.7	0.0	C9 H20 N

Line shape analysis of 10

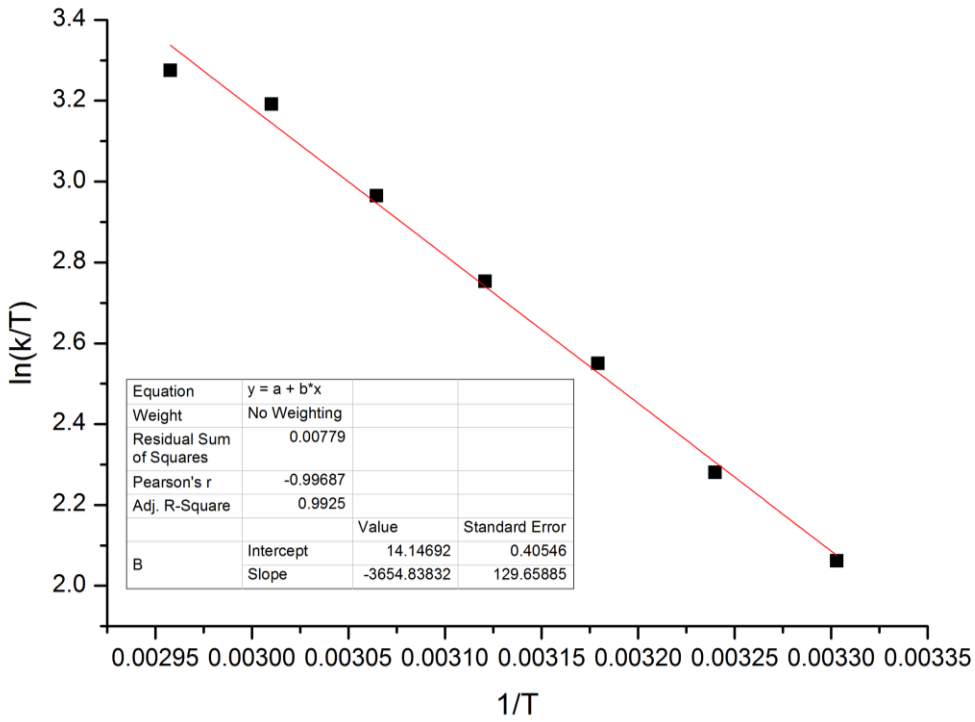

Table 1. ^{19}F NMR for Process A

temp/C	Temp (℃)	Rate	Temp (K)	1/T	ln(k/T)
25	29.7593	2.38E+03	302.7593	0.003303	2.061918
30	35.6498	3020	308.6498	0.00324	2.280805
35	41.5403	4030	314.5403	0.003179	2.550409
40	47.4308	5030	320.4308	0.003121	2.753509
45	53.3213	6330	326.3213	0.003064	2.965173
50	59.2118	8080	332.2118	0.00301	3.191374
55	65.1023	8940	338.1023	0.002958	3.274942

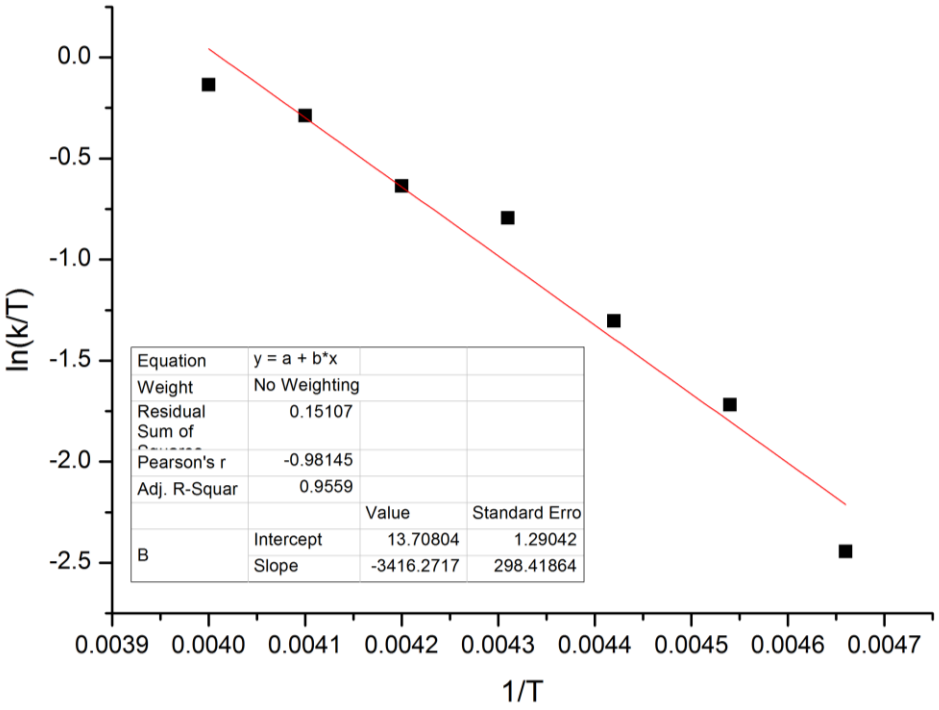

Table 2. ^{19}F NMR for Process B

temp/C	Temp (℃)	Rate	Temp (K)	1/T	ln(k/T)
-60	-70.3792	1.4	202.6208	0.004935	-4.97486
-55	-64.4887	6.22	208.5113	0.004796	-3.51222
-50	-58.5982	18.6	214.4018	0.004664	-2.44469
-45	-52.7077	39.5	220.2923	0.004539	-1.71865
-40	-46.8172	61.5	226.1828	0.004421	-1.30231
-35	-40.9267	105	232.0733	0.004309	-0.79309
-30	-35.0362	126	237.9638	0.004202	-0.63584
-25	-29.1457	183	243.8543	0.004101	-0.28708
-20	-23.2552	218	249.7448	0.004004	-0.13594

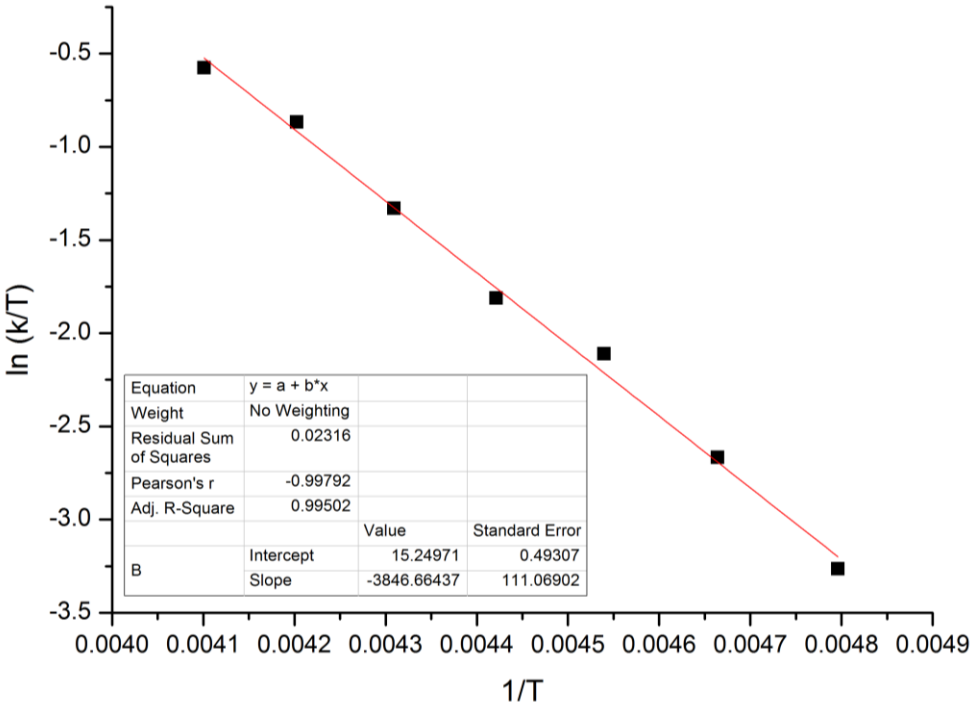

Table 3. ^{1}H NMR for Process B

temp/C	Temp (ºC)	Rate	Temp (K)	1/T	ln(k/T)
-60	-70.3792	3.59	202.6208	0.004935	-4.03318
-55	-64.4887	7.97	208.5113	0.004796	-3.26431
-50	-58.5982	14.9	214.4018	0.004664	-2.66649
-45	-52.7077	26.7	220.2923	0.004539	-2.11029
-40	-46.8172	37	226.1828	0.004421	-1.81043
-35	-40.9267	61.4	232.0733	0.004309	-1.32964
-30	-35.0362	100	237.9638	0.004202	-0.86695
-25	-29.1457	137	243.8543	0.004101	-0.57659
-20	-23.2552	247	249.7448	0.004004	-0.01105

Gradient = -ΔH*/R (in J mol-1)
Intercept = 23.8 + ΔS*/R (in J mol-1 K-1)

NMR	Process (T_c)	$\Delta H^{\ddagger}$ (kJ mol^{-1})	$\Delta S^{\ddagger}$ (J mol^{-1} K^{-1})	$\Delta G^{\ddagger}$ (T_c, kJ mol^{-1})
^{19}F	**A (313 K)**	32.1(5)	-75(2)	55.5(4)
^{19}F	**B (228 K)**	28(2)	-84(10)	48(3)
^{1}H	**B (228 K)**	32(1)	-71(4)	48(1)

Toepler Pump Calibration For Conversion of 13 to 15

	13
Mass (mg)	20
MW	1038.3
mmoles	0.019262256

Number mmoles gas admitted = $\frac{\Delta PV}{RT}$

0.36613346

R = 62.3237 cm^3 mmHg $mmol^{-1}$ K^{-1}
T = 298 K
ΔP = 80 mm Hg
V = 62.4 cm^3

Excess	19.0078186

X-ray Crystallography Data

[TMPH][μ-H(BArF$_{18}$)$_2$]·Et$_2$O (2·Et$_2$O)

Crystal data and structure refinement for ASH1106.

Identification code	ASH1106
Formula	C48 H19 B2 F36, C9 H20 N, C4 H10 O
Formula weight	1517.63
Temperature	173 K
Diffractometer, wavelength	OD Xcalibur 3, 0.71073 Å
Crystal system, space group	Triclinic, P-1
Unit cell dimensions	a = 12.0325(5) Å α = 90.233(4)°
	b = 15.7928(8) Å β = 92.367(4)°
	c = 17.3620(9) Å γ = 100.933(4)°
Volume, Z	3236.4(3) Å^3, 2
Density (calculated)	1.557 Mg/m^3
Absorption coefficient	0.164 mm^{-1}
F(000)	1528
Crystal colour / morphology	Colourless tablets
Crystal size	0.32 x 0.30 x 0.15 mm^3
θ range for data collection	3.10 to 28.53°
Index ranges	-14<=h<=15, -20<=k<=20, -14<=l<=23
Reflns collected / unique	24009 / 13209 [R(int) = 0.0305]
Reflns observed [F>4σ(F)]	7684
Absorption correction	Analytical
Max. and min. transmission	0.979 and 0.961
Refinement method	Full-matrix least-squares on F^2
Data / restraints / parameters	13209 / 343 / 1009
Goodness-of-fit on F^2	1.046
Final R indices [F>4σ(F)]	R1 = 0.0822, wR2 = 0.2189
R indices (all data)	R1 = 0.1380, wR2 = 0.2509
Largest diff. peak, hole	0.564, -0.491 eÅ^{-3}
Mean and maximum shift/error	0.000 and 0.001

Bond lengths [Å] and angles [°]

B(1)-C(1)	1.609(5)	C(3)-C(7)	1.515(7)
B(1)-C(17)	1.609(5)	C(4)-C(5)	1.391(5)
B(1)-C(9)	1.614(5)	C(5)-C(6)	1.390(5)
B(2)-C(41)	1.606(5)	C(5)-C(8)	1.484(5)
B(2)-C(33)	1.608(5)	C(7)-F(7A)	1.318(9)
B(2)-C(25)	1.622(5)	C(7)-F(7B)	1.320(8)
C(1)-C(6)	1.393(5)	C(7)-F(7C)	1.335(7)
C(1)-C(2)	1.398(5)	C(7')-F(7E)	1.290(13)
C(2)-C(3)	1.397(5)	C(7')-F(7D)	1.303(14)
C(3)-C(4)	1.366(5)	C(7')-F(7F)	1.307(14)
C(3)-C(7')	1.486(16)	C(8)-F(8C)	1.331(5)

C(8)-F(8A)	1.333(5)	C(43)-C(44)	1.383(5)
C(8)-F(8B)	1.336(5)	C(43)-C(47')	1.489(15)
C(9)-C(10)	1.396(5)	C(43)-C(47)	1.502(7)
C(9)-C(14)	1.406(5)	C(44)-C(45)	1.389(5)
C(10)-C(11)	1.389(5)	C(45)-C(46)	1.381(5)
C(11)-C(12)	1.392(5)	C(45)-C(48')	1.500(18)
C(11)-C(15)	1.496(5)	C(45)-C(48)	1.506(6)
C(12)-C(13)	1.383(5)	C(47)-F(47A)	1.307(8)
C(13)-C(14)	1.380(5)	C(47)-F(47B)	1.316(9)
C(13)-C(16')	1.492(17)	C(47)-F(47C)	1.318(7)
C(13)-C(16)	1.510(6)	C(47')-F(47D)	1.305(14)
C(15)-F(15C)	1.321(5)	C(47')-F(47E)	1.311(14)
C(15)-F(15B)	1.324(5)	C(47')-F(47F)	1.317(14)
C(15)-F(15A)	1.335(6)	C(48)-F(48B)	1.317(5)
C(16)-F(16C)	1.311(7)	C(48)-F(48A)	1.319(6)
C(16)-F(16B)	1.318(7)	C(48)-F(48C)	1.333(6)
C(16)-F(16A)	1.328(6)	C(48')-F(48D)	1.317(15)
C(16')-F(16E)	1.306(15)	C(48')-F(48F)	1.319(15)
C(16')-F(16F)	1.308(15)	C(48')-F(48E)	1.320(15)
C(16')-F(16D)	1.309(15)	N(50)-C(55)	1.523(5)
C(17)-C(22)	1.397(5)	N(50)-C(51)	1.543(5)
C(17)-C(18)	1.403(5)	C(51)-C(56)	1.506(6)
C(18)-C(19)	1.394(5)	C(51)-C(52)	1.527(5)
C(19)-C(20)	1.372(6)	C(51)-C(57)	1.527(6)
C(19)-C(23)	1.497(6)	C(52)-C(53)	1.510(6)
C(20)-C(21)	1.386(5)	C(53)-C(54)	1.533(7)
C(21)-C(22)	1.387(5)	C(54)-C(55)	1.542(6)
C(21)-C(24)	1.490(5)	C(55)-C(58)	1.510(6)
C(23)-F(23B)	1.305(5)	C(55)-C(59)	1.516(7)
C(23)-F(23A)	1.318(6)	O(60)-C(61)	1.405(5)
C(23)-F(23C)	1.333(6)	O(60)-C(63)	1.450(6)
C(24)-F(24B)	1.331(4)	C(61)-C(62)	1.465(7)
C(24)-F(24A)	1.334(5)	C(63)-C(64)	1.485(8)
C(24)-F(24C)	1.337(5)		
C(25)-C(26)	1.397(5)	C(1)-B(1)-C(17)	117.1(3)
C(25)-C(30)	1.397(5)	C(1)-B(1)-C(9)	114.0(3)
C(26)-C(27)	1.393(5)	C(17)-B(1)-C(9)	115.7(3)
C(27)-C(28)	1.378(5)	C(41)-B(2)-C(33)	116.0(3)
C(27)-C(31)	1.497(5)	C(41)-B(2)-C(25)	115.0(3)
C(28)-C(29)	1.397(5)	C(33)-B(2)-C(25)	114.9(3)
C(29)-C(30)	1.383(5)	C(6)-C(1)-C(2)	116.3(3)
C(29)-C(32)	1.489(5)	C(6)-C(1)-B(1)	119.9(3)
C(31)-F(31C)	1.328(5)	C(2)-C(1)-B(1)	123.8(3)
C(31)-F(31A)	1.328(5)	C(3)-C(2)-C(1)	121.6(3)
C(31)-F(31B)	1.337(5)	C(4)-C(3)-C(2)	120.8(3)
C(32)-F(32A)	1.336(5)	C(4)-C(3)-C(7')	111.5(7)
C(32)-F(32C)	1.339(5)	C(2)-C(3)-C(7')	127.0(7)
C(32)-F(32B)	1.340(5)	C(4)-C(3)-C(7)	121.3(4)
C(33)-C(34)	1.397(5)	C(2)-C(3)-C(7)	117.8(4)
C(33)-C(38)	1.419(5)	C(3)-C(4)-C(5)	119.1(3)
C(34)-C(35)	1.386(5)	C(6)-C(5)-C(4)	119.9(3)
C(35)-C(36)	1.387(5)	C(6)-C(5)-C(8)	119.8(3)
C(35)-C(39')	1.495(17)	C(4)-C(5)-C(8)	120.3(3)
C(35)-C(39)	1.500(6)	C(5)-C(6)-C(1)	122.4(3)
C(36)-C(37)	1.382(5)	F(7A)-C(7)-F(7B)	102.8(6)
C(37)-C(38)	1.378(5)	F(7A)-C(7)-F(7C)	105.9(7)
C(37)-C(40)	1.500(5)	F(7B)-C(7)-F(7C)	106.5(6)
C(39)-F(39A)	1.309(7)	F(7A)-C(7)-C(3)	116.8(5)
C(39)-F(39B)	1.312(7)	F(7B)-C(7)-C(3)	111.9(6)
C(39)-F(39C)	1.318(6)	F(7C)-C(7)-C(3)	112.1(5)
C(39')-F(39F)	1.309(14)	F(7E)-C(7')-F(7D)	107.1(12)
C(39')-F(39E)	1.311(15)	F(7E)-C(7')-F(7F)	110.0(12)
C(39')-F(39D)	1.312(14)	F(7D)-C(7')-F(7F)	105.1(12)
C(40)-F(40B)	1.335(5)	F(7E)-C(7')-C(3)	116.6(12)
C(40)-F(40C)	1.335(5)	F(7D)-C(7')-C(3)	108.6(12)
C(40)-F(40A)	1.343(5)	F(7F)-C(7')-C(3)	108.8(14)
C(41)-C(42)	1.395(5)	F(8C)-C(8)-F(8A)	106.6(4)
C(41)-C(46)	1.399(5)	F(8C)-C(8)-F(8B)	105.2(4)
C(42)-C(43)	1.392(5)	F(8A)-C(8)-F(8B)	105.7(3)

F(8C)-C(8)-C(5)	113.3(3)	C(28)-C(29)-C(32)	119.2(3)
F(8A)-C(8)-C(5)	112.4(4)	C(29)-C(30)-C(25)	122.3(3)
F(8B)-C(8)-C(5)	113.1(4)	F(31C)-C(31)-F(31A)	108.2(4)
C(10)-C(9)-C(14)	116.1(3)	F(31C)-C(31)-F(31B)	104.9(3)
C(10)-C(9)-B(1)	121.1(3)	F(31A)-C(31)-F(31B)	104.5(4)
C(14)-C(9)-B(1)	122.8(3)	F(31C)-C(31)-C(27)	113.5(4)
C(11)-C(10)-C(9)	122.3(3)	F(31A)-C(31)-C(27)	112.4(3)
C(10)-C(11)-C(12)	120.3(3)	F(31B)-C(31)-C(27)	112.7(3)
C(10)-C(11)-C(15)	119.6(3)	F(32A)-C(32)-F(32C)	105.9(4)
C(12)-C(11)-C(15)	120.1(3)	F(32A)-C(32)-F(32B)	106.6(3)
C(13)-C(12)-C(11)	118.3(3)	F(32C)-C(32)-F(32B)	104.8(4)
C(14)-C(13)-C(12)	121.3(3)	F(32A)-C(32)-C(29)	112.2(4)
C(14)-C(13)-C(16')	124.0(10)	F(32C)-C(32)-C(29)	112.8(3)
C(12)-C(13)-C(16')	114.6(9)	F(32B)-C(32)-C(29)	113.8(3)
C(14)-C(13)-C(16)	118.8(4)	C(34)-C(33)-C(38)	115.7(3)
C(12)-C(13)-C(16)	120.0(4)	C(34)-C(33)-B(2)	122.9(3)
C(13)-C(14)-C(9)	121.7(3)	C(38)-C(33)-B(2)	121.4(3)
F(15C)-C(15)-F(15B)	105.3(4)	C(35)-C(34)-C(33)	122.1(3)
F(15C)-C(15)-F(15A)	108.2(4)	C(34)-C(35)-C(36)	121.0(3)
F(15B)-C(15)-F(15A)	105.4(4)	C(34)-C(35)-C(39')	121.7(8)
F(15C)-C(15)-C(11)	113.0(4)	C(36)-C(35)-C(39')	117.2(8)
F(15B)-C(15)-C(11)	112.3(4)	C(34)-C(35)-C(39)	119.4(4)
F(15A)-C(15)-C(11)	112.2(4)	C(36)-C(35)-C(39)	119.6(4)
F(16C)-C(16)-F(16B)	107.7(5)	C(37)-C(36)-C(35)	118.0(3)
F(16C)-C(16)-F(16A)	103.4(5)	C(38)-C(37)-C(36)	121.4(3)
F(16B)-C(16)-F(16A)	107.1(5)	C(38)-C(37)-C(40)	119.8(3)
F(16C)-C(16)-C(13)	113.8(5)	C(36)-C(37)-C(40)	118.7(3)
F(16B)-C(16)-C(13)	112.0(5)	C(37)-C(38)-C(33)	121.7(3)
F(16A)-C(16)-C(13)	112.2(4)	F(39A)-C(39)-F(39B)	107.1(6)
F(16E)-C(16')-F(16F)	105.0(14)	F(39A)-C(39)-F(39C)	105.6(6)
F(16E)-C(16')-F(16D)	107.1(15)	F(39B)-C(39)-F(39C)	105.7(5)
F(16F)-C(16')-F(16D)	105.0(14)	F(39A)-C(39)-C(35)	111.4(5)
F(16E)-C(16')-C(13)	110.9(19)	F(39B)-C(39)-C(35)	113.0(5)
F(16F)-C(16')-C(13)	114(2)	F(39C)-C(39)-C(35)	113.5(5)
F(16D)-C(16')-C(13)	113.7(18)	F(39F)-C(39')-F(39E)	105.7(14)
C(22)-C(17)-C(18)	115.9(3)	F(39F)-C(39')-F(39D)	103.3(13)
C(22)-C(17)-B(1)	121.7(3)	F(39E)-C(39')-F(39D)	106.7(14)
C(18)-C(17)-B(1)	122.3(3)	F(39F)-C(39')-C(35)	115.5(16)
C(19)-C(18)-C(17)	121.7(3)	F(39E)-C(39')-C(35)	109.3(17)
C(20)-C(19)-C(18)	120.8(3)	F(39D)-C(39')-C(35)	115.5(16)
C(20)-C(19)-C(23)	119.2(4)	F(40B)-C(40)-F(40C)	106.0(3)
C(18)-C(19)-C(23)	119.9(4)	F(40B)-C(40)-F(40A)	106.8(3)
C(19)-C(20)-C(21)	118.9(3)	F(40C)-C(40)-F(40A)	105.9(4)
C(20)-C(21)-C(22)	120.1(3)	F(40B)-C(40)-C(37)	112.7(3)
C(20)-C(21)-C(24)	119.6(3)	F(40C)-C(40)-C(37)	113.1(3)
C(22)-C(21)-C(24)	120.2(3)	F(40A)-C(40)-C(37)	111.8(3)
C(21)-C(22)-C(17)	122.5(3)	C(42)-C(41)-C(46)	115.9(3)
F(23B)-C(23)-F(23A)	105.7(4)	C(42)-C(41)-B(2)	123.6(3)
F(23B)-C(23)-F(23C)	106.3(4)	C(46)-C(41)-B(2)	120.5(3)
F(23A)-C(23)-F(23C)	105.1(4)	C(43)-C(42)-C(41)	121.6(3)
F(23B)-C(23)-C(19)	114.2(4)	C(44)-C(43)-C(42)	121.5(3)
F(23A)-C(23)-C(19)	112.3(4)	C(44)-C(43)-C(47')	115.1(7)
F(23C)-C(23)-C(19)	112.6(4)	C(42)-C(43)-C(47')	123.2(7)
F(24B)-C(24)-F(24A)	106.6(3)	C(44)-C(43)-C(47)	119.9(4)
F(24B)-C(24)-F(24C)	104.9(3)	C(42)-C(43)-C(47)	118.6(4)
F(24A)-C(24)-F(24C)	105.5(4)	C(43)-C(44)-C(45)	117.6(3)
F(24B)-C(24)-C(21)	113.4(3)	C(46)-C(45)-C(44)	120.8(3)
F(24A)-C(24)-C(21)	112.4(3)	C(46)-C(45)-C(48')	118.0(12)
F(24C)-C(24)-C(21)	113.3(3)	C(44)-C(45)-C(48')	121.1(12)
C(26)-C(25)-C(30)	116.3(3)	C(46)-C(45)-C(48)	120.4(3)
C(26)-C(25)-B(2)	122.1(3)	C(44)-C(45)-C(48)	118.8(4)
C(30)-C(25)-B(2)	121.6(3)	C(45)-C(46)-C(41)	122.6(3)
C(27)-C(26)-C(25)	121.8(3)	F(47A)-C(47)-F(47B)	104.3(7)
C(28)-C(27)-C(26)	120.8(3)	F(47A)-C(47)-F(47C)	106.7(7)
C(28)-C(27)-C(31)	120.1(3)	F(47B)-C(47)-F(47C)	106.3(6)
C(26)-C(27)-C(31)	119.0(3)	F(47A)-C(47)-C(43)	110.6(6)
C(27)-C(28)-C(29)	118.4(3)	F(47B)-C(47)-C(43)	114.8(6)
C(30)-C(29)-C(28)	120.3(3)	F(47C)-C(47)-C(43)	113.5(6)
C(30)-C(29)-C(32)	120.5(3)	F(47D)-C(47')-F(47E)	102.6(11)

F(47D)-C(47')-F(47F)	106.0(12)	C(56)-C(51)-C(52)	112.4(4)
F(47E)-C(47')-F(47F)	105.8(12)	C(56)-C(51)-C(57)	109.1(3)
F(47D)-C(47')-C(43)	116.6(12)	C(52)-C(51)-C(57)	113.0(4)
F(47E)-C(47')-C(43)	112.6(12)	C(56)-C(51)-N(50)	105.4(3)
F(47F)-C(47')-C(43)	112.1(12)	C(52)-C(51)-N(50)	106.5(3)
F(48B)-C(48)-F(48A)	107.7(4)	C(57)-C(51)-N(50)	110.1(3)
F(48B)-C(48)-F(48C)	104.0(4)	C(53)-C(52)-C(51)	113.6(4)
F(48A)-C(48)-F(48C)	106.6(5)	C(52)-C(53)-C(54)	110.5(4)
F(48B)-C(48)-C(45)	113.7(4)	C(53)-C(54)-C(55)	114.2(4)
F(48A)-C(48)-C(45)	111.7(4)	C(58)-C(55)-C(59)	110.0(4)
F(48C)-C(48)-C(45)	112.6(4)	C(58)-C(55)-N(50)	110.6(4)
F(48D)-C(48')-F(48F)	106.3(15)	C(59)-C(55)-N(50)	105.2(3)
F(48D)-C(48')-F(48E)	105.7(15)	C(58)-C(55)-C(54)	113.1(4)
F(48F)-C(48')-F(48E)	104.7(15)	C(59)-C(55)-C(54)	111.2(4)
F(48D)-C(48')-C(45)	113(2)	N(50)-C(55)-C(54)	106.4(3)
F(48F)-C(48')-C(45)	114(3)	C(61)-O(60)-C(63)	114.0(4)
F(48E)-C(48')-C(45)	112(3)	O(60)-C(61)-C(62)	111.4(5)
C(55)-N(50)-C(51)	120.5(3)	O(60)-C(63)-C(64)	111.6(5)

$B[CH(C_6F_5)_2]_3$ (10)

Identification code	ASH1205
Formula	C39 H3 B F30, 1.5(C7 H8)
Formula weight	1190.43
Temperature	173 K
Diffractometer, wavelength	OD Xcalibur 3, 0.71073 Å
Crystal system, space group	Monoclinic, P2(1)/c
Unit cell dimensions	a = 24.3971(7) Å α = 90°
	b = 12.6719(3) Å β = 92.764(3)°
	c = 14.5724(5) Å γ = 90°
Volume, Z	4499.9(2) $Å^3$, 4
Density (calculated)	1.757 Mg/m^3
Absorption coefficient	0.189 mm^{-1}
F(000)	2348
Crystal colour / morphology	Colourless plates
Crystal size	0.48 x 0.44 x 0.14 mm^3
θ range for data collection	2.98 to 32.78°
Index ranges	-27<=h<=36, -18<=k<=17, -21<=l<=15
Reflns collected / unique	50254 / 15102 [R(int) = 0.0437]
Reflns observed [F>4σ(F)]	10074
Absorption correction	Analytical
Max. and min. transmission	0.973 and 0.927
Refinement method	Full-matrix least-squares on F^2
Data / restraints / parameters	15102 / 126 / 753
Goodness-of-fit on F^2	1.043
Final R indices [F>4σ(F)]	R1 = 0.0878, wR2 = 0.2337
R indices (all data)	R1 = 0.1244, wR2 = 0.2535
Largest diff. peak, hole	0.457, -0.440 $eÅ^{-3}$
Mean and maximum shift/error	0.000 and 0.001

Bond lengths [Å] and angles [°]

B(1)-C(3)	1.595(4)	C(6)-F(6)	1.332(3)
B(1)-C(1)	1.600(4)	C(6)-C(7)	1.381(5)
B(1)-C(2)	1.615(4)	C(7)-F(7)	1.341(3)
C(1)-C(4)	1.530(3)	C(7)-C(8)	1.380(4)
C(1)-C(10)	1.532(4)	C(8)-F(8)	1.334(3)
C(2)-C(22)	1.527(4)	C(8)-C(9)	1.384(4)
C(2)-C(16)	1.532(4)	C(9)-F(9)	1.343(3)
C(3)-C(34)	1.525(4)	C(10)-C(15)	1.385(4)
C(3)-C(28)	1.527(4)	C(10)-C(11)	1.391(4)
C(4)-C(9)	1.378(4)	C(11)-F(11)	1.346(3)
C(4)-C(5)	1.385(4)	C(11)-C(12)	1.380(4)
C(5)-F(5)	1.339(3)	C(12)-F(12)	1.336(4)
C(5)-C(6)	1.386(4)	C(12)-C(13)	1.382(4)

C(13)-F(13)	1.337(3)
C(13)-C(14)	1.379(5)
C(14)-F(14)	1.336(3)
C(14)-C(15)	1.385(4)
C(15)-F(15)	1.341(3)
C(16)-C(17)	1.385(4)
C(16)-C(21)	1.388(4)
C(17)-F(17)	1.338(4)
C(17)-C(18)	1.391(4)
C(18)-F(18)	1.339(5)
C(18)-C(19)	1.365(6)
C(19)-F(19)	1.341(4)
C(19)-C(20)	1.375(7)
C(20)-F(20)	1.341(4)
C(20)-C(21)	1.387(5)
C(21)-F(21)	1.345(4)
C(22)-C(23)	1.389(4)
C(22)-C(27)	1.393(4)
C(23)-F(23)	1.338(4)
C(23)-C(24)	1.387(4)
C(24)-F(24)	1.330(4)
C(24)-C(25)	1.380(5)
C(25)-F(25)	1.343(4)
C(25)-C(26)	1.362(6)
C(26)-F(26)	1.338(4)
C(26)-C(27)	1.385(5)
C(27)-F(27)	1.341(4)
C(28)-C(33)	1.385(4)
C(28)-C(29)	1.393(4)
C(29)-F(29)	1.338(3)
C(29)-C(30)	1.383(4)
C(30)-F(30)	1.340(3)
C(30)-C(31)	1.373(5)
C(31)-F(31)	1.330(3)
C(31)-C(32)	1.382(4)
C(32)-F(32)	1.337(3)
C(32)-C(33)	1.386(4)
C(33)-F(33)	1.349(3)
C(34)-C(39)	1.376(4)
C(34)-C(35)	1.395(4)
C(35)-F(35)	1.334(4)
C(35)-C(36)	1.391(5)
C(36)-F(36)	1.333(4)
C(36)-C(37)	1.381(6)
C(37)-F(37)	1.336(4)
C(37)-C(38)	1.380(5)
C(38)-F(38)	1.330(4)
C(38)-C(39)	1.391(4)
C(39)-F(39)	1.349(3)

C(3)-B(1)-C(1)	124.4(2)
C(3)-B(1)-C(2)	120.6(2)
C(1)-B(1)-C(2)	114.4(2)
C(4)-C(1)-C(10)	109.32(19)
C(4)-C(1)-B(1)	122.3(2)
C(10)-C(1)-B(1)	117.2(2)
C(22)-C(2)-C(16)	109.5(2)
C(22)-C(2)-B(1)	121.6(2)
C(16)-C(2)-B(1)	112.9(2)
C(34)-C(3)-C(28)	109.5(2)
C(34)-C(3)-B(1)	118.5(2)
C(28)-C(3)-B(1)	113.7(2)
C(9)-C(4)-C(5)	116.7(2)
C(9)-C(4)-C(1)	119.1(2)
C(5)-C(4)-C(1)	124.1(2)
F(5)-C(5)-C(4)	120.3(2)
F(5)-C(5)-C(6)	117.4(2)
C(4)-C(5)-C(6)	122.3(2)
F(6)-C(6)-C(7)	120.3(2)
F(6)-C(6)-C(5)	120.6(3)
C(7)-C(6)-C(5)	119.1(3)
F(7)-C(7)-C(8)	120.3(3)
F(7)-C(7)-C(6)	119.7(3)
C(8)-C(7)-C(6)	120.1(2)
F(8)-C(8)-C(7)	120.1(3)
F(8)-C(8)-C(9)	120.7(3)
C(7)-C(8)-C(9)	119.2(3)
F(9)-C(9)-C(4)	119.7(2)
F(9)-C(9)-C(8)	117.7(2)
C(4)-C(9)-C(8)	122.5(3)
C(15)-C(10)-C(11)	116.7(2)
C(15)-C(10)-C(1)	120.9(2)
C(11)-C(10)-C(1)	122.4(2)
F(11)-C(11)-C(12)	117.9(3)
F(11)-C(11)-C(10)	119.7(2)
C(12)-C(11)-C(10)	122.3(3)
F(12)-C(12)-C(11)	120.5(3)
F(12)-C(12)-C(13)	120.1(3)
C(11)-C(12)-C(13)	119.4(3)
F(13)-C(13)-C(14)	120.2(3)
F(13)-C(13)-C(12)	120.1(3)
C(14)-C(13)-C(12)	119.7(3)
F(14)-C(14)-C(13)	118.9(3)
F(14)-C(14)-C(15)	121.3(3)
C(13)-C(14)-C(15)	119.8(3)
F(15)-C(15)-C(14)	117.7(2)
F(15)-C(15)-C(10)	120.3(2)
C(14)-C(15)-C(10)	122.0(3)
C(17)-C(16)-C(21)	116.8(3)
C(17)-C(16)-C(2)	123.4(2)
C(21)-C(16)-C(2)	119.9(3)
F(17)-C(17)-C(16)	120.0(2)
F(17)-C(17)-C(18)	118.2(3)
C(16)-C(17)-C(18)	121.7(3)
F(18)-C(18)-C(19)	120.6(3)
F(18)-C(18)-C(17)	119.7(4)
C(19)-C(18)-C(17)	119.7(4)
F(19)-C(19)-C(18)	120.2(4)
F(19)-C(19)-C(20)	119.3(4)
C(18)-C(19)-C(20)	120.5(3)
F(20)-C(20)-C(19)	120.9(4)
F(20)-C(20)-C(21)	120.0(4)
C(19)-C(20)-C(21)	119.1(3)
F(21)-C(21)-C(20)	118.4(3)
F(21)-C(21)-C(16)	119.4(3)
C(20)-C(21)-C(16)	122.2(4)
C(23)-C(22)-C(27)	115.9(3)
C(23)-C(22)-C(2)	124.1(2)
C(27)-C(22)-C(2)	119.9(3)
F(23)-C(23)-C(24)	117.4(3)

F(23)-C(23)-C(22)	119.9(2)	C(30)-C(31)-C(32)	119.7(3)
C(24)-C(23)-C(22)	122.7(3)	F(32)-C(32)-C(31)	120.5(3)
F(24)-C(24)-C(25)	120.5(3)	F(32)-C(32)-C(33)	120.5(3)
F(24)-C(24)-C(23)	120.6(3)	C(31)-C(32)-C(33)	119.1(3)
C(25)-C(24)-C(23)	118.9(3)	F(33)-C(33)-C(28)	119.3(2)
F(25)-C(25)-C(26)	120.0(4)	F(33)-C(33)-C(32)	117.7(2)
F(25)-C(25)-C(24)	119.5(4)	C(28)-C(33)-C(32)	123.0(3)
C(26)-C(25)-C(24)	120.5(3)	C(39)-C(34)-C(35)	116.6(3)
F(26)-C(26)-C(25)	120.8(3)	C(39)-C(34)-C(3)	122.9(2)
F(26)-C(26)-C(27)	119.5(4)	C(35)-C(34)-C(3)	120.5(3)
C(25)-C(26)-C(27)	119.7(3)	F(35)-C(35)-C(36)	118.2(3)
F(27)-C(27)-C(26)	117.8(3)	F(35)-C(35)-C(34)	120.3(3)
F(27)-C(27)-C(22)	119.9(3)	C(36)-C(35)-C(34)	121.5(3)
C(26)-C(27)-C(22)	122.3(3)	F(36)-C(36)-C(37)	119.9(3)
C(33)-C(28)-C(29)	116.0(2)	F(36)-C(36)-C(35)	120.2(4)
C(33)-C(28)-C(3)	123.2(2)	C(37)-C(36)-C(35)	119.8(3)
C(29)-C(28)-C(3)	120.8(2)	F(37)-C(37)-C(38)	119.9(4)
F(29)-C(29)-C(30)	119.1(2)	F(37)-C(37)-C(36)	120.0(3)
F(29)-C(29)-C(28)	118.9(2)	C(38)-C(37)-C(36)	120.1(3)
C(30)-C(29)-C(28)	122.1(3)	F(38)-C(38)-C(37)	120.9(3)
F(30)-C(30)-C(31)	120.4(3)	F(38)-C(38)-C(39)	120.5(3)
F(30)-C(30)-C(29)	119.4(3)	C(37)-C(38)-C(39)	118.6(3)
C(31)-C(30)-C(29)	120.1(3)	F(39)-C(39)-C(34)	119.4(2)
F(31)-C(31)-C(30)	120.6(3)	F(39)-C(39)-C(38)	117.2(3)
F(31)-C(31)-C(32)	119.7(3)	C(34)-C(39)-C(38)	123.4(3)

[*t*Bu$_3$P→Li][B(C$_6$F$_5$)$_4$]

Identification code	ASH1306
Formula	C36 H27 B F20 Li P
Formula weight	888.30
Temperature	173 K
Diffractometer, wavelength	OD Xcalibur 3, 0.71073 Å
Crystal system, space group	Monoclinic, P2(1)/n
Unit cell dimensions	a = 10.9626(4) Å α = 90°
	b = 14.5968(4) Å β = 93.860(3)°
	c = 23.0765(6) Å γ = 90°
Volume, Z	3684.30(19) Å^3, 4
Density (calculated)	1.601 Mg/m^3
Absorption coefficient	0.204 mm^{-1}
F(000)	1784
Crystal colour / morphology	Colourless blocks
Crystal size	0.28 x 0.25 x 0.14 mm^3
θ range for data collection	3.00 to 28.79°
Index ranges	-11<=h<=13, -14<=k<=19, -30<=l<=21
Reflns collected / unique	15102 / 7948 [R(int) = 0.0213]
Reflns observed [F>4σ(F)]	5927
Absorption correction	Analytical
Max. and min. transmission	0.979 and 0.963
Refinement method	Full-matrix least-squares on F^2
Data / restraints / parameters	7948 / 162 / 581
Goodness-of-fit on F^2	1.036
Final R indices [F>4σ(F)]	R1 = 0.0461, wR2 = 0.0988
R indices (all data)	R1 = 0.0692, wR2 = 0.1091
Largest diff. peak, hole	0.276, -0.267 eÅ^{-3}
Mean and maximum shift/error	0.000 and 0.001

Bond lengths [Å] and angles [°]

Li(1)-F(38)	1.906(4)	C(5)-C(7)	1.551(9)
Li(1)-F(22)	1.907(4)	C(9)-C(11)	1.527(7)
Li(1)-C(39)	2.480(4)	C(9)-C(12)	1.530(6)
Li(1)-P(1)	2.503(4)	C(9)-C(10)	1.554(6)
Li(1)-C(44)	2.675(5)	C(1')-C(2')	1.532(7)
P(1)-C(1)	1.855(4)	C(1')-C(4')	1.553(10)
P(1)-C(9')	1.858(5)	C(1')-C(3')	1.561(9)
P(1)-C(5)	1.897(4)	C(5')-C(6')	1.537(7)
P(1)-C(1')	1.922(5)	C(5')-C(8')	1.545(8)
P(1)-C(9)	1.933(4)	C(5')-C(7')	1.546(11)
P(1)-C(5')	1.948(5)	C(9')-C(10')	1.532(7)
C(1)-C(4)	1.538(6)	C(9')-C(12')	1.547(8)
C(1)-C(3)	1.570(6)	C(9')-C(11')	1.554(10)
C(1)-C(2)	1.573(6)	B(20)-C(33)	1.650(3)
C(5)-C(8)	1.533(5)	B(20)-C(27)	1.652(3)
C(5)-C(6)	1.547(5)	B(20)-C(21)	1.656(3)

B(20)-C(39)	1.676(3)
C(21)-C(26)	1.386(3)
C(21)-C(22)	1.387(3)
C(22)-C(23)	1.373(3)
C(22)-F(22)	1.386(2)
C(23)-F(23)	1.341(3)
C(23)-C(24)	1.371(3)
C(24)-F(24)	1.343(2)
C(24)-C(25)	1.368(3)
C(25)-F(25)	1.343(3)
C(25)-C(26)	1.390(3)
C(26)-F(26)	1.346(2)
C(27)-C(28)	1.386(3)
C(27)-C(32)	1.396(3)
C(28)-F(28)	1.359(3)
C(28)-C(29)	1.381(3)
C(29)-F(29)	1.345(3)
C(29)-C(30)	1.371(4)
C(30)-F(30)	1.344(3)
C(30)-C(31)	1.362(4)
C(31)-F(31)	1.351(3)
C(31)-C(32)	1.385(3)
C(32)-F(32)	1.349(3)
C(33)-C(38)	1.378(3)
C(33)-C(34)	1.396(3)
C(34)-F(34)	1.353(3)
C(34)-C(35)	1.376(3)
C(35)-F(35)	1.342(3)
C(35)-C(36)	1.376(4)
C(36)-F(36)	1.341(3)
C(36)-C(37)	1.372(3)
C(37)-F(37)	1.342(3)
C(37)-C(38)	1.375(3)
C(38)-F(38)	1.394(2)
C(39)-C(44)	1.388(3)
C(39)-C(40)	1.397(3)
C(40)-F(40)	1.348(2)
C(40)-C(41)	1.372(3)
C(41)-F(41)	1.341(3)
C(41)-C(42)	1.374(3)
C(42)-F(42)	1.341(2)
C(42)-C(43)	1.367(3)
C(43)-F(43)	1.341(3)
C(43)-C(44)	1.388(3)
C(44)-F(44)	1.352(3)

F(38)-Li(1)-F(22)	99.69(19)
F(38)-Li(1)-C(39)	80.90(15)
F(22)-Li(1)-C(39)	85.53(15)
F(38)-Li(1)-P(1)	113.12(19)
F(22)-Li(1)-P(1)	119.4(2)
C(39)-Li(1)-P(1)	146.54(19)
F(38)-Li(1)-C(44)	111.41(18)
F(22)-Li(1)-C(44)	85.60(16)
C(39)-Li(1)-C(44)	30.94(8)
P(1)-Li(1)-C(44)	122.74(16)
C(1)-P(1)-C(5)	112.22(17)
C(9')-P(1)-C(1')	110.1(2)
C(1)-P(1)-C(9)	109.13(19)
C(5)-P(1)-C(9)	107.76(17)
C(9')-P(1)-C(5')	108.8(2)
C(1')-P(1)-C(5')	106.6(2)
C(1)-P(1)-Li(1)	114.31(16)
C(9')-P(1)-Li(1)	108.73(19)
C(5)-P(1)-Li(1)	108.50(15)
C(1')-P(1)-Li(1)	111.97(19)
C(9)-P(1)-Li(1)	104.44(15)
C(5')-P(1)-Li(1)	110.57(18)
C(4)-C(1)-C(3)	109.8(5)
C(4)-C(1)-C(2)	107.4(5)
C(3)-C(1)-C(2)	106.9(4)
C(4)-C(1)-P(1)	116.7(4)
C(3)-C(1)-P(1)	108.1(3)
C(2)-C(1)-P(1)	107.5(3)
C(8)-C(5)-C(6)	108.4(3)
C(8)-C(5)-C(7)	108.9(6)
C(6)-C(5)-C(7)	106.5(5)
C(8)-C(5)-P(1)	116.2(3)
C(6)-C(5)-P(1)	109.9(3)
C(7)-C(5)-P(1)	106.5(5)
C(11)-C(9)-C(12)	109.8(4)
C(11)-C(9)-C(10)	106.4(4)
C(12)-C(9)-C(10)	107.5(4)
C(11)-C(9)-P(1)	108.5(3)
C(12)-C(9)-P(1)	115.0(3)
C(10)-C(9)-P(1)	109.4(3)
C(2')-C(1')-C(4')	107.8(6)
C(2')-C(1')-C(3')	108.1(5)
C(4')-C(1')-C(3')	107.6(7)
C(2')-C(1')-P(1)	108.3(4)
C(4')-C(1')-P(1)	116.8(7)
C(3')-C(1')-P(1)	108.0(5)
C(6')-C(5')-C(8')	107.2(5)
C(6')-C(5')-C(7')	106.7(7)
C(8')-C(5')-C(7')	109.0(8)
C(6')-C(5')-P(1)	111.6(4)
C(8')-C(5')-P(1)	116.7(4)
C(7')-C(5')-P(1)	105.2(9)
C(10')-C(9')-C(12')	108.4(5)
C(10')-C(9')-C(11')	106.9(6)
C(12')-C(9')-C(11')	107.7(6)
C(10')-C(9')-P(1)	110.4(4)
C(12')-C(9')-P(1)	116.5(5)
C(11')-C(9')-P(1)	106.6(7)
C(33)-B(20)-C(27)	113.29(17)
C(33)-B(20)-C(21)	102.47(17)
C(27)-B(20)-C(21)	114.60(18)
C(33)-B(20)-C(39)	114.62(17)
C(27)-B(20)-C(39)	100.46(16)
C(21)-B(20)-C(39)	111.94(17)
C(26)-C(21)-C(22)	112.51(19)
C(26)-C(21)-B(20)	127.30(19)
C(22)-C(21)-B(20)	119.92(18)
C(23)-C(22)-F(22)	114.70(19)
C(23)-C(22)-C(21)	126.3(2)
F(22)-C(22)-C(21)	118.95(18)
C(22)-F(22)-Li(1)	143.53(17)
F(23)-C(23)-C(24)	120.9(2)
F(23)-C(23)-C(22)	120.9(2)
C(24)-C(23)-C(22)	118.2(2)
F(24)-C(24)-C(25)	120.5(2)
F(24)-C(24)-C(23)	120.4(2)
C(25)-C(24)-C(23)	119.1(2)
F(25)-C(25)-C(24)	119.7(2)
F(25)-C(25)-C(26)	120.0(2)
C(24)-C(25)-C(26)	120.2(2)
F(26)-C(26)-C(21)	121.26(19)
F(26)-C(26)-C(25)	115.2(2)
C(21)-C(26)-C(25)	123.5(2)
C(28)-C(27)-C(32)	113.0(2)
C(28)-C(27)-B(20)	119.64(19)
C(32)-C(27)-B(20)	126.9(2)
F(28)-C(28)-C(29)	115.9(2)
F(28)-C(28)-C(27)	118.78(19)
C(29)-C(28)-C(27)	125.4(2)
F(29)-C(29)-C(30)	120.9(2)
F(29)-C(29)-C(28)	120.5(2)
C(30)-C(29)-C(28)	118.7(3)

F(30)-C(30)-C(31)	120.8(2)	C(33)-C(38)-F(38)	119.99(19)
F(30)-C(30)-C(29)	120.0(3)	C(38)-F(38)-Li(1)	123.81(17)
C(31)-C(30)-C(29)	119.2(2)	C(44)-C(39)-C(40)	113.29(18)
F(31)-C(31)-C(30)	119.7(2)	C(44)-C(39)-B(20)	127.02(19)
F(31)-C(31)-C(32)	119.6(3)	C(40)-C(39)-B(20)	118.71(18)
C(30)-C(31)-C(32)	120.7(2)	C(44)-C(39)-Li(1)	82.32(16)
F(32)-C(32)-C(31)	115.7(2)	C(40)-C(39)-Li(1)	96.28(16)
F(32)-C(32)-C(27)	121.3(2)	B(20)-C(39)-Li(1)	100.96(16)
C(31)-C(32)-C(27)	123.1(2)	F(40)-C(40)-C(41)	116.49(19)
C(38)-C(33)-C(34)	112.0(2)	F(40)-C(40)-C(39)	119.19(18)
C(38)-C(33)-B(20)	128.87(18)	C(41)-C(40)-C(39)	124.3(2)
C(34)-C(33)-B(20)	118.87(19)	F(41)-C(41)-C(40)	120.9(2)
F(34)-C(34)-C(35)	116.75(19)	F(41)-C(41)-C(42)	119.57(19)
F(34)-C(34)-C(33)	118.7(2)	C(40)-C(41)-C(42)	119.5(2)
C(35)-C(34)-C(33)	124.6(2)	F(42)-C(42)-C(43)	120.8(2)
F(35)-C(35)-C(36)	119.8(2)	F(42)-C(42)-C(41)	119.7(2)
F(35)-C(35)-C(34)	120.5(2)	C(43)-C(42)-C(41)	119.4(2)
C(36)-C(35)-C(34)	119.7(2)	F(43)-C(43)-C(42)	120.3(2)
F(36)-C(36)-C(37)	120.8(2)	F(43)-C(43)-C(44)	120.3(2)
F(36)-C(36)-C(35)	120.4(2)	C(42)-C(43)-C(44)	119.4(2)
C(37)-C(36)-C(35)	118.8(2)	F(44)-C(44)-C(39)	121.13(18)
F(37)-C(37)-C(36)	120.4(2)	F(44)-C(44)-C(43)	114.8(2)
F(37)-C(37)-C(38)	120.8(2)	C(39)-C(44)-C(43)	124.1(2)
C(36)-C(37)-C(38)	118.8(2)	F(44)-C(44)-Li(1)	100.46(15)
C(37)-C(38)-C(33)	126.1(2)	C(39)-C(44)-Li(1)	66.74(15)
C(37)-C(38)-F(38)	113.85(19)	C(43)-C(44)-Li(1)	104.75(17)

$[Et_3Si–P\mathit{t}Bu_3]^+[B(C_6F_5)_4]^-$ (12)

Identification code	ASH1215
Formula	C24 B F20, C18 H42 P Si
Formula weight	996.63
Temperature	173 K
Diffractometer, wavelength	OD Xcalibur 3, 0.71073 Å
Crystal system, space group	Triclinic, P-1
Unit cell dimensions	a = 10.5254(7) Å α = 66.991(6)°
	b = 14.6409(9) Å β = 81.298(6)°
	c = 15.2885(9) Å γ = 80.888(6)°
Volume, Z	2130.8(3) $Å^3$, 2
Density (calculated)	1.553 Mg/m^3
Absorption coefficient	0.213 mm^{-1}
F(000)	1016
Crystal colour / morphology	Colourless blocks
Crystal size	0.48 x 0.28 x 0.20 mm^3
θ range for data collection	3.09 to 28.56°
Index ranges	-13<=h<=13, -19<=k<=18, -19<=l<=19
Reflns collected / unique	15109 / 15109 [R(int) = 0.0000]
Reflns observed [F>4σ(F)]	10594
Absorption correction	Analytical
Max. and min. transmission	0.972 and 0.940
Refinement method	Full-matrix least-squares on F^2
Data / restraints / parameters	15109 / 30 / 605
Goodness-of-fit on F^2	1.046
Final R indices [F>4σ(F)]	R1 = 0.0455, wR2 = 0.1153
R indices (all data)	R1 = 0.0715, wR2 = 0.1235
Largest diff. peak, hole	0.493, -0.586 $eÅ^{-3}$
Mean and maximum shift/error	0.000 and 0.001

Bond lengths [Å] and angles [°]

P(1)-C(1)	1.896(2)	C(5)-C(6)	1.532(3)
P(1)-C(9)	1.900(2)	C(9)-C(12)	1.526(3)
P(1)-C(5)	1.9018(19)	C(9)-C(11)	1.536(3)
P(1)-Si(1)	2.3788(8)	C(9)-C(10)	1.560(3)
Si(1)-C(13')	1.819(10)	C(13)-C(14)	1.503(5)
Si(1)-C(17)	1.874(2)	C(13')-C(14')	1.496(14)
Si(1)-C(15')	1.878(8)	C(15)-C(16)	1.468(5)
Si(1)-C(15)	1.889(4)	C(15')-C(16')	1.475(9)
Si(1)-C(13)	1.916(3)	C(17)-C(18)	1.521(3)
C(1)-C(4)	1.535(3)	B(1)-C(39)	1.644(3)
C(1)-C(3)	1.536(3)	B(1)-C(27)	1.655(3)
C(1)-C(2)	1.547(3)	B(1)-C(21)	1.655(3)
C(5)-C(8)	1.530(3)	B(1)-C(33)	1.660(3)
C(5)-C(7)	1.531(3)	C(21)-C(22)	1.379(3)

C(21)-C(26)	1.393(3)
C(22)-F(22)	1.356(2)
C(22)-C(23)	1.383(3)
C(23)-F(23)	1.346(2)
C(23)-C(24)	1.363(3)
C(24)-F(24)	1.346(2)
C(24)-C(25)	1.371(3)
C(25)-F(25)	1.343(2)
C(25)-C(26)	1.379(3)
C(26)-F(26)	1.355(2)
C(27)-C(32)	1.385(3)
C(27)-C(28)	1.392(3)
C(28)-F(28)	1.357(2)
C(28)-C(29)	1.383(3)
C(29)-F(29)	1.346(3)
C(29)-C(30)	1.371(3)
C(30)-F(30)	1.340(2)
C(30)-C(31)	1.370(3)
C(31)-F(31)	1.341(2)
C(31)-C(32)	1.377(3)
C(32)-F(32)	1.359(2)
C(33)-C(34)	1.375(3)
C(33)-C(38)	1.383(3)
C(34)-F(34)	1.339(2)
C(34)-C(35)	1.390(3)
C(35)-F(35)	1.341(2)
C(35)-C(36)	1.373(3)
C(36)-F(36)	1.344(2)
C(36)-C(37)	1.366(3)
C(37)-F(37)	1.352(2)
C(37)-C(38)	1.371(3)
C(38)-F(38)	1.366(2)
C(39)-C(44)	1.386(3)
C(39)-C(40)	1.386(3)
C(40)-F(40)	1.356(2)
C(40)-C(41)	1.382(3)
C(41)-F(41)	1.342(2)
C(41)-C(42)	1.373(3)
C(42)-F(42)	1.337(2)
C(42)-C(43)	1.374(3)
C(43)-F(43)	1.344(2)
C(43)-C(44)	1.380(3)
C(44)-F(44)	1.352(2)

C(1)-P(1)-C(9)	110.52(10)
C(1)-P(1)-C(5)	110.62(9)
C(9)-P(1)-C(5)	110.00(9)
C(1)-P(1)-Si(1)	107.21(7)
C(9)-P(1)-Si(1)	110.42(7)
C(5)-P(1)-Si(1)	108.01(6)
C(13')-Si(1)-C(17)	113.4(4)
C(13')-Si(1)-C(15')	85.3(6)
C(17)-Si(1)-C(15')	117.7(5)
C(13')-Si(1)-C(15)	88.9(5)
C(17)-Si(1)-C(15)	105.26(18)
C(17)-Si(1)-C(13)	109.91(13)
C(15')-Si(1)-C(13)	109.0(5)
C(15)-Si(1)-C(13)	114.4(2)
C(13')-Si(1)-P(1)	125.2(4)
C(17)-Si(1)-P(1)	107.46(8)
C(15')-Si(1)-P(1)	106.6(4)
C(15)-Si(1)-P(1)	114.07(16)
C(13)-Si(1)-P(1)	105.53(12)
C(4)-C(1)-C(3)	108.56(18)
C(4)-C(1)-C(2)	108.44(18)
C(3)-C(1)-C(2)	106.37(18)
C(4)-C(1)-P(1)	113.20(15)
C(3)-C(1)-P(1)	109.95(14)
C(2)-C(1)-P(1)	110.08(14)
C(8)-C(5)-C(7)	109.14(17)
C(8)-C(5)-C(6)	107.23(16)
C(7)-C(5)-C(6)	107.41(17)
C(8)-C(5)-P(1)	109.96(14)
C(7)-C(5)-P(1)	111.75(13)
C(6)-C(5)-P(1)	111.21(13)
C(12)-C(9)-C(11)	109.22(17)
C(12)-C(9)-C(10)	107.23(19)
C(11)-C(9)-C(10)	106.37(19)
C(12)-C(9)-P(1)	114.02(15)
C(11)-C(9)-P(1)	108.69(15)
C(10)-C(9)-P(1)	111.02(14)
C(14)-C(13)-Si(1)	111.2(3)
C(14')-C(13')-Si(1)	111.0(10)
C(16)-C(15)-Si(1)	122.9(4)
C(16')-C(15')-Si(1)	117.7(8)
C(18)-C(17)-Si(1)	114.12(18)
C(39)-B(1)-C(27)	101.18(15)
C(39)-B(1)-C(21)	113.43(15)
C(27)-B(1)-C(21)	113.74(15)
C(39)-B(1)-C(33)	112.84(15)
C(27)-B(1)-C(33)	114.51(15)
C(21)-B(1)-C(33)	101.69(14)
C(22)-C(21)-C(26)	113.15(17)
C(22)-C(21)-B(1)	127.23(16)
C(26)-C(21)-B(1)	119.28(16)
F(22)-C(22)-C(21)	121.13(17)
F(22)-C(22)-C(23)	114.64(17)
C(21)-C(22)-C(23)	124.22(19)
F(23)-C(23)-C(24)	120.18(18)
F(23)-C(23)-C(22)	120.1(2)
C(24)-C(23)-C(22)	119.8(2)
F(24)-C(24)-C(23)	120.5(2)
F(24)-C(24)-C(25)	120.3(2)
C(23)-C(24)-C(25)	119.22(18)
F(25)-C(25)-C(24)	119.72(18)
F(25)-C(25)-C(26)	121.1(2)
C(24)-C(25)-C(26)	119.15(19)
F(26)-C(26)-C(25)	116.36(18)
F(26)-C(26)-C(21)	119.19(17)
C(25)-C(26)-C(21)	124.44(19)
C(32)-C(27)-C(28)	112.46(18)
C(32)-C(27)-B(1)	119.83(17)
C(28)-C(27)-B(1)	126.88(17)
F(28)-C(28)-C(29)	114.54(19)
F(28)-C(28)-C(27)	121.39(18)
C(29)-C(28)-C(27)	124.1(2)
F(29)-C(29)-C(30)	119.3(2)
F(29)-C(29)-C(28)	120.6(2)
C(30)-C(29)-C(28)	120.1(2)
F(30)-C(30)-C(31)	120.9(2)

F(30)-C(30)-C(29)	120.2(2)	C(37)-C(38)-C(33)	125.10(19)
C(31)-C(30)-C(29)	118.8(2)	C(44)-C(39)-C(40)	113.02(17)
F(31)-C(31)-C(30)	120.1(2)	C(44)-C(39)-B(1)	118.83(16)
F(31)-C(31)-C(32)	120.9(2)	C(40)-C(39)-B(1)	127.75(17)
C(30)-C(31)-C(32)	119.0(2)	F(40)-C(40)-C(41)	114.94(16)
F(32)-C(32)-C(31)	115.54(18)	F(40)-C(40)-C(39)	120.72(16)
F(32)-C(32)-C(27)	118.86(18)	C(41)-C(40)-C(39)	124.34(18)
C(31)-C(32)-C(27)	125.6(2)	F(41)-C(41)-C(42)	119.68(18)
C(34)-C(33)-C(38)	113.29(17)	F(41)-C(41)-C(40)	120.67(18)
C(34)-C(33)-B(1)	127.42(17)	C(42)-C(41)-C(40)	119.65(18)
C(38)-C(33)-B(1)	118.96(16)	F(42)-C(42)-C(41)	120.82(19)
F(34)-C(34)-C(33)	121.31(17)	F(42)-C(42)-C(43)	120.32(19)
F(34)-C(34)-C(35)	114.91(17)	C(41)-C(42)-C(43)	118.86(18)
C(33)-C(34)-C(35)	123.78(19)	F(43)-C(43)-C(42)	120.28(18)
F(35)-C(35)-C(36)	119.78(18)	F(43)-C(43)-C(44)	120.42(19)
F(35)-C(35)-C(34)	120.5(2)	C(42)-C(43)-C(44)	119.30(19)
C(36)-C(35)-C(34)	119.75(19)	F(44)-C(44)-C(43)	115.97(17)
F(36)-C(36)-C(37)	121.0(2)	F(44)-C(44)-C(39)	119.22(16)
F(36)-C(36)-C(35)	120.3(2)	C(43)-C(44)-C(39)	124.81(18)
C(37)-C(36)-C(35)	118.72(18)		
F(37)-C(37)-C(36)	119.68(18)		
F(37)-C(37)-C(38)	121.00(19)		
C(36)-C(37)-C(38)	119.32(19)		
F(38)-C(38)-C(37)	115.77(17)		
F(38)-C(38)-C(33)	119.13(16)		

$[i\mathrm{Pr}_3\mathrm{Si}–\mathrm{P}t\mathrm{Bu}_3]^+[\mathrm{B}(\mathrm{C}_6\mathrm{F}_5)_4]^-$ (13)

Identification code	ASH1318
Formula	C24 B F20, C21 H48 P Si
Formula weight	1038.70
Temperature	173 K
Diffractometer, wavelength	Agilent Xcalibur PX Ultra A, 1.54184 Å
Crystal system, space group	Triclinic, P -1
Unit cell dimensions	a = 11.6772(5) Å α = 79.442(3)°
	b = 12.5736(4) Å β = 75.102(3)°
	c = 17.0286(6) Å γ = 77.292(3)°
Volume, Z	2335.61(15) Å^3, 2
Density (calculated)	1.477 Mg/m^3
Absorption coefficient	1.792 mm^{-1}
F(000)	1064
Crystal colour / morphology	Colourless blocks
Crystal size	0.30 x 0.28 x 0.20 mm^3
θ range for data collection	2.710 to 73.723°
Index ranges	-14<=h<=13, -15<=k<=10, -20<=l<=16
Reflns collected / unique	13549 / 8923 [R(int) = 0.0180]
Reflns observed [F>4σ(F)]	7708
Absorption correction	Analytical
Max. and min. transmission	0.773 and 0.666
Refinement method	Full-matrix least-squares on F^2
Data / restraints / parameters	8923 / 0 / 613
Goodness-of-fit on F^2	1.065
Final R indices [F>4σ(F)]	R1 = 0.0354, wR2 = 0.0896
R indices (all data)	R1 = 0.0418, wR2 = 0.0948
Largest diff. peak, hole	0.477, -0.305 eÅ^{-3}
Mean and maximum shift/error	0.000 and 0.001

Bond lengths [Å] and angles [°]

P(1)-C(9)	1.9129(15)	C(9)-C(11)	1.534(2)
P(1)-C(5)	1.9183(16)	C(9)-C(10)	1.538(2)
P(1)-C(1)	1.9221(16)	C(9)-C(12)	1.541(2)
P(1)-Si(1)	2.4843(5)	C(13)-C(14)	1.540(3)
Si(1)-C(13)	1.9148(17)	C(13)-C(15)	1.549(3)
Si(1)-C(16)	1.9159(18)	C(16)-C(17)	1.532(3)
Si(1)-C(19)	1.9182(19)	C(16)-C(18)	1.550(3)
C(1)-C(3)	1.534(2)	C(19)-C(20)	1.530(3)
C(1)-C(2)	1.542(2)	C(19)-C(21)	1.539(3)
C(1)-C(4)	1.545(2)	B(1)-C(31)	1.651(2)
C(5)-C(8)	1.537(3)	B(1)-C(43)	1.654(2)
C(5)-C(7)	1.542(3)	B(1)-C(49)	1.655(2)
C(5)-C(6)	1.544(3)	B(1)-C(37)	1.658(2)

C(31)-C(32)	1.390(2)
C(31)-C(36)	1.390(2)
C(32)-F(32)	1.353(2)
C(32)-C(33)	1.383(2)
C(33)-F(33)	1.344(2)
C(33)-C(34)	1.373(3)
C(34)-F(34)	1.343(2)
C(34)-C(35)	1.370(3)
C(35)-F(35)	1.348(2)
C(35)-C(36)	1.386(2)
C(36)-F(36)	1.346(2)
C(37)-C(42)	1.386(2)
C(37)-C(38)	1.397(2)
C(38)-F(38)	1.3506(18)
C(38)-C(39)	1.380(2)
C(39)-F(39)	1.3436(19)
C(39)-C(40)	1.377(3)
C(40)-F(40)	1.3403(19)
C(40)-C(41)	1.379(3)
C(41)-F(41)	1.343(2)
C(41)-C(42)	1.385(2)
C(42)-F(42)	1.3531(18)
C(43)-C(48)	1.389(2)
C(43)-C(44)	1.390(2)
C(44)-F(44)	1.353(2)
C(44)-C(45)	1.380(2)
C(45)-F(45)	1.345(2)
C(45)-C(46)	1.379(3)
C(46)-F(46)	1.339(2)
C(46)-C(47)	1.368(3)
C(47)-F(47)	1.346(2)
C(47)-C(48)	1.392(3)
C(48)-F(48)	1.348(2)
C(49)-C(54)	1.388(2)
C(49)-C(50)	1.397(2)
C(50)-F(50)	1.351(2)
C(50)-C(51)	1.375(3)
C(51)-F(51)	1.348(2)
C(51)-C(52)	1.371(3)
C(52)-F(52)	1.344(2)
C(52)-C(53)	1.379(3)
C(53)-F(53)	1.344(2)
C(53)-C(54)	1.386(2)
C(54)-F(54)	1.3532(19)

C(9)-P(1)-C(5)	108.72(7)
C(9)-P(1)-C(1)	108.50(7)
C(5)-P(1)-C(1)	108.59(8)
C(9)-P(1)-Si(1)	110.11(5)
C(5)-P(1)-Si(1)	109.99(6)
C(1)-P(1)-Si(1)	110.88(5)
C(13)-Si(1)-C(16)	110.51(8)
C(13)-Si(1)-C(19)	111.70(9)
C(16)-Si(1)-C(19)	111.86(9)
C(13)-Si(1)-P(1)	109.18(6)
C(16)-Si(1)-P(1)	108.07(6)
C(19)-Si(1)-P(1)	105.28(6)
C(3)-C(1)-C(2)	106.53(14)
C(3)-C(1)-C(4)	107.28(14)
C(2)-C(1)-C(4)	107.92(14)
C(3)-C(1)-P(1)	111.33(11)
C(2)-C(1)-P(1)	110.23(11)
C(4)-C(1)-P(1)	113.25(12)
C(8)-C(5)-C(7)	107.46(16)
C(8)-C(5)-C(6)	107.94(15)
C(7)-C(5)-C(6)	107.14(16)
C(8)-C(5)-P(1)	111.53(12)
C(7)-C(5)-P(1)	112.92(12)
C(6)-C(5)-P(1)	109.64(13)
C(11)-C(9)-C(10)	107.90(13)
C(11)-C(9)-C(12)	106.77(14)
C(10)-C(9)-C(12)	107.55(14)
C(11)-C(9)-P(1)	109.86(11)
C(10)-C(9)-P(1)	114.02(11)
C(12)-C(9)-P(1)	110.46(10)
C(14)-C(13)-C(15)	108.20(16)
C(14)-C(13)-Si(1)	118.97(14)
C(15)-C(13)-Si(1)	109.39(12)
C(17)-C(16)-C(18)	108.66(17)
C(17)-C(16)-Si(1)	118.00(13)
C(18)-C(16)-Si(1)	111.02(15)
C(20)-C(19)-C(21)	108.48(16)
C(20)-C(19)-Si(1)	113.48(15)
C(21)-C(19)-Si(1)	117.14(15)
C(31)-B(1)-C(43)	102.01(12)
C(31)-B(1)-C(49)	113.09(12)
C(43)-B(1)-C(49)	114.21(12)
C(31)-B(1)-C(37)	113.34(12)
C(43)-B(1)-C(37)	113.33(12)
C(49)-B(1)-C(37)	101.37(12)
C(32)-C(31)-C(36)	113.31(15)
C(32)-C(31)-B(1)	119.48(14)
C(36)-C(31)-B(1)	127.12(14)
F(32)-C(32)-C(33)	116.06(16)
F(32)-C(32)-C(31)	119.15(15)
C(33)-C(32)-C(31)	124.77(17)
F(33)-C(33)-C(34)	120.44(17)
F(33)-C(33)-C(32)	120.6(2)
C(34)-C(33)-C(32)	118.96(18)
F(34)-C(34)-C(35)	120.2(2)
F(34)-C(34)-C(33)	120.7(2)
C(35)-C(34)-C(33)	119.10(16)
F(35)-C(35)-C(34)	120.02(16)
F(35)-C(35)-C(36)	119.85(19)
C(34)-C(35)-C(36)	120.10(18)
F(36)-C(36)-C(35)	115.10(15)
F(36)-C(36)-C(31)	121.37(14)
C(35)-C(36)-C(31)	123.52(17)
C(42)-C(37)-C(38)	112.93(14)
C(42)-C(37)-B(1)	127.64(13)
C(38)-C(37)-B(1)	119.13(13)
F(38)-C(38)-C(39)	115.83(14)
F(38)-C(38)-C(37)	119.33(13)
C(39)-C(38)-C(37)	124.84(15)
F(39)-C(39)-C(40)	119.82(15)
F(39)-C(39)-C(38)	120.89(15)
C(40)-C(39)-C(38)	119.28(15)
F(40)-C(40)-C(39)	120.56(16)
F(40)-C(40)-C(41)	120.70(16)
C(39)-C(40)-C(41)	118.74(15)
F(41)-C(41)-C(40)	119.62(15)
F(41)-C(41)-C(42)	120.57(16)
C(40)-C(41)-C(42)	119.81(15)
F(42)-C(42)-C(41)	114.54(14)
F(42)-C(42)-C(37)	121.13(14)
C(41)-C(42)-C(37)	124.32(15)
C(48)-C(43)-C(44)	112.94(15)
C(48)-C(43)-B(1)	127.66(15)
C(44)-C(43)-B(1)	119.18(13)
F(44)-C(44)-C(45)	115.33(15)
F(44)-C(44)-C(43)	119.47(14)
C(45)-C(44)-C(43)	125.19(16)
F(45)-C(45)-C(46)	120.03(16)
F(45)-C(45)-C(44)	120.91(16)
C(46)-C(45)-C(44)	119.06(17)
F(46)-C(46)-C(47)	121.15(18)
F(46)-C(46)-C(45)	120.1(2)
C(47)-C(46)-C(45)	118.76(16)

F(47)-C(47)-C(46)	120.09(18)	F(51)-C(51)-C(50)	120.3(2)
F(47)-C(47)-C(48)	119.7(2)	C(52)-C(51)-C(50)	119.74(18)
C(46)-C(47)-C(48)	120.21(17)	F(52)-C(52)-C(51)	120.97(19)
F(48)-C(48)-C(43)	120.70(15)	F(52)-C(52)-C(53)	120.2(2)
F(48)-C(48)-C(47)	115.55(15)	C(51)-C(52)-C(53)	118.83(17)
C(43)-C(48)-C(47)	123.75(17)	F(53)-C(53)-C(52)	120.36(17)
C(54)-C(49)-C(50)	112.92(15)	F(53)-C(53)-C(54)	120.15(17)
C(54)-C(49)-B(1)	127.74(14)	C(52)-C(53)-C(54)	119.49(18)
C(50)-C(49)-B(1)	118.83(14)	F(54)-C(54)-C(53)	114.32(15)
F(50)-C(50)-C(51)	116.41(16)	F(54)-C(54)-C(49)	121.29(14)
F(50)-C(50)-C(49)	118.96(15)	C(53)-C(54)-C(49)	124.39(16)
C(51)-C(50)-C(49)	124.62(18)		
F(51)-C(51)-C(52)	119.99(18)		

$[t\mathrm{Bu}_3\mathrm{P}-{}^{13}\mathrm{C(O)O}-\mathrm{SiEt}_3][\mathrm{B}(\mathrm{C}_6\mathrm{F}_5)_4]$ (14)

Identification code	ASH1311
Formula	C19 H42 O2 P Si, C12 H28 P, 2(C24 B F20), 1.5(C6 H5 Cl)
Formula weight	2091.82
Temperature	173 K
Diffractometer, wavelength	OD Xcalibur 3, 0.71073 Å
Crystal system, space group	Triclinic, P-1
Unit cell dimensions	a = 14.2404(3) Å α = 110.506(2)°
	b = 17.8055(4) Å β = 102.188(2)°
	c = 19.5355(5) Å γ = 90.2856(18)°
Volume, Z	4518.0(2) Å^3, 2
Density (calculated)	1.538 Mg/m^3
Absorption coefficient	0.237 mm^{-1}
F(000)	2122
Crystal colour / morphology	Colourless blocks
Crystal size	0.59 x 0.43 x 0.31 mm^3
θ range for data collection	3.21 to 29.09°
Index ranges	-18<=h<=18, -20<=k<=24, -23<=l<=24
Reflns collected / unique	36359 / 19640 [R(int) = 0.0178]
Reflns observed [F>4σ(F)]	13872
Absorption correction	Analytical
Max. and min. transmission	0.949 and 0.912
Refinement method	Full-matrix least-squares on F^2
Data / restraints / parameters	19640 / 221 / 1307
Goodness-of-fit on F^2	1.022
Final R indices [F>4σ(F)]	R1 = 0.0598, wR2 = 0.1411
R indices (all data)	R1 = 0.0890, wR2 = 0.1609
Largest diff. peak, hole	1.237, -0.719 eÅ^{-3}
Mean and maximum shift/error	0.000 and 0.000

Bond lengths [Å] and angles [°]

Si(1)-O(2)	1.733(3)	C(9)-C(10')	1.370(14)
Si(1)-C(5)	1.844(4)	C(9)-C(10)	1.442(7)
Si(1)-C(7)	1.847(4)	C(11)-C(12)	1.539(8)
Si(1)-C(9)	1.855(4)	C(11)-C(14)	1.557(7)
O(2)-C(3)	1.308(4)	C(11)-C(13)	1.566(7)
C(3)-O(3)	1.209(4)	C(15)-C(16)	1.523(7)
C(3)-P(4)	1.851(4)	C(15)-C(17)	1.537(6)
P(4)-C(11)	1.856(5)	C(15)-C(18)	1.564(7)
P(4)-C(15')	1.860(13)	C(19)-C(22)	1.528(7)
P(4)-C(19')	1.880(12)	C(19)-C(21)	1.530(6)
P(4)-C(19)	1.897(4)	C(19)-C(20)	1.532(6)
P(4)-C(15)	1.899(5)	C(11')-C(13')	1.570(14)
P(4)-C(11')	1.928(13)	C(11')-C(14')	1.575(14)
C(5)-C(6)	1.516(6)	C(11')-C(12')	1.577(14)
C(7)-C(8)	1.495(6)	C(15')-C(16')	1.505(13)

C(15')-C(18')	1.505(13)	C(81)-C(86)	1.385(4)
C(15')-C(17')	1.520(13)	C(81)-C(82)	1.391(4)
C(19')-C(21')	1.527(14)	C(82)-F(82)	1.351(3)
C(19')-C(20')	1.531(13)	C(82)-C(83)	1.384(4)
C(19')-C(22')	1.533(13)	C(83)-F(83)	1.346(3)
P(30)-C(35)	1.866(3)	C(83)-C(84)	1.371(4)
P(30)-C(39)	1.869(3)	C(84)-F(84)	1.344(3)
P(30)-C(31)	1.877(3)	C(84)-C(85)	1.369(4)
C(31)-C(32)	1.531(5)	C(85)-F(85)	1.339(3)
C(31)-C(34)	1.537(5)	C(85)-C(86)	1.392(4)
C(31)-C(33)	1.537(5)	C(86)-F(86)	1.352(3)
C(35)-C(38)	1.530(4)	C(87)-C(92)	1.383(4)
C(35)-C(36)	1.540(5)	C(87)-C(88)	1.392(4)
C(35)-C(37)	1.542(5)	C(88)-F(88)	1.352(3)
C(39)-C(42)	1.533(5)	C(88)-C(89)	1.381(4)
C(39)-C(41)	1.536(4)	C(89)-F(89)	1.349(3)
C(39)-C(40)	1.538(5)	C(89)-C(90)	1.371(4)
B(50)-C(57)	1.646(4)	C(90)-F(90)	1.346(3)
B(50)-C(63)	1.655(4)	C(90)-C(91)	1.372(5)
B(50)-C(69)	1.659(4)	C(91)-F(91)	1.351(3)
B(50)-C(51)	1.664(4)	C(91)-C(92)	1.385(4)
C(51)-C(52)	1.383(4)	C(92)-F(92)	1.357(3)
C(51)-C(56)	1.385(4)	C(93)-C(98)	1.389(4)
C(52)-F(52)	1.352(3)	C(93)-C(94)	1.391(4)
C(52)-C(53)	1.389(4)	C(94)-F(94)	1.355(3)
C(53)-F(53)	1.339(4)	C(94)-C(95)	1.375(4)
C(53)-C(54)	1.373(5)	C(95)-F(95)	1.353(4)
C(54)-F(54)	1.346(3)	C(95)-C(96)	1.378(5)
C(54)-C(55)	1.367(5)	C(96)-F(96)	1.347(3)
C(55)-F(55)	1.350(4)	C(96)-C(97)	1.366(5)
C(55)-C(56)	1.384(4)	C(97)-F(97)	1.347(4)
C(56)-F(56)	1.351(4)	C(97)-C(98)	1.384(4)
C(57)-C(62)	1.374(4)	C(98)-F(98)	1.347(3)
C(57)-C(58)	1.423(4)	C(99)-C(104)	1.385(4)
C(58)-F(58)	1.334(4)	C(99)-C(100)	1.397(4)
C(58)-C(59)	1.362(5)	C(100)-F(100)	1.351(3)
C(59)-F(59)	1.347(4)	C(100)-C(101)	1.373(4)
C(59)-C(60)	1.351(6)	C(101)-F(101)	1.348(3)
C(60)-F(60)	1.351(4)	C(101)-C(102)	1.376(4)
C(60)-C(61)	1.389(6)	C(102)-F(102)	1.342(3)
C(61)-F(61)	1.338(4)	C(102)-C(103)	1.379(4)
C(61)-C(62)	1.390(5)	C(103)-F(103)	1.351(3)
C(62)-F(62)	1.359(4)	C(103)-C(104)	1.378(4)
C(63)-C(68)	1.386(4)	C(104)-F(104)	1.361(3)
C(63)-C(64)	1.391(4)	Cl(1)-C(111)	1.743(4)
C(64)-F(64)	1.354(3)	C(111)-C(112)	1.352(5)
C(64)-C(65)	1.375(4)	C(111)-C(116)	1.381(6)
C(65)-F(65)	1.348(3)	C(112)-C(113)	1.375(6)
C(65)-C(66)	1.375(4)	C(113)-C(114)	1.382(7)
C(66)-F(66)	1.342(3)	C(114)-C(115)	1.364(7)
C(66)-C(67)	1.370(4)	C(115)-C(116)	1.350(7)
C(67)-F(67)	1.340(3)	Cl(2)-C(121)	1.676(6)
C(67)-C(68)	1.387(4)	C(121)-C(122)	1.3900
C(68)-F(68)	1.357(3)	C(121)-C(126)	1.3900
C(69)-C(74)	1.386(4)	C(122)-C(123)	1.3900
C(69)-C(70)	1.388(4)	C(123)-C(124)	1.3900
C(70)-F(70)	1.351(3)	C(124)-C(125)	1.3900
C(70)-C(71)	1.379(4)	C(125)-C(126)	1.3900
C(71)-F(71)	1.342(3)		
C(71)-C(72)	1.375(4)	O(2)-Si(1)-C(5)	101.33(18)
C(72)-F(72)	1.341(3)	O(2)-Si(1)-C(7)	106.76(16)
C(72)-C(73)	1.372(4)	C(5)-Si(1)-C(7)	115.8(2)
C(73)-F(73)	1.345(3)	O(2)-Si(1)-C(9)	108.97(19)
C(73)-C(74)	1.387(4)	C(5)-Si(1)-C(9)	111.3(2)
C(74)-F(74)	1.350(3)	C(7)-Si(1)-C(9)	111.9(2)
B(80)-C(99)	1.653(4)	C(3)-O(2)-Si(1)	125.9(2)
B(80)-C(87)	1.654(4)	O(3)-C(3)-O(2)	125.8(3)
B(80)-C(93)	1.657(4)	O(3)-C(3)-P(4)	122.3(3)
B(80)-C(81)	1.663(4)	O(2)-C(3)-P(4)	111.8(2)

C(3)-P(4)-C(11)	106.4(2)	C(42)-C(39)-C(40)	106.6(3)
C(3)-P(4)-C(15')	111.1(5)	C(41)-C(39)-C(40)	109.0(3)
C(3)-P(4)-C(19')	104.9(5)	C(42)-C(39)-P(30)	108.3(2)
C(15')-P(4)-C(19')	118.8(6)	C(41)-C(39)-P(30)	111.4(2)
C(3)-P(4)-C(19)	103.72(18)	C(40)-C(39)-P(30)	110.4(2)
C(11)-P(4)-C(19)	114.0(2)	C(57)-B(50)-C(63)	113.2(2)
C(3)-P(4)-C(15)	107.39(19)	C(57)-B(50)-C(69)	102.3(2)
C(11)-P(4)-C(15)	112.8(3)	C(63)-B(50)-C(69)	114.4(2)
C(19)-P(4)-C(15)	111.7(2)	C(57)-B(50)-C(51)	113.7(2)
C(3)-P(4)-C(11')	104.5(6)	C(63)-B(50)-C(51)	102.0(2)
C(15')-P(4)-C(11')	109.2(7)	C(69)-B(50)-C(51)	111.7(2)
C(19')-P(4)-C(11')	107.3(7)	C(52)-C(51)-C(56)	112.8(3)
C(6)-C(5)-Si(1)	117.1(3)	C(52)-C(51)-B(50)	118.6(2)
C(8)-C(7)-Si(1)	114.8(3)	C(56)-C(51)-B(50)	128.4(3)
C(10')-C(9)-C(10)	59.5(10)	F(52)-C(52)-C(51)	119.1(2)
C(10')-C(9)-Si(1)	123.9(9)	F(52)-C(52)-C(53)	115.6(3)
C(10)-C(9)-Si(1)	118.2(4)	C(51)-C(52)-C(53)	125.3(3)
C(12)-C(11)-C(14)	109.2(5)	F(53)-C(53)-C(54)	120.3(3)
C(12)-C(11)-C(13)	109.9(6)	F(53)-C(53)-C(52)	121.2(3)
C(14)-C(11)-C(13)	107.3(5)	C(54)-C(53)-C(52)	118.5(3)
C(12)-C(11)-P(4)	108.9(4)	F(54)-C(54)-C(55)	120.5(3)
C(14)-C(11)-P(4)	111.3(5)	F(54)-C(54)-C(53)	120.2(3)
C(13)-C(11)-P(4)	110.1(4)	C(55)-C(54)-C(53)	119.3(3)
C(16)-C(15)-C(17)	110.5(5)	F(55)-C(55)-C(54)	119.9(3)
C(16)-C(15)-C(18)	106.2(4)	F(55)-C(55)-C(56)	120.3(3)
C(17)-C(15)-C(18)	107.6(5)	C(54)-C(55)-C(56)	119.7(3)
C(16)-C(15)-P(4)	108.9(4)	F(56)-C(56)-C(55)	114.6(3)
C(17)-C(15)-P(4)	110.9(4)	F(56)-C(56)-C(51)	121.0(3)
C(18)-C(15)-P(4)	112.6(3)	C(55)-C(56)-C(51)	124.4(3)
C(22)-C(19)-C(21)	108.1(5)	C(62)-C(57)-C(58)	113.7(3)
C(22)-C(19)-C(20)	109.0(4)	C(62)-C(57)-B(50)	128.4(3)
C(21)-C(19)-C(20)	108.5(4)	C(58)-C(57)-B(50)	117.8(3)
C(22)-C(19)-P(4)	108.3(4)	F(58)-C(58)-C(59)	117.5(3)
C(21)-C(19)-P(4)	112.5(3)	F(58)-C(58)-C(57)	119.1(3)
C(20)-C(19)-P(4)	110.4(4)	C(59)-C(58)-C(57)	123.4(3)
C(13')-C(11')-C(14')	106.4(12)	F(59)-C(59)-C(60)	119.7(3)
C(13')-C(11')-C(12')	107.5(11)	F(59)-C(59)-C(58)	119.9(4)
C(14')-C(11')-C(12')	106.4(12)	C(60)-C(59)-C(58)	120.4(4)
C(13')-C(11')-P(4)	107.0(12)	C(59)-C(60)-F(60)	121.9(4)
C(14')-C(11')-P(4)	111(2)	C(59)-C(60)-C(61)	119.6(3)
C(12')-C(11')-P(4)	117.5(14)	F(60)-C(60)-C(61)	118.5(4)
C(16')-C(15')-C(18')	113.1(11)	F(61)-C(61)-C(60)	121.2(4)
C(16')-C(15')-C(17')	112.6(10)	F(61)-C(61)-C(62)	119.9(4)
C(18')-C(15')-C(17')	113.9(11)	C(60)-C(61)-C(62)	118.9(3)
C(16')-C(15')-P(4)	108.3(12)	F(62)-C(62)-C(57)	121.1(3)
C(18')-C(15')-P(4)	103.2(16)	F(62)-C(62)-C(61)	115.0(3)
C(17')-C(15')-P(4)	104.6(11)	C(57)-C(62)-C(61)	123.9(3)
C(21')-C(19')-C(20')	109.5(11)	C(68)-C(63)-C(64)	112.8(2)
C(21')-C(19')-C(22')	110.2(11)	C(68)-C(63)-B(50)	127.9(2)
C(20')-C(19')-C(22')	108.3(11)	C(64)-C(63)-B(50)	119.0(2)
C(21')-C(19')-P(4)	107.3(15)	F(64)-C(64)-C(65)	116.3(2)
C(20')-C(19')-P(4)	108.9(15)	F(64)-C(64)-C(63)	118.8(2)
C(22')-C(19')-P(4)	112.6(11)	C(65)-C(64)-C(63)	124.9(3)
C(35)-P(30)-C(39)	115.39(15)	F(65)-C(65)-C(66)	119.6(3)
C(35)-P(30)-C(31)	114.10(15)	F(65)-C(65)-C(64)	121.0(3)
C(39)-P(30)-C(31)	114.25(15)	C(66)-C(65)-C(64)	119.4(3)
C(32)-C(31)-C(34)	110.8(3)	F(66)-C(66)-C(67)	121.1(3)
C(32)-C(31)-C(33)	109.1(3)	F(66)-C(66)-C(65)	120.1(3)
C(34)-C(31)-C(33)	106.6(3)	C(67)-C(66)-C(65)	118.9(3)
C(32)-C(31)-P(30)	112.0(2)	F(67)-C(67)-C(66)	120.2(3)
C(34)-C(31)-P(30)	108.0(2)	F(67)-C(67)-C(68)	120.2(3)
C(33)-C(31)-P(30)	110.3(2)	C(66)-C(67)-C(68)	119.6(3)
C(38)-C(35)-C(36)	109.6(3)	F(68)-C(68)-C(63)	120.7(2)
C(38)-C(35)-C(37)	109.6(3)	F(68)-C(68)-C(67)	114.9(2)
C(36)-C(35)-C(37)	106.6(3)	C(63)-C(68)-C(67)	124.4(3)
C(38)-C(35)-P(30)	111.1(2)	C(74)-C(69)-C(70)	113.3(2)
C(36)-C(35)-P(30)	110.4(2)	C(74)-C(69)-B(50)	126.7(2)
C(37)-C(35)-P(30)	109.4(2)	C(70)-C(69)-B(50)	119.4(2)
C(42)-C(39)-C(41)	111.0(3)	F(70)-C(70)-C(71)	116.1(2)

F(70)-C(70)-C(69)	119.1(2)	C(98)-C(93)-C(94)	113.6(3)
C(71)-C(70)-C(69)	124.8(3)	C(98)-C(93)-B(80)	126.6(2)
F(71)-C(71)-C(72)	119.6(2)	C(94)-C(93)-B(80)	119.3(2)
F(71)-C(71)-C(70)	121.3(3)	F(94)-C(94)-C(95)	115.8(3)
C(72)-C(71)-C(70)	119.1(3)	F(94)-C(94)-C(93)	119.7(2)
F(72)-C(72)-C(73)	120.0(3)	C(95)-C(94)-C(93)	124.4(3)
F(72)-C(72)-C(71)	120.8(3)	F(95)-C(95)-C(94)	120.8(3)
C(73)-C(72)-C(71)	119.2(3)	F(95)-C(95)-C(96)	119.8(3)
F(73)-C(73)-C(72)	120.0(3)	C(94)-C(95)-C(96)	119.3(3)
F(73)-C(73)-C(74)	120.4(3)	F(96)-C(96)-C(97)	120.6(3)
C(72)-C(73)-C(74)	119.6(3)	F(96)-C(96)-C(95)	120.5(3)
F(74)-C(74)-C(69)	121.6(2)	C(97)-C(96)-C(95)	118.9(3)
F(74)-C(74)-C(73)	114.3(2)	F(97)-C(97)-C(96)	120.0(3)
C(69)-C(74)-C(73)	124.1(3)	F(97)-C(97)-C(98)	119.8(3)
C(99)-B(80)-C(87)	101.4(2)	C(96)-C(97)-C(98)	120.2(3)
C(99)-B(80)-C(93)	113.0(2)	F(98)-C(98)-C(97)	115.1(3)
C(87)-B(80)-C(93)	114.7(2)	F(98)-C(98)-C(93)	121.4(3)
C(99)-B(80)-C(81)	114.2(2)	C(97)-C(98)-C(93)	123.5(3)
C(87)-B(80)-C(81)	112.8(2)	C(104)-C(99)-C(100)	112.6(2)
C(93)-B(80)-C(81)	101.3(2)	C(104)-C(99)-B(80)	128.1(2)
C(86)-C(81)-C(82)	113.4(2)	C(100)-C(99)-B(80)	118.9(2)
C(86)-C(81)-B(80)	126.6(2)	F(100)-C(100)-C(101)	116.4(2)
C(82)-C(81)-B(80)	119.5(2)	F(100)-C(100)-C(99)	118.7(2)
F(82)-C(82)-C(83)	116.2(2)	C(101)-C(100)-C(99)	124.9(3)
F(82)-C(82)-C(81)	119.5(2)	F(101)-C(101)-C(100)	121.0(3)
C(83)-C(82)-C(81)	124.4(3)	F(101)-C(101)-C(102)	119.5(3)
F(83)-C(83)-C(84)	119.9(2)	C(100)-C(101)-C(102)	119.5(3)
F(83)-C(83)-C(82)	120.8(3)	F(102)-C(102)-C(101)	120.7(3)
C(84)-C(83)-C(82)	119.3(3)	F(102)-C(102)-C(103)	120.7(3)
F(84)-C(84)-C(85)	120.1(3)	C(101)-C(102)-C(103)	118.6(3)
F(84)-C(84)-C(83)	120.5(3)	F(103)-C(103)-C(104)	121.0(3)
C(85)-C(84)-C(83)	119.4(2)	F(103)-C(103)-C(102)	119.3(3)
F(85)-C(85)-C(84)	119.9(3)	C(104)-C(103)-C(102)	119.7(3)
F(85)-C(85)-C(86)	120.7(3)	F(104)-C(104)-C(103)	114.5(2)
C(84)-C(85)-C(86)	119.4(3)	F(104)-C(104)-C(99)	120.8(2)
F(86)-C(86)-C(81)	121.3(2)	C(103)-C(104)-C(99)	124.7(2)
F(86)-C(86)-C(85)	114.6(2)	C(112)-C(111)-C(116)	123.0(4)
C(81)-C(86)-C(85)	124.1(3)	C(112)-C(111)-Cl(1)	118.2(3)
C(92)-C(87)-C(88)	113.2(2)	C(116)-C(111)-Cl(1)	118.8(3)
C(92)-C(87)-B(80)	127.4(2)	C(111)-C(112)-C(113)	117.7(4)
C(88)-C(87)-B(80)	118.9(2)	C(112)-C(113)-C(114)	120.0(4)
F(88)-C(88)-C(89)	116.2(2)	C(115)-C(114)-C(113)	120.8(4)
F(88)-C(88)-C(87)	119.4(2)	C(116)-C(115)-C(114)	119.8(4)
C(89)-C(88)-C(87)	124.5(3)	C(115)-C(116)-C(111)	118.7(5)
F(89)-C(89)-C(90)	119.9(3)	C(122)-C(121)-C(126)	120.0
F(89)-C(89)-C(88)	120.7(3)	C(122)-C(121)-Cl(2)	120.2(6)
C(90)-C(89)-C(88)	119.4(3)	C(126)-C(121)-Cl(2)	119.8(6)
F(90)-C(90)-C(89)	120.1(3)	C(121)-C(122)-C(123)	120.0
F(90)-C(90)-C(91)	120.8(3)	C(122)-C(123)-C(124)	120.0
C(89)-C(90)-C(91)	119.1(3)	C(125)-C(124)-C(123)	120.0
F(91)-C(91)-C(90)	119.9(3)	C(124)-C(125)-C(126)	120.0
F(91)-C(91)-C(92)	120.5(3)	C(125)-C(126)-C(121)	120.0
C(90)-C(91)-C(92)	119.6(3)		
F(92)-C(92)-C(87)	120.8(2)		
F(92)-C(92)-C(91)	114.9(2)		
C(87)-C(92)-C(91)	124.3(3)		

[*t*Bu$_3$P–^{13}C(O)O–Si*i*Pr$_3$][B(C$_6$F$_5$)$_4$] (15)

Identification code	ASH1303
Formula	C24 B F20, C22 H48 O2 P Si
Formula weight	1082.71
Temperature	173 K
Diffractometer, wavelength	OD Xcalibur 3, 0.71073 Å
Crystal system, space group	Monoclinic, P2(1)/n
Unit cell dimensions	a = 15.2074(3) Å α = 90°
	b = 20.7944(4) Å β = 90.3103(18)°
	c = 15.3016(3) Å γ = 90°
Volume, Z	4838.74(16) Å^3, 4
Density (calculated)	1.486 Mg/m^3
Absorption coefficient	0.197 mm^{-1}
F(000)	2216
Crystal colour / morphology	Colourless blocks
Crystal size	0.44 x 0.37 x 0.16 mm^3
θ range for data collection	3.14 to 32.74°
Index ranges	-23<=h<=22, -29<=k<=31, -21<=l<=22
Reflns collected / unique	55662 / 16114 [R(int) = 0.0294]
Reflns observed [F>4σ(F)]	10695
Absorption correction	Analytical
Max. and min. transmission	0.975 and 0.929
Refinement method	Full-matrix least-squares on F^2
Data / restraints / parameters	16114 / 0 / 640
Goodness-of-fit on F^2	1.040
Final R indices [F>4σ(F)]	R1 = 0.0735, wR2 = 0.2034
R indices (all data)	R1 = 0.1116, wR2 = 0.2355
Largest diff. peak, hole	0.983, -0.636 eÅ^{-3}
Mean and maximum shift/error	0.000 and 0.000

Bond lengths [Å] and angles [°]

Si(1)-O(2)	1.747(2)	C(14)-C(17)	1.528(4)
Si(1)-C(5)	1.860(4)	C(14)-C(16)	1.554(5)
Si(1)-C(8)	1.877(4)	C(18)-C(21)	1.536(5)
Si(1)-C(11)	1.888(3)	C(18)-C(20)	1.546(5)
O(2)-C(3)	1.306(3)	C(18)-C(19)	1.559(6)
C(3)-O(3)	1.198(3)	C(22)-C(23)	1.522(5)
C(3)-P(4)	1.881(3)	C(22)-C(24)	1.540(5)
P(4)-C(18)	1.869(3)	C(22)-C(25)	1.554(6)
P(4)-C(14)	1.889(3)	B(30)-C(43)	1.653(3)
P(4)-C(22)	1.908(3)	B(30)-C(31)	1.660(3)
C(5)-C(6)	1.517(6)	B(30)-C(37)	1.660(3)
C(5)-C(7)	1.533(7)	B(30)-C(49)	1.664(3)
C(8)-C(10)	1.539(5)	C(31)-C(32)	1.389(3)
C(8)-C(9)	1.542(5)	C(31)-C(36)	1.391(3)
C(11)-C(12)	1.532(5)	C(32)-F(32)	1.355(3)
C(11)-C(13)	1.536(5)	C(32)-C(33)	1.395(4)
C(14)-C(15)	1.526(4)	C(33)-F(33)	1.342(3)

C(33)-C(34)	1.363(5)
C(34)-F(34)	1.349(3)
C(34)-C(35)	1.367(5)
C(35)-F(35)	1.343(3)
C(35)-C(36)	1.386(4)
C(36)-F(36)	1.352(3)
C(37)-C(38)	1.387(3)
C(37)-C(42)	1.394(3)
C(38)-F(38)	1.349(3)
C(38)-C(39)	1.387(4)
C(39)-F(39)	1.347(3)
C(39)-C(40)	1.374(5)
C(40)-F(40)	1.338(3)
C(40)-C(41)	1.373(5)
C(41)-F(41)	1.351(3)
C(41)-C(42)	1.387(4)
C(42)-F(42)	1.348(3)
C(43)-C(44)	1.384(3)
C(43)-C(48)	1.398(3)
C(44)-F(44)	1.358(3)
C(44)-C(45)	1.390(4)
C(45)-F(45)	1.355(3)
C(45)-C(46)	1.363(4)
C(46)-F(46)	1.349(3)
C(46)-C(47)	1.373(4)
C(47)-F(47)	1.341(3)
C(47)-C(48)	1.389(3)
C(48)-F(48)	1.342(3)
C(49)-C(50)	1.393(3)
C(49)-C(54)	1.394(3)
C(50)-F(50)	1.353(3)
C(50)-C(51)	1.393(4)
C(51)-F(51)	1.346(3)
C(51)-C(52)	1.379(5)
C(52)-F(52)	1.340(3)
C(52)-C(53)	1.374(5)
C(53)-F(53)	1.348(4)
C(53)-C(54)	1.380(4)
C(54)-F(54)	1.357(3)

O(2)-Si(1)-C(5)	111.21(14)
O(2)-Si(1)-C(8)	100.59(13)
C(5)-Si(1)-C(8)	113.57(17)
O(2)-Si(1)-C(11)	105.08(12)
C(5)-Si(1)-C(11)	111.19(17)
C(8)-Si(1)-C(11)	114.35(16)
C(3)-O(2)-Si(1)	125.62(18)
O(3)-C(3)-O(2)	125.9(3)
O(3)-C(3)-P(4)	119.8(2)
O(2)-C(3)-P(4)	114.16(19)
C(18)-P(4)-C(3)	105.55(14)
C(18)-P(4)-C(14)	113.59(15)
C(3)-P(4)-C(14)	111.23(12)
C(18)-P(4)-C(22)	112.71(17)
C(3)-P(4)-C(22)	100.61(13)
C(14)-P(4)-C(22)	112.19(14)
C(6)-C(5)-C(7)	109.2(4)
C(6)-C(5)-Si(1)	114.7(3)
C(7)-C(5)-Si(1)	114.3(3)
C(10)-C(8)-C(9)	110.5(3)
C(10)-C(8)-Si(1)	112.2(3)
C(9)-C(8)-Si(1)	115.3(3)
C(12)-C(11)-C(13)	110.5(3)
C(12)-C(11)-Si(1)	113.0(3)
C(13)-C(11)-Si(1)	114.1(2)
C(15)-C(14)-C(17)	110.3(3)
C(15)-C(14)-C(16)	105.6(3)
C(17)-C(14)-C(16)	107.5(3)
C(15)-C(14)-P(4)	113.3(2)
C(17)-C(14)-P(4)	110.9(2)
C(16)-C(14)-P(4)	109.0(2)
C(21)-C(18)-C(20)	108.2(3)
C(21)-C(18)-C(19)	107.0(3)
C(20)-C(18)-C(19)	109.1(3)
C(21)-C(18)-P(4)	111.8(3)
C(20)-C(18)-P(4)	110.2(2)
C(19)-C(18)-P(4)	110.5(3)
C(23)-C(22)-C(24)	110.1(3)
C(23)-C(22)-C(25)	107.1(3)
C(24)-C(22)-C(25)	108.9(3)
C(23)-C(22)-P(4)	109.0(2)
C(24)-C(22)-P(4)	111.2(2)
C(25)-C(22)-P(4)	110.5(2)
C(43)-B(30)-C(31)	102.83(18)
C(43)-B(30)-C(37)	112.56(18)
C(31)-B(30)-C(37)	113.30(17)
C(43)-B(30)-C(49)	113.92(17)
C(31)-B(30)-C(49)	113.33(18)
C(37)-B(30)-C(49)	101.36(18)
C(32)-C(31)-C(36)	112.8(2)
C(32)-C(31)-B(30)	127.7(2)
C(36)-C(31)-B(30)	119.3(2)
F(32)-C(32)-C(31)	120.8(2)
F(32)-C(32)-C(33)	115.2(2)
C(31)-C(32)-C(33)	124.0(2)
F(33)-C(33)-C(34)	120.5(3)
F(33)-C(33)-C(32)	119.8(3)
C(34)-C(33)-C(32)	119.7(3)
F(34)-C(34)-C(33)	120.5(3)
F(34)-C(34)-C(35)	120.1(3)
C(33)-C(34)-C(35)	119.4(2)
F(35)-C(35)-C(34)	120.5(2)
F(35)-C(35)-C(36)	120.4(3)
C(34)-C(35)-C(36)	119.2(3)
F(36)-C(36)-C(35)	115.6(2)
F(36)-C(36)-C(31)	119.6(2)
C(35)-C(36)-C(31)	124.8(2)
C(38)-C(37)-C(42)	113.1(2)
C(38)-C(37)-B(30)	127.7(2)
C(42)-C(37)-B(30)	118.91(19)
F(38)-C(38)-C(39)	114.7(2)
F(38)-C(38)-C(37)	121.2(2)
C(39)-C(38)-C(37)	124.1(2)
F(39)-C(39)-C(40)	120.0(3)
F(39)-C(39)-C(38)	119.9(3)
C(40)-C(39)-C(38)	120.1(2)
F(40)-C(40)-C(41)	120.4(3)
F(40)-C(40)-C(39)	120.9(3)
C(41)-C(40)-C(39)	118.7(2)
F(41)-C(41)-C(40)	120.3(3)
F(41)-C(41)-C(42)	120.2(3)
C(40)-C(41)-C(42)	119.5(3)
F(42)-C(42)-C(41)	115.9(2)
F(42)-C(42)-C(37)	119.6(2)
C(41)-C(42)-C(37)	124.5(2)
C(44)-C(43)-C(48)	113.4(2)
C(44)-C(43)-B(30)	126.8(2)
C(48)-C(43)-B(30)	119.6(2)
F(44)-C(44)-C(43)	121.4(2)
F(44)-C(44)-C(45)	114.9(2)
C(43)-C(44)-C(45)	123.7(2)
F(45)-C(45)-C(46)	120.0(2)
F(45)-C(45)-C(44)	119.8(3)
C(46)-C(45)-C(44)	120.3(3)
F(46)-C(46)-C(45)	120.9(3)
F(46)-C(46)-C(47)	119.9(3)
C(45)-C(46)-C(47)	119.2(2)
F(47)-C(47)-C(46)	120.0(2)

F(47)-C(47)-C(48)	120.9(3)	F(51)-C(51)-C(50)	119.8(3)
C(46)-C(47)-C(48)	119.1(2)	C(52)-C(51)-C(50)	119.8(2)
F(48)-C(48)-C(47)	116.6(2)	F(52)-C(52)-C(53)	120.9(3)
F(48)-C(48)-C(43)	119.1(2)	F(52)-C(52)-C(51)	120.4(3)
C(47)-C(48)-C(43)	124.3(2)	C(53)-C(52)-C(51)	118.8(3)
C(50)-C(49)-C(54)	113.0(2)	F(53)-C(53)-C(52)	119.9(3)
C(50)-C(49)-B(30)	127.0(2)	F(53)-C(53)-C(54)	120.5(3)
C(54)-C(49)-B(30)	119.8(2)	C(52)-C(53)-C(54)	119.5(3)
F(50)-C(50)-C(51)	114.9(2)	F(54)-C(54)-C(53)	115.9(2)
F(50)-C(50)-C(49)	121.1(2)	F(54)-C(54)-C(49)	119.1(2)
C(51)-C(50)-C(49)	123.9(2)	C(53)-C(54)-C(49)	124.9(2)
F(51)-C(51)-C(52)	120.4(3)		